EUROPEAN AVIATION SAFETY AGENCY
AGENCE EUROPÉENNE DE LA SÉCURITÉ AÉRIENNE
EUROPÄISCHE AGENTUR FÜR FLUGSICHERHEIT

Research Project EASA.2011/01

CODAMEIN-II – Composite Damage Metrics and Inspection (high energy blunt impact threat) – 2nd phase

easa.europa.eu

Bishop GmbH Aeronautical Engineers www.bishop-gmbh.com		Hamburg (D)

REPORT

Department: Research Project: CODAMEIN II	Report No.: PBH100337 A
Type: Test / FEA Classification: PUBLIC	Project Reference: RBH100730A Customer Reference: EASA.2011.NP.24

Subject: **EASA.2011.NP.24 "Composite Damage Metrics and Inspection" (CODAMEIN II)**

Summary:

This report documents the outcomes of the EASA CODAMEIN II research project. The main objectives of this project were, based on the outcomes of the EASA.2010.C13 CODAMEIN project, to perform another series of high energy blunt impact tests on a similar test panel representing hybrid fuselage structure of a CS-25 Aircraft. Two static load cycles were performed within the panel test using a test set-up similar to CODAMEIN with an increased boundary stiffness. A maximum impact energy of 1443 J was induced to the panel and local damage was generated in the centre shear ties. The damage onset threshold was found to be 970 J. Based on the outcomes of CODAMEIN and the investigations of the University of California San Diego (UCSD), a typical damage sequence was anticipated which involved shear tie damage and failure as the first stage of damage. The study indicated that this damage process is stable and basic changes in the test set-up or the panel design would be required to change the mode of first damage. Based on the objective to retain the test panel in a reparable condition for further tests, no damage beyond damage of the centre shear ties was generated.

The results of the impact test were analysed and set in comparison with the results of the CODAMEIN test and the tests performed by the UCSD.

An advanced numerical model was developed which was used to perform FE Analyses of the impact test including the damage sequence. Furthermore, a sensitivity study was performed using FEA to assess the influence and significance of factors governing the formation of impact damage with low visibility.

Date: 14.02.2013	Prepared:	Checked:		Approved:	Archive:
	Peter Haase	Rodney Thomson	Peter Bishop	Emmanuel Isambert	\Work_Packages\EASA_CODAMEIN_II_RBH100730A\D_Documentation\1_Report\Final_Report\
Signature					

Distribution		Issue:	Date:	No. Pages	Changed pages:	Valid from/for:
Peter Haase Peter Bishop Rodney Thomson Emmanuel Isambert Simon Waite Elena Garcia Sanchez Archive *Cover Sheet	Bishop-GmbH Bishop-GmbH ACS Australia EASA EASA EASA	A	14.02.2013	179	Initial version	A350 / B787

CODAMEIN II

Composite **Da**mage **Me**trics and **In**spection

EASA.2011.NP.24

Report

Peter Haase

14 February 2013

Bishop GmbH - Aeronautical Engineers

Blankeneser Bahnhofstraße 12

22587 Hamburg – Germany

Table of contents

List of figures

List of tables

List of references

No.	Title
[1]	Mikulik, Z., Haase, P.:CODAMEIN (Composite Damage Metrics and Inspection), EASA.2010.C13, Final Report, 31 Jan 2012
[2]	Perez, I.: Proposal for "Testing of the 2nd CODAMEIN Panel", Offer Ref. 2011_L_5810209430_5354, Issue 3, 14 Dec 2011
[3]	Kim, H.: Impact Damage Formation on Composite Aircraft Structures, FAA Joint Advanced Materials & Structures (JAMS) 6th Annual Technical Review Meeting, Seattle, WA, 19-20 May 2010
[4]	Kim, H., DeFrancisci, G., Chen, Z.M., Rhymer, J., Funai, S., Tippman, J.: Impact Damage Formation on Composite Aircraft Structures, FAA Joint Advanced Materials & Structures (JAMS) 2011 Technical Review Meeting, San Diego, CA, 20-21 April 2011
[5]	Kim, H.: Safety Management Initiative on High Energy Blunt Impact, CMH-17 PMC Forum, Kansas City, MO, 1 March 2011
[6]	Jacobson, D.:SDC Support of Bishop Stiffened Fuselage Panel – Summary Report (Rev A), PO EASA.2010.C13.SDC, 13 June 2011
[7]	Pringle, T.: Preventing ramp and ground accidents, Transport Canada, www.tc.gc.ca, 2010
[8]	International Air Transport Association: Ground damage prevention programme targets 10% cost reduction, Industry Times, Edition 7, September, Article 4, 2005
[9]	Haase, P.: EASA.2011.NP.24 "Composite Damage Metrics and Inspection (CODAMEIN) II", 1st Interim Report, 12.04.2012
[10]	Hernandez, O.: Applus LGAI, Mechanical Testing Laboratory, Facilities Breakdown, October 2012

[11]	**Bergo Soto, R.: Non-destructive Testing Inspection Report, Report No. 12/31702927, 15. October 2012**
[12]	**Kim, H.: Frame03 Test Video – Wide Area Blunt Impact, https://www.youtube.com/watch?v=TJofm5MuLoc, available 25.10.2012**
[13]	**Kim, H.: Frame03 Test Video – Blunt Impact High Speed Video, https://www.youtube.com/watch?v=bBXhcQNbcl8, available 25.10.2012**
[14]	**"DCB ENF Data 20120808.xls", ACS Australia, August 2012**
[15]	**Abaqus Analysis User's Manual, Version 6.11**
[16]	**European Aviation Safety Agency: General acceptable means of compliance for airworthiness of products, parts and appliances, Annex II AMC 20-29: Composite Aircraft structure, July 2010**
[17]	**Mikulik, Z.: Blunt Impact on Composite-Metallic Aircraft Structure: Overview of the EASA / Bishop GmbH Research Project, 2011 FAA / EASA / Industry Composite Transport Fatigue, Damage Tolerance, Maintenance & Crashworthiness Workshop, Atlanta, May 18, 2011**
[18]	**Mikulik, Z.; High Energy, low Velocity Blunt Impact on a Composite-Metallic Aircraft Structure, CMH-17 PMC European Coordination Meeting, Delft, September 28, 2011**
[19]	**Mikulik, Z.: Damage Criticality and Inspection Concerns of Composite – Metallic Aircraft Structures subjected to high Energy, low Velocity Blunt Impact, 4th European Conference on Materials and Structures in Aerospace, Hamburg, February 8, 2012**
[20]	**Bishop, P.: CODAMEIN II (Composite Damage Metrics and Inspection), EASA-funded research project, Aerospace Structural Impact Dynamics International Conference, Wichita, November 6-9, 2012**
[21]	**Bishop, P.: CODAMEIN II (Composite Damage Metrics and Inspection), EASA-funded research project, 14th Annual Ground Handling International Conference, Milan, November 26-29, 2012**

List of acronyms

ACI	Airports Council International
ACS	Advanced Composite Structures
BC	Boundary Condition
CFRP	Carbon Fibre Reinforced Plastics
CODAMEIN	Composite Damage Metrics and Inspection
CS	Certification Specification
DBH	Internal Naming of Bishop GmbH Engineering Drawings
DCB	Double Cantilever Beam
DOF	Degree Of Freedom
EASA	European Aviation Safety Agency
ENF	End Notch Flexure
FAA	Federal Aviation Administration
FE / FEA	Finite Element / Finite Element Analysis
Frm	Frame
GSE	Ground Service Equipment
LC	Load Cycle
LL	Limit Load
LVDT	Linear Variable Differential Transformer
NDT	Non-Destructive Testing
ST	Shear Tie
Str	Stringer
UCSD	University of California San Diego
UD	Uni-Directional
UL	Ultimate Load

Acknowledgements

This work was funded by European Aviation Safety Agency (EASA) under contract EASA.2011.C20. The research was supervised by Dr Simon Waite. Technical guidance was provided throughout the project by Elena Garcia Sanchez and Dr Simon Waite.

The author would like to thank Dr. Rodney Thomson of ACS Australia for his intensive expert advice and support of the numerical investigations throughout the entire research.

The contribution of Prof. Hyonny Kim, Gabriela DeFrancisci and Zhi Ming Chen of the University of California San Diego, who supported the CODAMEIN II research by supplying material for the test panel and with updates on the high energy blunt impact research of the UCSD and who enabled a further alignment of the numerical investigations of Bishop GmbH and the UCSD is highly appreciated.

Executive summary

In the second phase of the EASA CODAMEIN program, high energy blunt impact damage on a hybrid aircraft structure was investigated. Based on the CODAMEIN investigation, the initiation and progression of damage in composite/metallic hybrid aeroplane fuselage structures, caused by a collision with a ground service equipment vehicle, equipped with a rubber bumper, was investigated. A static impact test on a hybrid design 5-frame, 4-stringer fuselage panel was performed. Predictions of the damage initiation and progression were made using Finite Element Analyses. For this numerical investigation, high detail Finite Element models of the fuselage structure were generated and analysed. The performance of the Finite Element models was assessed in comparison with the static tests of CODAMEIN and CODAMEIN II using an increased amount of test instrumentation in the CODAMEIN II test.

Finite Element Models of different detail levels were created, covering the range between coupon level models and a fuselage barrel model. Material damage and degradation were integrated in models including the model of the test panel. The damage modes and the damage process that were found in the tests of CODAMEIN and CODAMEIN II, were represented by the test panel model. A sensitivity study provided knowledge about the sensitivity of the Finite Element modelling approach to all parameters that may influence the model response and especially the damage initiation and damage progression behaviour.

The investigation has been coordinated with the research of Prof. Hyonny Kim and his research group at the University of California San Diego. The investigation of hybrid fuselage structure within CODAMEIN complements their research on all composite fuselage structures in collaboration with FAA and Boeing Co.. The author would also like to thank UCSD for the supply of composite material out of UCSD's stock for the fabrication of the CODAMEIN II test panel.

Based on the general results of the CODAMEIN investigation, detailed knowledge about the damage processes, the influence of the boundary conditions and approaches of representation by Finite Element Analyses was gained. The confidence in the used Finite Element modelling approaches was increased, which proposes further usage of the Finite Element modelling approaches for the investigation of different impact scenarios and different fuselage structures. The gained information also clearly proposed further experimental investigation benefitting from the performed investigations, to validate Finite Element models and to extend the investigation to different boundary conditions and different test specimen designs that represent further relevant regions of aircraft fuselages and different fuselage material configurations and designs.

1 Introduction

1.1 Background

Advanced carbon fibre reinforced polymer composite materials are being used more extensively in the aerospace industry today. After already having a long history in military aviation and secondary structure of civil aircraft, the high stiffness to weight ratio and fatigue resistance bring carbon fibre composites in much more extensive use for primary structure of large civil aircraft. One of the most important issues in changing from conventional metallic alloys to composite materials is to ensure that there are no compromises in the level of safety [Mikulik, Haase 2012]. Aircraft certification requires the demonstration of the capacity of structure with manufacturing flaws or structure damaged during aircraft service, to carry ultimate load (UL) throughout the entire aircraft life or limit load (LL) for a substantiated inspection period with the demand for sooner detection of damages that weaken the structure closer to LL capability. High energy blunt impact during ground service often generates damage of the category 2 or 3 of the definition in the EASA AMC 20-29 (see Figure 1) which must be respected in the certification process. Such impact may also result in higher category damage which must be reported and repaired immediately. Therefore, it becomes necessary to understand the boundaries between category 2/3 and category 5 respectively [Mikulik, Haase, 2012].

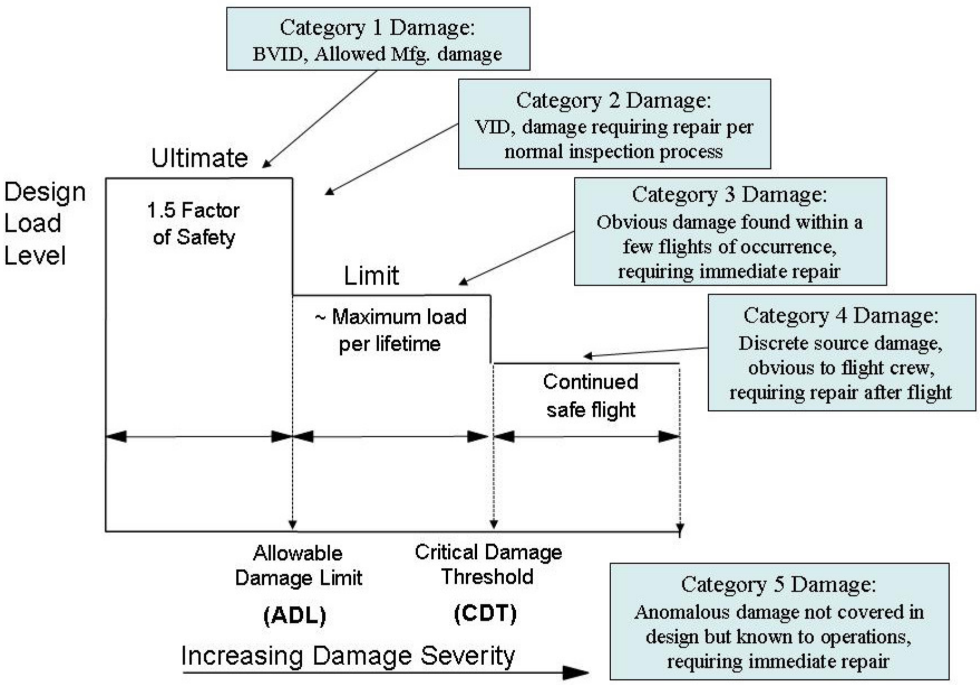

Figure 1 Schematic diagram showing design load levels versus categories of damage severity [EASA, 2010]

One specific area of interest is blunt impact of ground vehicles with aircraft fuselage.

The aviation industry has acknowledged the risks associated with serious ground operation incidents and accidents. Consequences of these events result in aircraft damage, delays and financial cost to the industry. In 2000, the Airports Council International (ACI) reported that US$3 billion of losses were caused by airport ground vehicles colliding with aircraft, aircraft hitting each other or other objects around the airport [Pringle 2010]. Narrowing down the focus to aircraft damage during ground operations, it has been reported that 50% of major damage has been recorded to be caused by baggage vehicles while 60% of minor damage was caused by collision of aircraft with ground vehicles [IATA 2005, Mikulik, Haase 2012].

The aim of CODAMEIN was to investigate the relationship between damage severity and visible damage caused by high energy blunt impact due to a collision with a ground service vehicle. The conditions of such events have been examined and a representative scenario for testing and numerical analysis has been developed in collaboration with Prof. Hyonny Kim's group at the University of California San Diego (UCSD). Numerical analyses were performed to assess the boundary conditions for an impact test on a hybrid design fuselage panel.

The aim of the CODAMEIN was to investigate the conditions of impact damage with low or no visibility, caused by high energy blunt impact, specifically focusing on collisions by ground service equipment (GSE) vehicles that use protective rubber bumpers. With the use of composite materials, this type of damage is of special interest since potential significant structural damage may be barely visible or invisible on the structure's outer surface.

The results of the CODAMEIN tests confirmed the initial assumptions on the level of damage. Significant structural damage was generated in a static test that implemented fuselage-like boundary conditions and a typical size GSE rubber bumper, that impacted the fuselage at low velocity.

1.2 Aims and objectives of the research

The investigation for CODAMEIN II intended to improve the understanding of the formation of blunt impact damage with no or low visibility, based on the results obtained from CODAMEIN. To achieve this, a structural test and detailed FE Analyses were planned.

The case of a GSE vehicle colliding with an aircraft fuselage was studied by performing a quasi-static impact test on a fuselage panel by a steel plate equipped with a circular shaped rubber bumper. Based on the knowledge gained from CODAMEIN, the focus of CODAMEIN II was to be concentrated on the assessment of structural damage initiation and the damage sequence. The boundary conditions of the test were to be verified with respect to a possible change towards a boundary stiffness that is more critical for damage initiation. A model for numerical analysis was to be developed, which enables the prediction of damage in the structure. The understanding of damage initiation and propagation was to be advanced, based on the impact conditions determined in the CODAMEIN investigation.

For this, both the approach of testing and FE analysis were to be adapted in order to gain more detailed information on the initiation and propagation of damage. Based on the test of CODAMEIN which used a basic set-up of instrumentation, the data acquisition was planned to be expanded to gain a greater amount of information about the initiation and progress of damage and the global test panel behaviour. The measurement data from the test was intended to be used to more accurately validate the FE model. The implementation of damage models and model refinements were intended to enable the FE Analysis to reflect the high energy blunt impact sequence beyond the initiation of failure.

1.3 Damage sequence as result of blunt impact

Both the test and the FE analysis of CODAMEIN showed that the radii of the shear ties can be expected to show the first failure in terms of delamination and rupture. The test in CODAMEIN II is expected to be loaded to a higher indentation. The damage that was detected in the CODAMEIN test (shear tie delamination and rupture, frame-stringer contact, frame rotation), has also been documented in UCSD's panel tests. The resulting events of damage after multiple shear tie failures are expected to be similar as well. Severing of the stringers or stringer delamination and finally significant frame or stringer damage due to stringer-frame contact are expected in the CODAMEIN II test. This order of damage, expected prior to the detailed FE analysis of the CODAMEIN II test scenario is shown in Table 1.

Table 1 Expected order of damage events in test

Damage stage	Type of damage	
1	Delamination and breakage of shear ties	Frame rotation
2	Frame-stringer contact	
3	Stringer severing, delamination	
4	Massive frame or stringer damage due to frame-stringer contact	

Compared to the testing within CODAMEIN, more information was expected to be gained from the CODAMEIN II test. Based on advanced results from FE analysis, which covered a possible change in boundary stiffness, an investigation of more extensive damage with low or no external visibility was expected.

1.4 Outcomes of CODAMEIN

Within CODAMEIN , a hybrid design test panel was designed to provide a representative fuselage structure of a modern long range CS-25 aeroplane with a primary structure mainly made of composite material. The panel design was based on the same general lay-out of the test panels used in the UCSD research. Contrary to the full composite design of UCSD's test panels that incorporate C-frames, the CODAMEIN test panel used

Aluminium Z-frames. By performing FE Analyses of the test panel alongside a full fuselage barrel model, the boundary conditions for a suitable test were assessed. Physical properties of current GSE vehicles have been analysed. Using reports of GSE-to-aircraft collision incidents, representative levels of the impact parameters were found. Since the high energy blunt impact of a vehicle, equipped with a rubber bumper, was found to be a main threat for the generation of impact damage with low or no visibility on a composite aircraft fuselage, an impact case using a common circular GSE rubber bumper was chosen for investigation. A quasi-static test was performed by loading the panel in three cycles. The first load cycle was run until the first noticeable load drop, which was also highlighted by an audible event. Since A-scan inspection showed no delamination in the skin, delamination in the shear tie radii was expected to be the first point of damage onset. The failure threshold energy for the first damage onset was 1270 J, which represents a vehicle with a mass of 2500 kg impacting the fuselage with a velocity of 1 m/s. The second load cycle was stopped when several shear ties in the panel centre showed significant radius cracking (see Figure 2), which accompanied a continuous softening of the panel. Besides the multiple shear tie damage, which was clearly visible in the loaded state and became invisible after unloading, no further damage was detected either visually or by A-scan.

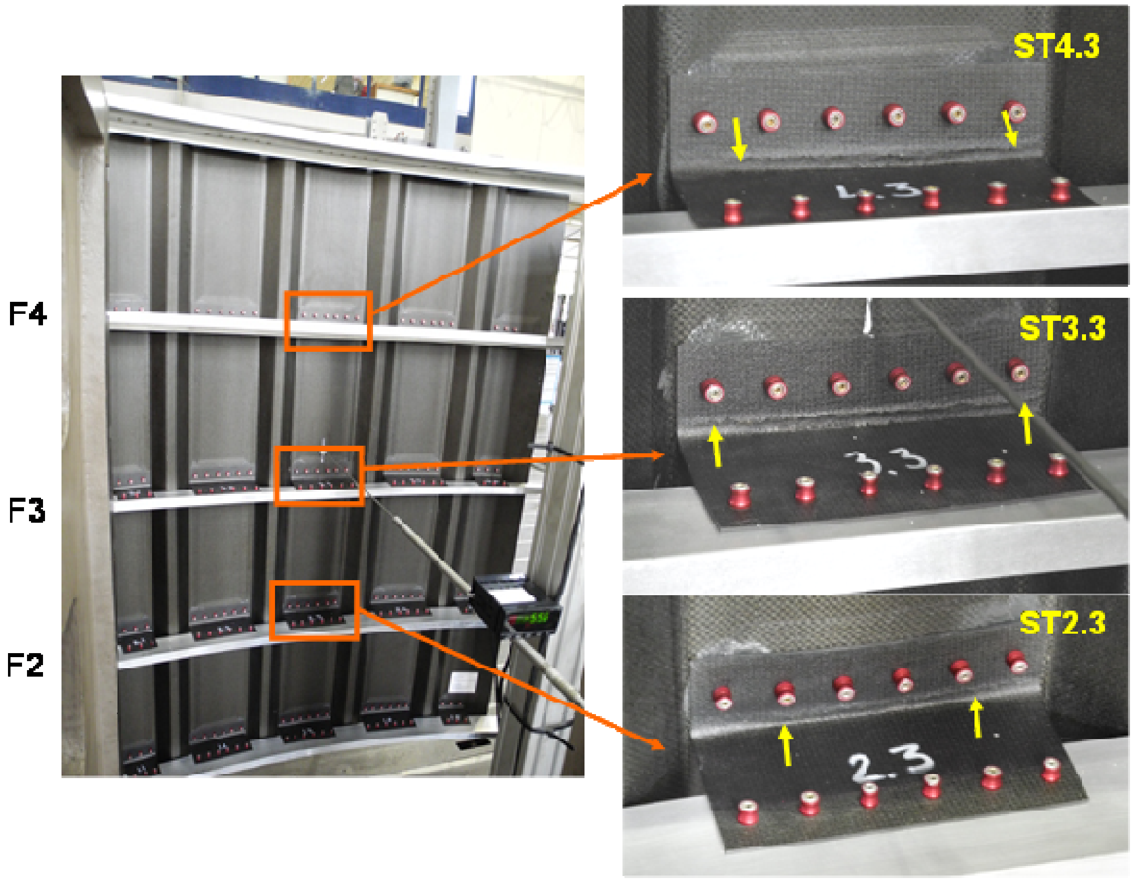

Figure 2 Shear tie damage in CODAMEIN 2nd load cycle [Mikulik, Haase 2012]

In the third load cycle, several shear ties failed, the centre frames came into contact with the centre stringers and the frames showed significant rotation. The third load cycle was stopped just before the estimated point of plastic deformation of the frames in order to prevent permanent deformation of the panel. A maximum energy of 2660 J was applied in the performed load cycles. The final inspection showed damage and failure of several shear ties as well as minor surface damage to the frames and stringers due to contact between those parts. The shear tie failure and stringer damage at frame 3 is shown in Figure 3. No delamination was detected in the skin and the stringers after the test.

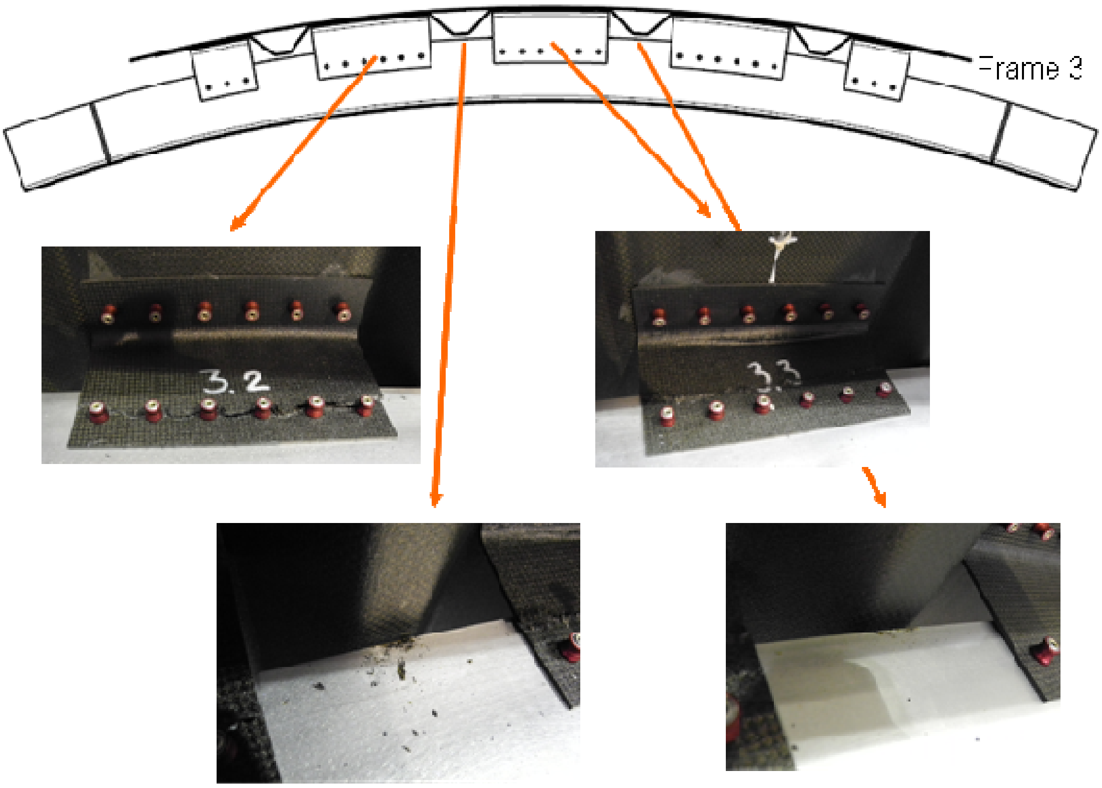

Figure 3 Shear tie failure and stringer damage in CODAMEIN 3rd load cycle [Mikulik, Haase 2012]

1.5 Outcomes of the UCSD research

The FAA-funded research work of Prof. Hyonny Kim's team at the UCSD uses a multi-step investigation of damage in composite fuselage structures caused by high energy blunt impacts. The aim of UCSD's research is to characterize blunt impact threats and locations and to understand damage formation and its relationship to visual detectability [Kim 2010]. Both quasi-static and dynamic tests have been performed on panels of differing sizes that are based on the part design concept which also influenced the design of the CODAMEIN / CODAMEIN II test panels. The design of UCSD's test panels incorporates a composite skin, composite omega stringers, composite C-frames and composite shear ties. The test panel types “stringer specimen” and “frame specimen” are shown in Figure 4.

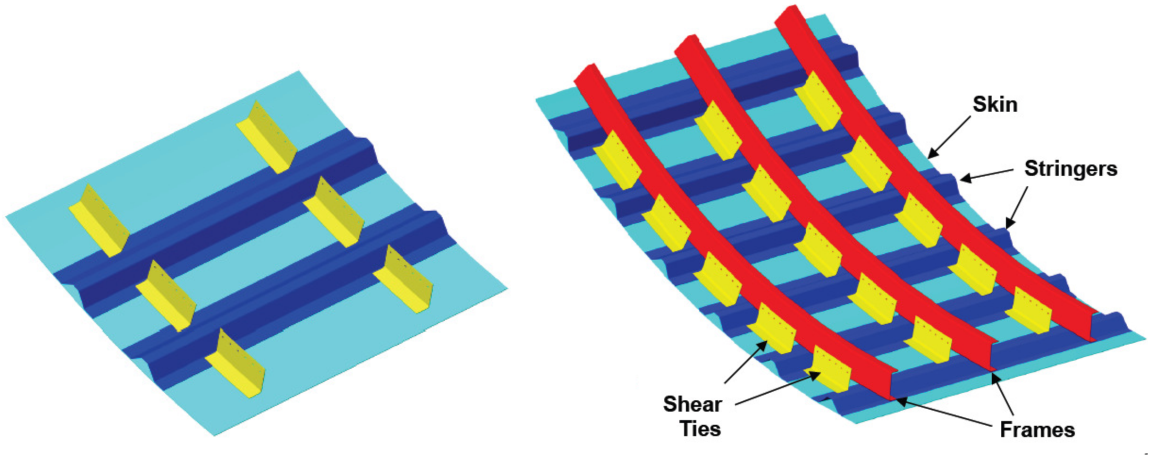

Figure 4 UCSD “stringer specimen”, “frame specimen” [Kim 2010]

UCSD’s research considered various parameters which affect the high energy blunt impact type. Different types of impactors were used such as small scale rigid impactors (see Figure 5) as well as small length and full size OEM rubber bumpers commonly used in GSE vehicles. A series of various boundary conditions, linked to various levels of detail of the specimens, were involved. Furthermore, the position of the impact with reference to the panel’s stiffeners was varied.

The tests performed by the UCSD generated valuable information on the influence of the different incorporated factors on the development of damage in the composite structure.

Impactor type:

The various impactor types that were used in the tests are displayed in Figure 5. The small rigid and rubber bumper impactors were used for the “stringer specimens”. The 0.5 m long circular rubber bumper was used to impact the “frame specimens”.

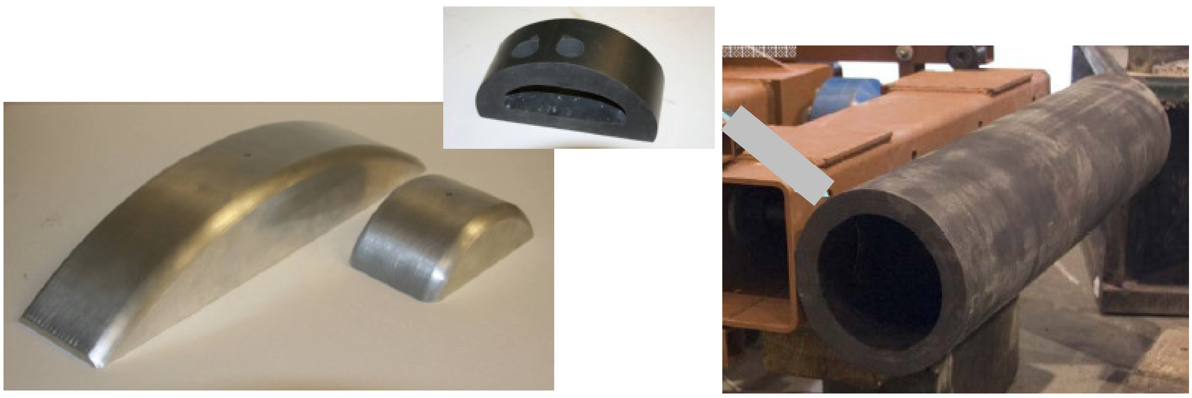

Figure 5 Impactor types: Rigid, Rubber Bumper (small scale D-shaped, 0.5 m long circular) [Kim 2010, Kim 2011]

The impact tests using small scale rigid impactors generated local and detectable damage to the skin. At relatively low indentation load levels, the skin was locally delaminated and failed by cracking in subsequent loading. The different rubber bumper impactors were found to cause more critical damage in the structure. Due to their softness and flexibility, the rubber bumpers distribute the load over a wider region of the structure which implies direct loading of some of the stiffeners. The detected damage in the rubber bumper impact test was skin delamination in the area surrounding the impact location and various types of stiffener damage or failure. The C-scan images of two "stringer specimens" impacted by a rigid impactor and a rubber bumper are displayed in Figure 6. The figures show local skin damage caused by the rigid bumper. This damage was clearly visibly detectable. The impact by the rubber bumper caused widespread damage such as stringer foot and shim delamination but no visibly detectable skin damage.

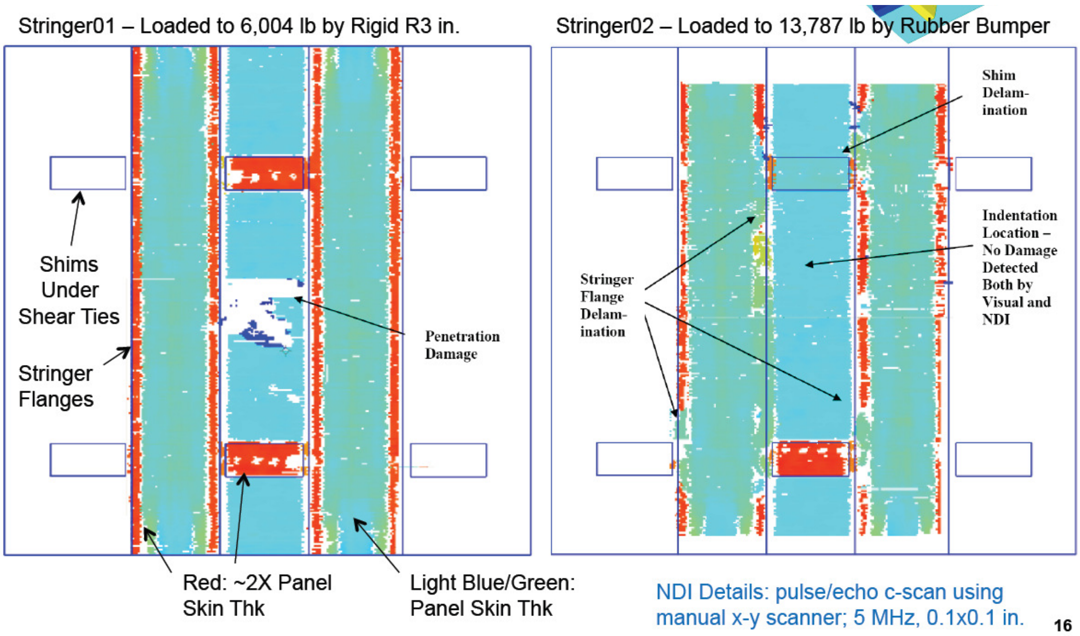

Figure 6 C-scan images of "stringer specimens", "stringer01", "stringer02" [Kim 2010]

<u>Impact location:</u>

The tests incorporated indentation of the panels directly on the skin with the bumper parallel to the stringers, at the centre line of a stringer (position 1 in Figure 7), on one stringer foot (position 2 in Figure 7) or equidistant between two stringers (position 3 in Figure 7). Regarding the creation of damage with low or no external visibility, the impact position on the skin between two stringers proved to be the most critical since the impacts on the other positions did create visible damage in the skin. In the large scale tests, massive damage was created in the stringers, the frames and the shear ties, as well as severing of parts with still no external visible damage.

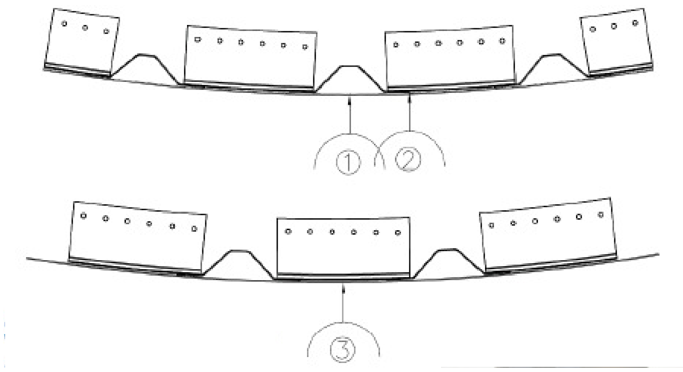

Figure 7 Impact positions at "stringer specimen" [Kim 2010]

Boundary Condition type:

The different kinds of test panel size incorporated various levels of detail and boundary conditions. While the small scale specimens did not include frames and were attached to a rigid structure through the shear ties (see Figure 8), the large scale specimens included frames which were attached to the test fixture. The small scale specimens allowed only for local skin and shear tie deformation. The attachments of the large scale specimens incorporated rotational and translational degrees of freedom (DOF) and stiffness, simulating the behaviour of the surrounding fuselage structure (see Figure 9).

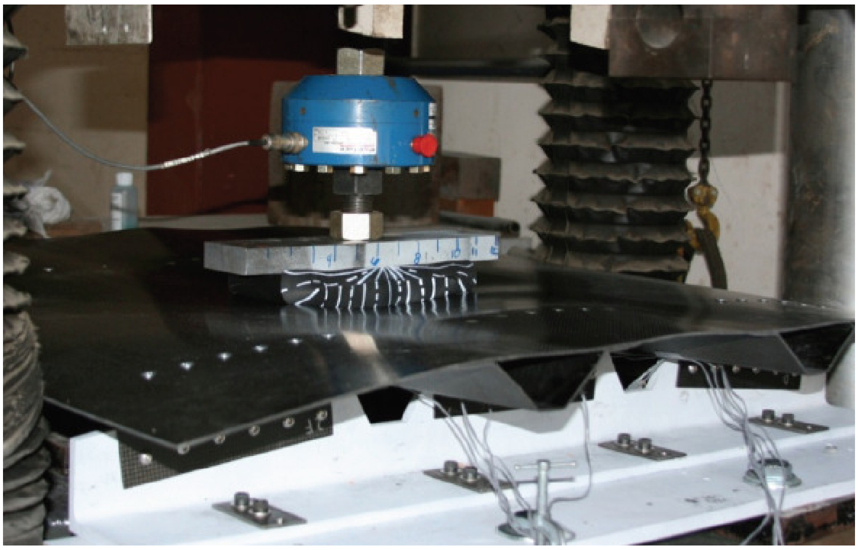

Figure 8 Set-up of "stringer specimen" [Kim 2010]

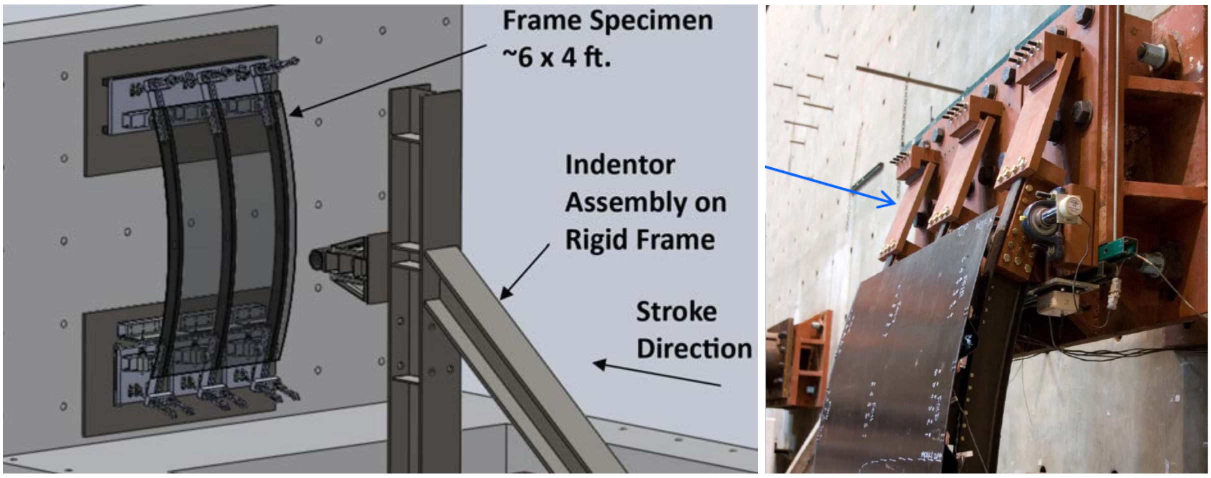

Figure 9 Set-up of "frame specimen" [Kim 2010]

Results:

The UCSD tests with rubber bumper impactors delivered valuable results regarding generation of barely visible damage. A progressive failure sequence was established, which explains the single steps of local damage, stiffness reduction and load diversion. The typical order of damage events of a 5-stringer 3-frame panel impacted by a rubber bumper between two stringers, first shows shear tie crushing, then delamination and multiple shear tie failure, followed by contact between the frames and the stringers and a rotation of the frames. The frame to stringer contact then leads to a local failure of either the stringer or the frame. A load-displacement plot of a "frame specimen" test is shown in Figure 10. It shows the load-displacement plots of the four single loadings which show numerous load drops, indicating local damage initiation and progress.

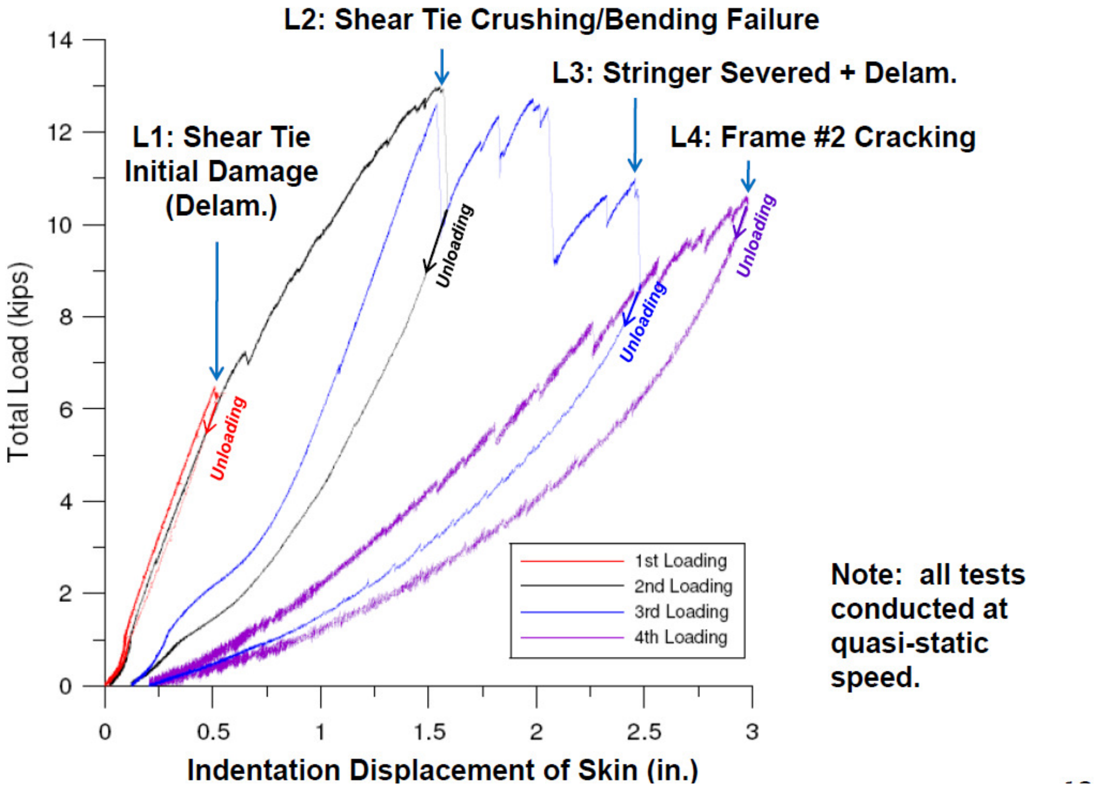

Figure 10 Load-Displacement plot of a "frame specimen" test [Kim 2010]

The damage progression sequence that the UCSD found in its tests is shown in Figure 11. It shows the order of events during the loading of the test panels, including the different paths of events that are possible at several points of the test. The displayed process gives also an indication of the damage sequence that is expected for the CODAMEIN II test. Especially at the branch points of the chart, the design variations such as the different frame types (composite C-frame, Aluminium Z-frame) influence the sequence of damage events. The rotation of the frames, especially after coming into contact with the centre stringers, will have a major influence on the following progress of the panel damage.

The video recordings of a dynamic blunt impact test of UCSD have been published [Kim 2012].

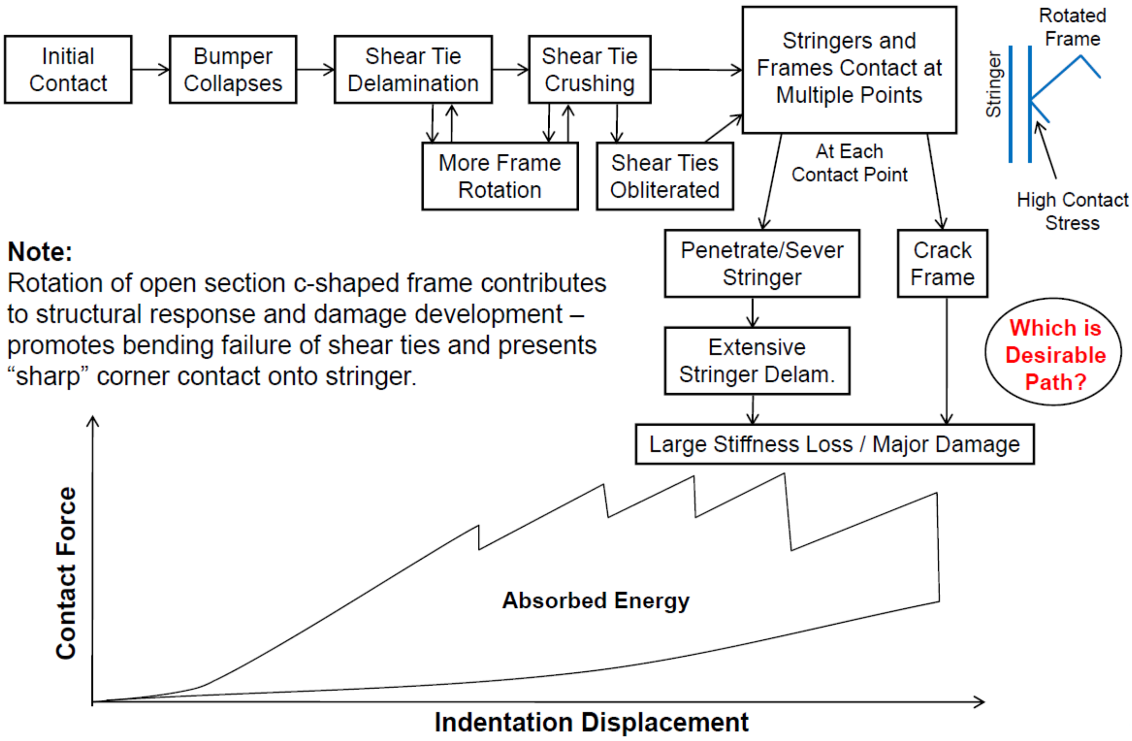

Figure 11 Sequence of Damage [Kim 2010]

1.6 Factors influencing the damage sequence

Several factors were assumed to have influence on the damage sequence of the test panel. A modification of the part dimensions and the relation of their dimensions would most likely influence the damage sequence. Previous tests have shown that the shear ties are the first parts to be damaged and fail. The usage of shear ties of a higher stiffness and strength would transfer the first damage and failure to other components. In fuselage regions with a very thick skin, the skin would likely get damaged earlier or as the first kind of damage.

The loading rate which correlates with the velocity of the impact might also influence the damage sequence. The range of probable impacts by GSE is assumed to be quasi-static up to slowly dynamic. Impact events with higher velocities would reduce the risk of remaining undetected or unreported as they are expected to generate visible damage. A static impact case was investigated since this type of loading provides the highest amount of information about the damage sequence and leaves the test controllable which permits reactions on the response of the specimen.

The position of the impact, the impactor size and its orientation relating to the fuselage orientation are also parameters that are expected to significantly influence the damage sequence. Since the impact situation using a rubber bumper of 1 m length and impacting the skin between two stringers was indicated to be the most critical case in terms of the creation of impact damage with no or low visibility by the investigations of UCSD, and since it provides a maximum of comparability with the outcomes of CODAMEIN and with the UCSD investigations, the impact situation was not changed for CODAMEIN II.

2 Methodology

Based on the results of CODAMEIN and the investigations performed by UCSD, several general approaches were considered for CODAMEIN II. Since all activities conducted within CODAMEIN and by UCSD showed individual pros and cons the approach with a maximum of comparability and flexibility was chosen. The points that were assessed for the choice of the CODAMEIN II methodology were the test panel design, the test set-up, especially the boundary conditions, the type of loading and the process of testing.

The re-use of the CODAMEIN test set-up and test fixtures was decided. A change of the boundary stiffness within the test fixtures was expected. Since an advancement of the FEA fuselage barrel model was part of the CODAMEIN II objectives and an increased stiffness of the barrel was expected as consequence of the involvement of more stiffening structure details, an increase of the test boundary stiffness was anticipated. A similar test method to CODAMEIN was anticipated. No major design change of the test panel was desired since the comparability of results between the CODAMEIN and CODAMEIN II tests as well as between the tests and the FE analyses and between the CODAMEIN / CODAMEIN II and UCSD investigations was rated as one of the most important objectives. A minor design change to the panel boundary was integrated to reduce the risk of undesired boundary failure of the panel. The extent of test monitoring and data recording was significantly increased to gain more detailed information from the test performance. Based on the limitations in the FE representation that were found within CODAMEIN, numerous new approaches and new feature integrations were planned for CODAMEIN II, also generating significantly more and more precise information about the test panel performance, also covering the post-damage range.

3 Implementation

The objectives that were planned for the test set-up, the test performance and the numerical investigation were implemented according to the project tasks. The proceeding within the CODAMEIN project was the basis for the implementation of CODAMEIN II, although the weighting was changed towards an increased ratio of numerical investigation and test evaluation. Due to the constraints in the capacities of the specimen manufacturer and the test lab, early decision making and scheduling were confirmed to be two of the most important tasks within the project. Reacting to the outcomes of the research of the UCSD and the findings of the numerical investigation within CODAMEIN II, the test objectives were adapted by EASA to gain the maximum outcome and the best comparability with the previous investigation and the UCSD activities, also in relation to objectives future investigations based on CODAMEIN II.

4 Test Panel

A test panel which represents a region of an aircraft fuselage, has been manufactured for the static high energy blunt impact test. The location of the test panel within the fuselage of a CS-25 large aircraft would be in the low rear fuselage, close to a cargo door (a field area local to the door, but not reflecting the local reinforcement typical of such structure). This region is one of the relevant regions for this investigation since the hybrid fuselage design might be used in this region and this region is one of the areas that are prone for the investigated type of damage.

4.1 Panel design

A hybrid design fuselage test panel will be investigated in CODAMEIN II. The design is based on that of CODAMEIN test panel which was defined based on a modern CS-25 aircraft design and the research work of the UCSD. While the UCSD focused on a full composite design for its research, the hybrid set-up was chosen to represent the passenger and cargo door surrounds of a fuselage as mentioned in 4. The panel with an overall size of approx. 1930 mm x 1830 mm implies a CFRP skin, four co-cured CFRP omega-stringer, five Aluminium Z-frames and L-shaped CFRP shear ties. An overview of the CODAMEIN II panel design is shown in Figure 15. The CODAMEIN II test panel incorporates a minor design change from the CODAMEIN panel. The planned testing aims to reach a higher level of deformation of the panel, compared to the completed test.

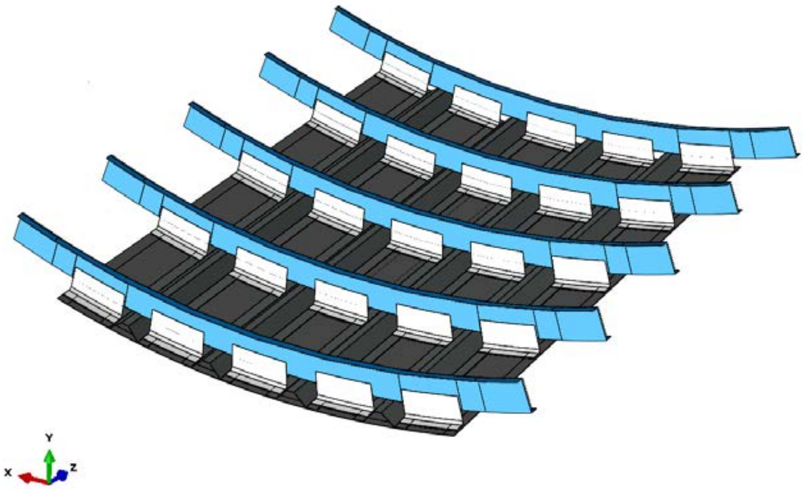

Figure 12 Overview of the CODAMEIN II panel

The shear ties are fastened to the skin (and stringer feet) and to the frames using countersunk and protruding head Hi Lok fasteners (see Figure 13).

Figure 13 Fastener attachment of Shear Ties [Jacobson 2011]

3D models of the main components of the CODAMEIN II test panel (skin, -frame, Omega-stringer, L-shear tie) are displayed in Figure 14.

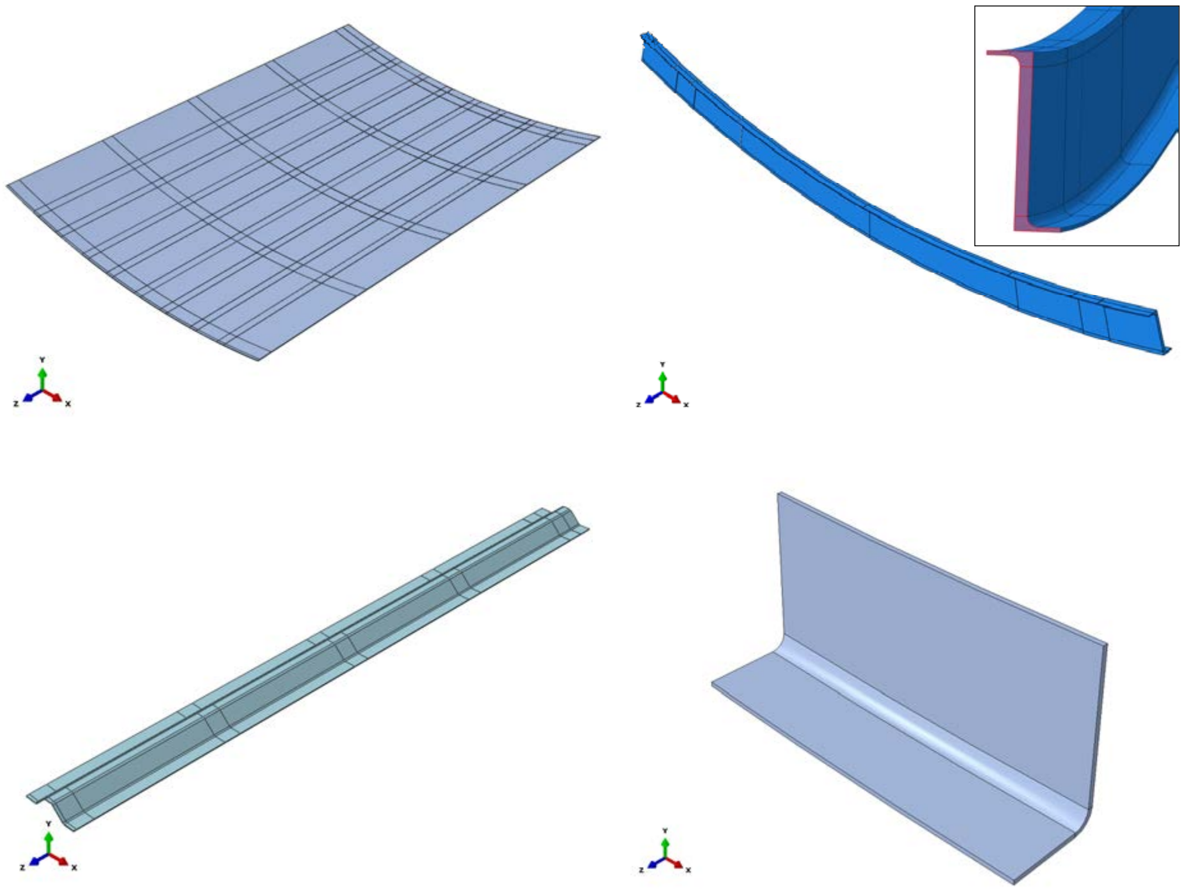

Figure 14 Panel components: Skin, Frame, Stringer, Shear Tie

The materials used to manufacture the CODAMEIN II panel are identical to those used for the CODAMEIN panel. These are Aluminium Al7075-T6 for the frames and aerospace grade carbon fibre reinforced plastic material, Cytec X840 Z60 12k UD tape and Cytec X840 Z60 PW Fabric. The lay-ups of the composite parts, which are also identical to the CODAMEIN lay-ups, are shown in Table 2. The types of fasteners used are steel Hi-Lok.

Table 2 CODAMEIN, CODAMEIN II: Part Composite Lay-ups

Skin	
Material	Orientation
Fabric	0
UD	0
UD	45
UD	90
UD	-45
UD	0
UD	45
UD	90
UD	-45
UD	-45
UD	90
UD	45
UD	0
UD	-45
UD	90
UD	45
UD	0
Fabric	0

Stringer	
Material	Orientation
Fabric	0
UD	0
UD	45
UD	-45
UD	90
UD	45
UD	-45
UD	0
UD	0
UD	-45
UD	45
UD	90
UD	-45
UD	45
UD	0
Fabric	0

Shear Tie	
Material	Orientation
Fabric	45
Fabric	0
Fabric	45
Fabric	0
Fabric	45
Fabric	45
Fabric	0
Fabric	45
Fabric	0
Fabric	45
Fabric	0
Fabric	45

The CODAMEIN II panel under assembly is depicted in Figure 15

Figure 15 CODAMEIN II test panel

For the CFRP skin and stringers, aerospace grade carbon fibre reinforced unidirectional tape (X840 Z60 12k) and plain weave fabric (X840 Z60 PW) prepreg of Cytec Industries were used. Usage of the same material as for the CODAMEIN panel could be achieved. The Z-frames were manufactured from Aluminium 7075-T6 and Hi-Lok fasteners were used to attach the shear ties to the skin, the stringer feet and the frames.

4.1.1 Similarity to the CODAMEIN test panel design

The CODAMEIN II panel is generally similar to the CODAMEIN panel. It incorporates a minor design change at the panel boundary. The modifications are implemented to reinforce the boundary region of the frames. The CODAMEIN II testing originally aimed to reach a higher level of deformation of the panel, compared to the CODAMEIN test. To ensure the frame ends do not undergo critical deformation at high loads, the end reinforcement was extended. Full size shear ties instead of half size shear ties were used also at the outer positions. An overview of the panel designs for CODAMEIN and CODAMEIN II is shown in Figure 16 [Haase 2012].

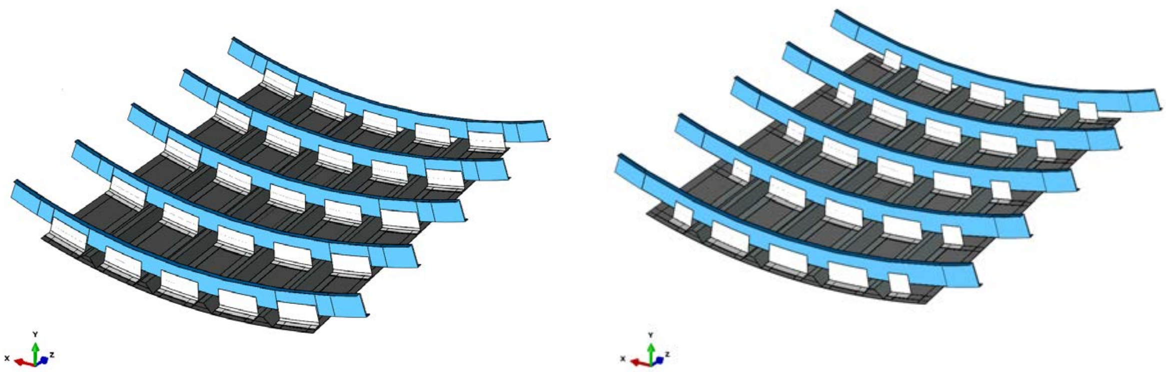

a) b)

Figure 16 Overview of the CODAMEIN II (a)) and CODAMEIN (b)) panels [Haase 2012]

Figure 17 shows an axial view of the CODAMEIN panel. The frame end region, which was modified for the CODAMEIN II panel, is highlighted. In order to reduce the free length between the outer shear ties and the frame clamping, full size outer shear ties were used for the CODAMEIN II panel instead of half width shear ties. Furthermore, the frame web thickness was increased in three steps (see Figure 18). Thus the frame end was reinforced more gradually.

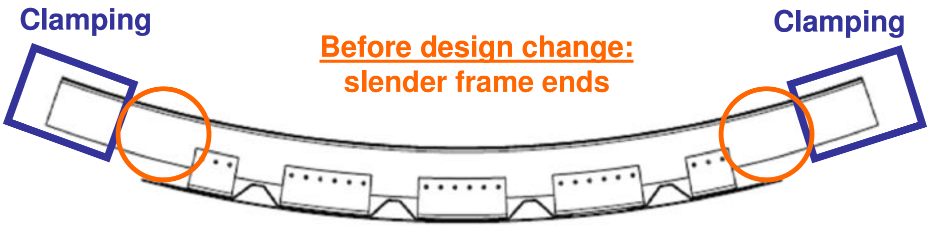

Figure 17 Panel axial view; frame ends

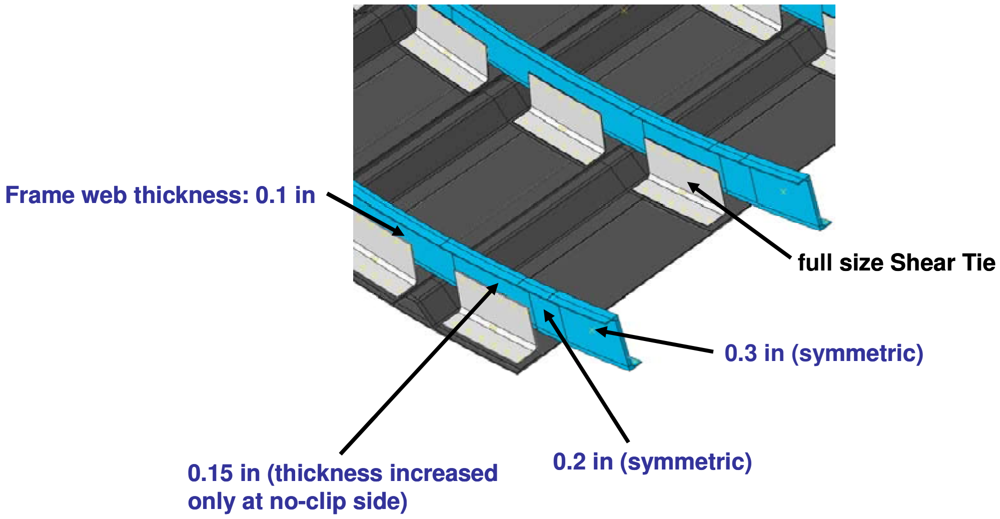

Figure 18 Detail: Frame End Reinforcement

Possible consequences of the frame end design change might be the promotion of frame failure close to the first step of frame reinforcement or shear tie failure at the outer positions. The design change was supported by Prof. Hyonny Kim who leads the associated investigation at UCSD. It achieves an additional similarity to the UCSD test panels. The composite frames of the UCSD test panels are reinforced by gradually adding composite plies at the frame ends.

4.1.2 Similarity to the UCSD test panel designs

The test panel design of CODAMEIN and CODAMEIN II is based on the component design of UCSD test panels. The UCSD performed numerous tests on specimens of different sizes and levels of detail which imply a size similar to the CODAMEIN / CODAMEIN II panel. A set of standard components has been used for all performed tests. Thus the material, lay-up and cross section of the test panel’s skin, stringers, frames and shear ties were maintained throughout the impact testing program. The size of the test panels, the number of involved components and the boundary conditions have all been changed. Figure 19 shows the UCSD test panel types, “stringer panel” and “frame panel”.

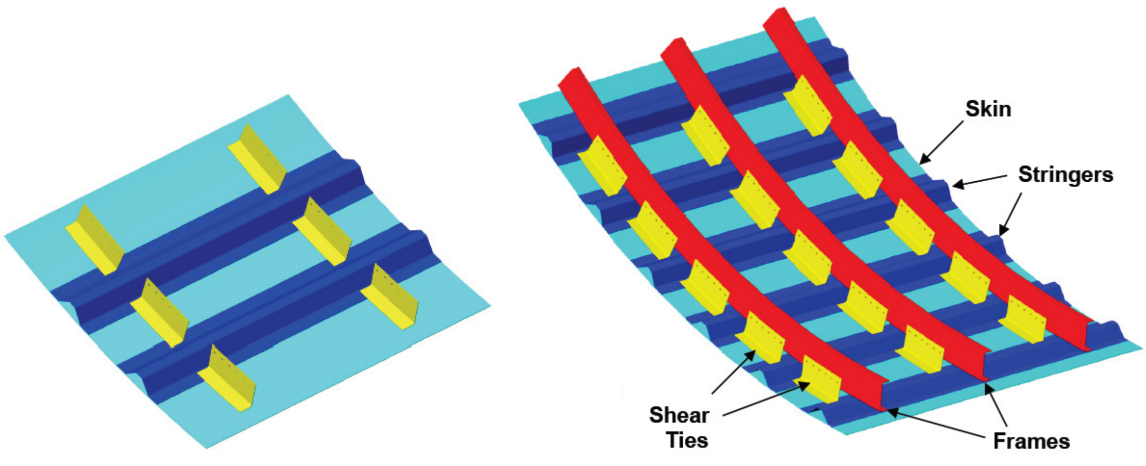

Figure 19 UCSD "Stringer Panel" and "Frame Panel"

All the UCSD test panels incorporate composite C-frames. Instead, the CODAMEIN and CODAMEIN II test panels use Aluminium Z-frames. The Z-frame, which was chosen for the CODAMEIN and CODAMEIN II panels to create a hybrid design panel, is displayed in Figure 20. This picture also shows the composite C-frame which UCSD uses for its comparable investigation on a full composite fuselage design.

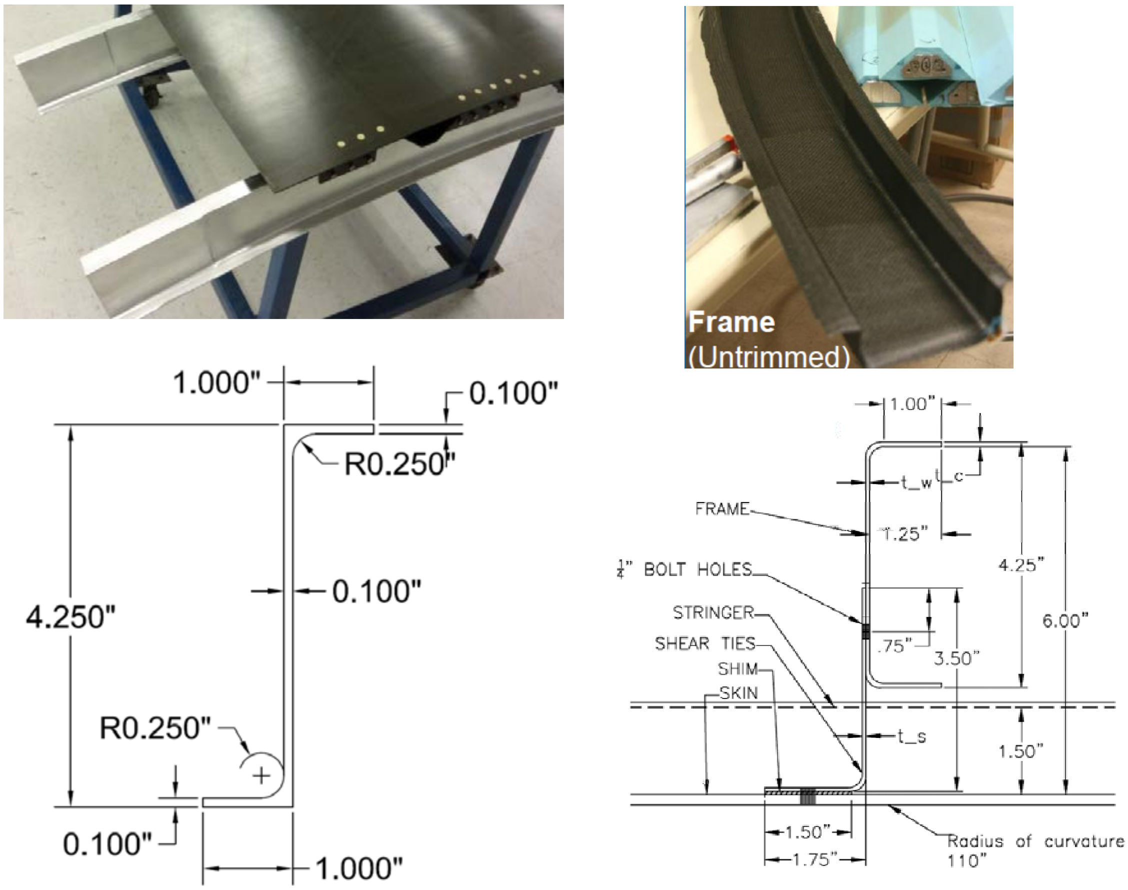

Figure 20 Z-Frame section, UCSD C-Frame section [Kim 2011]

The geometry of the composite Omega-Stringers and composite L-Shear Ties, which are identical for the UCSD test panels and the CODAMEIN / CODAMEIN II panels, are shown in Figure 21.

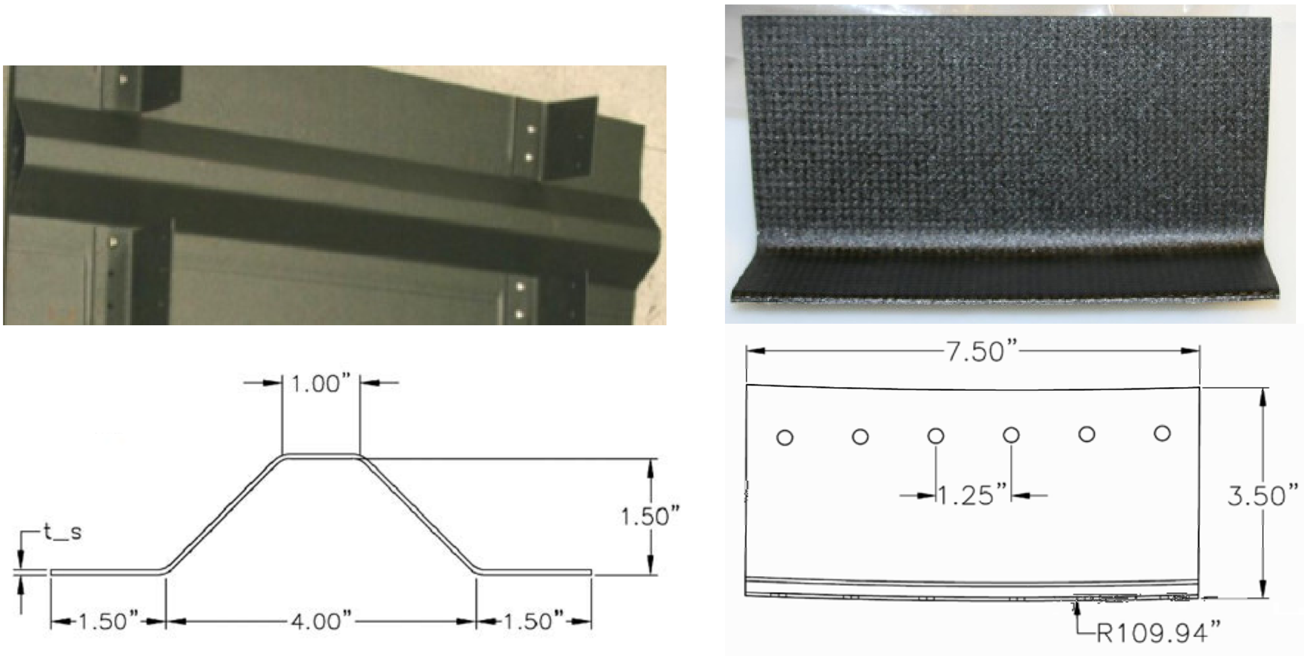

Figure 21 Omega Stringer Section, L-Shear Tie [Kim 2011]

4.2 Manufacturing

The manufacturing of the CODAMEIN II panel was based on the procedures of the CODAMEIN panel manufacturing, with high similarity to the manufacturing of the UCSD large test panels (see [Haase, 2012]). The skin was made using hand lay-up. The four stringers were laid up on the skin using silicon cores, and co-cured in an autoclave. The shear ties were laid up using an adapted tool and cured in the autoclave. The aluminium frames were machined using a CNC machine. Hi_Lok fasteners were used to attach the shear ties to the skin and to the frames.

5 Testing

The static test that was conducted within CODAMEIN II is described below.

5.1 Test Lab

The test was performed in the Applus LGAI test lab in Bellaterra (near Barcelona) in Spain. The mechanical test lab in which the test was set up, is depicted in Figure 22. The basic test set-up and the tooling for the test was the same as for the CODAMEIN test.

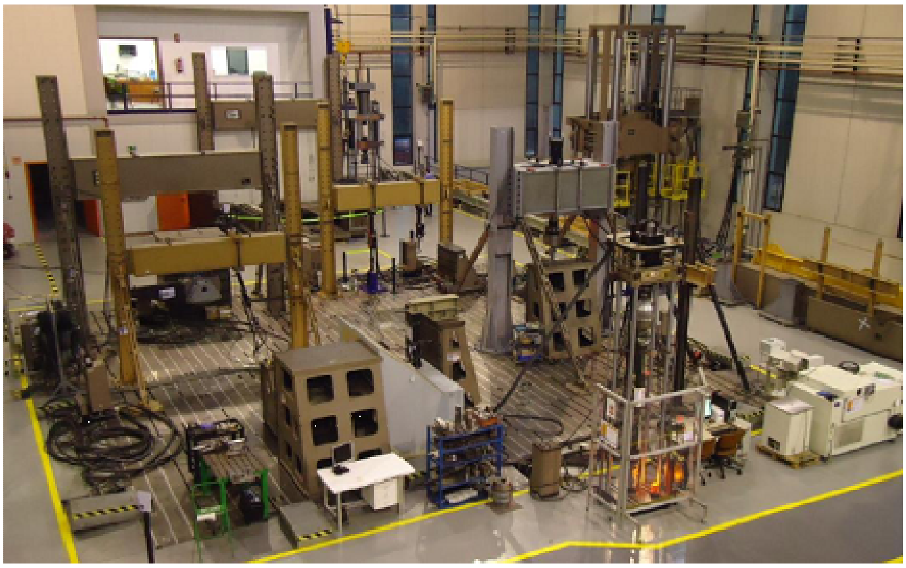

Figure 22 Applus LGAI test lab [Hernandez 2012]

5.2 Objectives

The aim of the CODAMEIN II test was to test a hybrid design fuselage panel similar to the CODAMEIN test panel. Thus, a static test was conducted. Compared to dynamic loading, this method offers the possibility of performing several load cycles. Thus different levels of damage can be attained in a stepwise manner and an inspection of the panel is possible between load cycles. The actuator used for the test was a 250 kN hydraulic cylinder equipped with a 250 kN load cell. The main objective of the test was to investigate the damage sequence by loading the panel to a load level which creates several subsequent types of damage. The boundary stiffness for the test was changed in accordance to numerical analyses of a fuselage barrel model.

Compared to the CODAMEIN test, the recording of a higher amount of data was intended. To achieve this, the instrumentation set-up described in 5.7 was used.

Since the damage sequence of the first CODAMEIN test and comparable tests performed by the (UCSD) showed that shear ties always were the first parts that failed, the test objectives were changed by EASA. To be able to replace the shear ties with stronger ones after the test and to perform a second test campaign with the actual panel, it was decided to not load the panel above shear tie failure in the actual test.

5.3 Boundary conditions

A schematic of the boundary conditions applied to the three inner frames of the test panel is displayed in Figure 23.

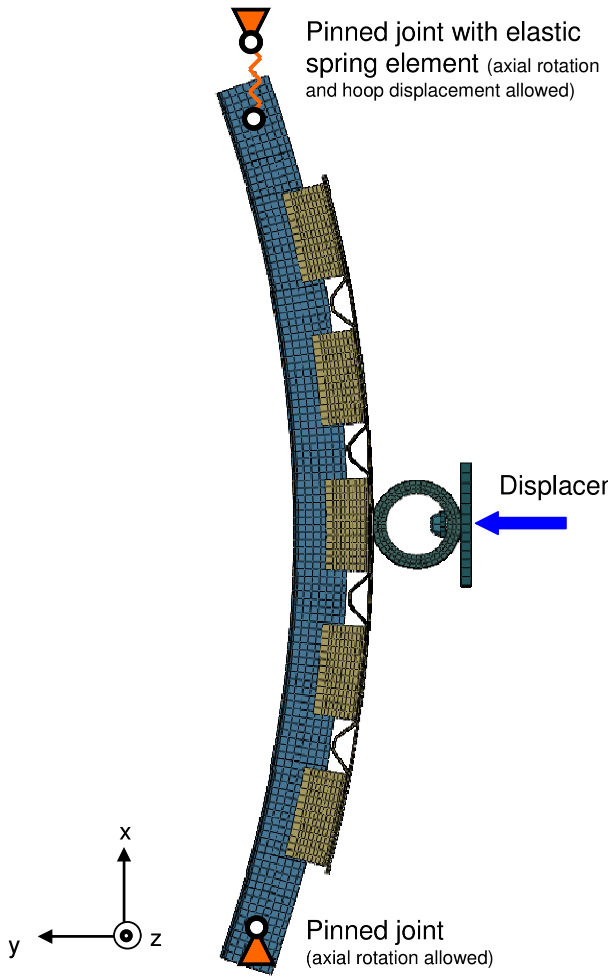

Figure 23 CODAMEIN boundary conditions (top view)

In order to achieve boundary conditions which are in a realistic range and most critical in creating visible structural damage, the stiffness of the springs in the elastic test fixtures can be modified. The spring stiffness that creates the most critical boundary stiffness was determined by numerical analyses.

For the numerical analyses, an improved FE model of the test panel was created, based on the results of the FE analyses within CODAMEIN. A FE model with a generally higher level of detail was used in order to reduce numerical errors caused by geometrical simplification and to provide information about damage onset and the post-damage behaviour of the panel.

Using the FE model of the test panel, a sensitivity analysis was performed to assess the test fixture spring stiffness which creates the most critical state for damage of the panel.

To justify the boundary conditions for the panel, an advanced FE model of a complete fuselage barrel was used (see Figure 24). Included is a higher level of detail compared to the model generated in CODAMEIN. The barrel model was used to prove the boundary stiffness of the test panel and is able to represent a realistic aircraft fuselage structure. The impact region was set below the main floor. This region of a fuselage, which is prone for collisions with GSE vehicles, is well represented by the 5-frame, 4-stringer test panel.

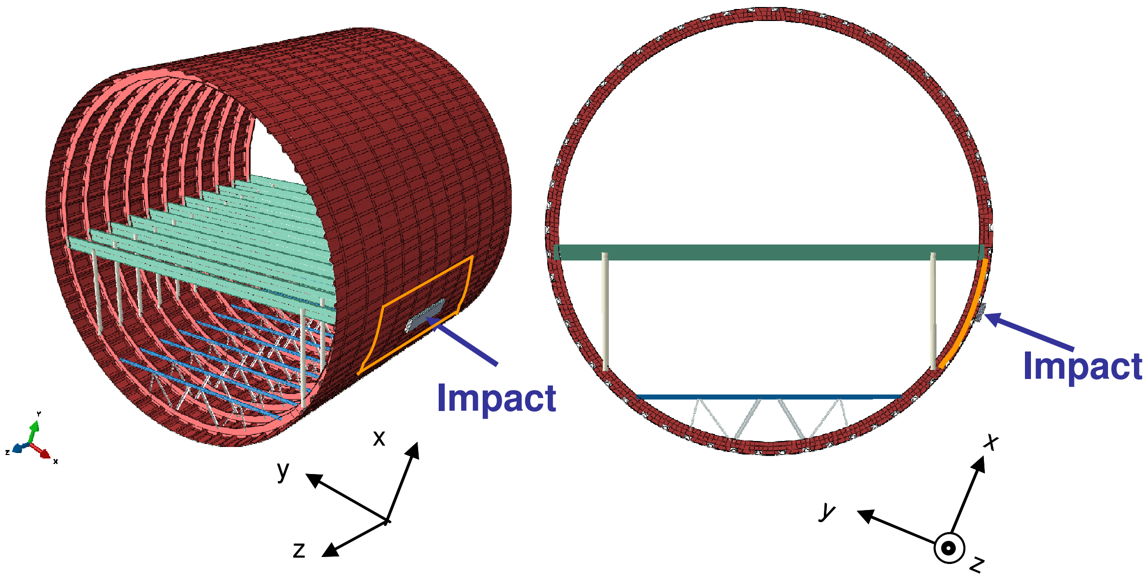

Figure 24 Full Fuselage Barrel FE Model

5.4 Test set-up

The CODAMEIN II test incorporated the test set-up and test fixtures that were also used in the CODAMEIN test. An identical configuration, attaching the three inner frames, has been defined at the project launch. The test panel is mounted in an upright position with the stringers in the vertical direction. The actuator is installed horizontally with the rubber bumper aligned vertically. Two different types of test fixtures attached the frame ends to two strong walls. The test set-up is displayed in Figure 25, and the components named in Figure 26.

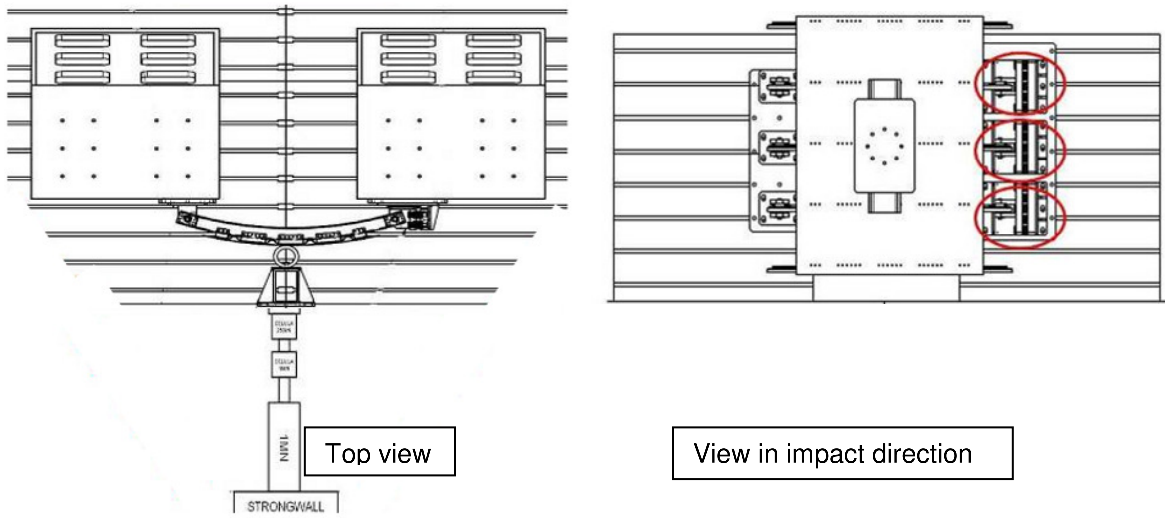

Figure 25 Test set-up: schematic top view, outside view [Perez 2011]

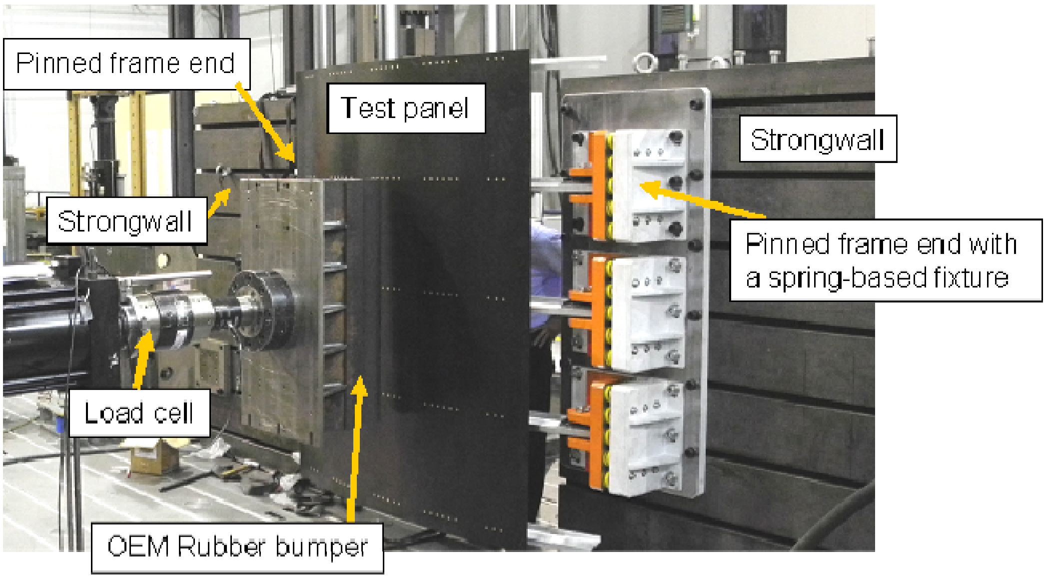

Figure 26 Test set-up: main components [Perez 2011]

The two different types of test fixtures, that attach the three inner frames, are shown in see Figure 27.

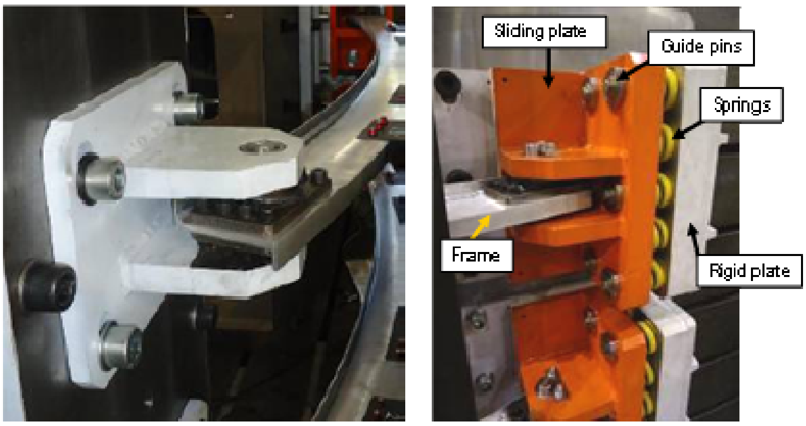

Figure 27 Frame attachments: pinned fixture, pinned fixture with hoop dir. springs [Perez 2011]

The test fixtures that imply a pin joint and translational spring stiffness normal to the impact direction are displayed in detail in Figure 28. The fixtures consist of a fixed part and a movable part. The movable part is supported by each six guide pins and guide bushings (with graphite pads for low friction) moving on them. Furthermore, when the springs get compressed, the movable part is guided by gliding pads that transfer the impact load from the movable part of the test fixtures to the test rig.

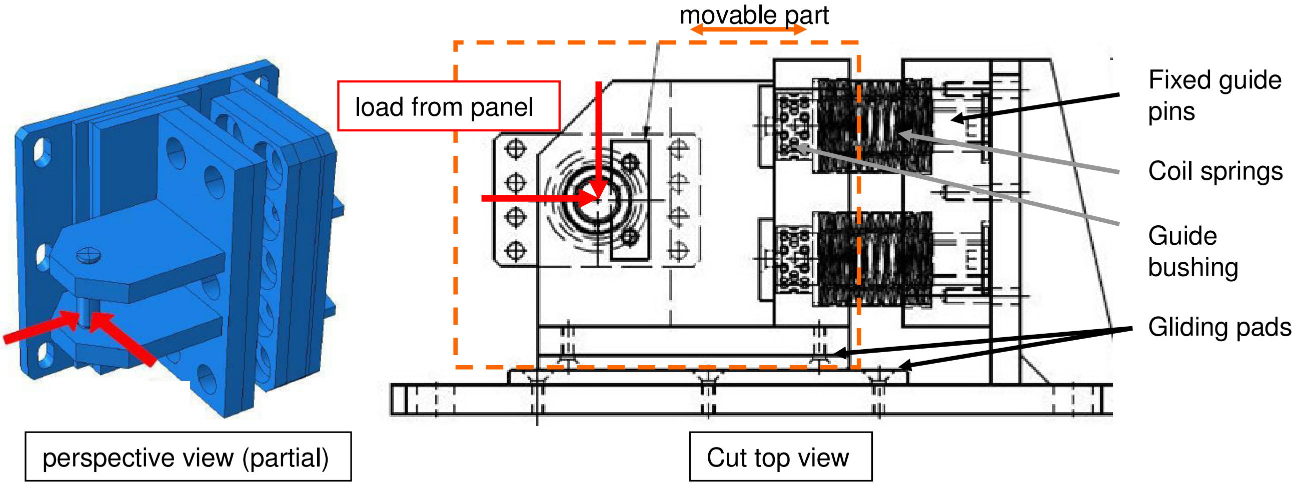

Figure 28 Test fixture with springs: two views

One end of each of the three inner three frames is held by a bolt connection that allows for rotation about the panel axis. The second type of attachment at the opposite ends of the three inner frames consists of an identical type of bolt connection which allows for rotation about the panel axis. Additionally this attachment permits hoop displacement (perpendicular to the impact direction). Through the use of arrays of coil springs, the stiffness behaviour of the surrounding fuselage structure is represented [Haase 2012] solely by this hoop direction boundary stiffness.

The springs in the test fixtures have been replaced for the CODAMEIN II test. After having used spring arrays with a stiffness of 8.5 kN/mm at each of the inner three frames in the CODAMEIN test, spring arrays with a stiffness of 9.5 kN/mm were used for the CODAMEIN II test. This adjustment to the boundary condition was made as a result of the full barrel analysis described in section 5.3.

The test set-up of the CODAMEIN II test is depicted in Figure 29, showing the panel inside surface prepared for the video correlation system in a), showing the panel outside and the impactor as well as the pin and spring fixtures in b) and the pin fixtures in c)

a) b) c)

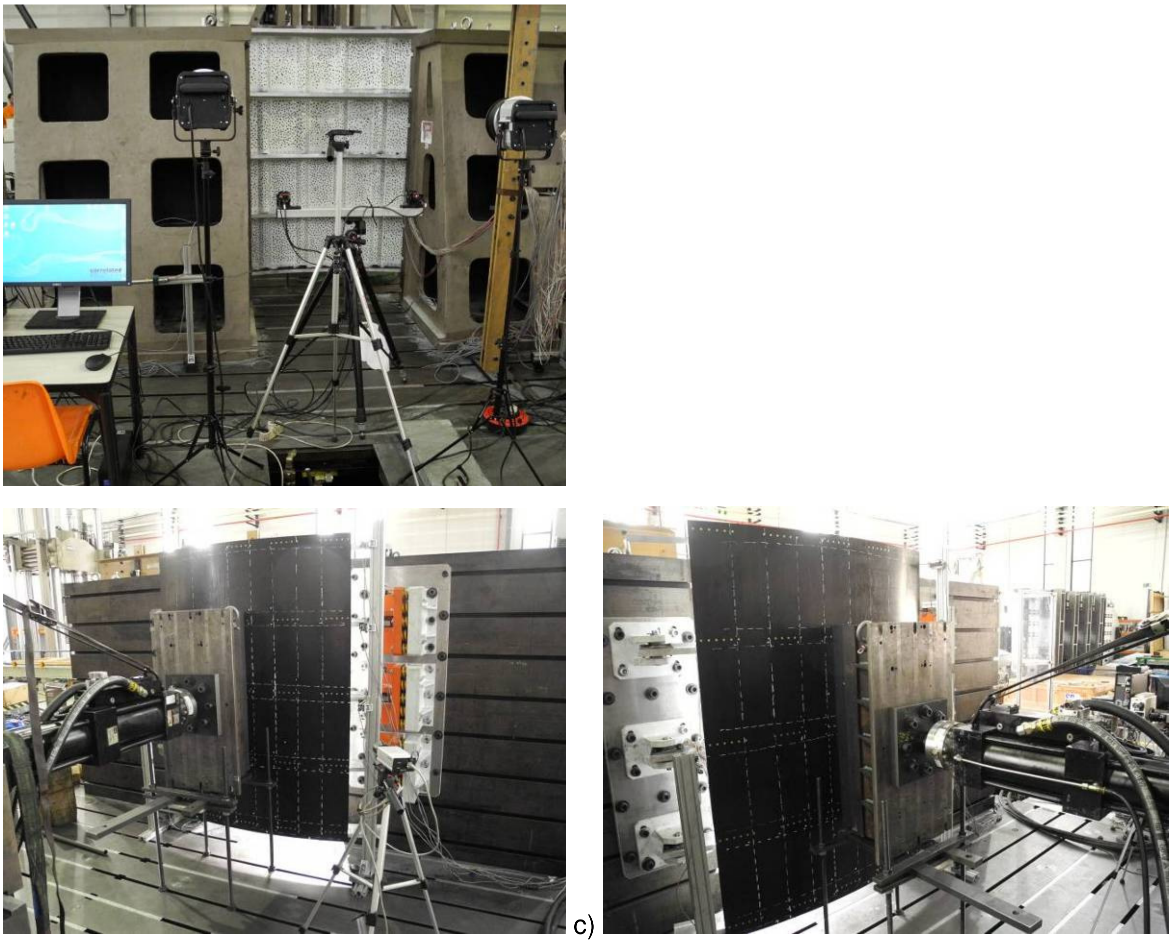

Figure 29 Set-up of CODAMEIN II Test

5.5 Testing methodology

For CODAMEIN II, a similar test method to that of CODAMEIN was defined. Three load cycles were intended, in which three significant states of damage were planned to be reached.

- First damage: expected: load drop due to damage of the radii of the centre shear ties
- Multiple shear tie failure and frame – stringer contact
- Global failure caused by stringer breakage or massive frame plastic deformation

Based on the knowledge of the shear ties being the parts to most likely fail first, which was proven by the CODAMEIN research and the associated UCSD research, EASA changed the test objectives. A future repair of the test panel including the replacement of the shear ties with a stronger design was anticipated. Thus the objective of the test was to generate damage only in the shear ties and to not damage the remaining structure. Target loads similar to the CODAMEIN load cycle maximum loads were defined. The test was stopped after the second load cycle to not risk the generation of damage apart from shear tie damage. Based on the CODAMEIN test, a sudden multiple shear tie failure leading to immediate frame – stringer contact was expected in the 3rd load cycle.

5.6 Load sequence

The impact test consisted of two of the planned three load cycles. The respective maximum load of each load cycle was chosen according to the load cycle stop events that were also used in the CODAMEIN test. Each load cycle was stopped at the target load and was held at constant actuator displacement for some minutes for documentation of the panel deformation and damage state. Subsequently the panel was unloaded, inspected visually and by A-Scan before starting the next load cycle. See Figure 30 for the loading scheme including the inserted deformation energy.

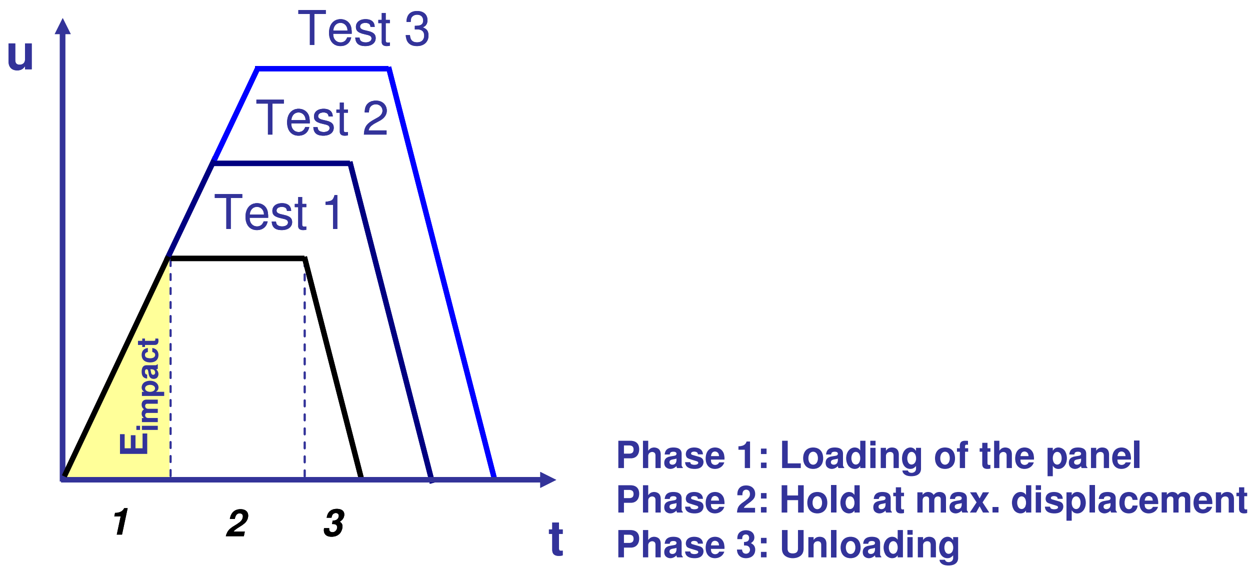

Figure 30 Loading scheme for three load cycles

The actuator was moved with a velocity of 25 mm/min in the phase of contact establishment between the panel and the bumper. After the panel and the bumper came into contact, the actuator velocity was reduced to 2 mm/min, until it was stopped at the maximum load. The unloading was done with a velocity of 10 mm/min (see Figure 31).

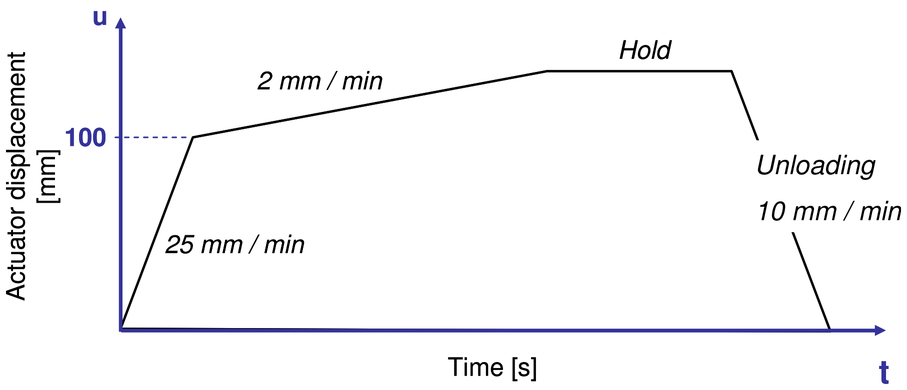

Figure 31 Loading velocity for one load cycle

The actuator operating system used "soft stop" and "hard stop" limits. The soft stop limits led to an automatic hold at every significant load drop and permitted a phase for assessment of the appearance of the panel and of the instrumentation recordings before it was decided to continue loading or to stop.

5.7 Instrumentation

The positions within the test panel, where measurement instrumentation was positioned or where the behaviour of the panel was described in the test or in the numerical analyses, were defined according to the numbering system that is displayed in Figure 32.

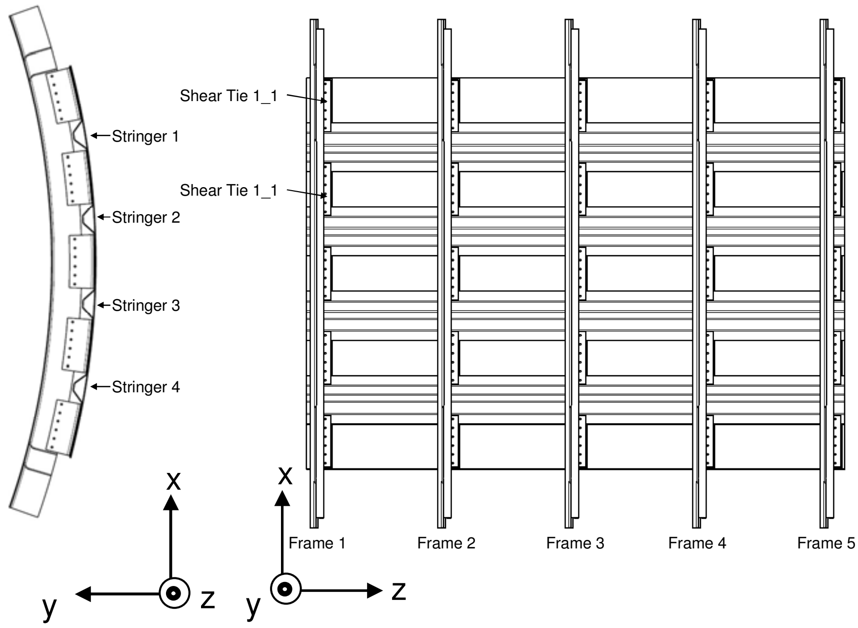

Figure 32 Component numbering

The instrumentation used for the CODAMEIN II test was extended, based on the experience gained from the CODAMEIN test. The basic configuration, implemented in the CODAMEIN test, measured the displacement of the actuator and the skin at a point close to the centre shear tie 3.3. Two cameras recorded the behaviour of the panel from an inside and an outside view (see Figure 33).

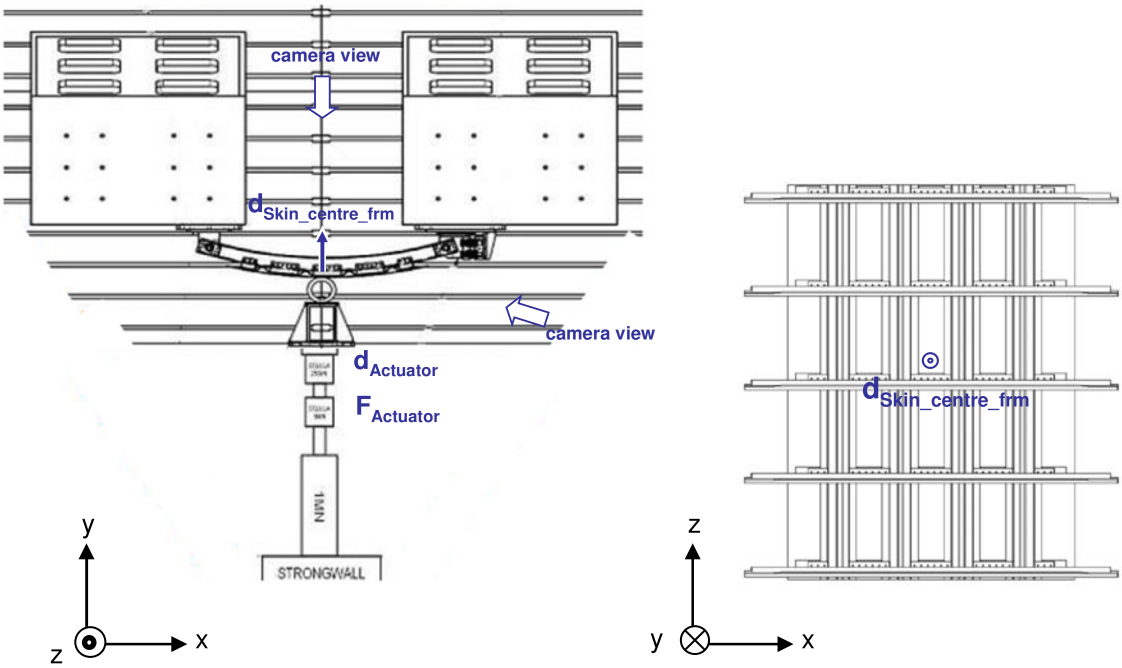

Figure 33 Instrumentation of the CODAMEIN test

The following instrumentation was used in the CODAMEIN II test.

- 1 Load Cell at the hydraulic actuator
- 7 LVDTs to measure displacements and rotations plus the actuator displacement gauge
- 30 Strain Gauges at the skin, a stringer, the centre frame and two shear ties
- Video Correlation System (similar to ARAMIS) on the panel inside
- 2 Video Cameras on the panel inside and outside

Figure 34 shows the positions of the used LVDTS, at which displacements (LVDT 1 to 4 plus actuator displacement gauge) and rotations (LVDT 5 to 7) were recorded.

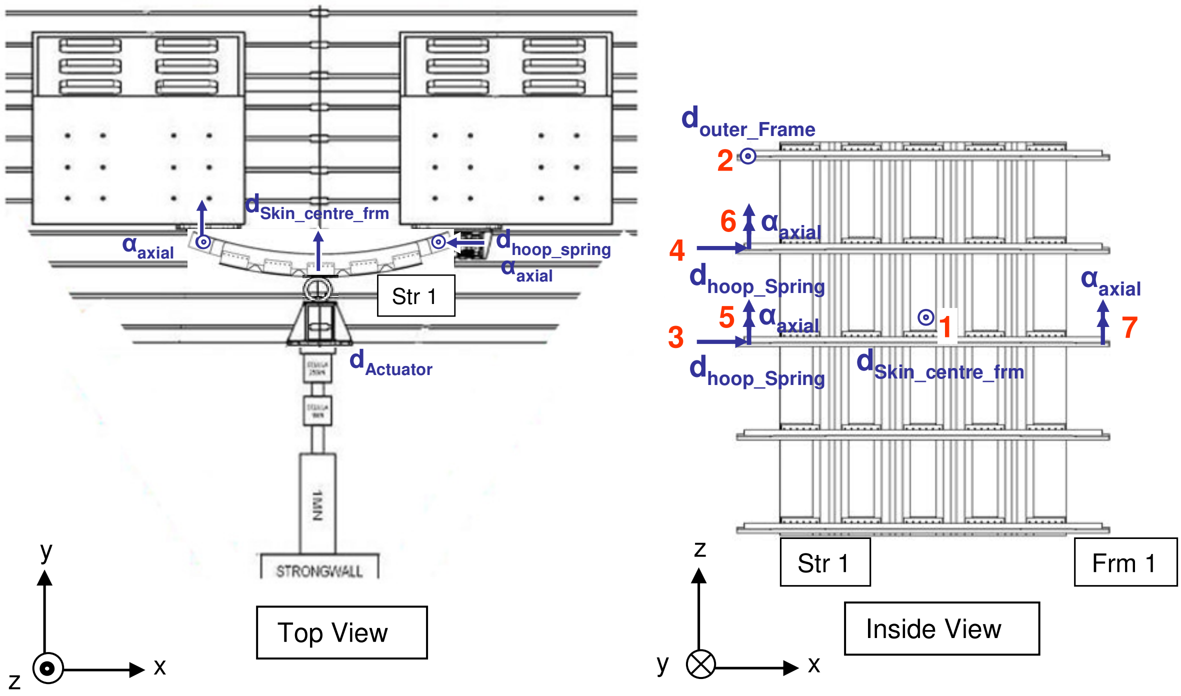

Figure 34 Measurement positions for displacement and rotation

Photos of the LVDTs installed in the test set-up are displayed in Figure 35 (a): LVDT 1, b): LVDT 7, c): LVDTs 2 to 6).

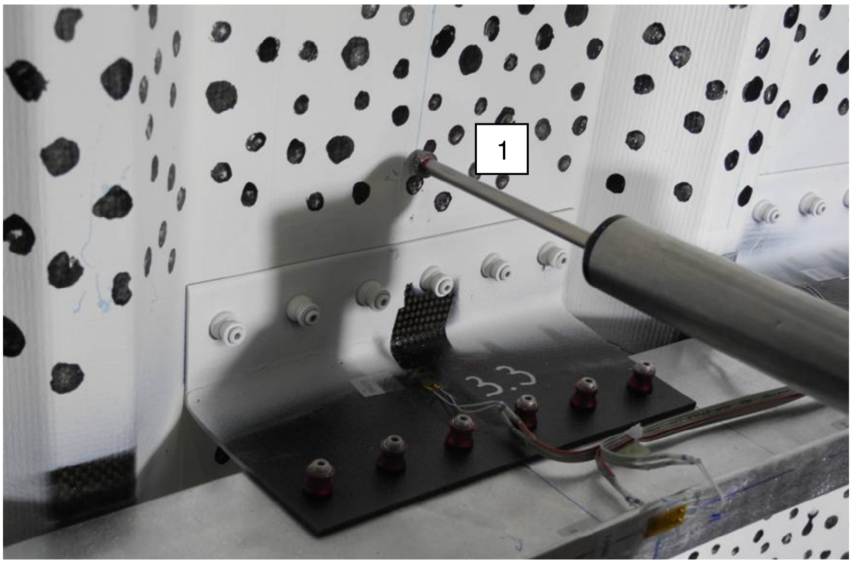

a)

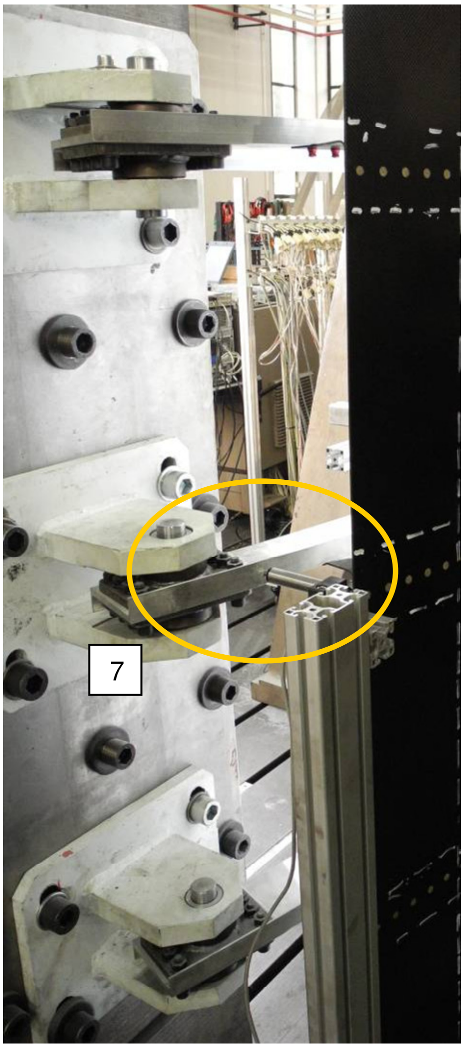

b)

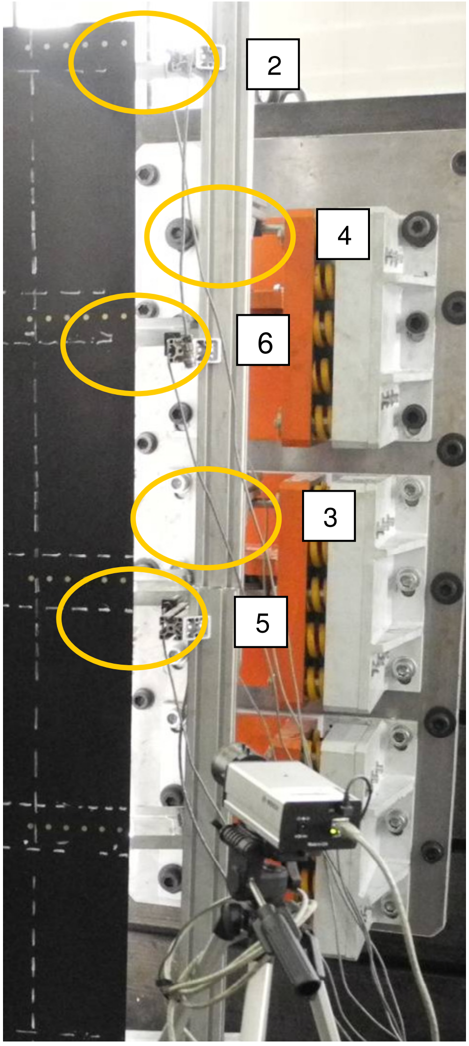

c)

Figure 35 LVDTs in the test set-up

The positions of the 30 strain gauges are depicted in Figure 36 and Figure 37. These figures also show the channel numbers of the strain gauges. On the skin and the stringer no. 3, strains were measured on the panel inside. At the frames and shear ties, strain gauges were applied back-to-back on both sides of the part to obtain information about bending. All used strain gauges were of the type HBM K-LY41-b/350-4L-5MS with a grid length of 10 mm. A drawing showing the strain gauge definition can be found in Appendix B.

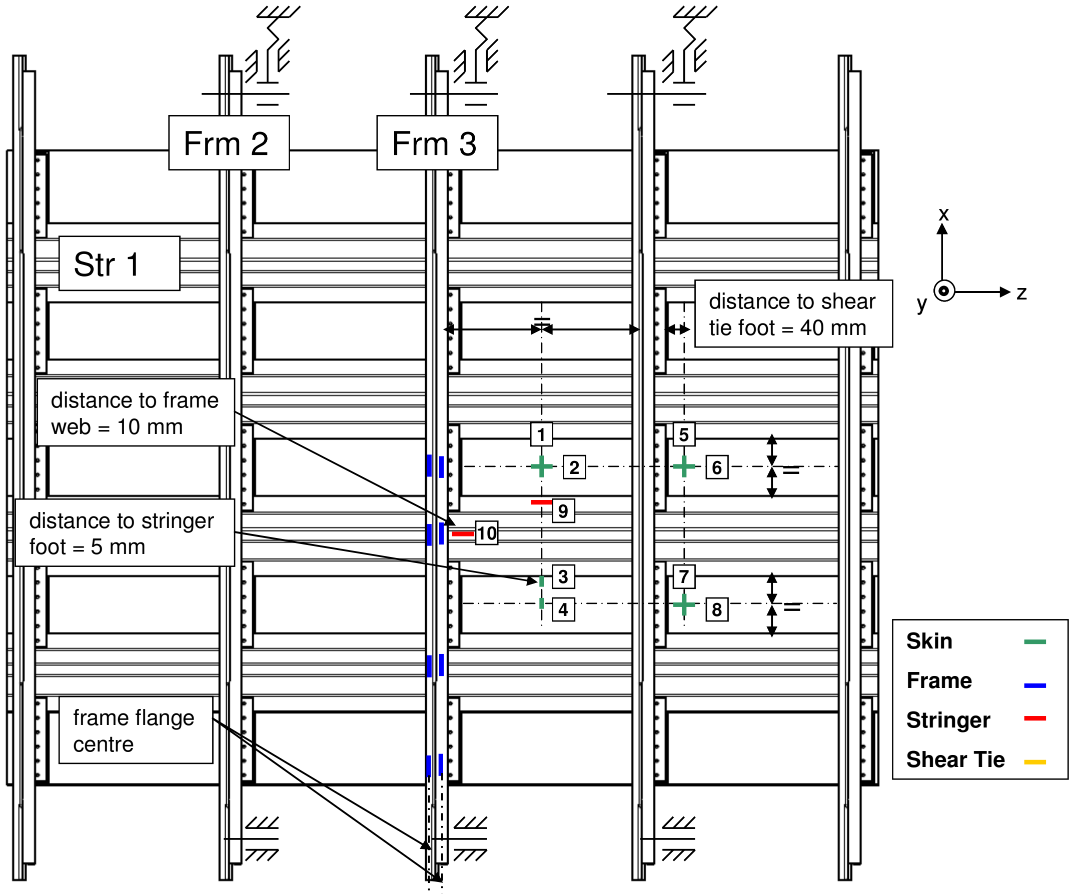

Figure 36 Strain Gauge positions: inside view

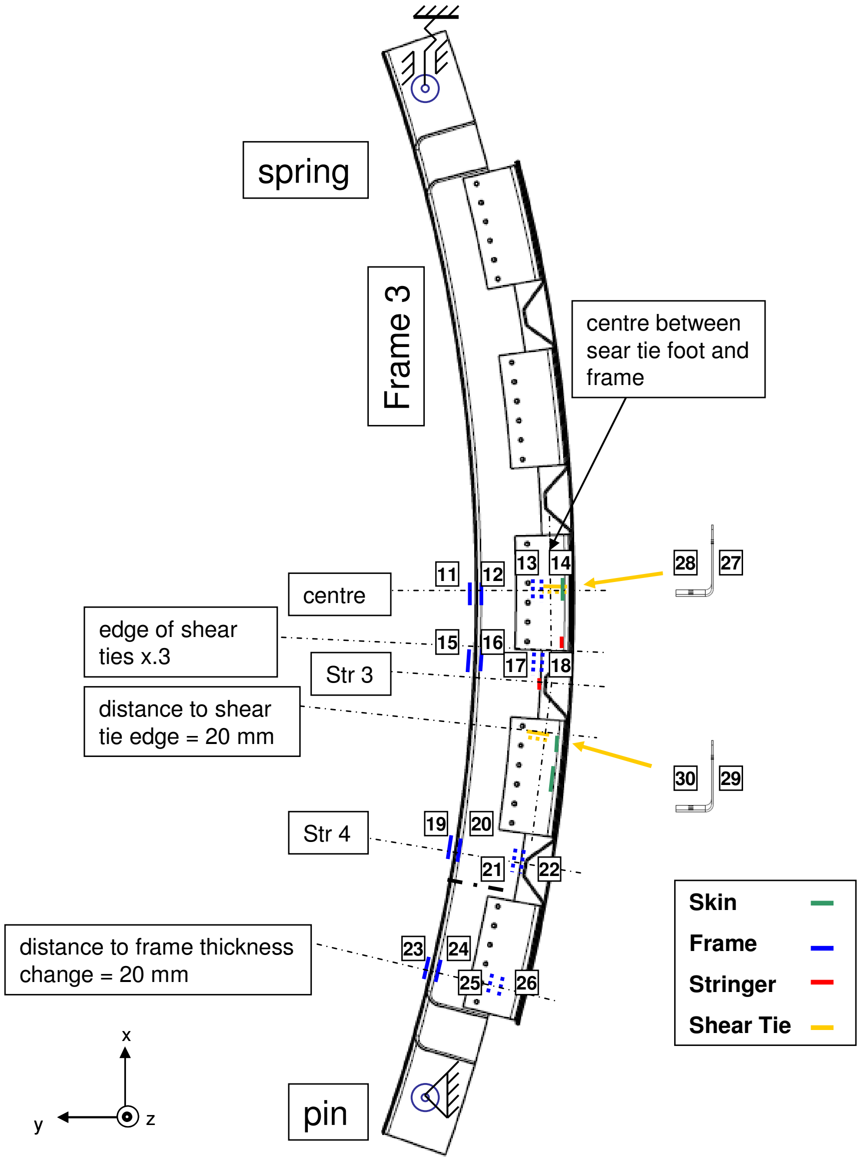

Figure 37 Strain Gauge positions; axial view

Figure 38 shows the strain gauges on the test panel. The skin channels have been covered for the paint preparation for the video correlation system, the inner frame channels at each frame position are clearly visible.

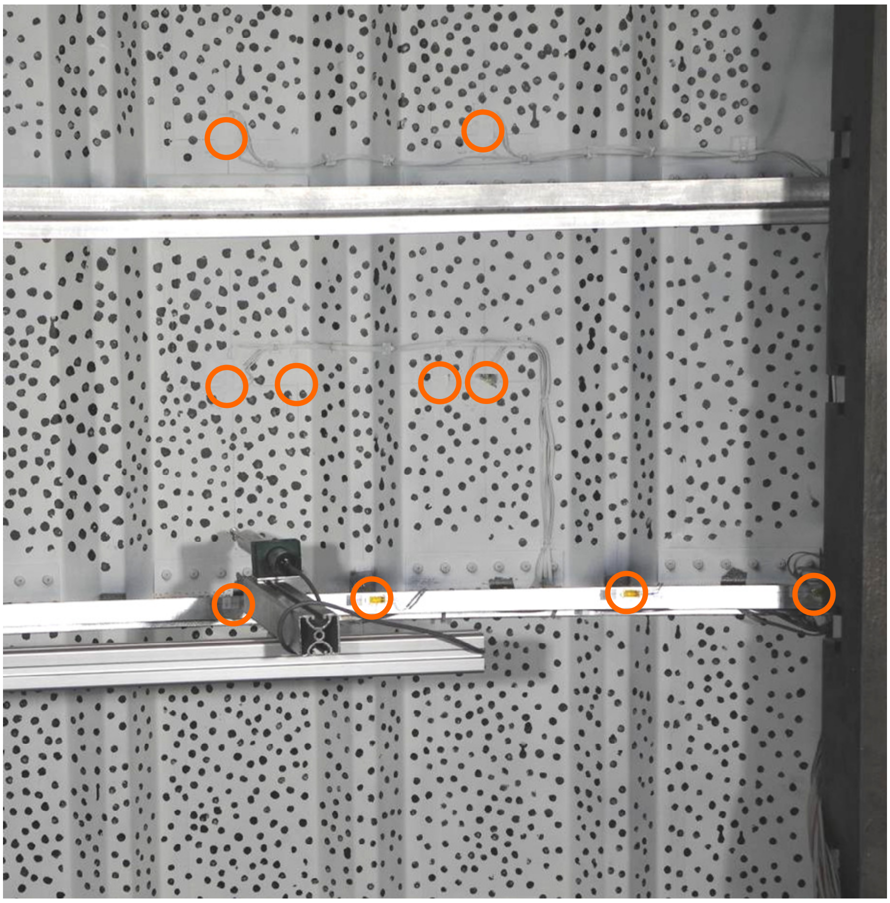

Figure 38 Strain Gauge positions on the panel

The force, displacements and strains were recorded with a frequency of 10 Hz.

A video correlation system (comparable to the ARAMIS system) was used to capture the displacement of the panel inside. Based on the initial state of the panel, the system is able to record and visualize the displacement in every direction at every taken snapshot. The visible field covered almost the entire inside of the panel. The system recorded snapshots at manually defined points of the load cycles which were at every 5 kN of load and at every event at which the loading was stopped.

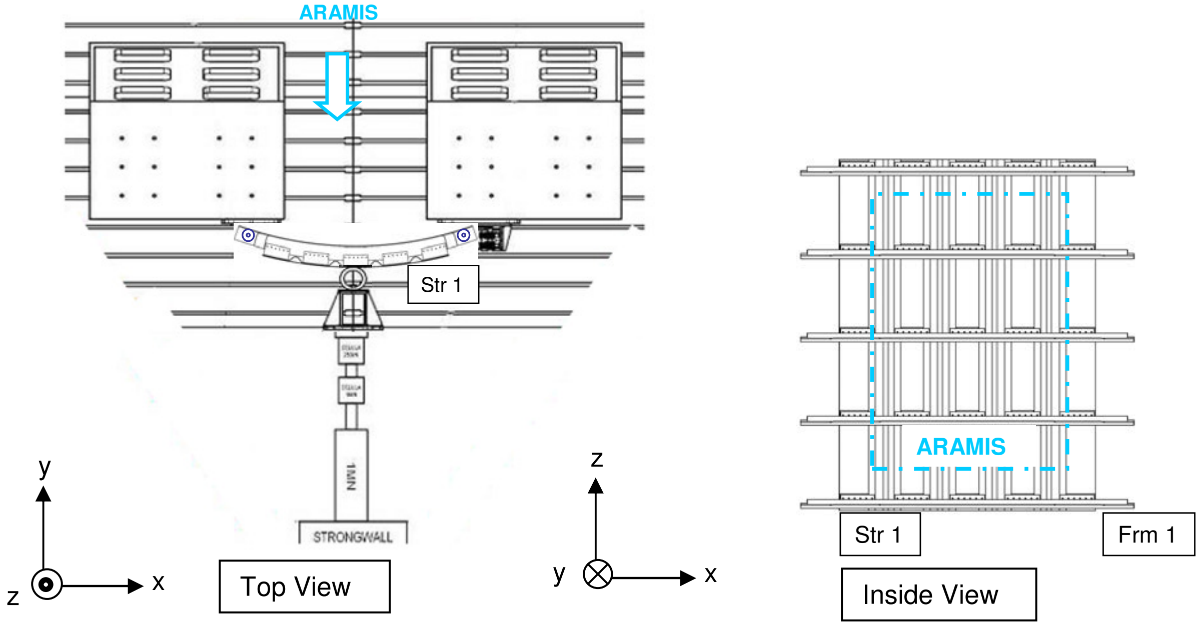

Figure 39 ARAMIS measurement field

Figure 40 shows the inside of the test panel which has been prepared for the video correlation system by applying white paint and black dots. The picture also shows the two small cameras of the system and two spotlights. Using the two cameras, the video correlation system is able to record the displacement of the black dots 3-dimensionally.

Figure 40 Test Panel and video correlation system equipment

Videos were recorded using two cameras that were positioned as shown in Figure 41. One camera covered the inside of the panel. The second camera view enclosed one side of the panel outside, the flexible test fixtures and the impact zone. A third camera was used to record the actuator load. A combined recording showing all three camera views in one video was provided by the test lab.

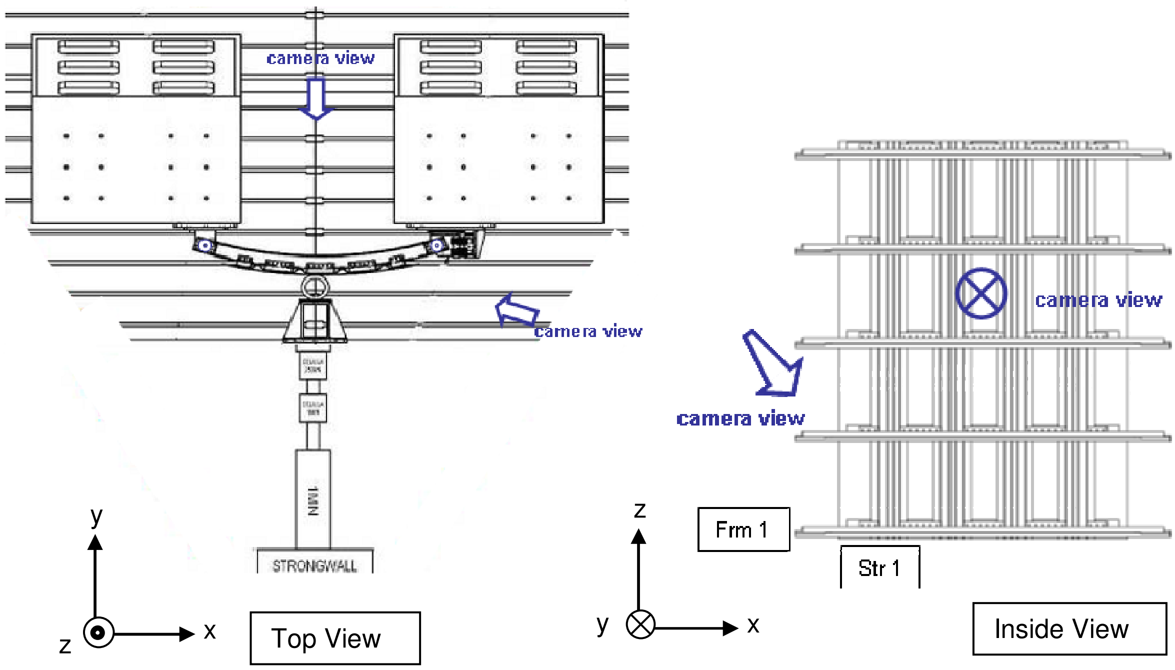

Figure 41 Video camera positions

5.8 Inspection

Before the initial loading and after each load cycle, the panel will be visually inspected and scanned by NDT using a hand-held A-Scan system. In performing these repeated scans, the initial state of the panel is assessed and therefore it is possible to detect subsequent damage initiation and track its progression. The inspection pattern of the CODAMEIN test was the basis of the CODAMEIN II inspection pattern. This covers all regions which are prone to interlaminar failure under loading. The skin zone which is contacted by the impactor bumper will be inspected as well as all zones of co-cured part connections such as the stringer feet and the shim regions underneath the shear ties. Additionally, the stringer caps will be scanned to detect potential damage that is initiated before stringer-frame contact, and damage that is caused by this contact. The scan pattern for the A-Scan is displayed in Figure 42. The panel outer edges (as highlighted in Figure 43) were additionally scanned in the initial NDT.

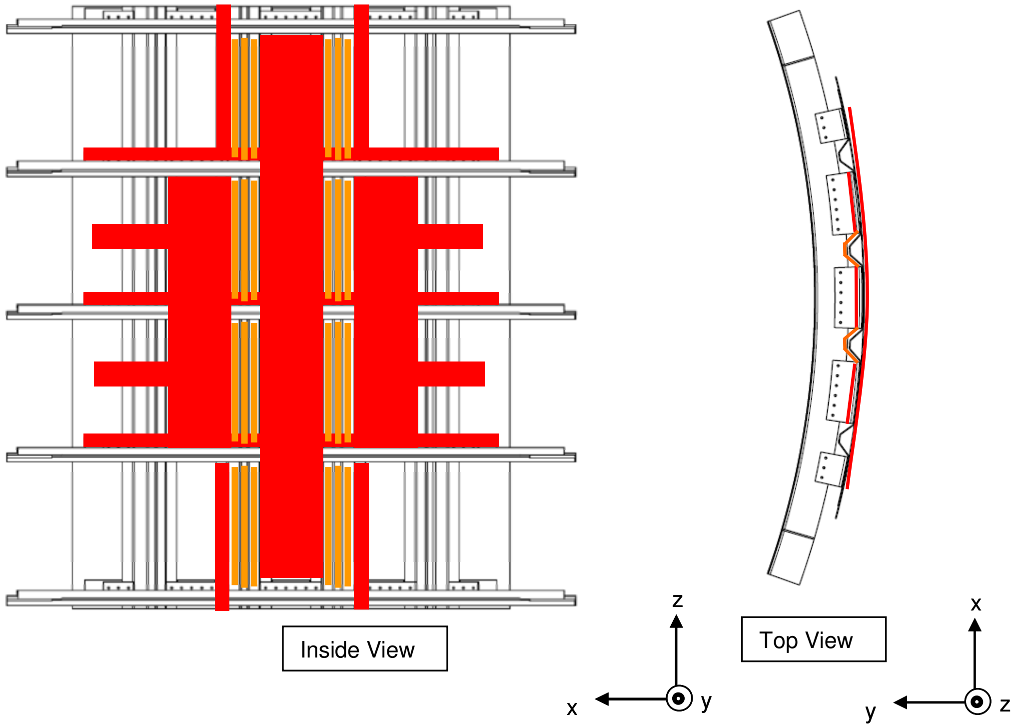

Figure 42 A-Scan inspection pattern

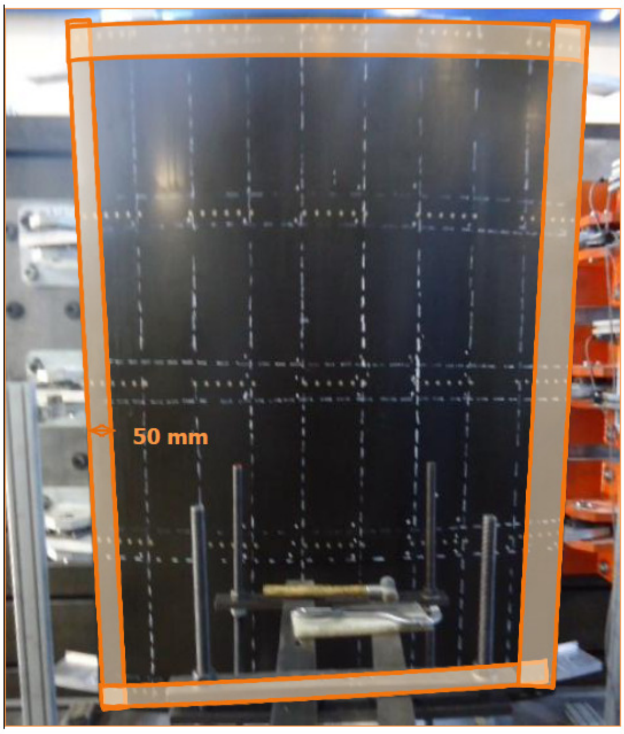

Figure 43 A-scan inspection pattern for the initial NDT [Bergo Soto 2012]

5.9 Test results

Two load cycles have been performed on the panel test. The first load cycle was stopped at 39.5 kN, which is lower, compared to the CODAMEIN test (45 kN), due to a damage event that caused a load drop. The second load cycle was run up to the load of the second load cycle of CODAMEIN, 57.0 kN.

Since EASA had stated the intention to use the test panel again in another test, the target load and damage situation of the current test was reduced. Thus the stop criterion for this test was defined as the failure of shear ties which was expected to happen prior to any damage to other parts of the panel.
After a discussion between Bishop and EASA representatives after the second load cycle, on the possibilities and risks of continuation of the test, it was decided to perform no further load cycle. Based on the result of the first CODAMEIN test and the tests of UCSD, it was assumed that the expected shear tie failure would lead to contact between the stringers and frames. This event was expected to occur suddenly and with no possibility to be stopped. To avoid any potential damage, especially to the stringers, it was decided to not continue loading up to shear tie failure.

Apart from the actuator displacement gauge, all LVDT readings were negative. They have been displayed with positive sign in the following charts. The loading phase as well as the unloading phase of each measurement is displayed.

At the positions where strain gauges were applied on both sides of a part, the strains were displayed as well as the membrane component and the bending component. These components were calculated using the following equations.

- $E_{Membrane}=(E_{Side\ 1}+E_{Side\ 2})/2$ Eq. 1
- $E_{Bending}=(E_{Side\ 1}-E_{Side\ 2})/2$ Eq. 2

Due to the time required for the post processing by the test lab, the outputs of the video correlation system and the video recordings are not available yet for this report.

5.9.1 Load cycle 1

The first load cycle was run up to a load of 39.5 kN and stopped at a damage event which caused a load drop of 1 kN. The only visible evidence of damage after the first load cycle was a crack in the radius of the centre shear tie no. 3.3 (see Figure 44) which covered ¾ of the width of the shear tie.

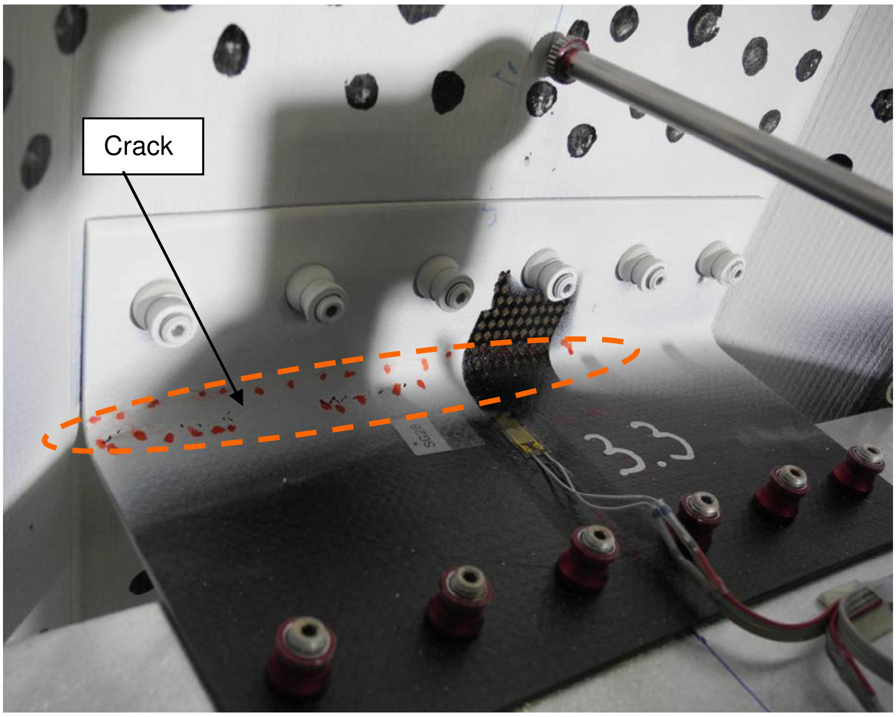

Figure 44 Damage after 1st load cycle: Crack in the centre shear tie no. 3.3

The video correlation system captured the distribution of displacement in impact direction as shown in Figure 45 at the loads 10 kN, 20 kN, 30 kN and at the maximum load of the 1st load cycle, 39.2 kN.

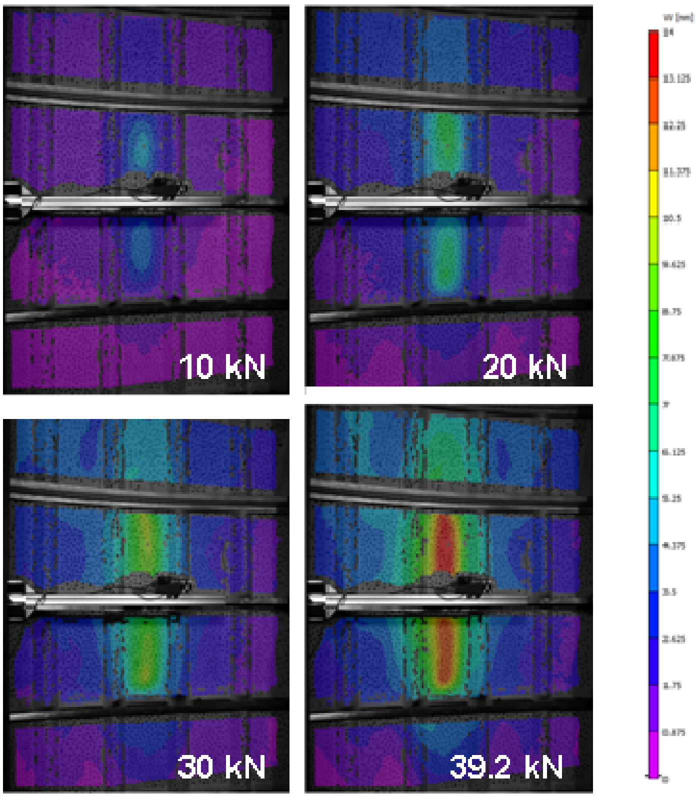

Figure 45 Panel displacement in impact direction (video correlation system) at three load levels and max. load

The readings of the load cell, of the LVDTS and of the strain gauges are displayed in Figure 46 toFigure 48. The strain recordings of the load cycle 1 can be found in .Appendix C.

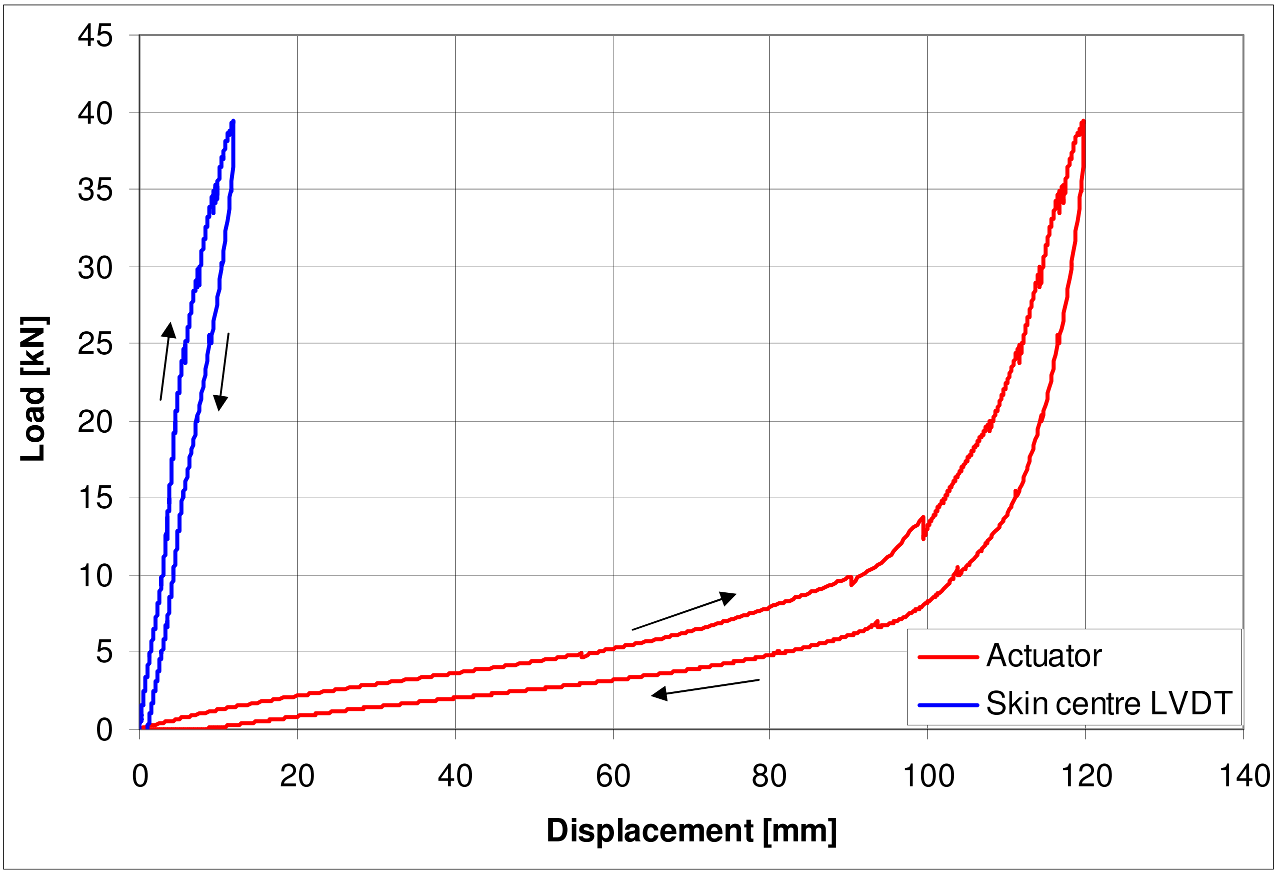

Figure 46 Load-Displacement: Actuator and Skin centre displacement

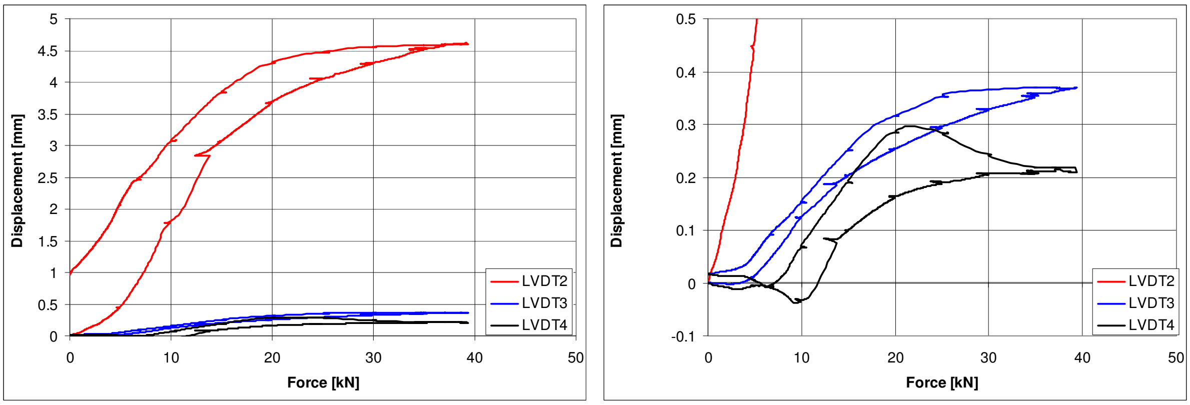

Figure 47 Displacement of LVDTs 2,3,4 vs. Actuator Load, 2 scales

The displacement vs. load chart of LVDTs 5, 6 and 7, used to measure rotations, are shown in Figure 48.

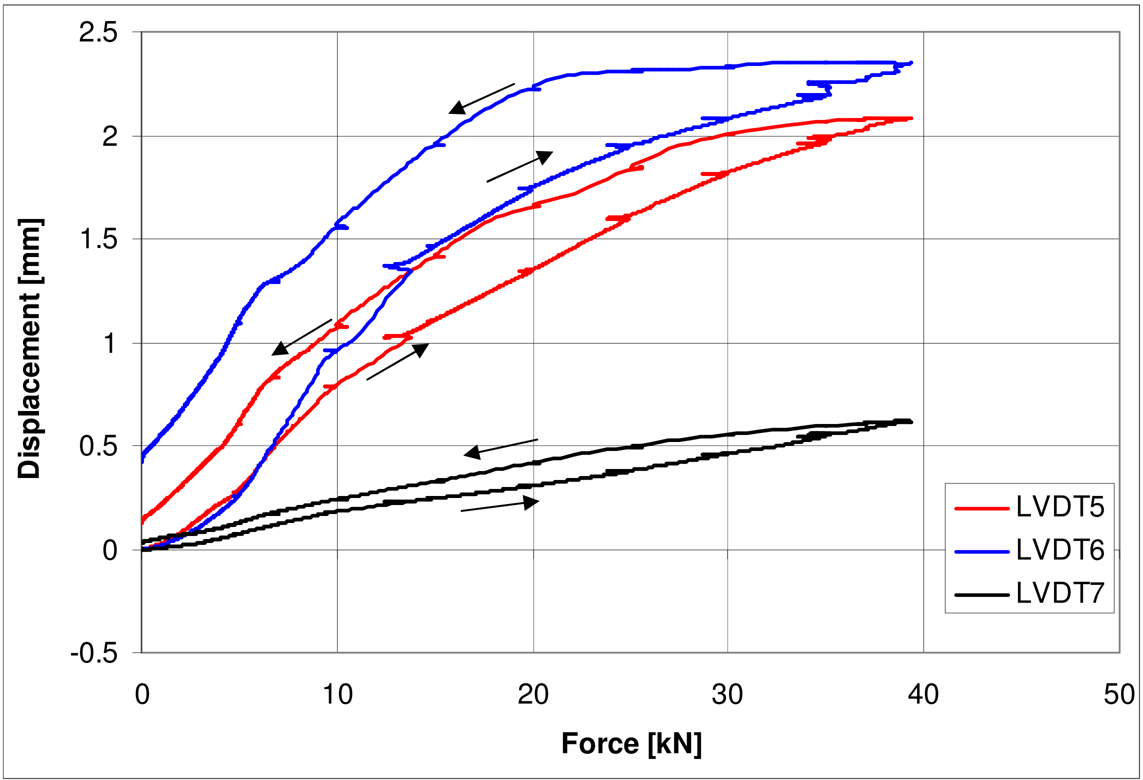

Figure 48 Displacement of LVDTs 5,6,7 vs. Actuator Load

The crack observed in the centre shear tie ST 3-3 was set in relation to the audible event that caused the first load drop and caused the stop of the first load cycle. NDT was performed after unloading, which did not find any damage. In addition to the skin, the flat regions of the centre shear ties were scanned by the NDT. Due to the curvature, it was not able to scan the shear tie radii in which damage was visible.

5.9.2 Load cycle 2

The second load cycle was run up to a load of 57 kN which corresponds to the maximum load of the second load cycle of the CODAMEIN test. After exceeding the maximum load of the 1st load cycle, damage onset and damage growth mechanisms were audible in terms of single cracking sounds or continuous cracking sounds which were assigned to the damage to the two centre shear ties ST 2.3 and ST 3.3 as well as ST 3.4. No load drop appeared prior to the maximum load of the 2nd load cycle. Figure 49 shows the panel inside at maximum load. The slight out of plane bending of the three centre frames is visible.

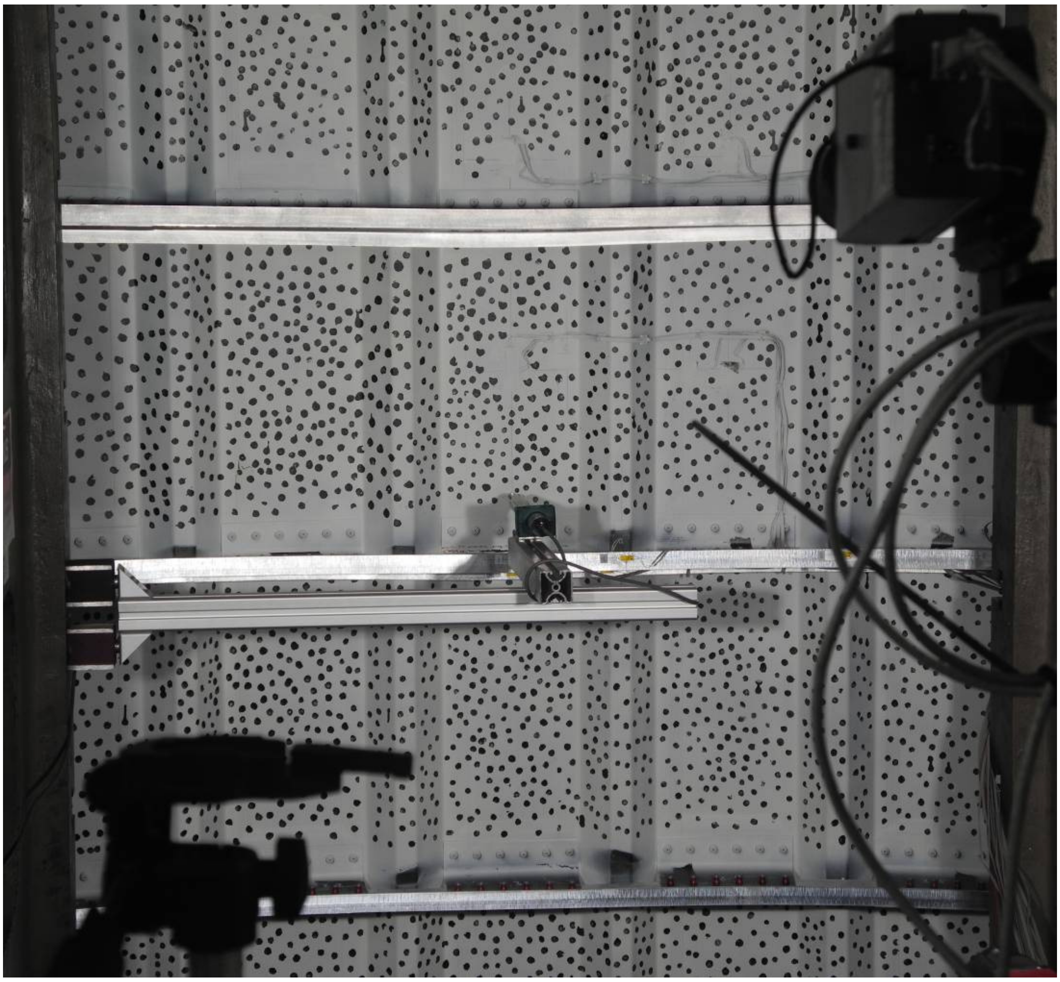

Figure 49 Panel inside at 2nd load cycle max. load

The distribution of the panel displacement in the impact direction is displayed at six load levels in Figure 50. At the maximum load of 57 kN, a displacement of 130 mm was measured. The damage event at maximum load led to a load drop to approx. 54 kN. With a relaxing of the centre frame from its torsion and after further unloading to 50 kN, the displacement distribution changed to the final displayed state in Figure 50.

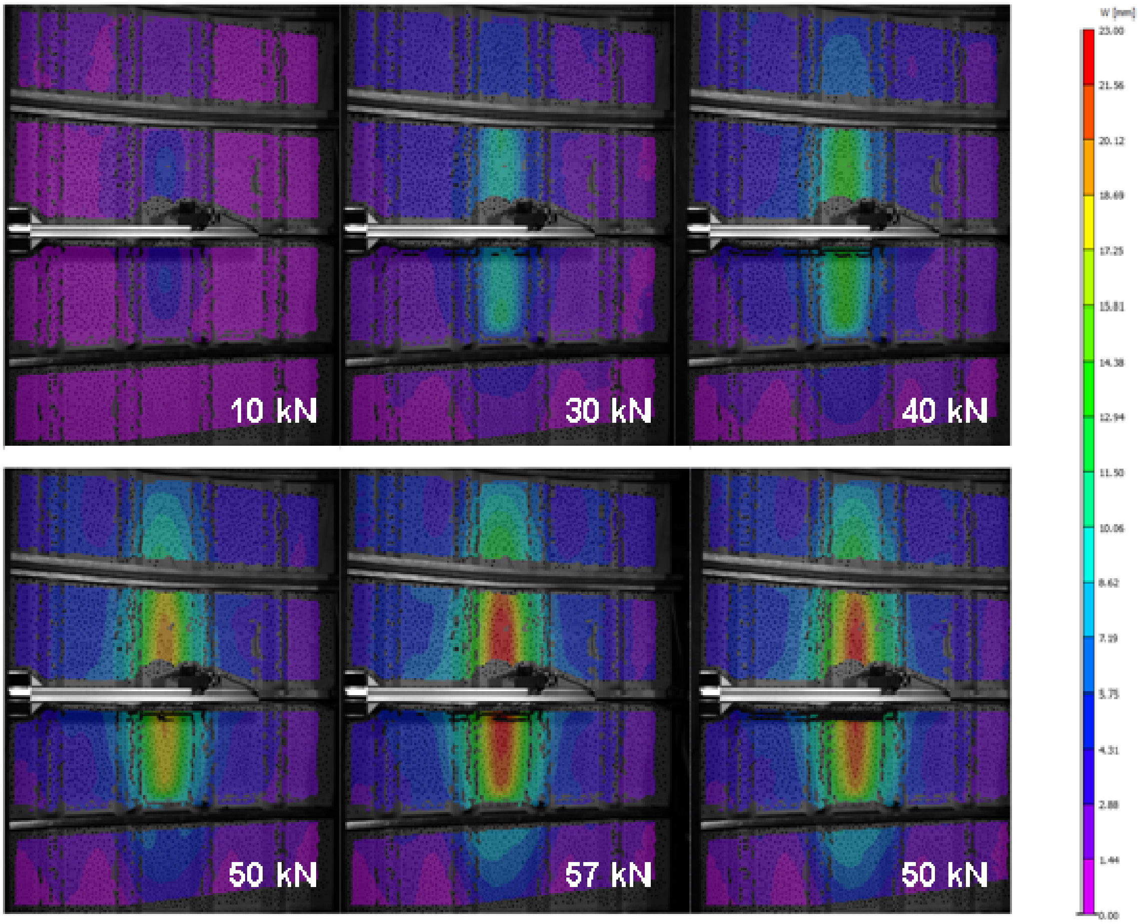

Figure 50 Max. panel displacement in impact direction (video correlation system): four load levels, max. load, past load drop

After unloading the 2nd load cycle, the shear tie no. 2.3 exhibited initial cracking in the radius (see a) of Figure 51) along with delamination marks at the side of the radius (see b) of Figure 51). The crack in the shear tie no. 3.3 developed through the full width of the shear tie (see a) of Figure 52). Delamination was visible on both sides of the radius (see b) of Figure 52). The shear tie no. 3.3 also showed a crack along the entire width of the radius (see a) of Figure 53) and delamination of the radius (see b) of Figure 53). The delamination marks indicated delamination of multiple plies throughout the thickness of the shear ties and covering approximately the full radius curvature.

a) 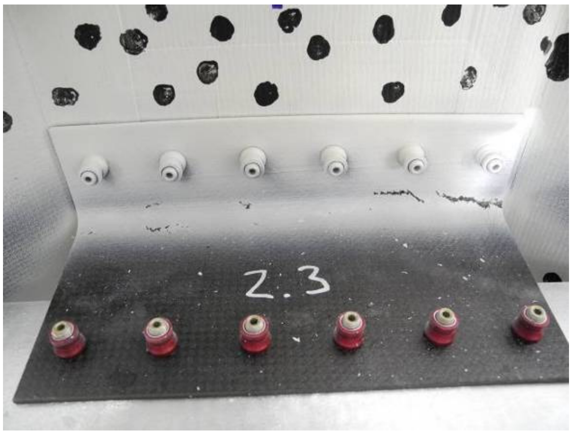

b) 

Figure 51 Shear Tie no. 2.3 after 2nd load cycle

a) 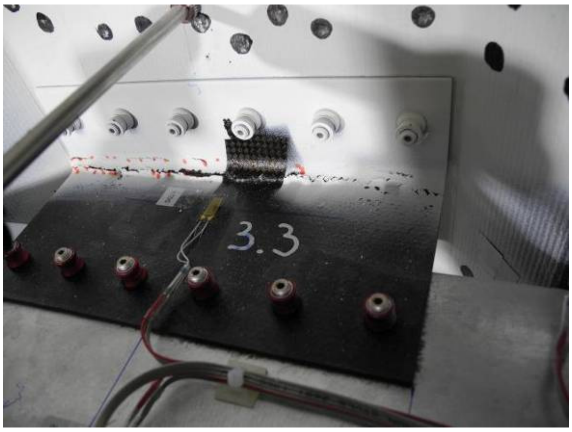

b) 

Figure 52 Shear Tie no. 3.3 after 2nd load cycle

a) 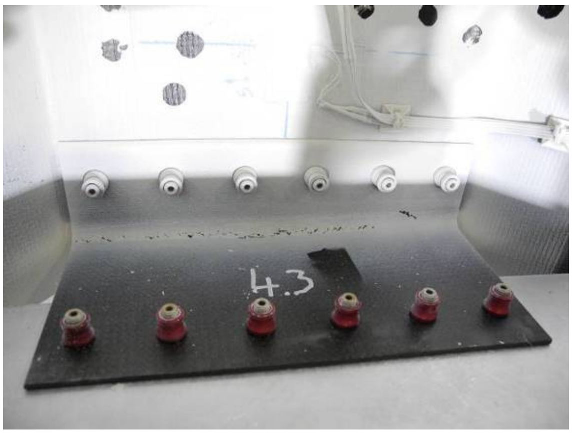

b) 

Figure 53 Shear Tie no. 3.4 after 2nd load cycle

The readings of the load cell and of the LVDTs are displayed in Figure 54 and Figure 55.The strain gauge readings of the 2nd load cycle can be found in Appendix C.

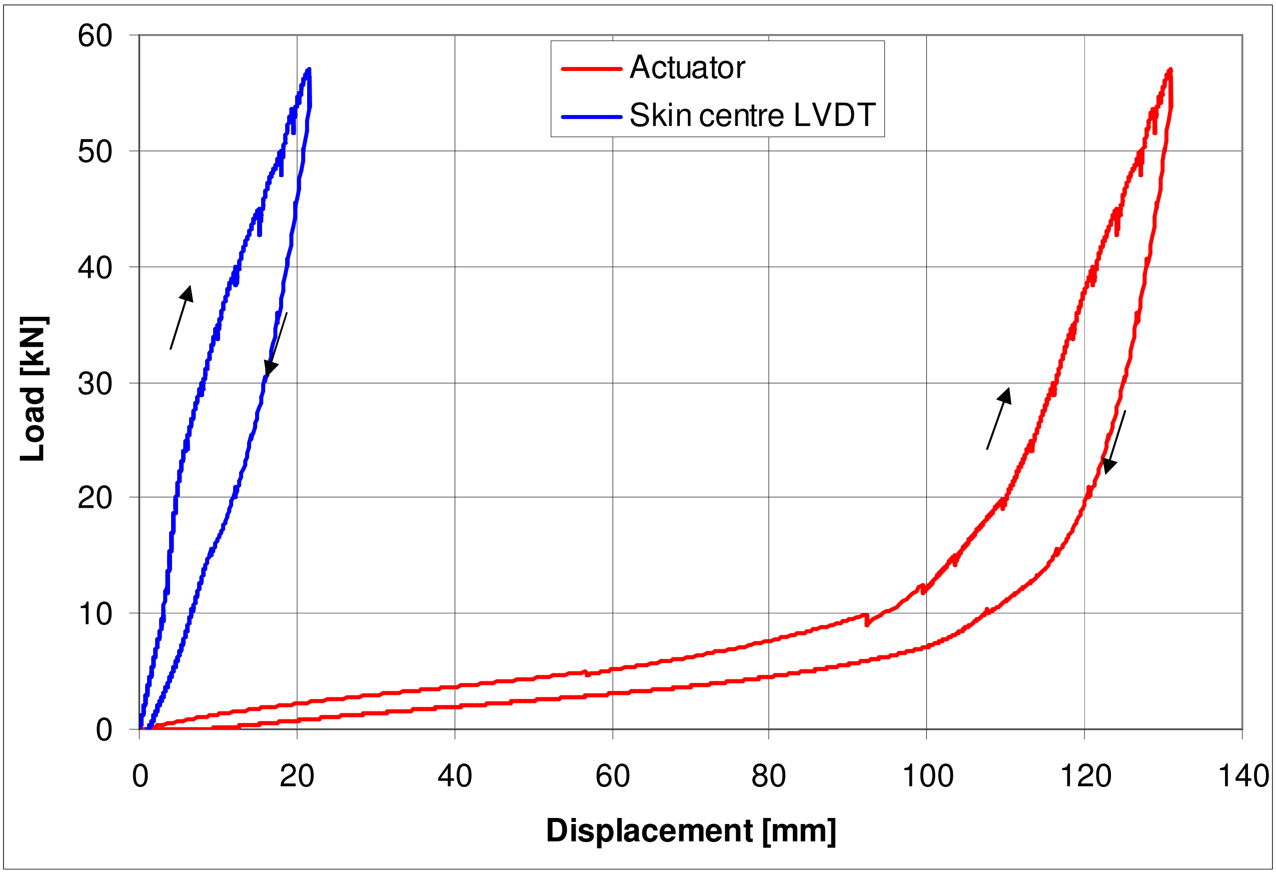

Figure 54 Load-Displacement: Actuator and Skin centre displacement

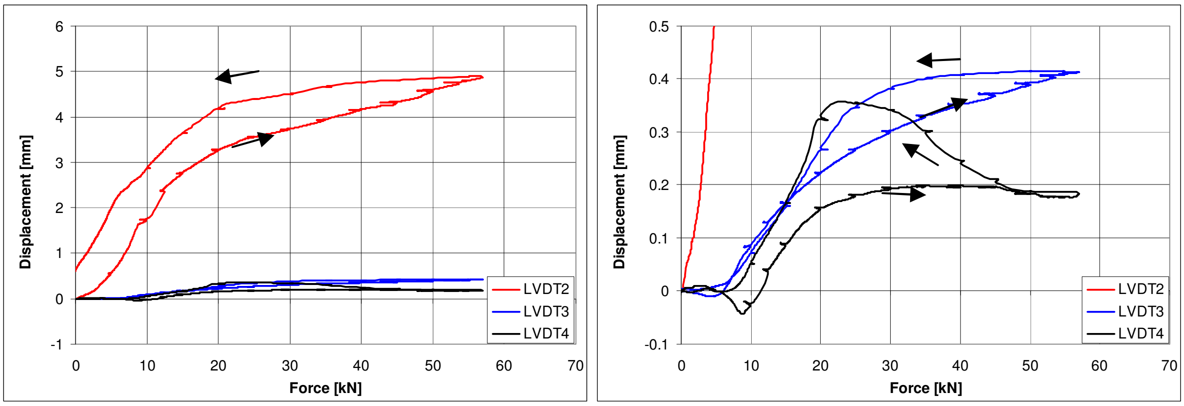

Figure 55 Displacement of LVDTs 2,3,4 vs. Actuator Load, 2 scales

5.9.3 Load cycles: Summary

The load-displacement charts of the actuator displacement and the skin centre displacement, in the first and second load cycle, are displayed in Figure 56. The panel settling and first damage is visible as an offset towards a higher displacement in the second load cycle.

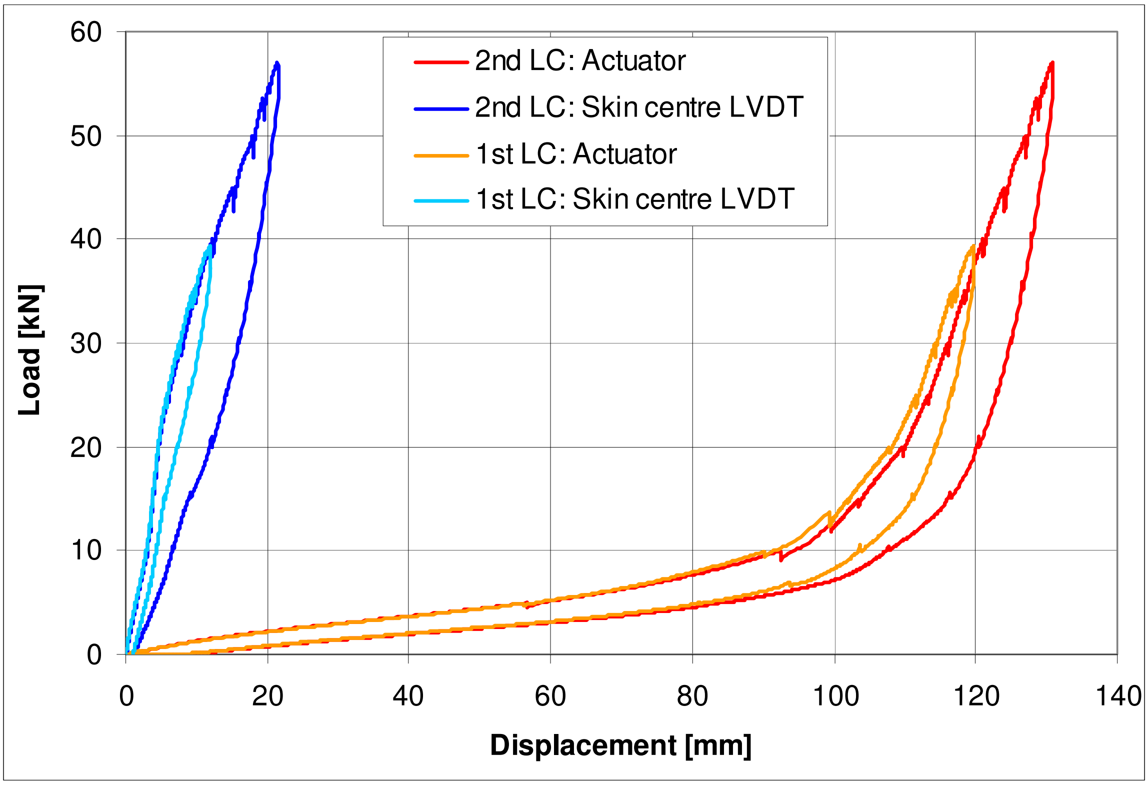

Figure 56 Load-Displacement of the 1st and 2nd load cycle

The energy that was applied to impact the test panel was calculated using the actuator force and the corresponding displacement. Figure 57 shows the energies that were needed to load the entire system consisting of the test panel and the rubber bumper. The second type of energy curve displayed in Figure 57 is related to the displacement of the skin centre of the panel and thus excludes the compression of the rubber bumper. The deviation of these two types of energy curves gives and indication about the level of energy that is necessary to compress the rubber bumper. The energies achieved in the two performed load cycles as well as the bumper compression energies that were calculated in the way described above, are listed in Table 3. The included energy dissipation reflects the reduction in the actuator force on the unloading path compared to the loading path, relating to the panel. The actuator deformation is not taken into account here.

Table 3 Energy levels of the test load cycles

	1st Load cycle	2nd Load cycle
Energy at first indication of damage	757 J	-
Maximum energy of the load cycle	974 J	1443 J
Bumper compression energy (calculated)	707 J	726 J
Energy dissipation during load cycle (panel only)	80 J	290 J

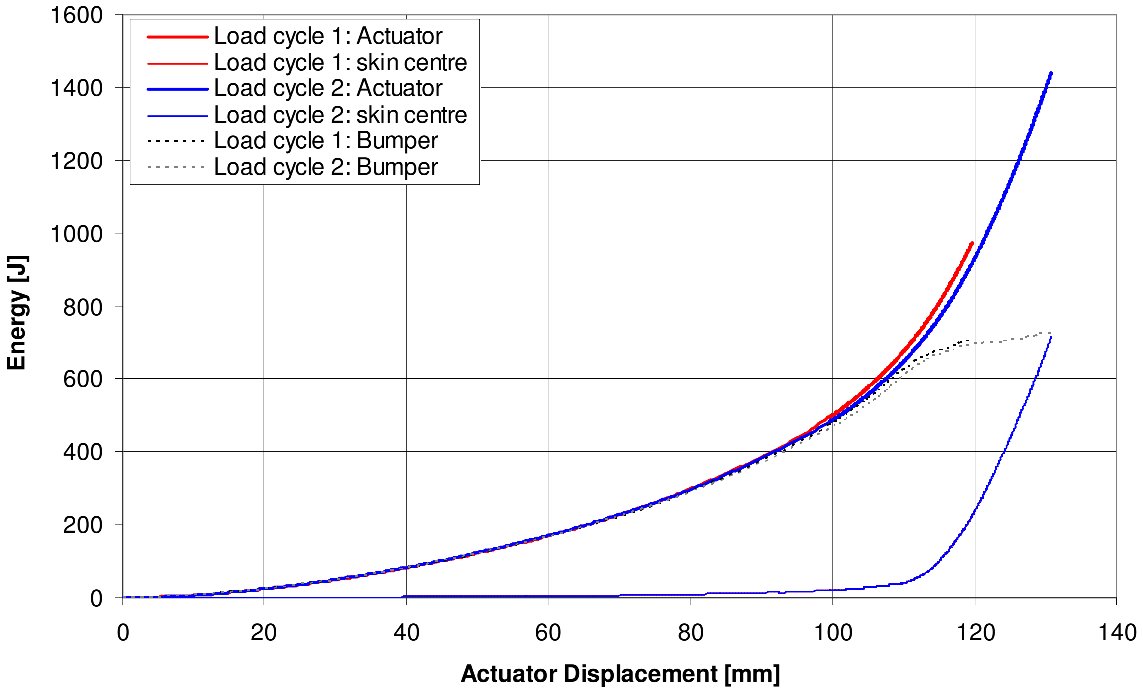

Figure 57 Energy levels in the 1st and 2nd load cycle

5.9.4 Comparison with the CODAMEIN test results

The first and second load cycles of the CODAMEIN II test and of the CODAMEIN test are compared using the global load-displacement readings of the two tests (see Figure 58 for the 1st load cycles and Figure 59 for the 2nd load cycles). The displacement of the 1st load cycle was lost at the final load drop in the CODAMEIN test since the used LVDT lost contact with the skin. The skin displacements show close agreement up to 25 kN applied load. At loads above 25 kN, the CODAMEIN II panel behaved softer which indicates faster damage growth in the shear ties. The load-displacement curves of the actuators show more deviations, in the low load phase and at the maximum load. In comparison with the skin displacement chart, this indicates different compression behaviour of the rubber bumper. It was compressed for the first time in the first load cycle of the CODAMEIN test which possibly made it behave softer in later compressions. The skin displacements indicate no influence of the higher boundary stiffness in the CODAMEIN II test at this low load level. The two displacement slopes rather indicate a stiffer response of the rubber bumper in the CODAMEIN II test.

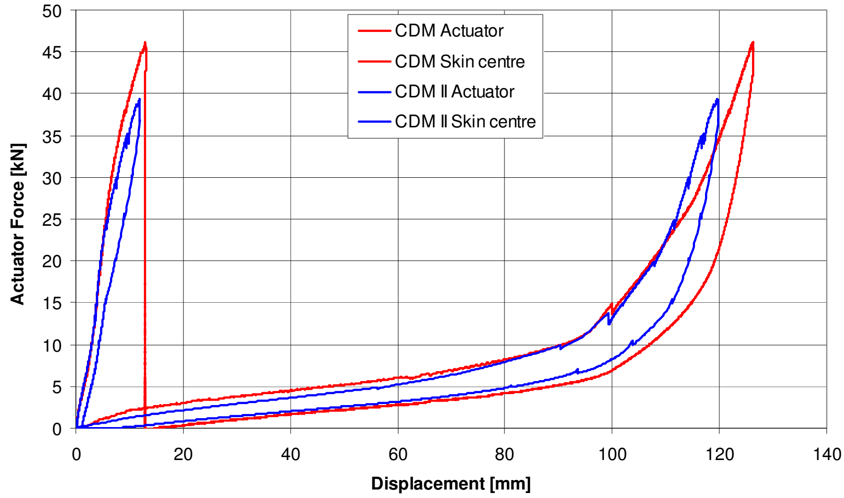

Figure 58 Load-displacement of test 1st load cycle: CODAMEIN II, CODAMEIN

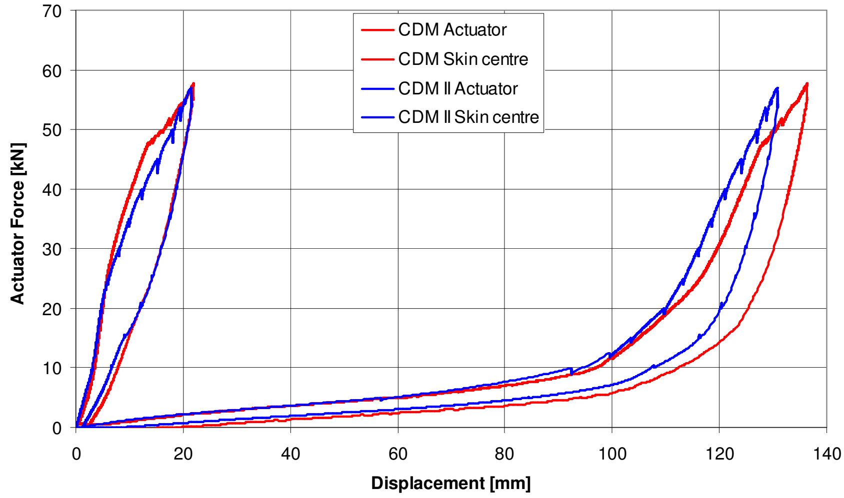

Figure 59 Load-displacement of test 2nd load cycle: CODAMEIN II, CODAMEIN

A comparison of the damage after the 2nd load cycle of the CODAMEIN II test with the damage within the 2nd load cycle of the CODAMEIN test is given in Figure 60. The white paint which was used for the video correlation system in the CODAMEIN test, allowed for a good visibility of the damage of the shear tie radii, mainly affecting the centre shear tie ST3_3. The cracks in the shear tie radii became invisible after the 1st and 2nd load cycle in the CODAMEIN test. The loaded state in the 2nd load cycle is therefore displayed. Damage onset was observed at slightly lower load in the CODAMEIN II test, possibly due to the different visibility caused by the paint used in CODAMEIN II. The symmetry of the shear tie radius damage was clearer in the CODAMEIN test. The tolerances in the test set-up and the alignment of the rubber bumper are higher than in test set-ups with rigid impactors. Fibre damage on the surface of the shear ties radius, clearly visible in the CODAMEIN test, was not observed in the CODAMEIN II test.

Figure 60 Damaged ST3.3: CDM II, after 2nd load cycle, CDM, in 2nd load cycle

5.10 Inspection results

The panel has been inspected visually and by NDT (A-scan) prior to testing and after each load cycle.

After damage was found visually at the centre shear tie no.3.3, an A-scan was also performed on the flat and accessible regions of the centre shear ties and the protruding parts of the two centre stringers, as shown in Figure 61.

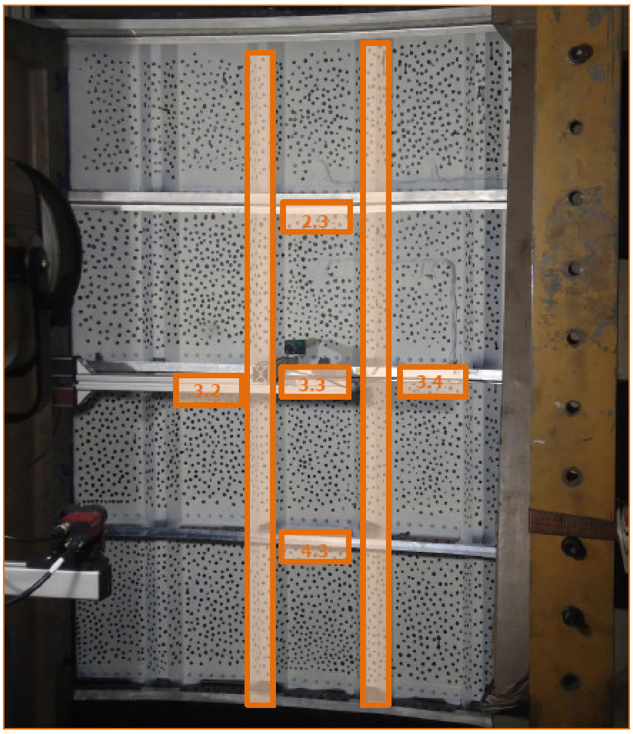

Figure 61 Additional A-scan pattern on the panel inside [Bergo Soto 2012]

The scanned shear ties are displayed in Figure 62.

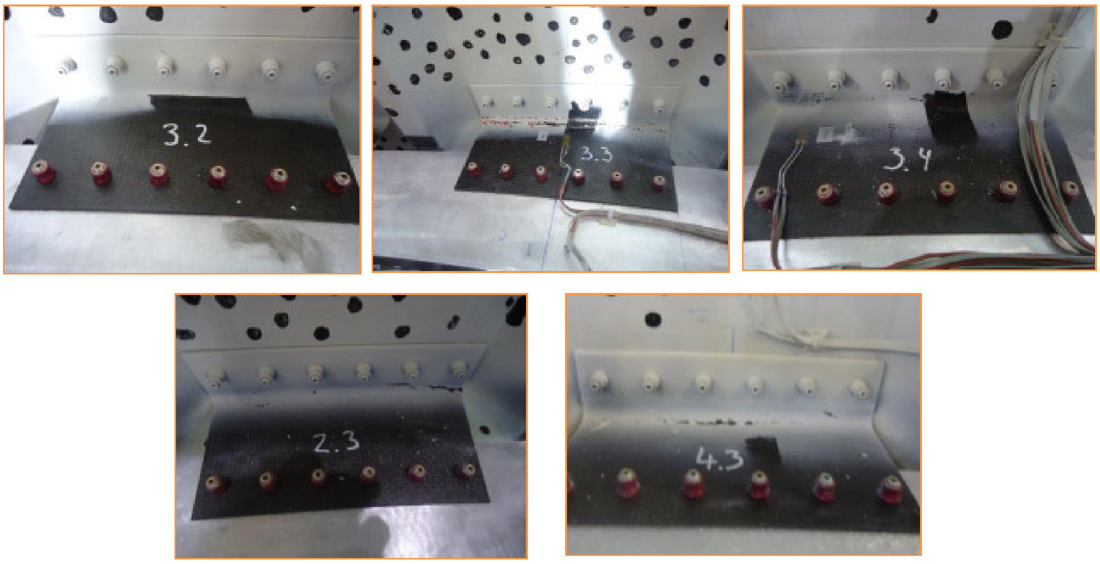

Figure 62 Shear Ties that were A-scanned after the first load cycle [Bergo Soto 2012]

None of the NDT scans, before the test and after the two performed load cycles, revealed any damage in the panel. The damage that was visually found in the radii of three shear ties, could not be reached by the NDT probe due to the curvature of the surface. None of these damages reached the flat regions of the shear ties which were scanned. It is possible that more precise inspection could be achieved in the future if the shear ties were disassembled from the panel.

The test panels of CODAMEIN and CODAMEIN II are stored at Bishop GmbH, Blankeneser Bahnhofstr. 12, 22587 Hamburg

6 Numerical investigation

A numerical model of the test panel as well as several additional FE models were generated and advanced throughout the project to deliver the desired test simulation data and information on parameter sensitivity.

6.1 Objectives of the FE model and analyses

One main objective of CODAMEIN II was the development of a numerical model that permits the simulation of the investigated impact case and which predicts the sequence of structural damage that is caused by the impact. Such a model can be used to predict further load cases, different panel designs or different materials in future work.

Based on the numerical models of CODAMEIN which were generated to simulate the stiffness of the hybrid structure, the detail level has been increased in several ways. All FE analyses were conducted using Abaqus 6.11. While an implicit integration scheme was used in CODAMEIN, an explicit integration was adopted in CODAMEIN II to better deal with the large non-linearities. The panel FE model used for CODAMEIN II is depicted in Figure 63.

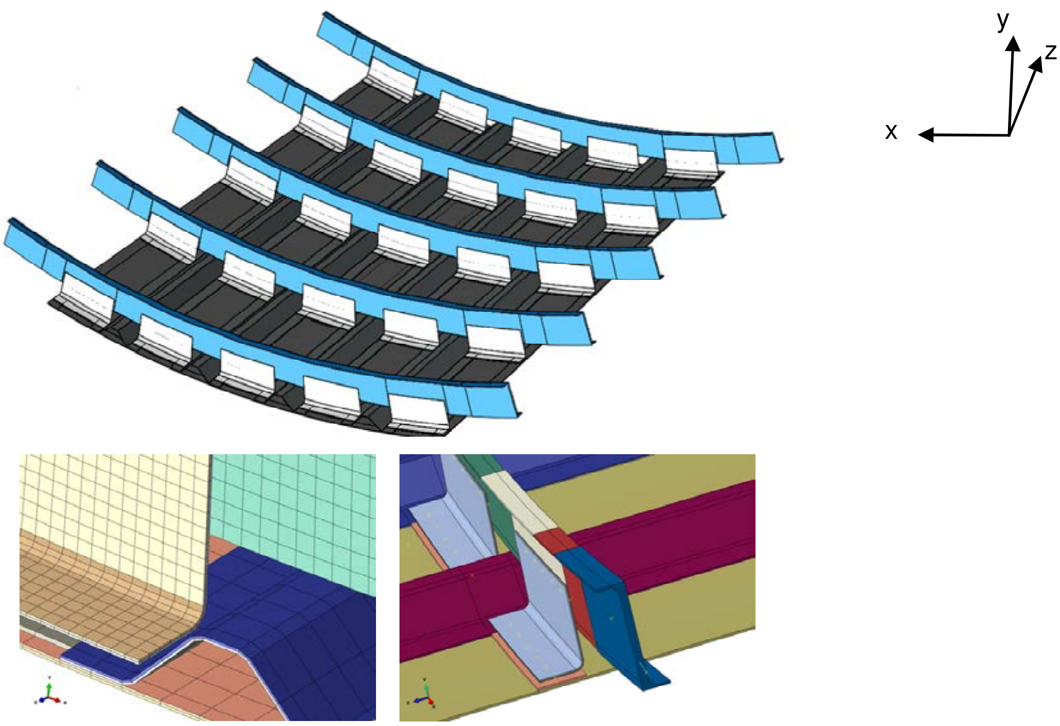

Figure 63 CODAMEIN II panel FE model: overview, details

6.1.1 Higher geometrical detail level

The FE models used in CODAMEIN provided a flexible base with a medium level of detail. With the results of the numerical analyses and the test in CODAMEIN, the most relevant points for potential higher detail investigation have been determined. To reach a higher geometrical detail level, the basic element type of the model was changed from Shell to Continuum Shell. Table 4 compares the detail level of the FE models of CODAMEIN and CODAMEIN II in terms of element types and numbers.

Table 4 Number of elements: CODAMEIN, CODAMEIN II

	CODAMEIN	CODAMEIN II
Number of shell elements	15443	0
Number of solid elements	5538	14831
Number of continuum shell elements	0	39896
Total number of elements	20981	54727

The Shear Ties which were found to be the most critical parts in CODAMEIN, were modelled with a finer mesh and with involvement of the bending radius which is the key region regarding damage and failure. Instead of shell elements, two layers of continuum shells were used to allow prediction of delamination damage. The frame parts of the CODAMEIN model and the CODAMEIN II model are depicted in Figure 64.

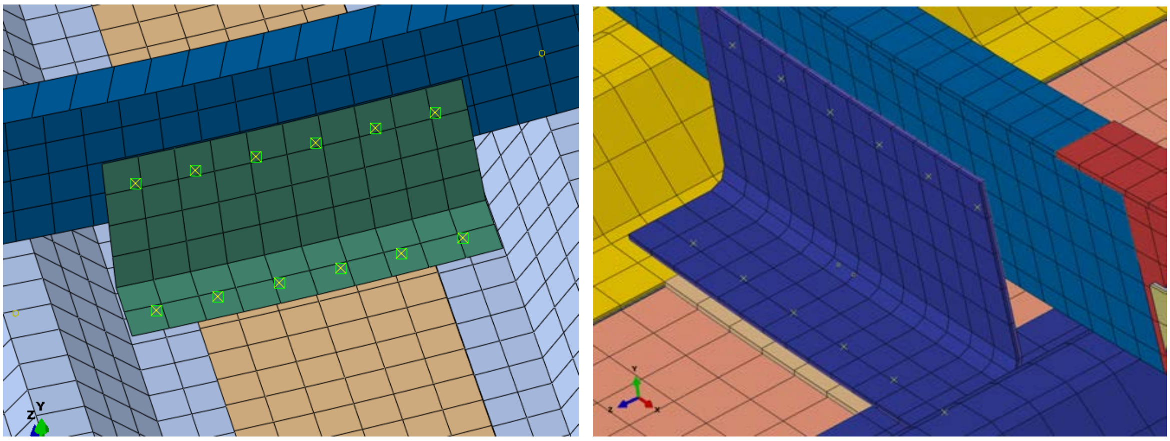

Figure 64 Shear Ties in the CODAMEIN and the CODAMEIN II model

The geometrical detail level of the frames was also increased to improve the representation of the reinforcement at the frame ends and of the bending stiffness of the frames. The profile radii were accurately represented using continuum shell elements as shown in Figure 65.

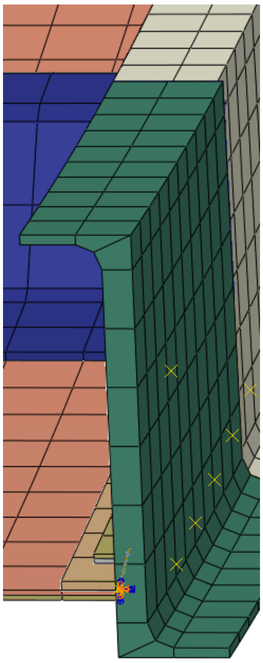

Figure 65 Frame (End attachment region)

6.1.2 Damage / Failure capabilities

The advancements of the panel FE model based on the CODMAMEIN test and FE analysis results implied the ability to develop damage and degradation. The defined parameters for the composite materials applied the Hashin damage criterion which enables ply-wise intralaminar damage and degradation. To integrate interlaminar damage in terms of delamination, the relevant composite parts were modelled using two element layers through the thickness. By the definition of a cohesive surface contact between the two layers, physical delamination was enabled. The connection of the parts that were co-cured during the manufacturing was represented by a cohesive surface definition that allowed for delamination. The rivet connection of the shear ties to the skin and the frames was modelled using 1D fastener elements. The failure of fasteners in tension or shear was also integrated although fastener failure did not occur in the tests of CODAMEIN, CODAMEIN II or in the FE analyses. The used damage and failure models are described in more detail in the respective sub-chapters for materials, contact definitions and connector elements (6.2.2, 6.2.5 and 6.2.6).

6.1.3 Investigation of boundary conditions

The boundary conditions of the CODAMEIN set-up have been further assessed within CODAMEIN II. The basic test set-up remained unchanged for CODAMEIN II. The spring stiffness of the coil springs within the test fixtures was the parameter which could be modified to influence the boundary behaviour of the set-up. FE analyses have been performed using the panel model and an advanced version of the barrel model (see Figure 66) that was introduced within CODAMEIN to assess the influence of the boundary stiffness.

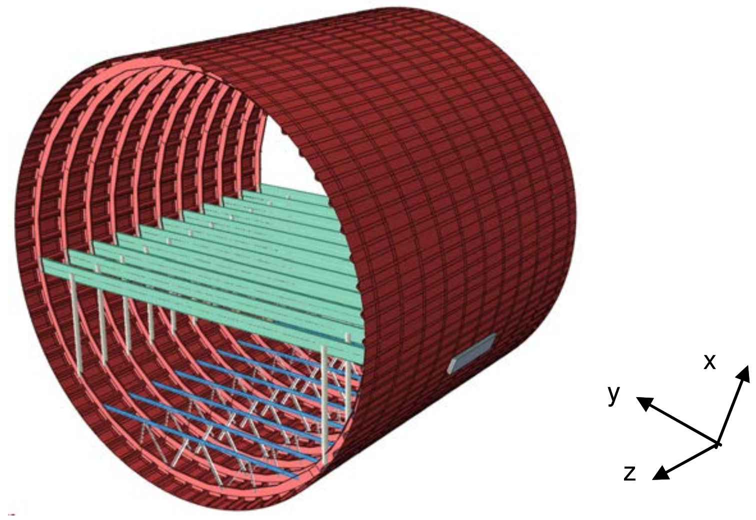

Figure 66 CODAMEIN II barrel FE model

The boundary stiffness was changed, based on the results of the barrel model FE analyses. The influence of the 3-frame attachment that was selected for the test, against an attachment of all 5 frames was also assessed using FE analyses.

6.2 Description of the panel FE model

A shell model was used to represent the test panel in CODAMEIN. During the FEA work within CODAMEIN, several difficulties were identified, which were not solvable within the scope of CODAMEIN yet were registered as objectives for a CODAMEIN II FE panel model. For CODAMEIN II, a new panel model was generated with the aim to cover as many of these points as possible. The existing models could not be used since the fundamental modelling techniques were changed.

6.2.1 General

Based on the outcomes of CODAMEIN, the general precision level of the FE model was increased. Several features were included to enable damage, degradation and failure and different element types were used which require a complete re-modelling of the test panel instead of a modification of the existing CODAMEIN model. The explicit solver of Abaqus delivered solutions for the analysed cases for which the standard solver failed to provide results. The panel model is displayed in Figure 67.

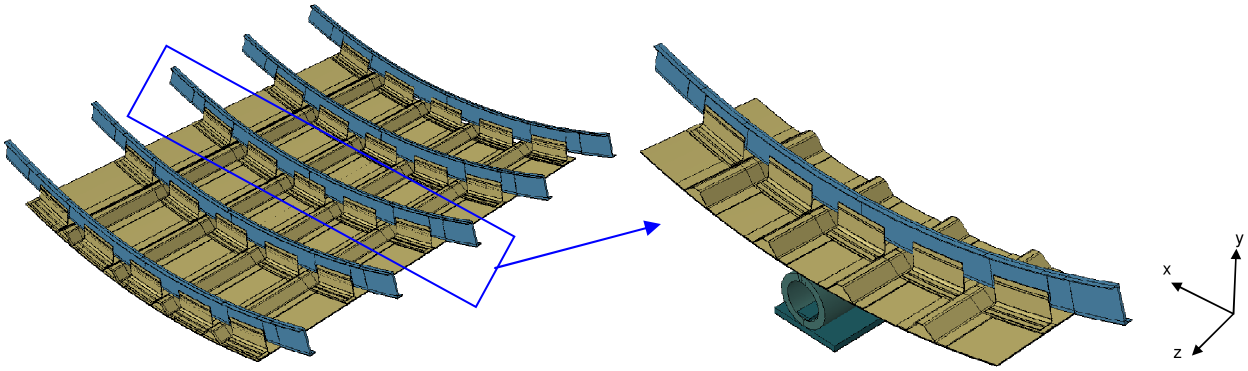

Figure 67 Panel FE model and centre cut-out view

6.2.2 Materials

The materials of the CODAMEIN II panel were identical to those of the CODAMEIN panel. The hybrid design panel consists of a composite skin with composite Omega-stringers and composite shear ties which are connected to Aluminium Z-frames. The shear ties are connected to the skin and the frames using steel Hi-Lok fasteners with Aluminium collars.

Figure 68 CODAMEIN II panel within the quality check

The specific materials used for the CODAMEIN II panels are listed in Table 5.

Table 5 Materials of the CODAMEIN II panel

Material	Usage
Cytec X84-Z60 UD 12k Tape	Skin, Stringers
Cytec X840-Z60 Pw Fabric	Skin, Stringers, Shear Ties
Al 7075-T6	Frames
Rubber NBR	Bumper

The drawings of the panel and all parts can be found in Appendix B. The material usage and the composite lay-ups of the parts are included in the drawings.

Within CODAMEIN II, no material tests were defined. The used material data was partially taken from the composite material data sheets of the material supplier Cytec. Generic data was used for the remaining material properties.

The Hashin damage criterion that is implemented in Abaqus [Abaqus, 2012] was used to model the damage initiation and progress in the composite materials. This criterion uses the material's strength components for fiber and matrix, in tension, compression and shear direction.

X^T (Tension longitudinal), X^C (Compression longitudinal),
Y^T (Tension transversal), Y^C (Compression transversal),
S^L (Shear longitudinal), S^T (Shear transversal)

The damage onset is defined for the modes fibre tension and compression, matrix tension and compression as well as shear, according the equations below [Abaqus, 2012].

Fiber tension $(\hat{\sigma}_{11} \geq 0)$: $$F_f^t = \left(\frac{\hat{\sigma}_{11}}{X^T}\right)^2 + \alpha\left(\frac{\hat{\tau}_{12}}{S^L}\right)^2 \quad \text{Eq. 3}$$

Fiber compression $(\hat{\sigma}_{11} < 0)$: $$F_f^c = \left(\frac{\hat{\sigma}_{11}}{X^C}\right)^2 \quad \text{Eq. 4}$$

Matrix tension $(\hat{\sigma}_{22} \geq 0)$: $$F_m^t = \left(\frac{\hat{\sigma}_{22}}{Y^T}\right)^2 + \left(\frac{\hat{\tau}_{12}}{S^L}\right)^2 \quad \text{Eq. 5}$$

Matrix compression $(\hat{\sigma}_{22} < 0)$: $F_m^c = \left(\frac{\hat{\sigma}_{22}}{2S^T}\right)^2 + \left[\left(\frac{Y^C}{2S^T}\right)^2 - 1\right]\frac{\hat{\sigma}_{22}}{Y^C} + \left(\frac{\hat{\tau}_{12}}{S^L}\right)^2$ Eq. 6

The effective stress tensors $\hat{\sigma}_{11}$, $\hat{\sigma}_{22}$ and $\hat{\tau}_{12}$ are calculated as $\hat{\sigma} = M\sigma$ Eq. 7

with the damage operator M that is equal to zero as long as no damage has set on.

$$M = \begin{bmatrix} \frac{1}{(1-d_f)} & 0 & 0 \\ 0 & \frac{1}{(1-d_m)} & 0 \\ 0 & 0 & \frac{1}{(1-d_s)} \end{bmatrix} \quad \text{Eq. 8}$$

Using the damage variables d_f , d_m and d_s.

$$d_f = \begin{cases} d_f^t & if\ \hat{\sigma}_{11} \geq 0 \\ d_f^c & if \hat{\sigma}_{11} < 0 \end{cases} \quad \text{Eq. 9}$$

$$d_m = \begin{cases} d_m^t & if\ \hat{\sigma}_{22} \geq 0 \\ d_m^c & if \hat{\sigma}_{22} < 0 \end{cases} \quad \text{Eq. 10}$$

$$d_s = 1 - (1-d_f^t)(1-d_f^c)(1-d_m^t)(1-d_m^c) \quad \text{Eq. 11}$$

Damage progression is defined in terms of energy law with linear softening of the material. The damaged elasticity matrix C_D has the form of Eq. 10.

$$C_D = \frac{1}{D}\begin{bmatrix} (1-d_f)E_1 & (1-d_f)(1-d_m)\upsilon_{21}E_1 & 0 \\ (1-d_f)(1-d_m)\upsilon_{12}E_2 & (1-d_m)E_2 & 0 \\ 0 & 0 & (1-d_s)GD \end{bmatrix} \quad \text{Eq. 12}$$

With $D = 1 - (1-d_f)(1-d_m)\upsilon_{12}\upsilon_{21}$ Eq. 13

For the four damage modes, the function of the equivalent stress and equivalent displacement shows the linear stiffness prior to damage onset and a linear degradation from damage onset. If unloaded at the point B, after damage onset at point A (Figure 69), the structure relaxes back to the origin of the equivalent stress – equivalent displacement chart, dissipating the energy G^C (see Abaqus Analysis User's Manual 23.3.3, [Abaqus, 2012]).

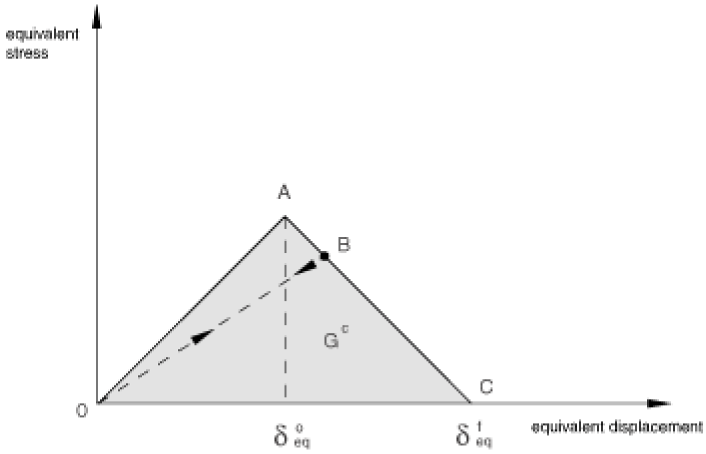

Figure 69 Equivalent stress - equivalent displacement [Abaqus, 2012]

The rubber material of the bumper was represented by a simplified linear elastic isotropic material since no specific hyper elastic material data was available for this material.

6.2.3 FE Mesh

After a shell model was used to perform static simulations in CODAMEIN, a continuum shell model was generated for CODAMEIN II, which was simulated in explicit analyses. This modelling approach permits an improved geometrical precision, reduces inaccuracies due to section offsets and provides through-thickness outputs. Linear continuum shell elements of the type SC8R were used for all composite parts and the frames. The impactor structure was meshed using linear solid elements C3D8R, the rubber bumper was meshed using linear solid elements with incompatible modes (C3D8I) that provide improved bending behaviour. The size of elements was chosen with the aim to provide sufficient analysis accuracy, an appropriate element dimension ratio and an optimal match between the meshes of the parts connected in the assembly. These conditions were in opposition to the aim to achieve the maximum possible element size in order to allow for reasonable solution times. All part meshes are displayed in Figure 70 to Figure 74.

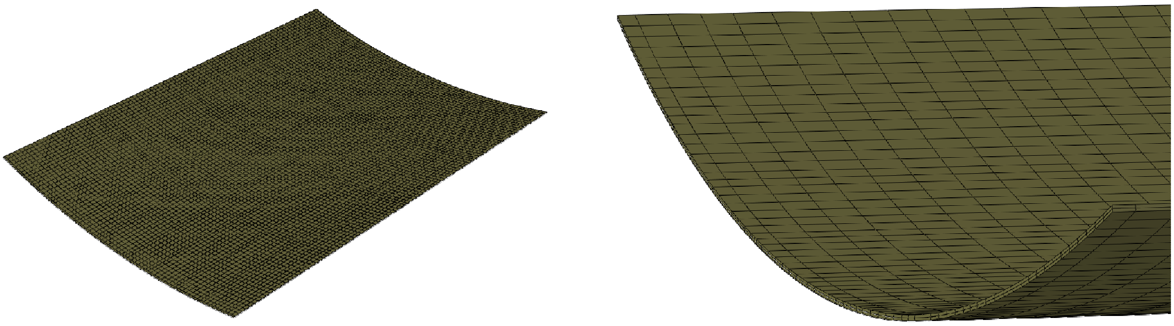

a) b)

Figure 70 Skin mesh: a) overview, b) detail

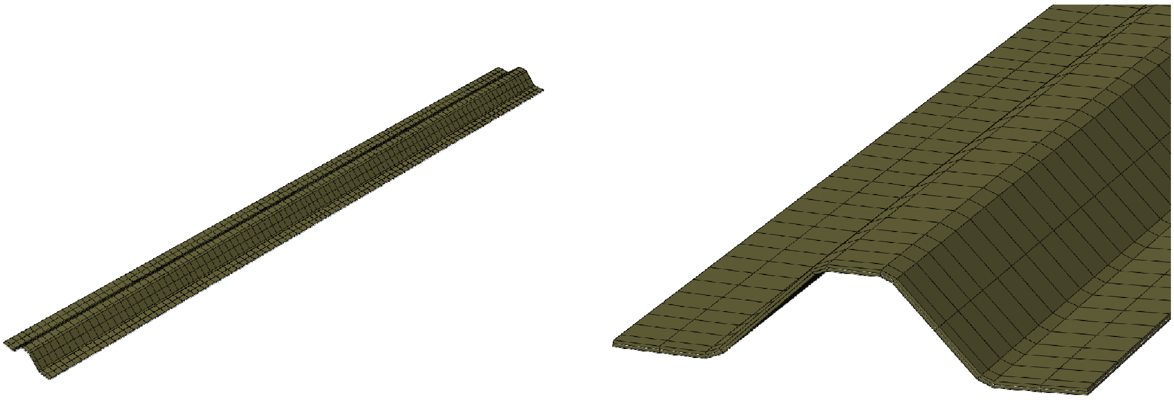

a) b)

Figure 71 Stringer mesh: a) overview, b): detail

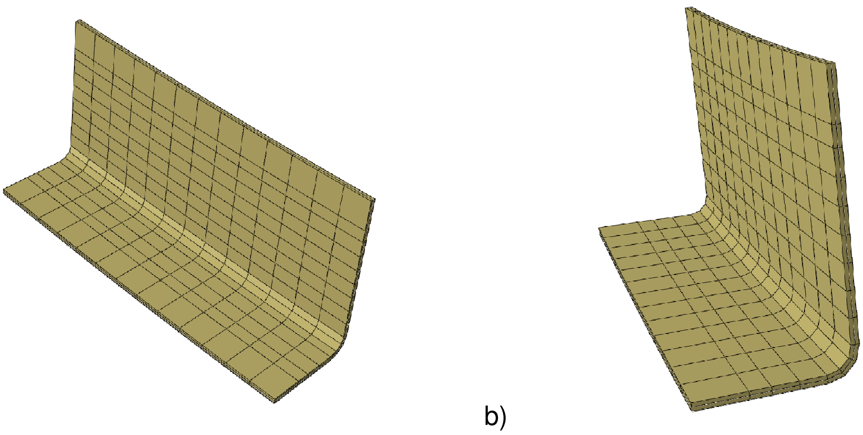

a) b)

Figure 72 Shear tie mesh: a) overview, b) detail

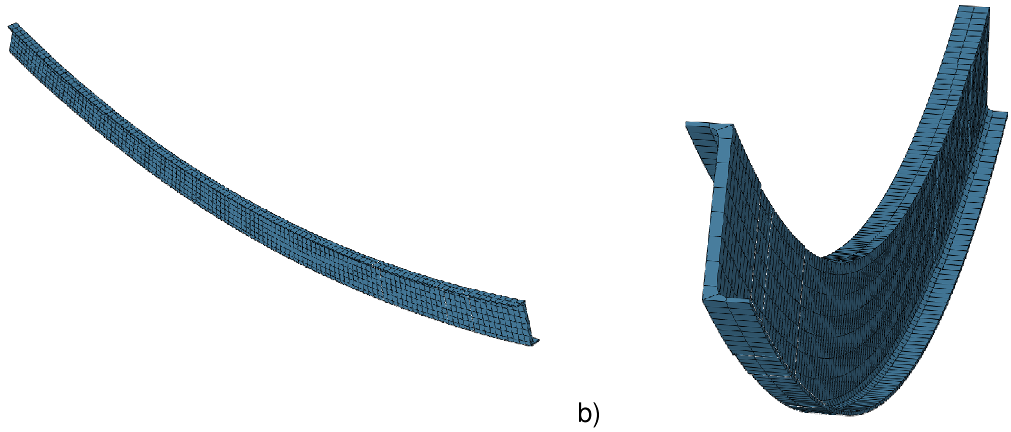

a) b)

Figure 73 Frame mesh: a) overview, b) detail

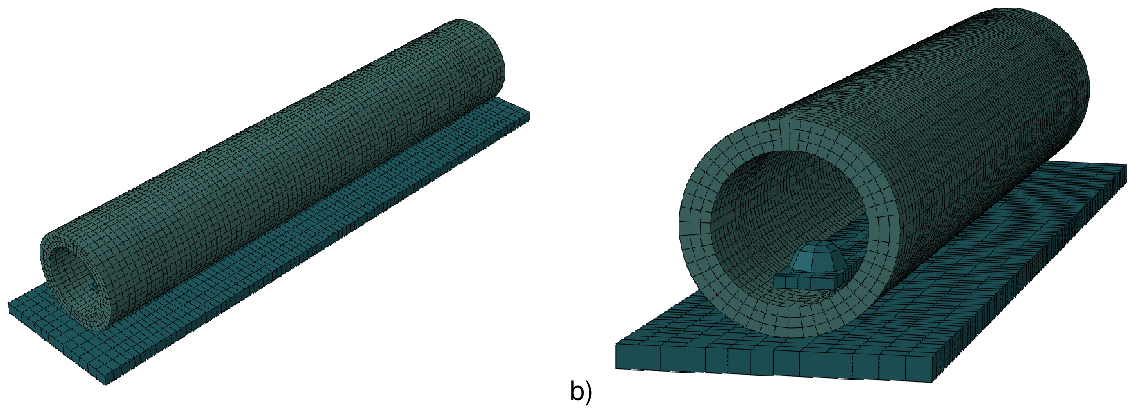

a) b)

Figure 74 Rubber bumper mesh: a) overview, b) detail

The most critical elements that drove the incrementation of the explicit analyses were the smallest elements in the section radii of the stringers and the shear ties. No simplification was done to these regions since especially the shear tie radii were the most relevant regions for damage onset and progression within the model. Since the achieved elementation of the model still required an inadequate solution time, mass scaling was allowed at low magnitude. The mass scaling function of Abaqus allows for an automatic increase of mass for the elements that are most critical for the solution minimum time increment which can significantly reduce the computation time. The mass scaling factor was held below 10 which means that the mass of several elements in the shear tie and stringer radii was increased by a maximum factor of 10 throughout the entire analysis. The computation time could be reduced to approx. 40 h on 4 CPUs for a panel analysis.

6.2.4 Boundary conditions

The boundary conditions of the panel analyses were chosen to represent the test set-up. Figure 75 shows the axial view of the set-up.

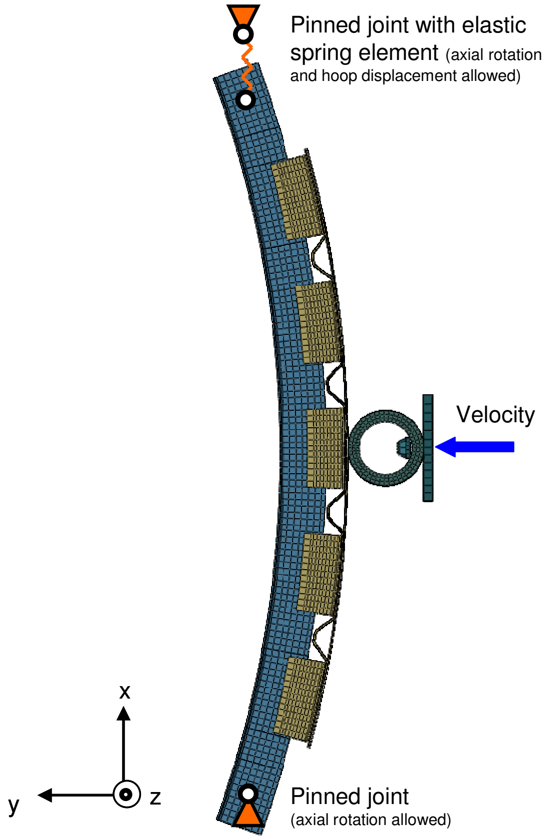

Figure 75 Panel boundary conditions, axial view

Boundary conditions were defined at the ends of the three inner frames. Coupling constraints with reference points represented the steel fittings at the frame ends (see Figure 76).At the frame ends which were attached by a bolt connection in the test set-up, a boundary conditions that only permits longitudinal rotation, was defined on the fitting reference point. At the other frame ends that were mounted to the spring test fixtures in the test set-up, longitudinal rotation and transverse translation, relating to the impact direction was permitted. An axial connector and a fixed reference point were used to represent the spring stiffness of one test fixture.

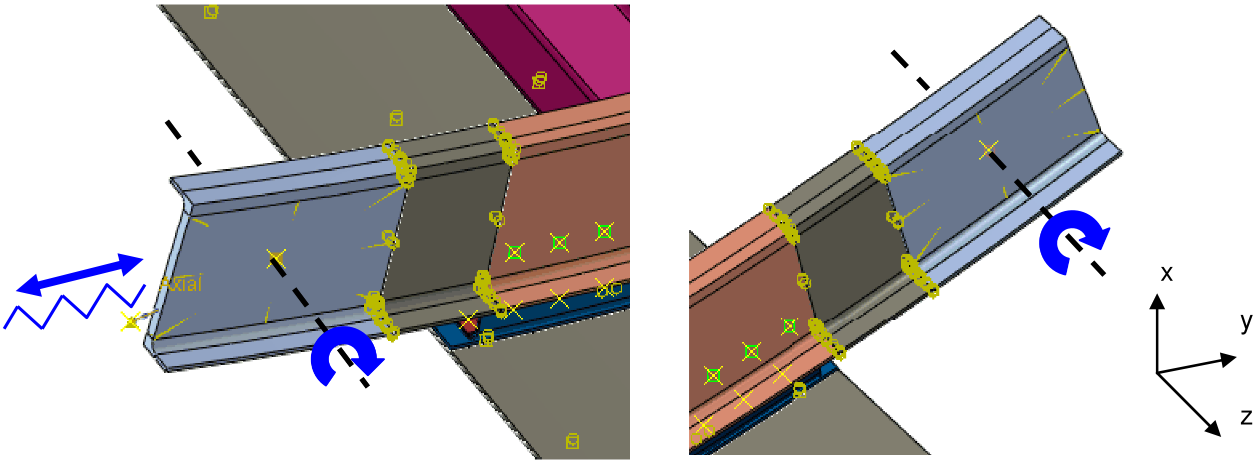

Figure 76 Frame end boundary conditions: spring side, bolt side

The impact was simulated dynamically using a velocity of 1 m/s while the test was done with static loading. Simulating a lower impact velocity was not possible due to the resulting extreme computation time. Dynamic effects in the analyses were noticed an assessed as far as possible. The influence of the dynamic loading was noticed and judged acceptably low.

The loading of the FE simulations was defined as constant velocity load for the simulation of the loading phase. The impact velocity was also defined as initial condition to achieve a steady start phase of the loading.. The velocity of 1 m/s was held for 0.2 s which resulted in a movement of the impactor of 200 mm.

The spring stiffness of the test fixtures in CODAMEIN were determined using FE analyses of a simplified fuselage barrel model. In this model, the detailed panel was extended to a full barrel using simplified modelling of the structure.

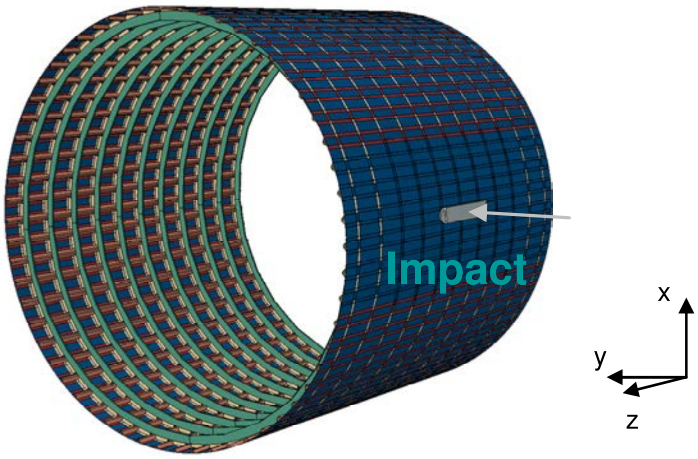

Figure 77 CODAMEIN barrel model

The degree of indentation in relation to the force of a statically loaded impactor was used to adjust the boundary stiffness of the panel.

In CODAMEIN II, the barrel model was advanced by including further fuselage structure in the FE model. The additional structure such as floor beams and load struts increased the stiffness of the barrel exposed to the blunt impact which was located in a position 21° under the horizontal axis. This position at the lower fuselage is both a likely position where ground service equipment such as belt loaders might impact the fuselage and a position of maximum distance to the reinforcing inner structure which permits high indentation and thus the risk of creation of impact damage with low visibility.

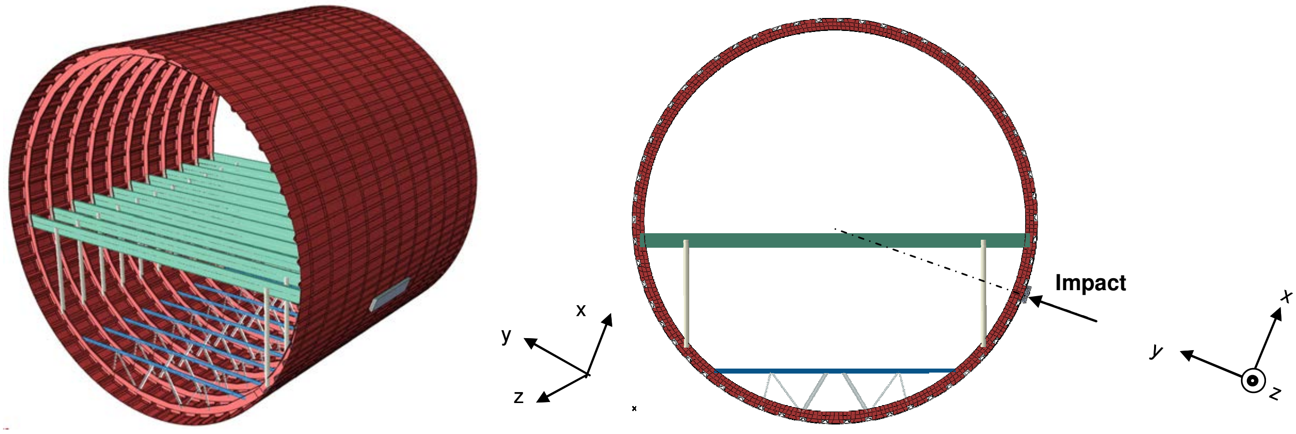

Figure 78 CODAMEIN II barrel FE model

The FE analyses of the improved barrel model indicated a small increase of stiffness. Although the response in this stage has been highly dynamic, a stiffness increase of approximately 12 % was found.
Even though the stiffness of the panel boundary is not directly connected to the indentation of the panel, the feasible range for a stiffness increase of the springs in the test fixtures from the CODAMEIN test was also approx. 12%. Thus, this level of spring stiffness increase was chosen for the COAMEIN II test. The springs within the test fixtures (spring stiffness in CODAMEIN: 850 N/mm, see Figure 79) were replaced with springs of a higher stiffness (950 N/mm).

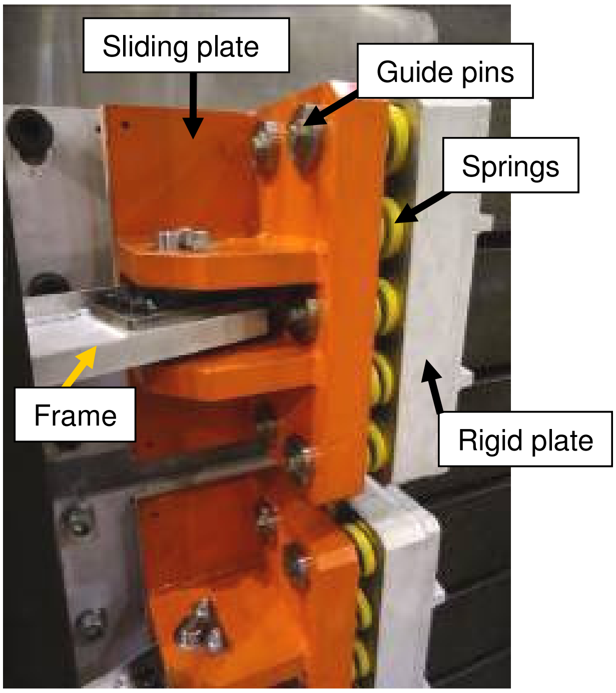

Figure 79 Coil springs within the test fixtures

The friction within the test fixtures was not included in the FE model. Friction within the test fixtures was assumed to have low influence; however its magnitude could not be assessed. However the test indicated an unexpected significant influence of friction due to tolerances and imperfect alignment within the test fixtures and with the panel. The test fixtures would have to be tested separately to assess their influence and to consider it in the simulations.

6.2.5 Contact definitions

Contact was defined between the rubber bumper and the panel skin, at the inside of the rubber bumper, and between all parts of the panel which were connected during manufacturing or which could contact during the impact. A general contact definition was used to realize most of the contacts as “hard” contacts. These contacts permitted no intersection and used a friction coefficient of 0.3. The connection of the composite parts that were co-cured in the panel manufacturing, like the skin and the stringers was represented by a cohesive surface definition which was also used in all parts that were modelled as two stacked layers of elements with the ability to delaminate, like the skin, the two inner stringers and the shear ties. The splitting of the composite parts into two layers of elements permitted delamination ability throughout the entire panel model. The usage of three or four element layers would not supply a significantly higher precision of the delamination / debond representation. The modelling of composite parts in full detail (including all plies as separate element layers) is only possible for very small detail models. The cohesive surface interaction uses a generalized traction separation behaviour and is similar to that of cohesive elements assuming a very small thickness. The uncoupled traction – separation behaviour uses one normal stiffness as well as two shear stiffnesses K_{NN}, K_{SS} and K_{TT} and does not couple the normal and shear separations. The quadratic stress criterion is defined for damage onset. With the peak stress values t^0 of the one normal and the two shear stress components, the damage parameter is defined as follows.

$$\left\{\frac{\langle t_n \rangle}{t_n^0}\right\}^2 + \left\{\frac{t_s}{t_s^0}\right\}^2 + \left\{\frac{t_t}{t_t^0}\right\}^2 = 1 \qquad \text{Eq. 14}$$

The linear energy law was defined for the damage propagation, which correlates with the representation of damage of the composite materials. The composite surface behaves linearly elastic before reaching the traction of damage onset and softens linearly afterwards (see Figure 80).

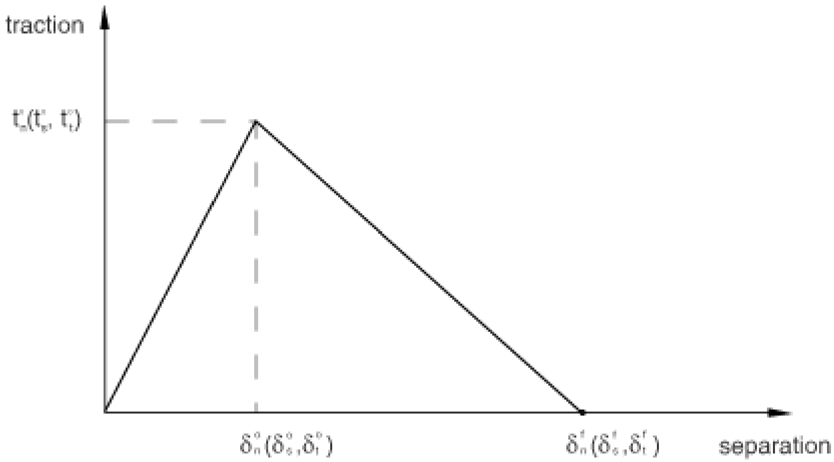

Figure 80 Traction separation of the damage propagation [Abaqus, 2012]

In the used criterion, the fracture energies of the single modes are mixed using the power law.

$$\left\{\frac{G_n}{G_n^C}\right\}^\alpha + \left\{\frac{G_s}{G_s^C}\right\}^\alpha + \left\{\frac{G_t}{G_t^C}\right\}^\alpha = 1 \qquad \text{Eq. 15}$$

The meshes of the parts were defined to match in the locations of initial contact. Even though non-matching meshes are preferred for contact definitions, the initial intersections of the surfaces due to the curved panel shape could be avoided by the matching meshes. The influence of a small offset of the contacting meshes was assessed in a detail model which showed no different behaviour due to this adjustment.

6.2.6 Connector elements

Connector elements were used to represent the springs within the panel test fixtures and the fasteners which attached the shear ties to the skin and to the frames. The used connectors were 1D-elements which connected two points with a individual relationship between their degrees of freedom (DOF).

Axial connectors were used to represent the springs in the test fixtures at one side of the panel (see Figure 81). The pin joints at the frame ends were given one translational DOF. The connectors with the axial stiffness of the springs used in the test, connected those pin joints to fully fixed points.

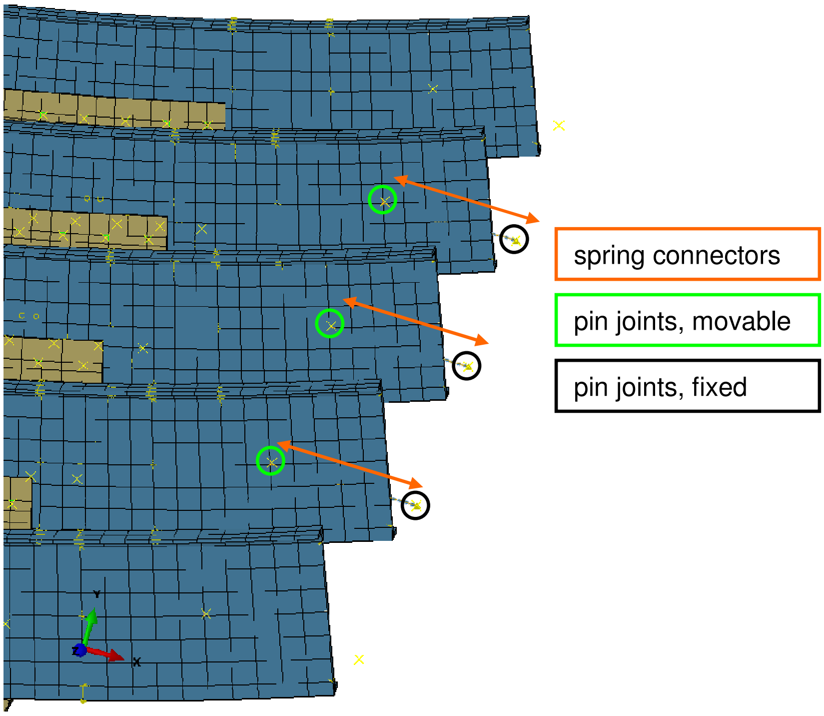

Figure 81 Connectors representing springs in the test fixtures

The fasteners that attached the shear ties to the skin and to the frames were modelled as fasteners (Figure 82). The fastener feature of Abaqus allows the connection of points on different surfaces which do not need to be nodes of the mesh. These reference points are automatically coupled to the adjacent nodes of the mesh using distributing couplings. A single connector element or, like in this case of selection of several element layers in the fastening direction, a chain of connectors is generated between each pair of nodes. The present type definition “cartesian + cardan” allows the assignment of properties in all DOF. For the representation of the fasteners, translational elasticities as well as axial and shear strengths were defined. Thus, fastener failure was possible however did not occur in the test or in the FEA. The fasteners attaching the shear ties to the skin were replaced by local tie constraints (DOF equalization of node pairs) to reduce the tendency of elements within the shear tie feet to undergo hourglassing modes that caused delamination. Due to the pressure loading by the rubber bumper, neither significant tension nor significant shear was applied to these fasteners.

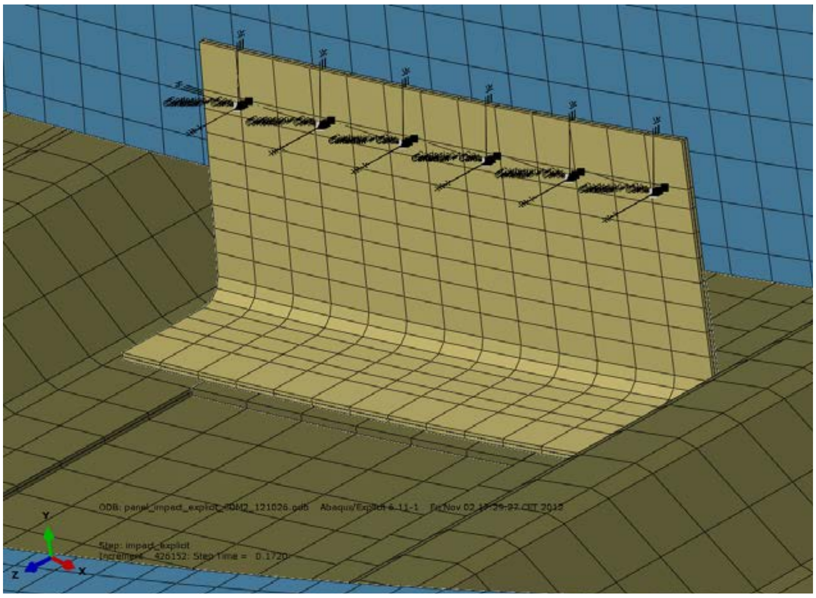

Figure 82 Connectors: fasteners attaching shear ties to the frames

Another connector was added to attach the rubber bumper to the impactor plate using the plate and bolts inside the bumper (see Figure 83). The clamping of the rubber bumper using the inner steel plate was integrated in the single analysis step of the panel analyses. While the bumper started to compress against the panel, it got clamped to the impactor plate. Since an external clamping load disturbed the load recording of the impactor, this attachment force was transferred to a connector which was gradually loaded in tension direction in the start phase of the impact analyses.

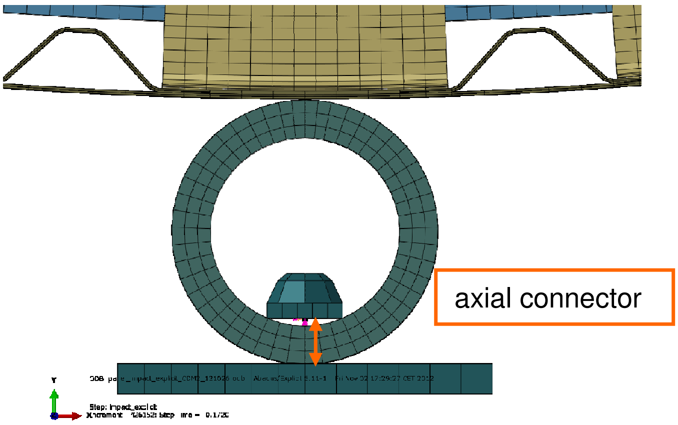

Figure 83 Connector fixing the rubber bumper attachment plate

6.2.7 Rubber bumper modelling

The finite element representation of the rubber bumper is expected to have significant influence on the behaviour of the impacted panel. Since the complete modelling of the rubber bumper proved to be complicated, a simplified pre-compressed part was used in CODAMEIN. The limitations of this simplification are the missing simulation of the impact phase prior to the complete compression of the bumper in which both the bumper and the panel get deformed. Furthermore, the contribution of the bumper attachment tooling on its inside to the load distribution could not be covered by the simplified bumper modelling. Within CODAMEIN II, a solution for the modelling of the undeformed rubber bumper was found. The inner attachment tooling consisting of a steel plate and two bolts was integrated in the model. The inclusion of the bumper compression phase enabled a comparison of the whole impact process with the test. The final representation of the rubber bumper is shown in Figure 84 in the undeformed state and as a cut view of the meshed and deformed combination with the panel.

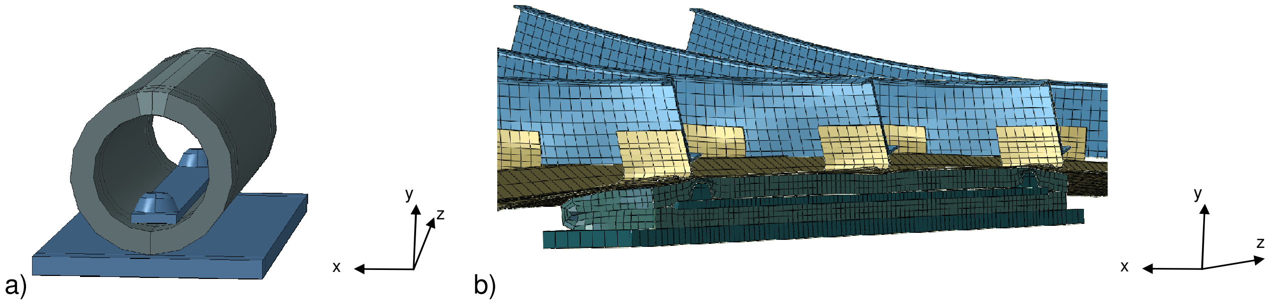

Figure 84 Rubber bumper assembly: a): geometry, b) cut view of the meshed deformed state

6.3 Sensitivity study

Sensitivity studies have been performed to assess the contribution of several parameters of the test panel FE model behaviour under the impact load. The goal of the performed analyses was to validate the FE model of the test panel using the results of the CODAMEIN test. The parameters that were found to have main influence on the formation of damage, especially of damage with no or low visibility, consist of physical parameters such as part geometries and material parameters, which must be represented as accurate as possible by the numerical analyses, as well as modelling techniques and analysis parameters. For these factors, the minimum of influence on the analysis results or a maximum of understanding of their influence and thus a possibility of adjustment for a minimal final influence were important. As not all relevant material parameters of the used material were known, several properties such as the shear modulus and the fracture toughnesses of the composite materials had to be estimated using data of similar materials. These parameters were also assessed by the sensitivity study.
The physical parameters considered to have main influence are:

- Stiffness of the composite material
- Strength of the composite material
- Energy release rates in damage progression of the composite material
- Thickness of the composite material plies and entire parts

Factors which were relevant for the performance of the FE analyses are:

- Element size
- Critical time increment
- Loading rate
- Mass scaling

By performing a series of FE analyses, the influence of these factors has been assessed using several different FE models.

A limitation of the performed sensitivity study was the unavailability of material test data. The manufacturer of the composite material supplied data sheets from which the basic material parameters were taken. Detailed information on the behaviour of the used composite lay-ups were not available since coupon tests were not possible within the project. In a series of parametric FE analyses, the behaviour of detail models and sub-models was assessed. A comparison with a test was possible only for the CODAMEIN test, performed in 2011.

For that, the entire panel model was used to simulate the conditions of the CODAMEIN test. Using coupon test and simulation data available from a previous test, [ACS Australia, 2012], FE models using the element type of the CODAMEIN II panel model were tested in comparison with these test results. This comparison was valid only for the used materials and lay-ups which were different from those of CODAMEIN II. The results of the performed sensitivity study for the test panel details, materials and composite lay-ups of CODAMEIN II thus delivered information on the limits of the respective model. Full influence on the test panel could only be assessed in simulations of the full panel. The number of simulations of the full panel was limited by the high analysis time demand (more than 40 h per run).

6.3.1 FE models: global / detail

Additional to the test panel FE model, several models with different detail levels were used to perform the sensitivity analyses. Even though using the panel model for most of the parameter variation studies would probably have delivered the most valuable outcome, the number of possible analyses with the panel model is limited due to its long computation time. Thus, smaller, efficient models have been used to perform most of the sensitivity study analyses, which enabled the variation of parameters and a direct comparison of the results. However, the performance of the detail models could be judged in relation to the respective model and could not be fully related to the panel model. A final series of analyses was done with the full panel model to verify several indications given by the detail model analyses. These panel analyses enabled the elimination of several factors the model might have been sensitive to.

<u>Panel model</u>

The panel model, shown in Figure 85 is the base FE model which was used for the prediction of the CODAMEIN II test (see 6.2).

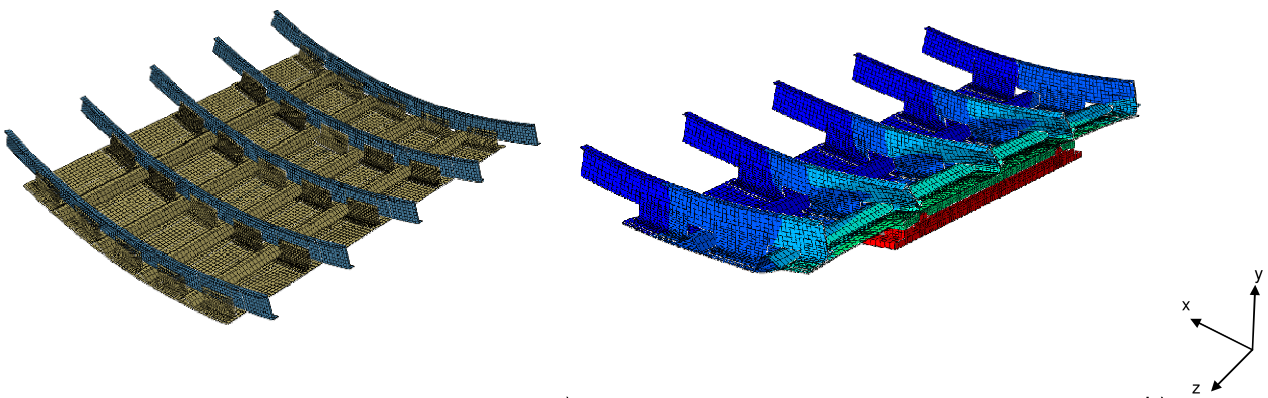

a) b)

Figure 85 Panel model (a)), cut view of deformed panel model (b))

Shear tie model

For the assessment of the damage behaviour of the cohesive connections and of the composite material, a model of a single shear tie has been used. Analogue to the panel model, this shear tie was modelled as two layers of continuum shell elements. Thus, delamination as well as in-plane damage and failure of the used composite material could be tested with this model, shown in Figure 86.

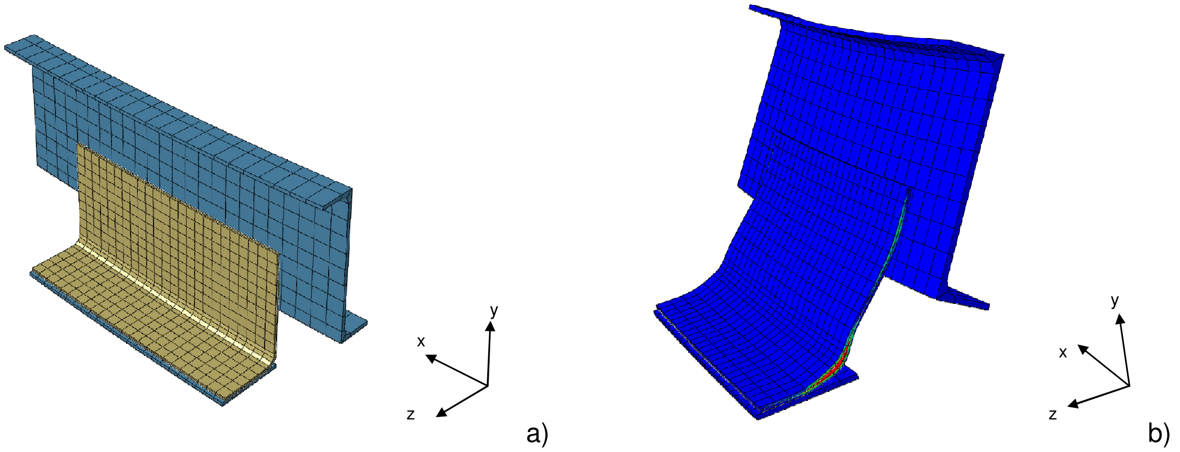

Figure 86 Shear tie detail model (a)), deformed / debonded shear tie detail model (b))

Sub-model: single shear tie

As an improvement of the single shear tie detail model, a sub-model of the panel centre region was generated using the Abaqus sub-model approach. While the single shear tie model was loaded with a simplified bending load case, this sub-model used the displacement output of an analysis of the complete panel model as displacement input and thus enabled more realistic boundary conditions and loading. The sub-model is shown in Figure 87.

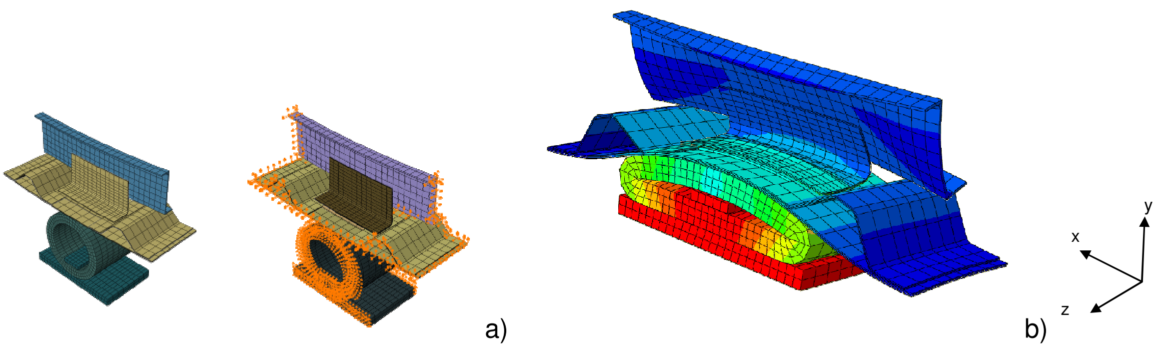

Figure 87 Shear tie sub-model (a)), deformed shear tie sub-model (b))

Bumper compression model

After a solution was found to integrate an undeformed circular rubber bumper in the panel simulation and thus to simulate the compression and the resulting pressure distribution on the skin of the panel, the load-displacement behaviour of the circular bumper was assessed using different rubber stiffnesses. A model in which the rubber bumper was pushed against a rigid surface, was used for this examination (see Figure 88). This model also delivered the amount of energy which is needed to compress the rubber bumper.

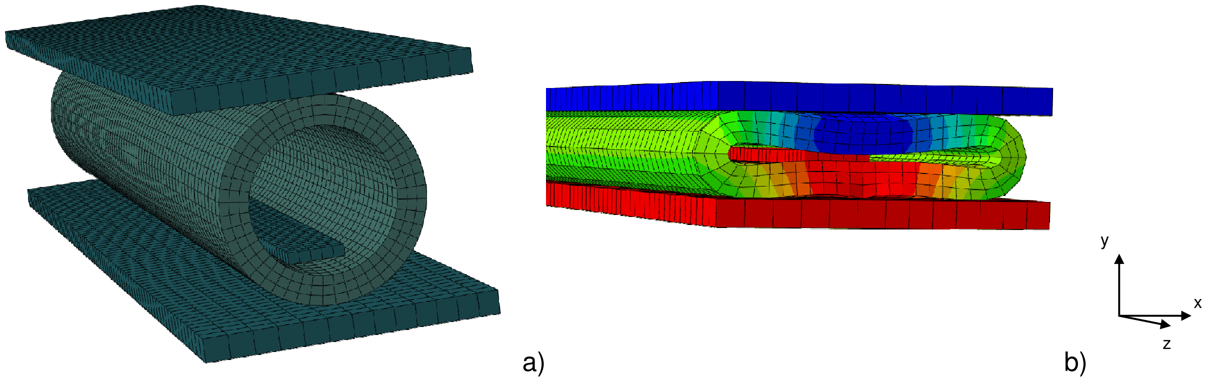

Figure 88 Bumper compression model (a)), deformed bumper compression model (b))

DCB, ENF model

Simulations of coupon interlaminar fracture tests have been performed to assess the accordance of a FE model to test results. Based on test data for a composite material and lay-up, different to that of CODAMEIN II, models of a standard double cantilever beam (DCB, see Figure 89 a),c)) and an End Notch Flexure (ENF, see Figure 89 b),d)) specimen have been created.

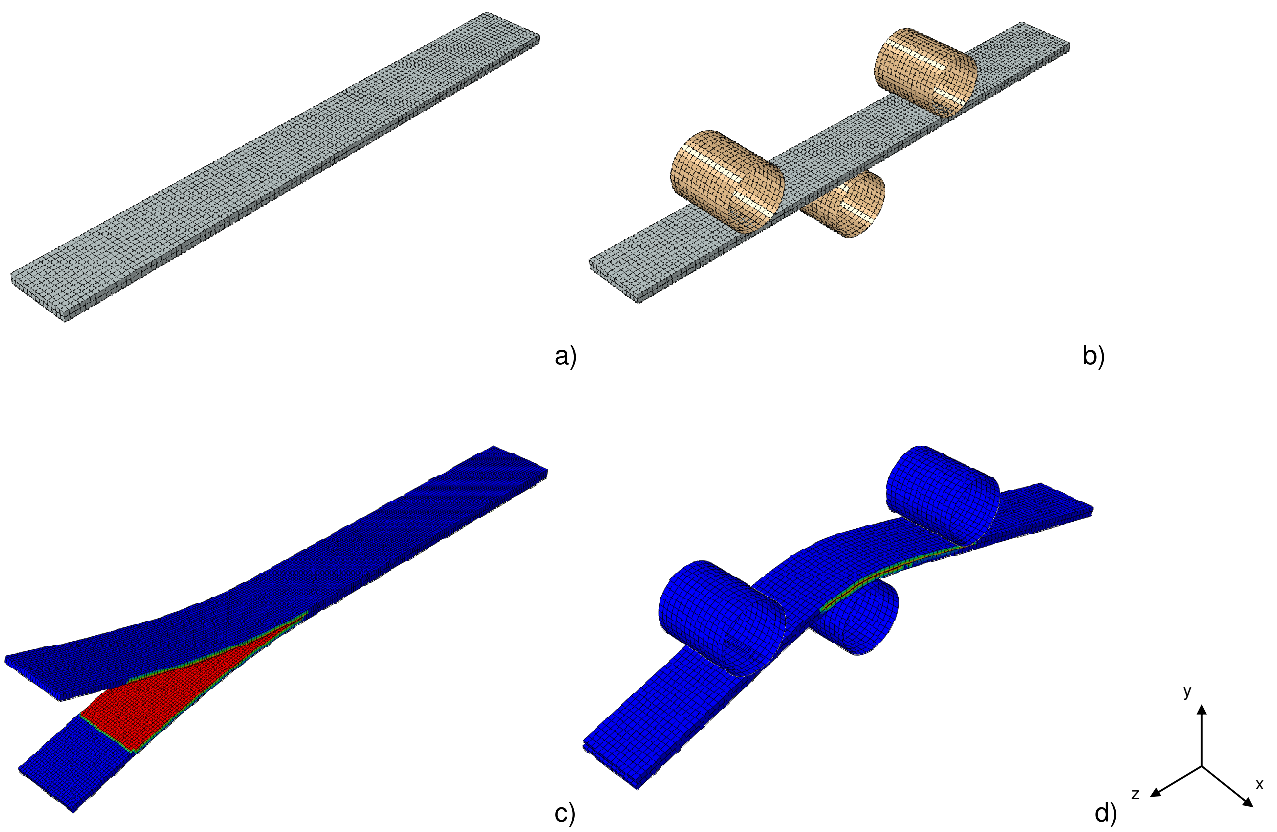

Figure 89 DCB (a)) and ENF (b)) model, deformded, debonded DCB (c)) and ENF (d)) model

6.3.2 Results of the sensitivity study

The parameters of the test panel FE model that were expected to have main influence on its response to the blunt impact loading, have been tested in the sensitivity study. Those parameters are:

- 6.3.2.1 Element size
- 6.3.2.2 Loading rate
- 6.3.2.3 Mass scaling
- 6.3.2.4 Strength of the adhesive surface
- 6.3.2.5 Damage progression of the adhesive material
- 6.3.2.6 Strength of the composite material
- 6.3.2.7 Damage progression of the composite material
- 6.3.2.8 Shear tie strength
- 6.3.2.9 Stiffness of the rubber bumper
- 6.3.2.10 Impactor mass

Several parameters that were assessed within the sensitivity study using detail models did not deliver outcomes which could be directly transferred to the panel model. Thus several additional analyses have been done subsequently on the panel model. The outcomes of these panel simulations are described within the results of the panel FEA (6.4).

6.3.2.1 Element size

The element size for the panel model was chosen with the aim to achieve the largest possible elements while respecting all geometric features which were judged meaningful. Thus, the bending radius of the shear ties has been modelled using three circumferencial elements to gain a maximum of information in this most critical region. Along the section of the stringer, each one element was added to represent the radii and to smooth these transitions. The elements in the radii of the shear ties and the stringer parts drive the incrementation of the explicit analyses.

A local refinement was done for the shear tie foot and flange to permit a less restricted deformation of the softening shear tie material after damage onset at the bending radius. The refined elements did not reach the size of the elements in the radius.

The influence of the mesh size was assessed by analyses with the DCB model. Especially for the debond process, the element size showed significant influence. When using a fine mesh (element size = 1 mm), the debond progressed relatively smooth still with several rows of nodes disconnecting at one time. When using a coarser mesh (5 mm, up to 10 mm), a much more noisy load-displacement behaviour is generated. A much higher force threshold has to be reached to debond a node row. The number of node rows that debond at one time, is at least as high as for the finer mesh, which means that a significant length gets debonded at one time, which in dynamic analyses also causes significant acceleration and vibration of the debonded regions. The load-displacement chart in this case shows a much higher damage onset load and much more noise than for the finer mesh. Figure 90 shows the DCB model with an element size of 10 mm, unloaded and with an opening of approx. 20 mm. These two states are also depicted for a DCB with an element size of 5 mm (see Figure 91) and an element size of 1 mm (see Figure 92).

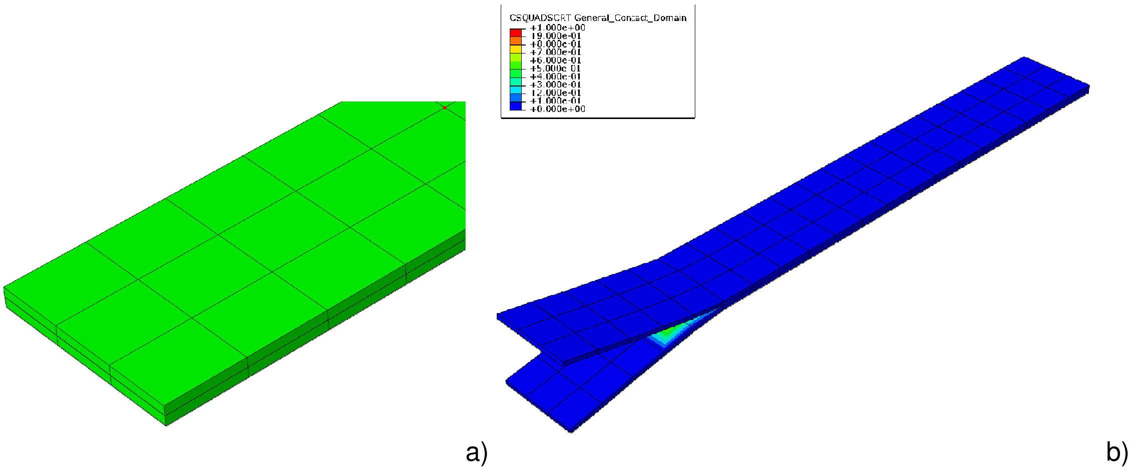

Figure 90 DCB: element length = 10 mm, unloaded (a)), opened 20 mm (b))

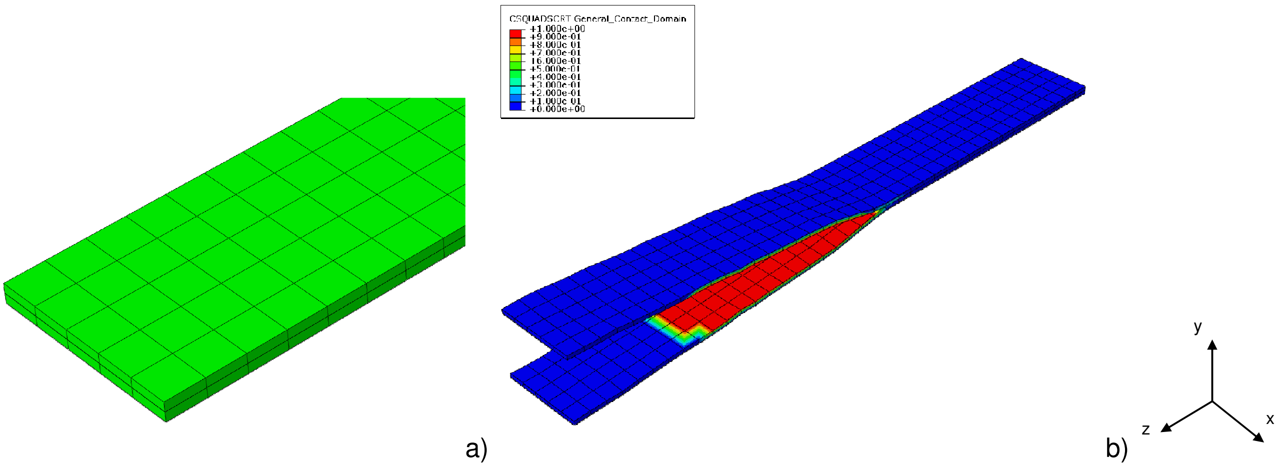

Figure 91 DCB: element length = 5 mm, unloaded (a)), opened 20 mm (b))

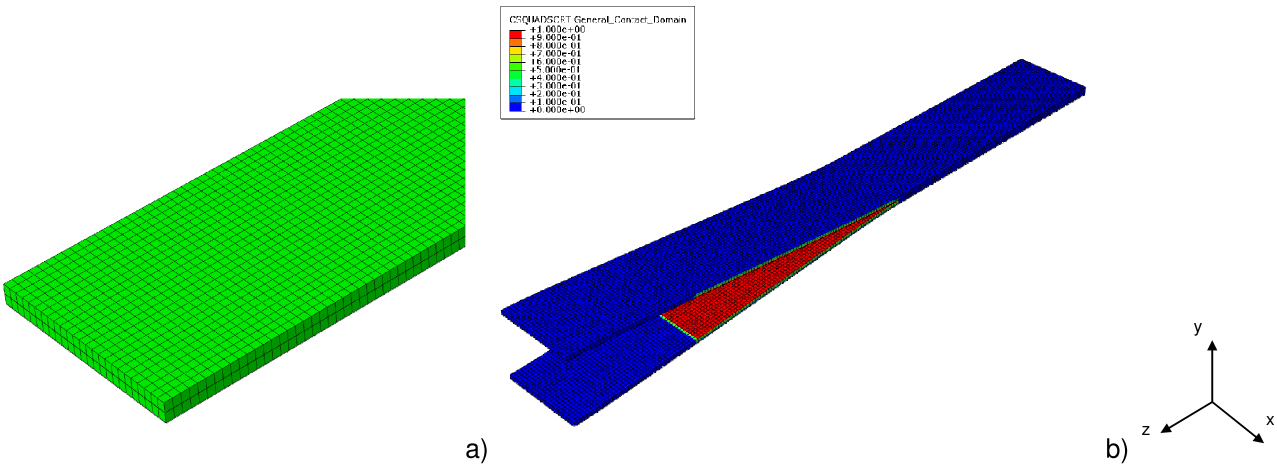

Figure 92 DCB: element length = 1 mm, unloaded (a)), opened 20 mm (b))

The shear ties of the panel model which are the most prone parts to delamination, have an element size between 4 mm and 15 mm. The smallest elements are located in the radius which is the region of typical damage onset in this application (see Figure 93).

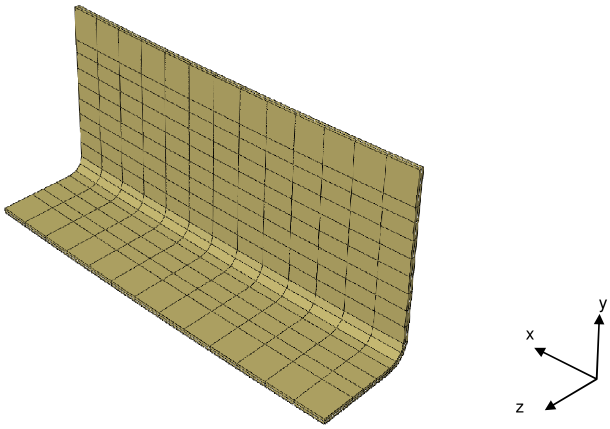

Figure 93 Shear tie of the panel model

The load-displacement chart in Figure 94 shows the slopes of DCB simulations with different element sizes. This chart clearly shows that a larger element size, within a debond process, causes several node rows to fail simultaneously. This implies a higher load that is necessary to initiate a partial failure of the bondline and a high level of noise due to vibration since high strain levels get released each time. The DCB simulations visualized in this chart implied non-typical DCB boundary conditions. Thus, the chart depicts the different response of different element sizes, not the typical DCB load-displacement behaviour.

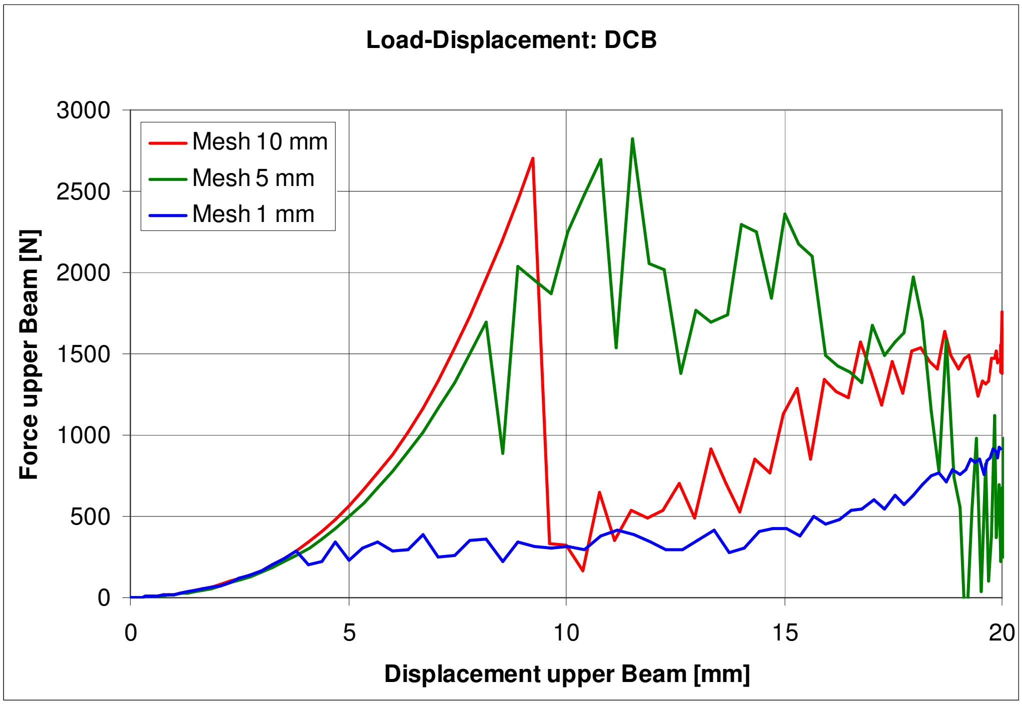

Figure 94 Load-Displacement of DCB analyses with different mesh sizes

The studies that have been performed on the debond behaviour indicate that a finer mesh would improve the debond behaviour which reflects delamination in the panel model. For the performed panel analyses, the mesh was not refined based on the sensitivity study with the detail models. Due to its overall size, the element size of the panel model is limited to a minimum element size that keeps the overall model manageable. To be able to perform FE analyses with the panel model using reasonable levels of computation power and time, also mass scaling was used in a limited range. See the sensitivity study item “c) mass scaling” for explanation.

6.3.2.2 Loading rate

The chosen impact velocities of the FE analyses were limited by the overall computation time. In order to reach a feasible analysis time for the panel model, the impact velocity of 1m/s was used. This is a higher loading rate than that of the test (25 mm/s, 2 mm/s). No clear information could be gained from a test simulation that was done on the panel model and a loading rate that was 10% (100 mm/s) of the original loading rate. No completed solution was achieved after a significant computation time. In contrast to the simulation using the original loading rate, earlier load peaks were found while the shear tie failure was not reached in this test (see Figure 95).

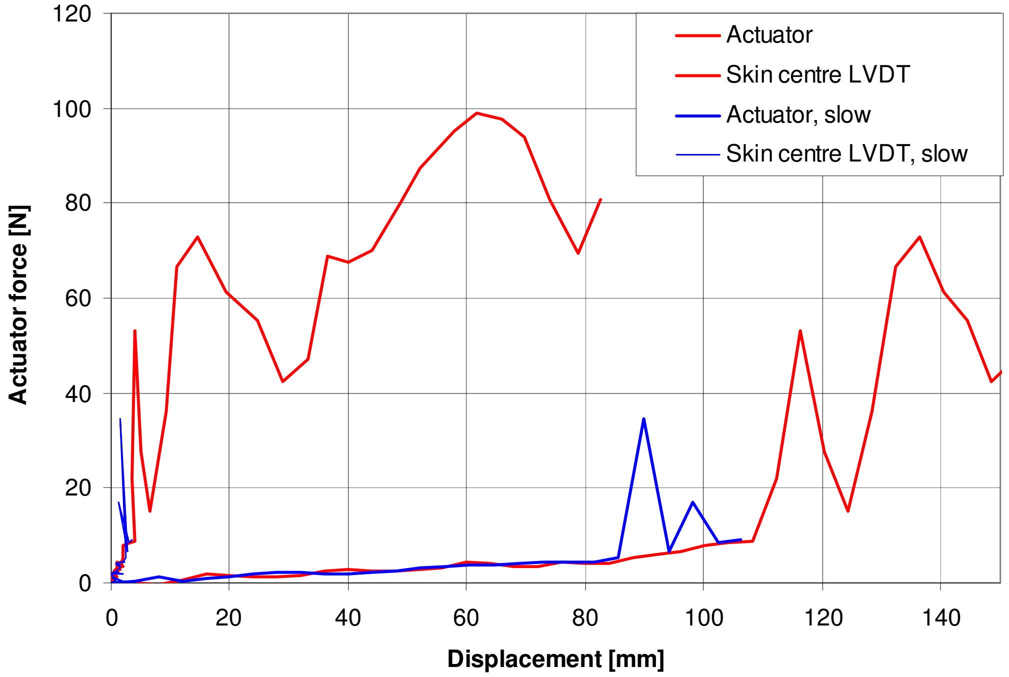

Figure 95 Load-displacement: original, reduced loading rate

Generally, a lower loading rate of the analyses would have required a much higher level of mass scaling which is expected to be highly adverse for the quality of the gained results.

6.3.2.3 Mass scaling

The mass scaling option of the Abaqus Explicit solver was used to reduce the computation time. This option increases the mass of the most critical elements within the model artificially to increase the critical time increment and hence to reduce the computation time. The mass scaling settings have been chosen to allow the increase of mass for the most critical elements, which are located in the shear tie and stringer radii for the panel model, by a maximum factor that did not exceed 10. This level of mass scaling is expected to have sufficiently small influence on the behaviour of the panel model. The actual effect is an increased inertia for the affected regions. Detail models in which the cohesive interaction was investigated, tended to undergo hourglassing effects. These models, when simulated with higher levels of mass scaling, led to significant hourglassing modes in the cohesive zones. This effect could not be eliminated by any tested modelling technique. Yet in the panel model with its level of mass very localised scaling, elements did not show that tendency towards hourglassing modes. Figure 96 shows the load-displacement chart of two performed DCB analyses, without mass scaling and with a uniform mass scaling factor of 25. The damage onset stress and the slope of material degradation are not changed by the mass scaling. Yet it generates significant noise in the chart. At every debonding of node pairs, the scaled mass causes vibration which influences the subsequent debonding steps.

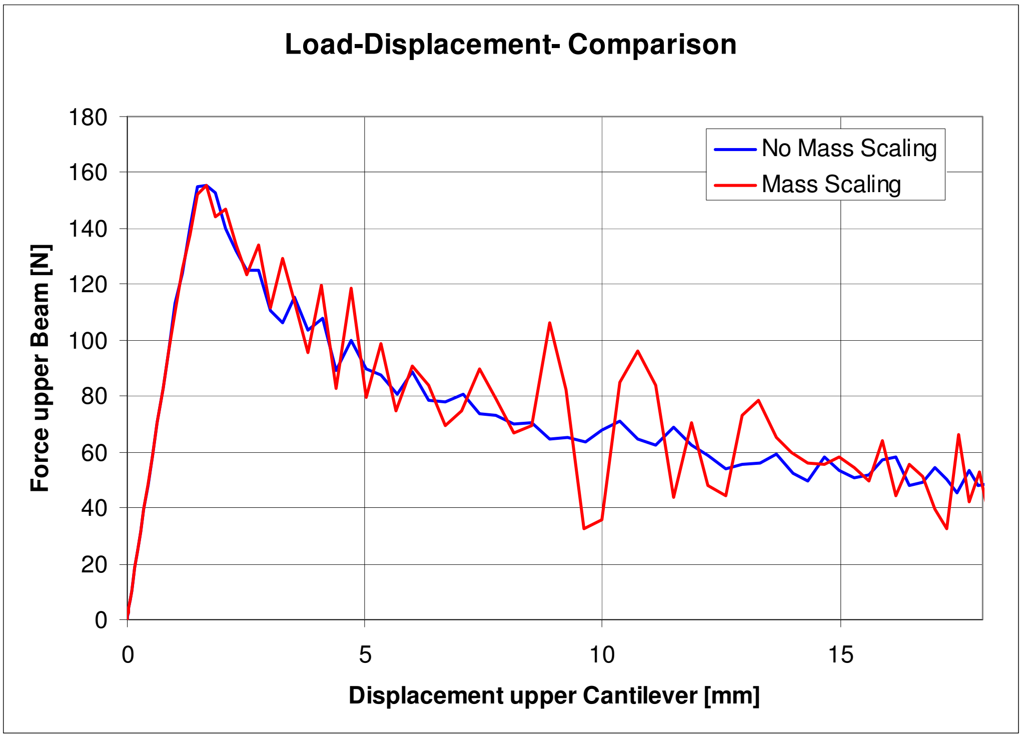

Figure 96 Load-Displacement of DCB analyses: with and without mass scaling

To verify the influence of mass scaling on the panel model, an analysis without any mass scaling was done. The global load-displacement chart (see Figure 97) shows no deviation between these two analyses.

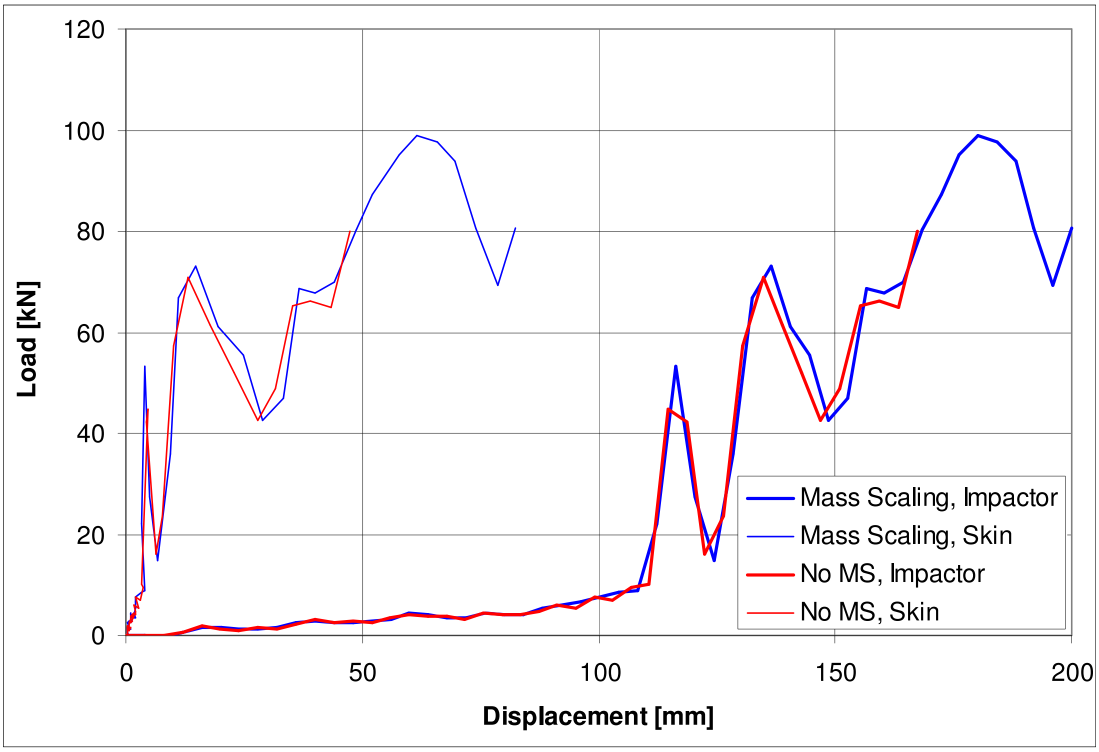

Figure 97 Load-Displacement: Panel model with / without mass scaling

6.3.2.4 Strength of the adhesive surface

To respect delamination damage and failure in the panel FE model, the parts relevant for this kind of damage / failure were modeled using two layers of continuum shell elements. The two layers were connected with a cohesive surface formulation which enabled damage in terms of physical separation of the two layers, as displayed in Figure 98.

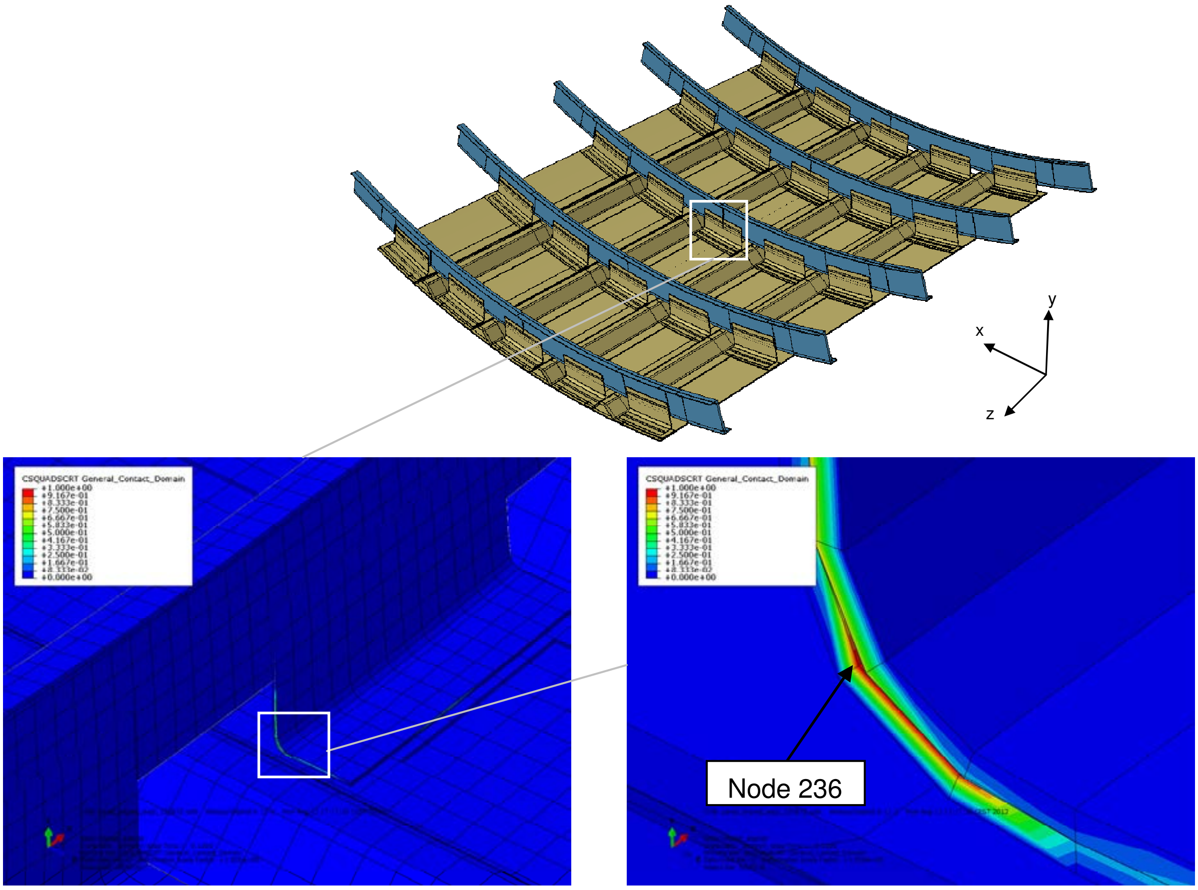

Figure 98 Delamination of a shear tie: failure criterion output

For the integration of the cohesive surface, the thickness of the relevant parts was split into each two halves of identical thickness containing each one half of the respective composite lay-up. The properties of the cohesive surface connecting the two element layers of each lay-up have been defined in terms of an uncoupled traction separation law. The quadratic stress criterion was used to define damage of the cohesive surface. Damage evolution was implemented using the linear energy law (see Abaqus Analysis User's Manual 23.3.3 [Abaqus, 2012]).

The used material parameters for damage onset stress and damage progression energy release rate could not be tested against material test data. The performance of the FE analyses was investigated using data of Double Cantilever Beam (DCB) and End Notch Flexure (ENF) coupon tests [ACS Australia, 2012]. The materials in these tests were different to the ones used for the CODAMEIN II panel. The DCB and ENF FE models were created according to the parameters of the available test data. Their response could be assessed according to the test results.

Increasing the cohesive strength by 1.5 had only small influence on the response of the Shear Tie Sub-model. In this model, only the centre shear tie was affected by the variation. The global response of the underlying panel model remained identical. The sequence of the damage criterion is shown for a node in the shear tie outer part's radius (see Figure 98). A node at the shear tie's edge was chosen since the cohesive damage starts at the edges of the centre shear tie. As shown in Figure 99, the damage sequence is only slightly delayed by the modification.

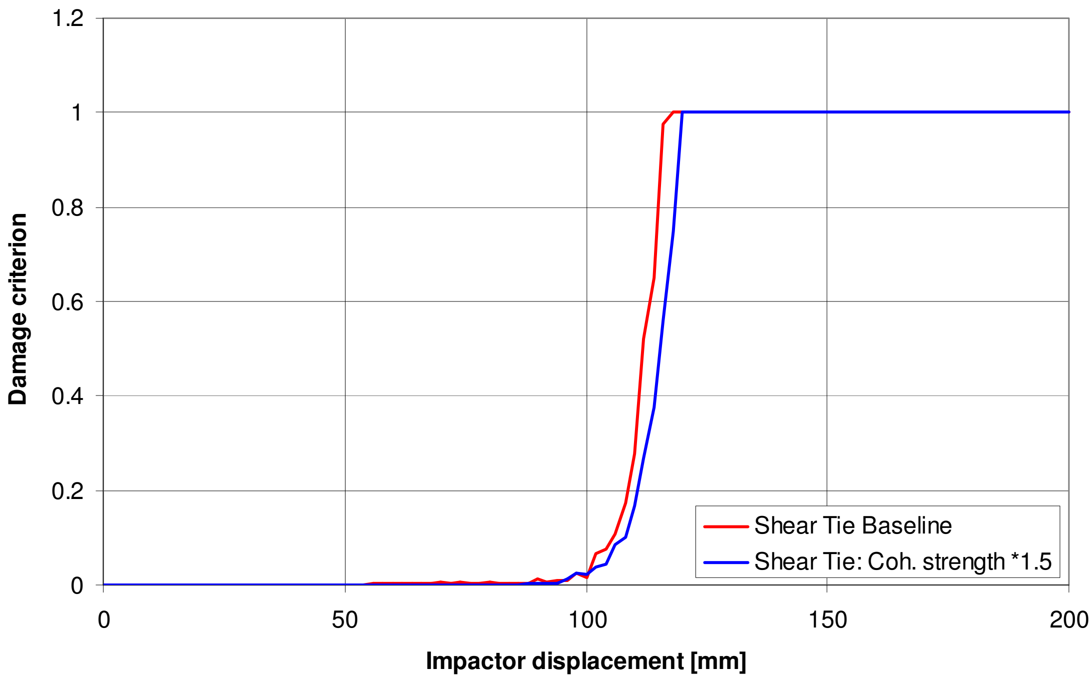

Figure 99 Shear tie delamination onset in sub-model, radius, edge

A further assessment of the strength of the cohesive surface was done using the ENF model. Since the ENF model was defined to represent a test performed by ACS Australia, it implied material properties and a composite lay-up that are different to those of CODAMEIN II. E.g. the cohesive surface strength of the ENF model was lower than that of CODAMEIN II. Since the material parameters are still in the same order of magnitude, the influence of changes of the cohesive properties can in principle be transferred to the materials of CODAMEIN II. As shown in Figure 100, an increase of the cohesive strength by the factor 2 or even factor 3.5 has an influence on the point of damage onset. Yet very high variations are necessary for significant changes in the ENF response. Apart from the relevance to CODAMEIN II, a main outcome of the simulation of the present ENF test was that the cohesive strength must be significantly increased to approach the specimen response of the test.

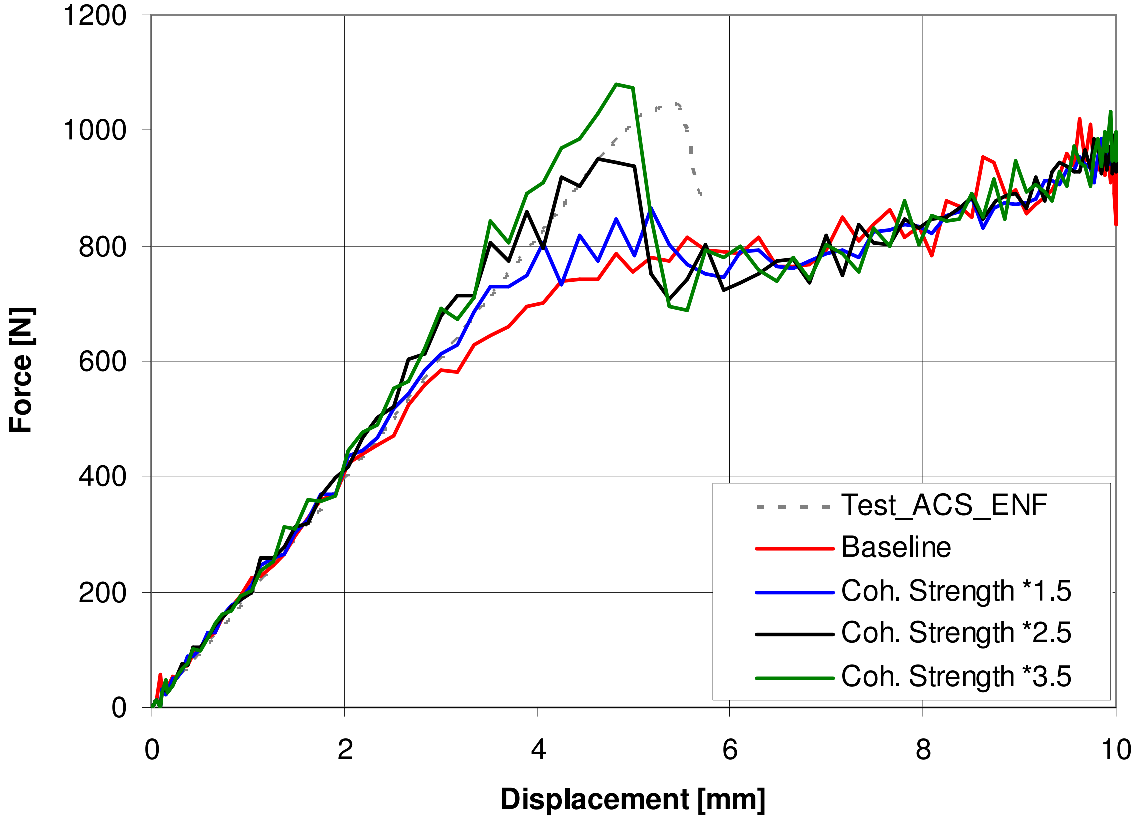

Figure 100 ENF test, FEA: different cohesive strengths

6.3.2.5 Damage progression of the adhesive material

The DCB test generates cohesive damage and failure in mode I. The comparison of the FEA and the ACS test data showed a significantly different pre-damage stiffness which ACS explained to be expectable due to the limitations of the test. The damage sequence however showed good accordance. The stress level of damage onset was slightly overestimated by the FEA. The comparison with FEA using twice respectively half of the energy release rate indicated that a reduction to 75% would have matched the test best. The damage parameters could be adjusted for a specific mesh size to match the test result. This could be done in future work. The load-displacement chart of the test and the simulation is depicted in Figure 101.

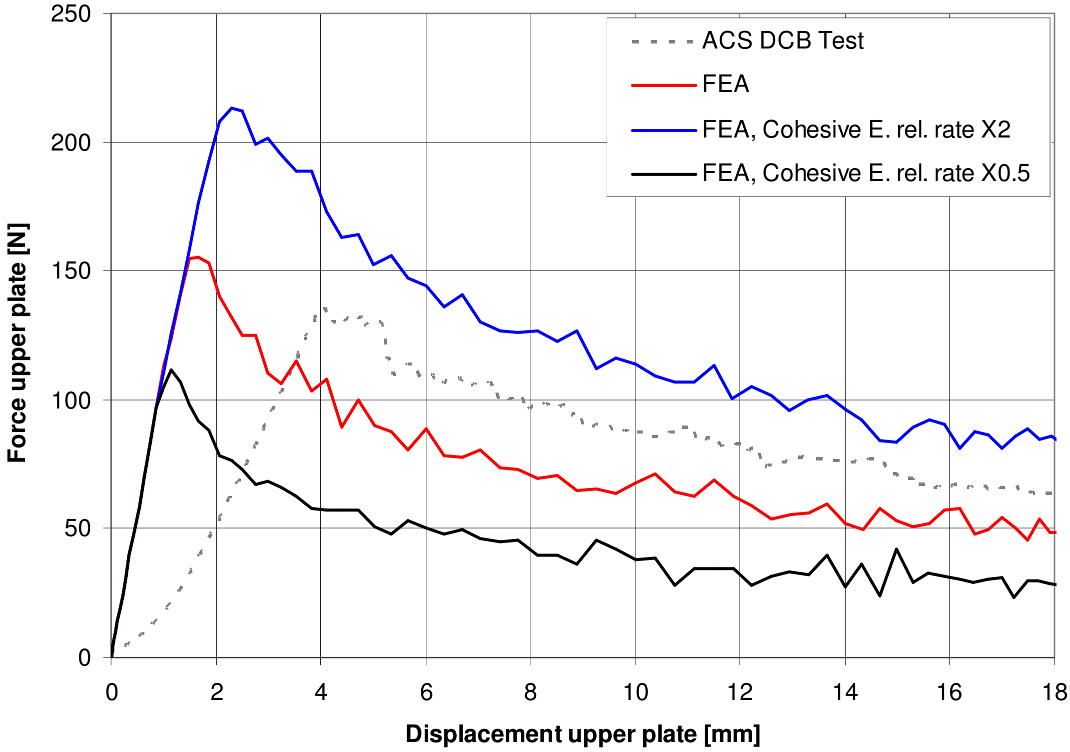

Figure 101 Load-Displacement of the DCB test and analysis

In the ENF test, the cohesive fails in mode II. Due to the short and progressive damage phase up to failure, it is more complicated to match the typical ENF load-displacement slope with FEA, compared to the DCB test.

While the comparison with the DCB test indicated that the energy release rate values should be slightly decreased, the ENF comparison indicated an increase of the energy release rates or of the strengths. Since increasing the energy release rate (factor 3.5) only changed the damage progression phase slightly, the strengths were instead increased (factor 5) which lead to a better match with the test load-displacement chart. See a load-displacement chart of the test and several FE analyses below.

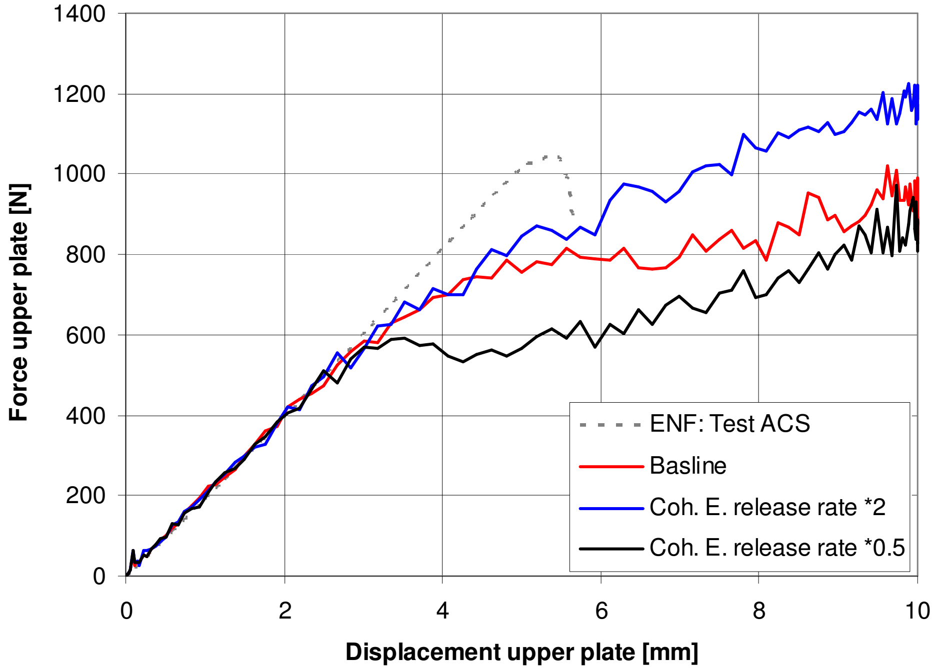

Figure 102 Load-Displacement of the ENF test and analysis

Hence no final tendency for an over- or underestimation of the damage progression can be taken from this assessment, performed on the DCB and ENF test information from ACS, using different material and lay-up than CODAMEIN II. To reduce deviations in the behavior of the FEA, caused by the FE modeling, the FE panel model is compared to the CODAMEIN test data. The usage of the smaller detail models and sub-models could not be used to gain clear information for the adjustment of the cohesive damage parameters.

6.3.2.6 Strength of the composite material

The composite material damage onset (strength) and damage propagation parameters were varied using a sub-model of the centre region of the panel, including one shear tie. The damage behavior of the shear tie under the present loading which was derived from the deformation of a panel analysis, has been changed in a limited range. For all parameter studies using the shear tie sub-model, the change of the response was limited by the boundary conditions at all cut-out surfaces, which were identical for all performed analyses. The strength parameters of the used Hashin damage criterion were varied as a set for both the UD and the fabric material. The point of damage onset was thereby changed. Also the mode which set on damage first, changed partially. Three cases of this study with their respective points of damage onset are shown below. With the original material parameters, the sub-model failed at 118 mm of impactor displacement in fibre compression mode at one outer edge of the radius (see Figure 103).

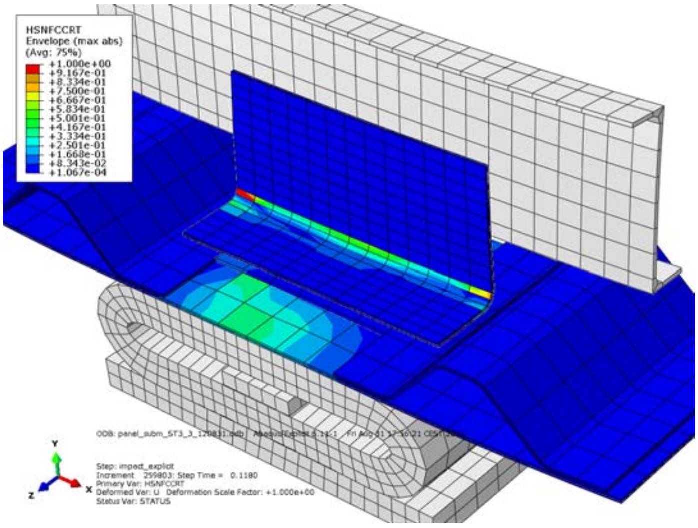

Figure 103 Shear Tie sub-model: ST damage onset, original material parameters

After increasing the strength values of the two composite materials by the factor 1.5, damage onset was found at 130 mm of impactor displacement, also in fibre compression mode and at the outer edges of the radius (see Figure 104).

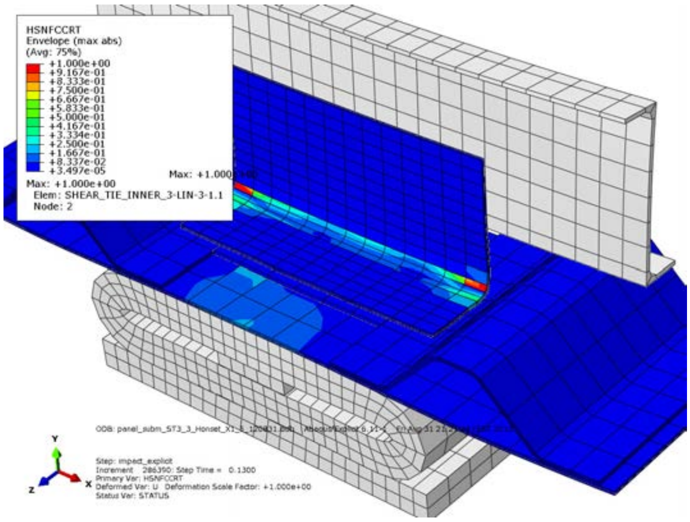

Figure 104 Shear Tie sub-model: ST damage onset, composite strength *1.5

The strength of the two composite materials was reduced to one half of the original values. This modification led to a significantly earlier damage onset. Fibre compression damage set on in the shear tie radius at an impactor displacement of 58 mm (see Figure 105). In this configuration, material damage set on even earlier in the skin, at both sides of the shim pad-up underneath the shear tie. This kind of damage was not found in the panel model or in the test and might be related to the sub-model boundary conditions in connection with modified material properties.

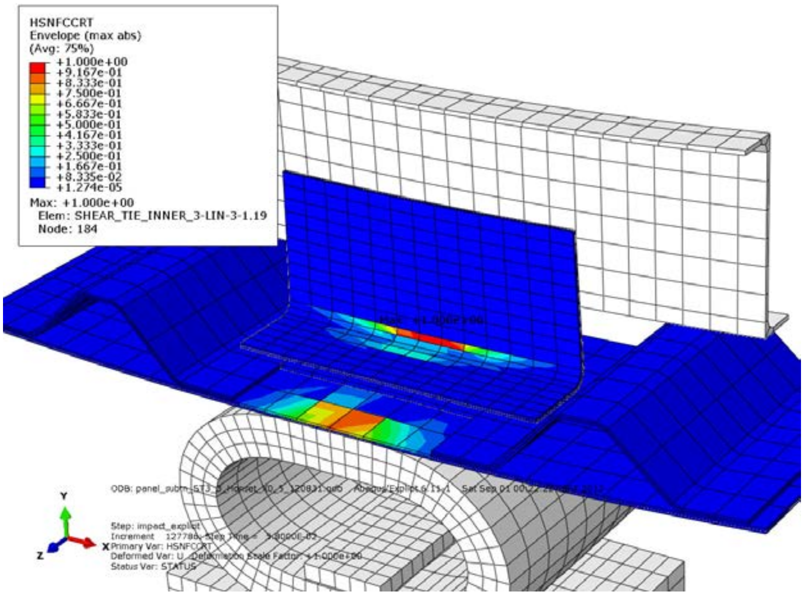

Figure 105 Shear Tie sub-model: ST damage onset, composite strength *0.5

More appropriate information about the influence of changed properties of the composite material on the response of the structure can only be derived from analyses of the panel model.

6.3.2.7 Damage progression of the composite material

The variation of the energy release rates of the composite materials which govern the damage propagation had only small influence on the response of the shear tie sub-model. The modification of all components of the energy release rates between 0.5 and 1.5 times the baseline value created a change in the deformation sequence of the shear tie which was not clearly visible. A difference gets obvious in the distribution of the damage parameters within the shear tie parts at high deformation. Figure 106 shows the distribution of the fibre compression damage parameter at an impactor displacement of 160 mm. Figure 107 and Figure 108 show the distribution of the fibre compression damage parameter at the same impactor displacement using a factor of 0.5 and 1.5 for the damage progression energy release rates.

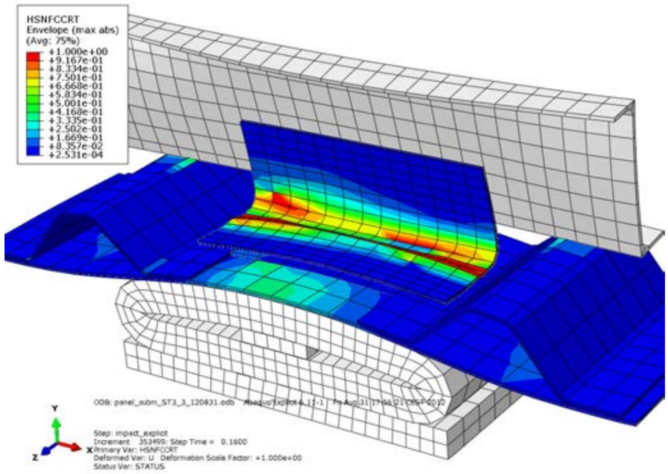

Figure 106 Shear tie sub-model: ST composite damage propagation, original material parameters

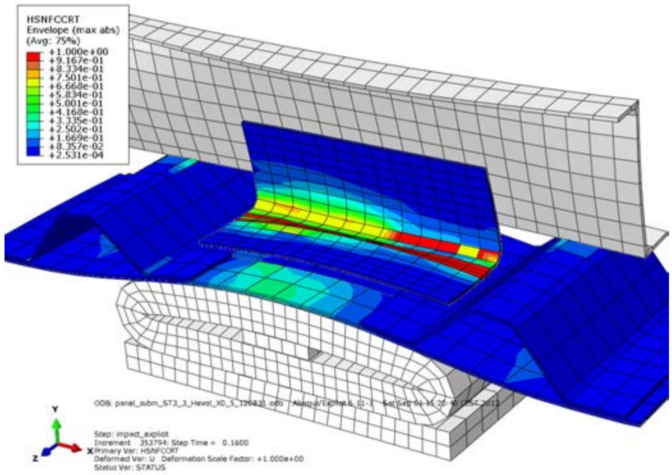

Figure 107 Shear tie sub-model: ST composite damage propagation *0.5

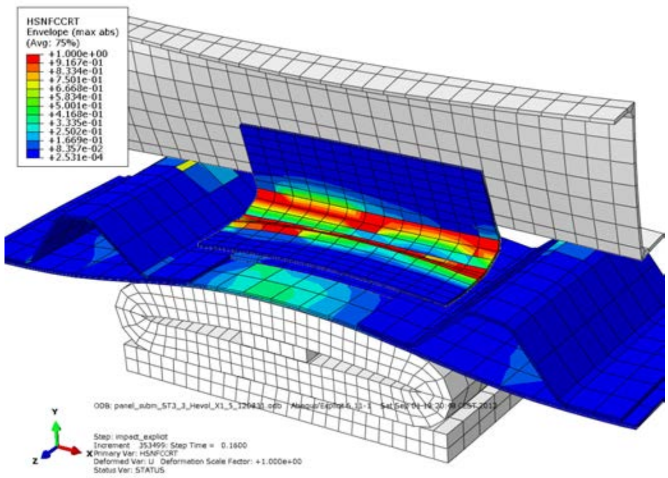

Figure 108 Shear tie sub-model: ST composite damage propagation *1.5

Figure 109 and Figure 110 show the displacements of the shear tie radius centre region for the three material configurations. The position of the displacements is marked in Figure 111. The displacement U2 in impact direction has a very similar slope for the three configurations (see Figure 109).

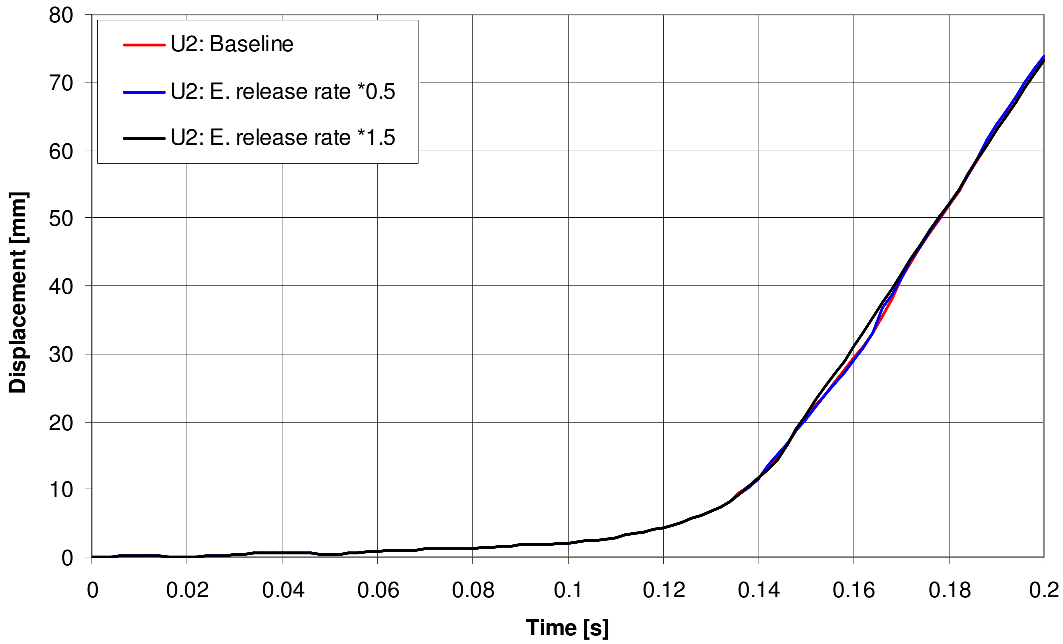

Figure 109 Displacements in impact direction: ST radius 3 material configurations

The displacement U3 in stringer direction shows more significant deviations of the three configurations slopes (see Figure 110). It illustrates how the damage propagation of the composite material influences the bending deformation of the shear tie radius.

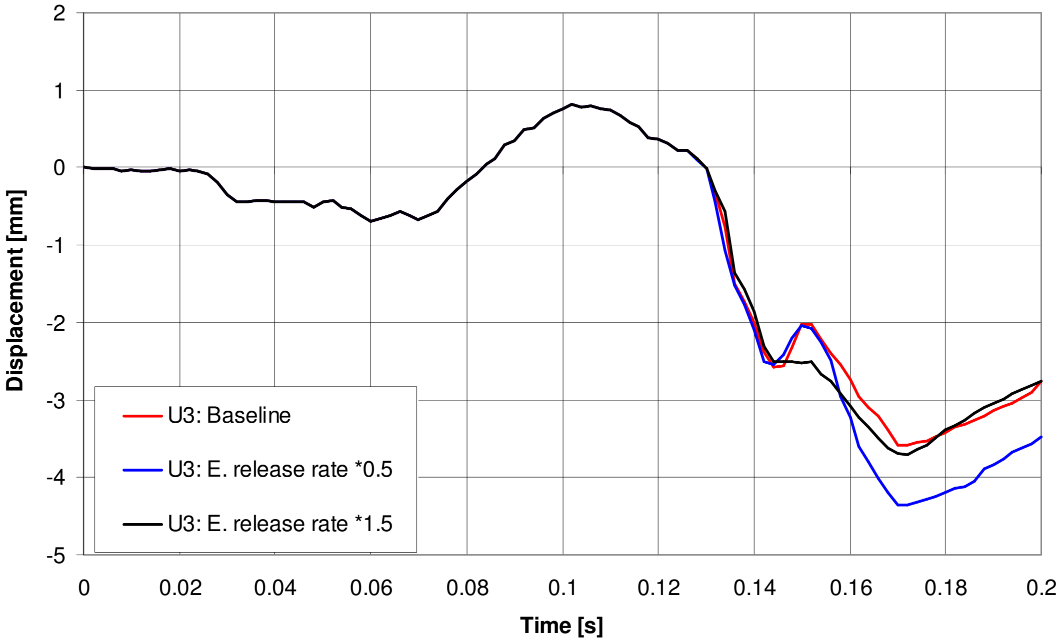

Figure 110 Displacements in stringer direction: ST radius 3 material configurations

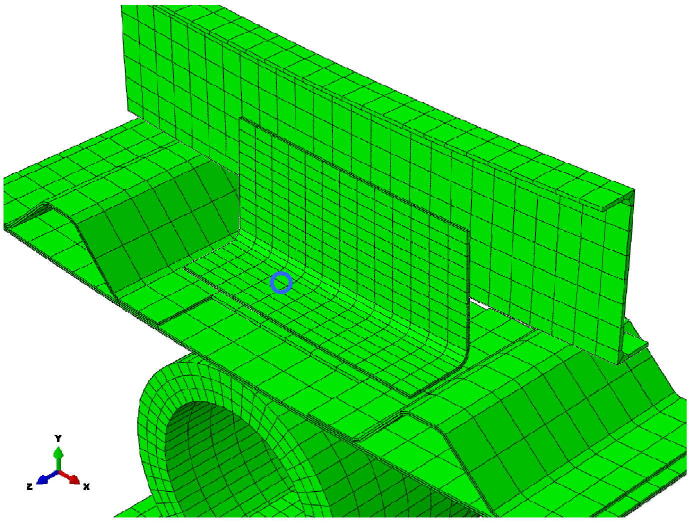

Figure 111 Shear tie sub-model: position of displacement outputs

Depending on the limited detail level of the mesh, the damaged elements soften and fold towards the skin (see Figure 112).

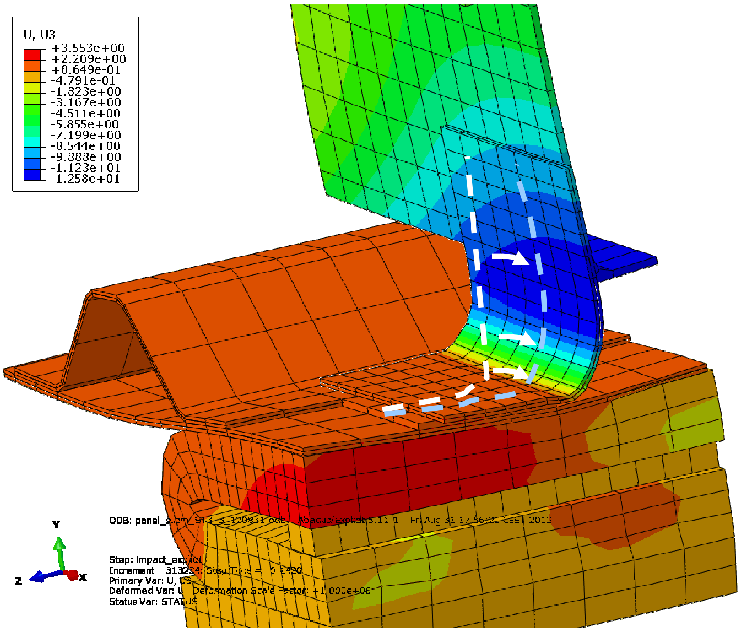

Figure 112 Shear tie deformation, cut view

The parameter study using the shear tie sub-model could give an indication of how the response of a composite part sustaining significant damage changes due to a variation of the damage propagation parameters. The influence on the response of the panel could only be assessed by performing analyses on the panel model.

6.3.2.8 Shear tie strength

It was found in the CODAMEIN test as well as in the tests of the UCSD, that the shear ties are the most prone parts to failure under the loading conditions which the rubber bumper generates. The option of using stronger shear ties was discussed. The information, how damage does form if the shear ties do not get damaged first, was of interest. The UCSD has performed tests using metallic shear ties which were significantly stiffer than the original composite shear ties. The influence of stronger shear ties on the CODAMEIN II panel has been assessed by FEA. For this simulation, the thickness of the shear ties was not changed. Instead, the stiffness and the strength of the composite material of the shear ties were increased by 50%. Simulations using the sub-model did not generate satisfying results. Due to the size of the sub-model and the constant boundary deformation, no change of the damage behaviour could be generated for this model. Analyses of the full panel model were used for the assessment of the influence of the shear tie strength. The load-displacement charts of the initial panel model, of the panel model with stronger shear tie and of the CODAMEIN test result are shown in Figure 113.

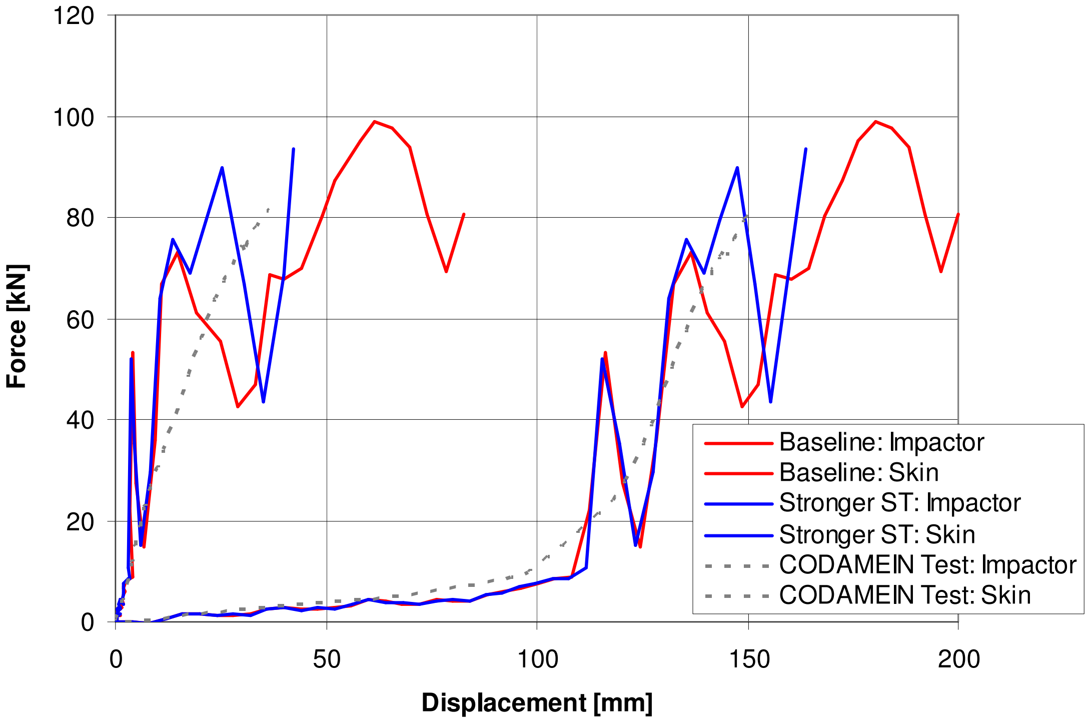

Figure 113 Load-displacement of FEA (baseline, stronger ST) and CODAMEIN test

The modification of the shear ties towards stronger parts was not sufficient to change the damage sequence of the panel model. The load level at the first shear tie failure was increased which led to an improved correlation of the FE analysis with the CODAMEIN test results. This result indicates that a significantly higher stiffness of the shear ties would be necessary to generate a different general damage sequence in the panel. To increase the stiffness and strength of the shear ties, their lay-up would have to be reinforced with additional plies as the used composite material is of typical aviation type. The L-shape of the used shear ties also offers possibilities for a change towards a stiffer design (e.g. T-shape or clip - and - cleat design).

The changed shear tie design that was tested by the UCSD, used Aluminium material an increased thickness by 25% and a modified geometry fitting two more rivets in the shear tie - frame connection. This modification increased the sustained load and changed the damage and failure occurrence (and thus the damage sequence). The shear ties did not fail any more. The frames also did not rotate significantly. Instead, the frames failed locally, in the region of the attachment of the load – transferring shear ties. As the frame – stringer contact was prevented, which finally led to full frame separation near the attachments in UCSD tests, the failure was then kept local in the region of impact. The general detectability did not change due to the shear tie modification.

6.3.2.9 Stiffness of the rubber bumper

Since no material test data for the rubber bumper was available and thus no hyperelastic properties could be defined for the rubber material, it was idealized as a linear isotropic material. To assess the influence of different rubber stiffnesses on the response of the circular bumper shape, a series of FE analyses was performed in which the rubber bumper was compressed against a quasi-rigid surface as displayed in Figure 114.

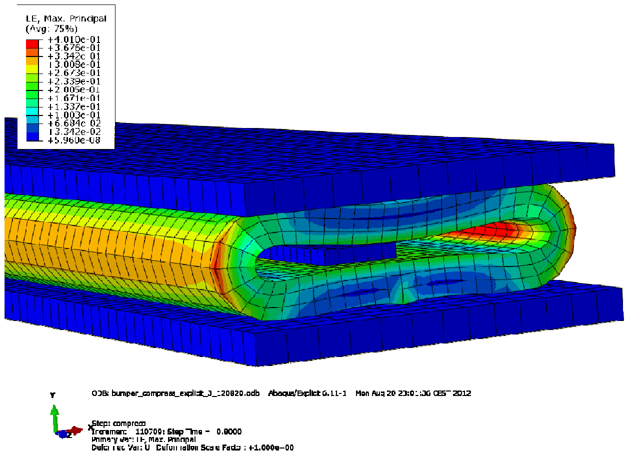

Figure 114 FE model of the compressed rubber bumper

The different Young's moduli (between 0.5 Mpa and 8 MPa) led to an almost linear relationship between the applied loads and the stiffness (see Figure 115). The force offset that is obvious in Figure 115 was caused by the force that was raised by the steel attachment plate inside the rubber bumper which attached it to the support plate and acted counter wise to the compression force. An attachment force of 9000 N was used to fix the rubber bumper to the support plate and to cause the related deformation.

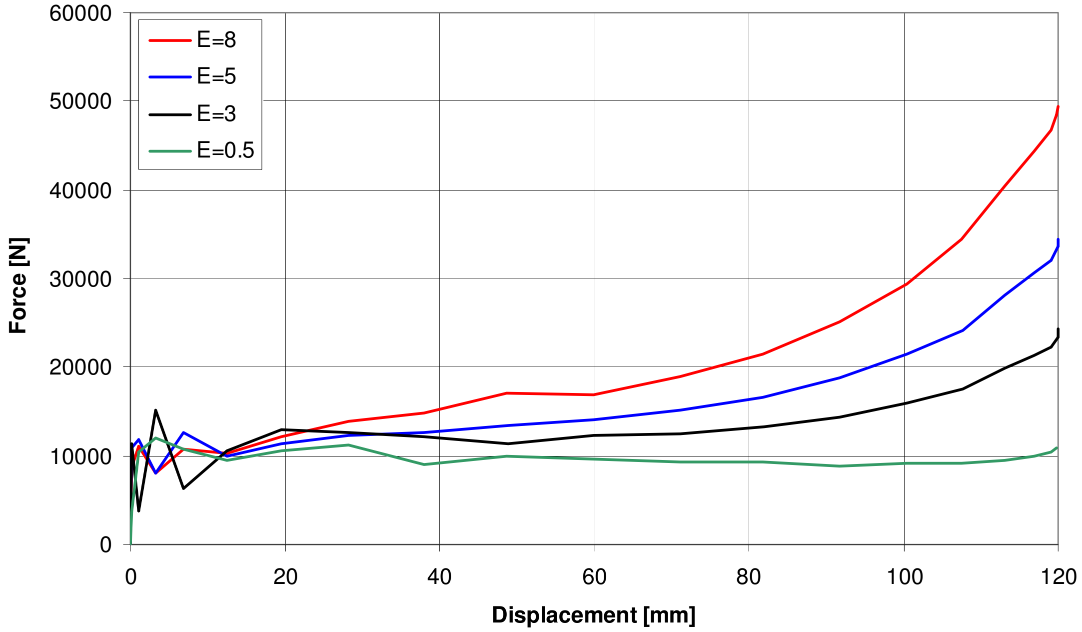

Figure 115 Load-displacement: Rubber bumper compression, different stiffnesses

The force that was applied to the attachment steel plate to fix the rubber bumper to the support steel plate was subsequently replaced by a connector force between the two steel plates. Thus the attachment force did not influence the loading of the impactor any more. Figure 116 shows two additional bumper compression analyses which imply the changed bumper attachment. That modification removed the force offset and also the load fluctuating at the beginning of the process.

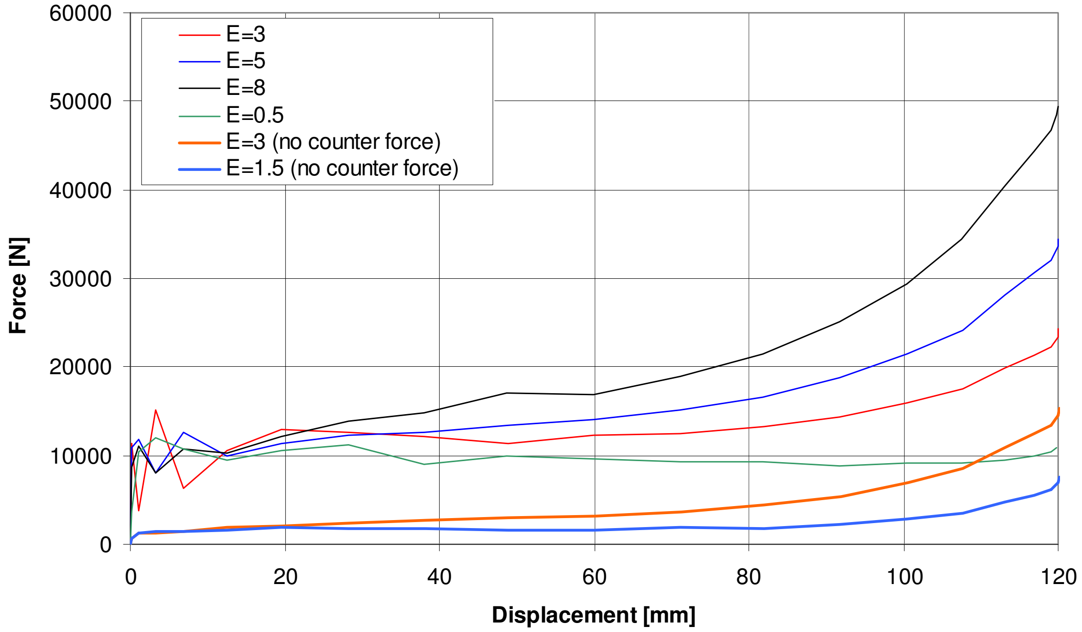

Figure 116 Load-displacement: Rubber bumper compression, changed bumper attachment

The rubber's Young's modulus of 3 MPa showed the best correlation of the panel model with the test results. The low rubber stiffness led to element distortion in the regions where the attachment bolts touch and compress the opposite side of the rubber bumper. Thus, the rubber the stiffness was locally increased to 8 MPa in these regions of the bumper which are exposed to small levels of bending only. A detail of the bumper assembly is given in Figure 117.

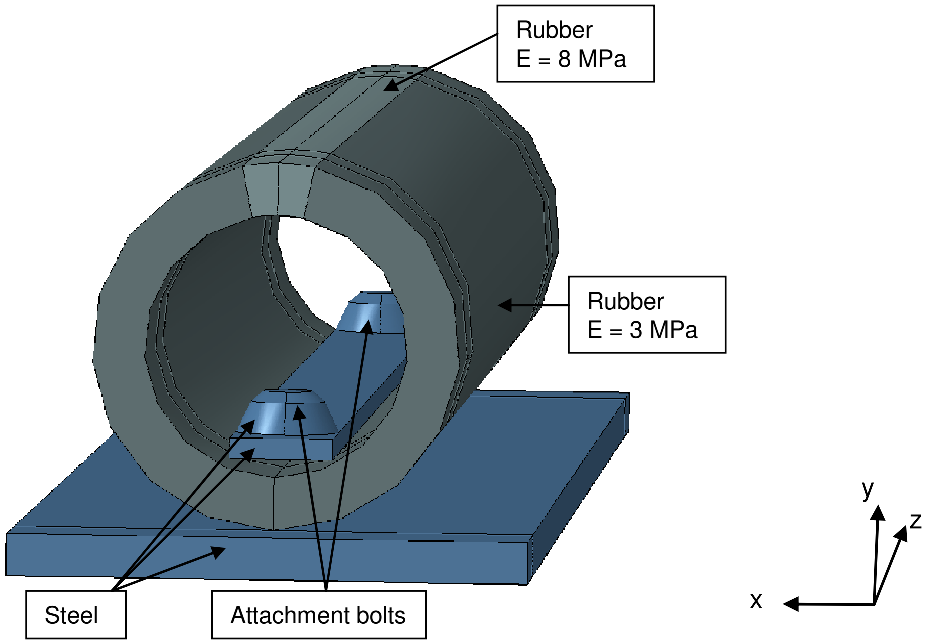

Figure 117 Rubber bumper and attachment

6.3.2.10 Impactor mass

The performed FE analyses with the panel model generated a load-displacement slope with an up-down peak in the range of full compression of the rubber bumper and of increasing load transfer into the panel (see Figure 113). In this region also the damage of the centre shear ties initiated. To evaluate the influence of the impactor mass on the panel response, this mass was increased. The increase of the impactor load was defined in combination with variations of the material parameters. In this way, the influence of the single material parameters on the panel response could be compared with the done detail model analyses. Based on the results of the detail analyses, the material values of the panel model were adjusted with the aim to improve the match between the panel FEA and test response. The significant change of the impactor mass did not influence the undesired peaks in the load-displacement chart. However the material adjustments which were done in the same process eliminated this effect and achieved an improved match of the FEA with the test results of the CODAMEIN test.

6.4 Results of the FE panel analysis

6.4.1 Panel response

The FE model of the test panel was developed to a state which provided a good accordance with the test panel behaviour. The global load-displacement as well as the relevant types of damage were represented by the FE model. Figure 118 shows the load-displacement relating to the actuator displacement and the skin centre displacement in actuator direction. The first peak of the charts represents the first major damage mode of the panel through failure of the centre shear ties. The subsequent frame-stringer contact allowed for further loading of the panel up to the global force peak at which point the frames started to massively deform plastically.

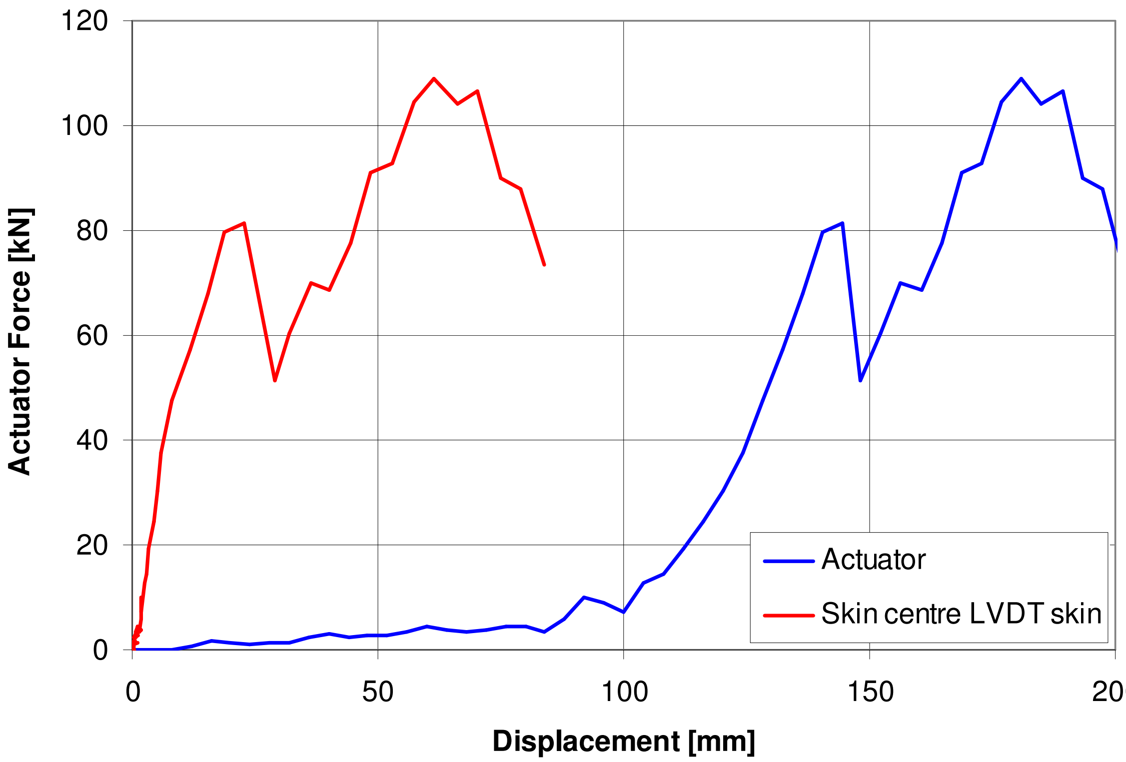

Figure 118 Load-displacement: panel FEA

To illustrate the tendency of deformation of the panel in the final state of the FE analysis, corresponding to an actuator displacement of 200 mm, it is shown in Figure 119.

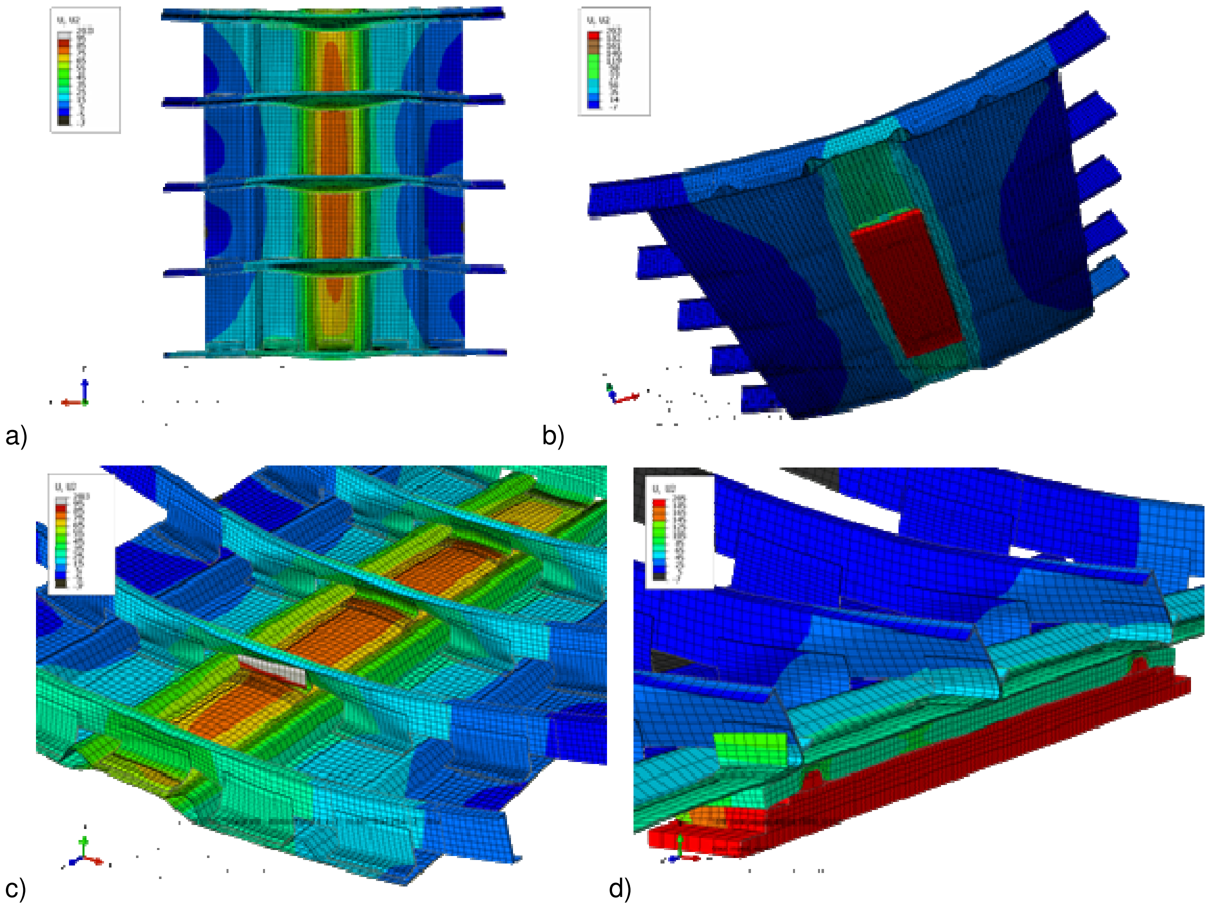

Figure 119 Deformed panel model displaying the impact direction displacement in 4 views

The maximum value of the used mass scaling was approx. 10 for the two centre stringers. This increased the overall mass of the panel model by approx. 3%.

6.4.2 LVDT comparison

A comparison of the load-displacement measured in the test and generated by the FEA is shown in Figure 120. The slopes of the load-displacement curves relating to the actuator displacement show good agreement. The FEA result exhibits minor dynamic influence on the results in the low load phase. The displacements measured at the skin centre, next to the shear tie ST3_3 show an offset between the test and the FEA which is expected to be caused by the material properties assumed for the rubber bumper. The rubber bumper was modelled using dimensions measured at the test bumper. The material was represented by simplified linear elastic material whose stiffness was adjusted within the FEA sensitivity study. Further adjustments were not done to the rubber bumper representation.

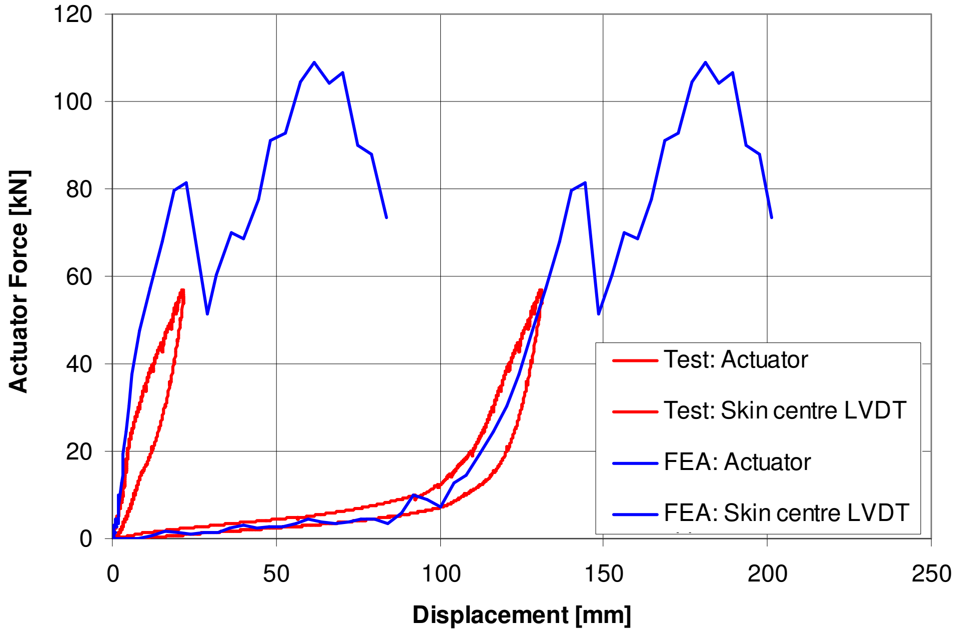

Figure 120 Load-displacement: FEA and Test

A first comparison of the detailed readings of displacements and strains of the test and the FE analysis is given below. The test data post-processing and reporting by the test lab is not finished yet. In this comparison, the FEA results are compared to the readings of the 2nd load cycle of the CODAMEIN II test.

The positions of the LVDTs that were used in the test, as well as their numbering are described in the chapter "Testing" and displayed again in Figure 121.

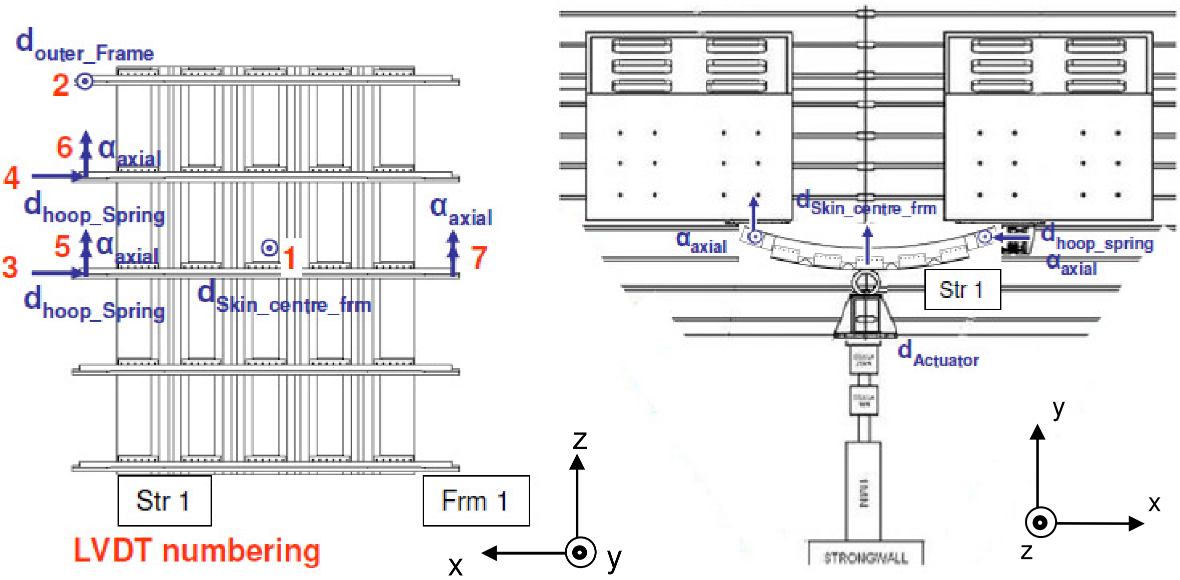

Figure 121 LVDT positions and numbering

In the comparison of the displacements measured by LVDTs (see Figure 122), the offset of the skin centre displacement is shown, which was also indicated by the global load-displacement charts of the test and the FEA. The displacement of the free end of frame 5 in the impact direction was not reflected by the FEA which showed a slight motion in positive impact direction instead of the negative motion measured in the test.

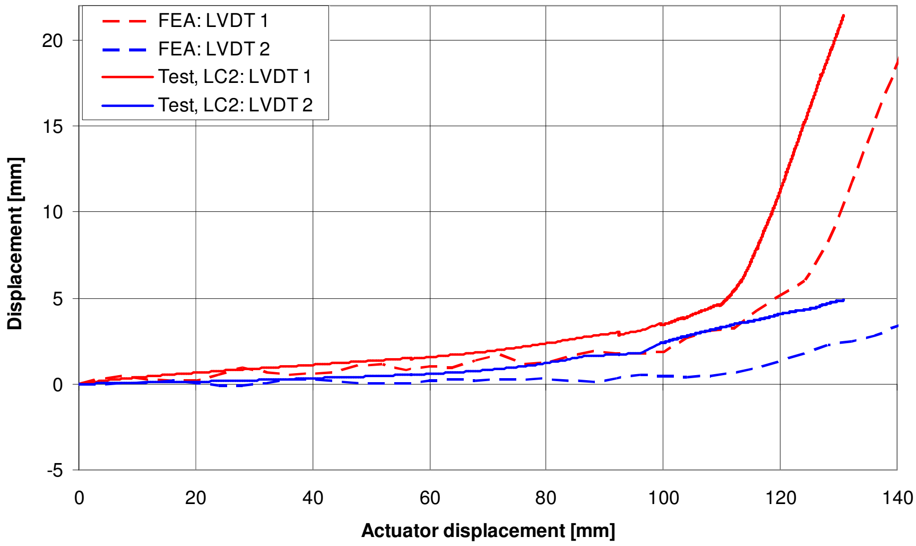

Figure 122 Test and FEA: Displacements of LVDTs 1,2

The compression of the spring-based test fixtures was significantly overestimated by the FEA. The general magnitude of compression was found to be very low (see Figure 123).

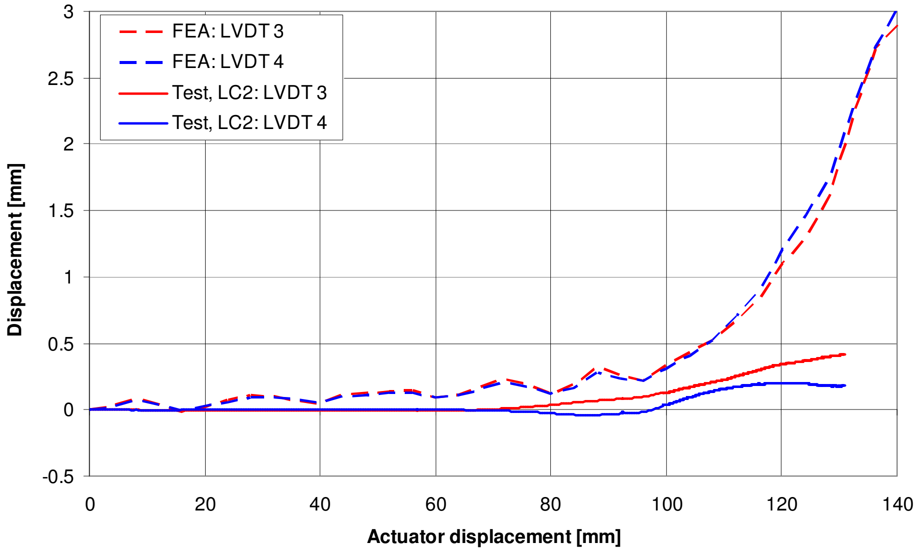

Figure 123 Test and FEA: Displacements of LVDTs 3,4

The LVDTs 5 and 6 which assessed the rotation of the frame ends 3 and 4 were clearly underestimated by the FEA. Figure 124 shows the measured displacements from which the rotations can be calculated.

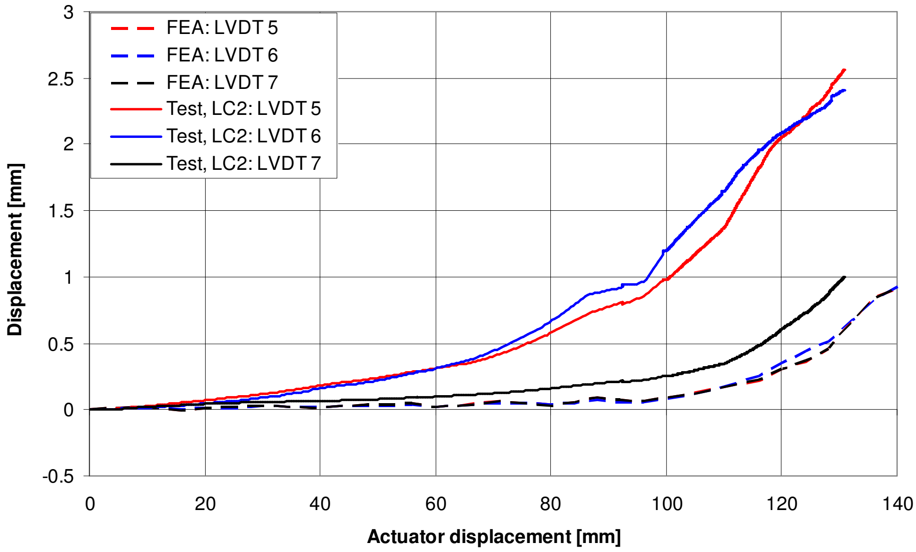

Figure 124 Test and FEA: Displacements of LVDTs 5,6,7

The deviations in the measured boundary displacements and rotations between the test and the FEA propose an assessment of the friction and damping behaviour of the massive test fixtures which were modelled as perfectly elastic and frictionless in the FEA. The mass of the test fixtures is assumed to cause friction when the test fixtures get compressed since it is not carried by the gliding pads but by the guiding pins of the springs. Independent from the effect of the test fixtures' mass, the described deviations may also indicate that the linear motion within the test fixtures undergoes some friction. As an effect the compression stiffness of the test fixtures was obviously increased beyond the spring stiffness. For clarification of the assumed friction influence, a partial 3D model of the test fixture is displayed in Figure 125. The points where friction is induced and the acting loads are highlighted in this figure. The mass of the movable part of the test fixture and the mass of the panel may generate nameable friction at the guide pins. The actuator load is transferred through the gliding pads where also friction may occur corresponding to the actuator load.

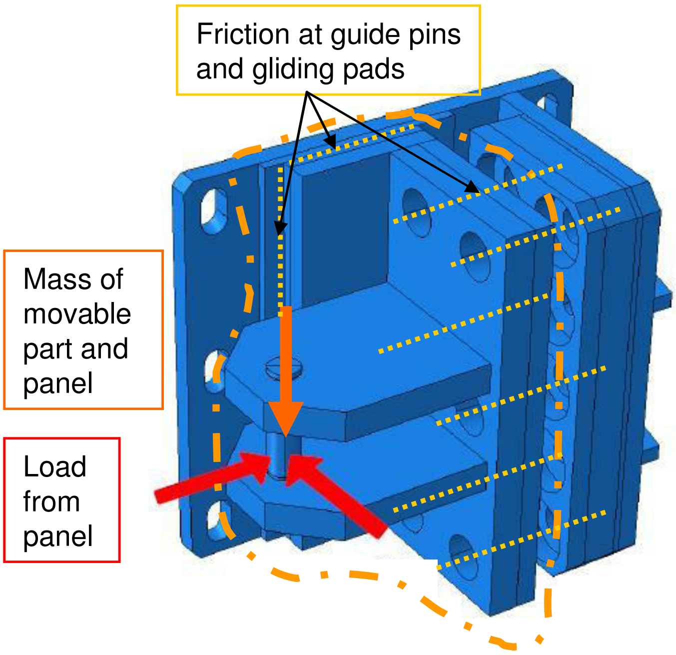

Figure 125 Test fixture: mass influence and friction

In the test, the displacement of the panel in impact direction was recorded by a video correlation system. This displacement has been compared to the FEA results at significant load levels. The offset between the displacements in the impact direction between the test and the FEA that was captured by LVDT1, could be found in the displacement plots in Figure 126 as well. The distribution of indentation along the panel centre in stringer direction was not represented exactly by the FEA which shows indentation peaks near the centre shear ties of the frames 2 and 4 and less indentation at the centre frame 3. Figure 126 shows the panel at maximum load in the 1st load cycle, at 39.2 kN (the closest available load of the FEA was 37.4 kN).

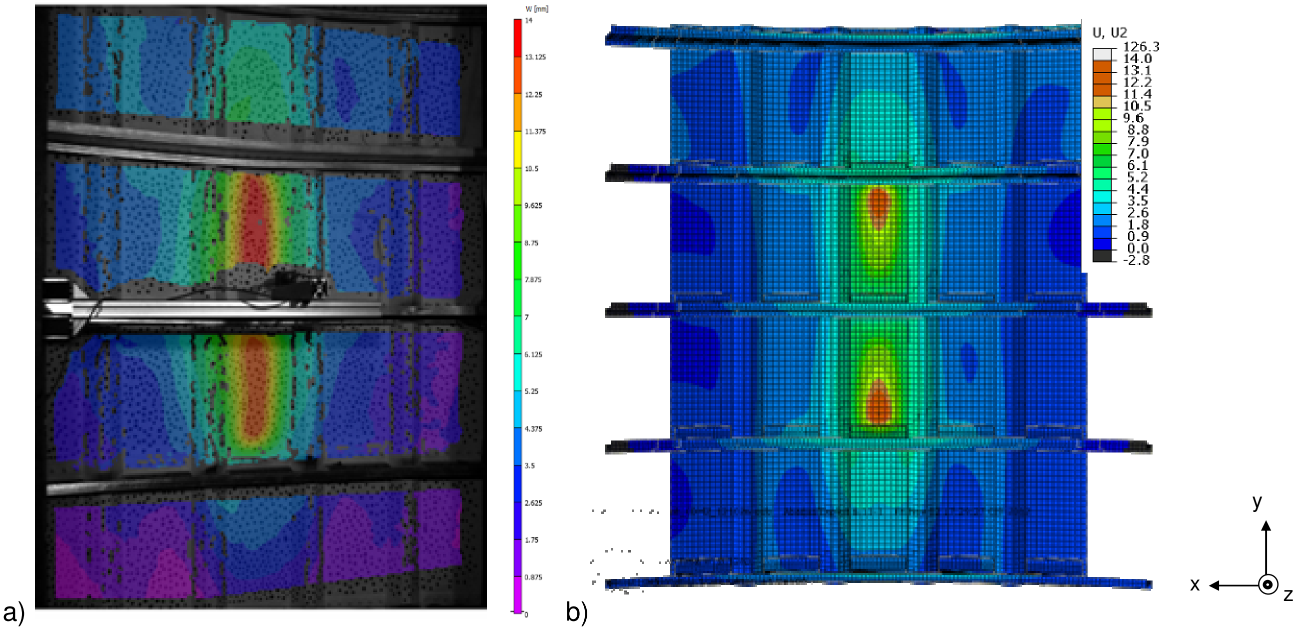

Figure 126 Displacement in impact direction, a): Test, 1st load cycle, b): 39.2 kN, FEA: 37.4 kN

A state of low deformation within the 2nd load cycle is displayed for a comparison between the test and the FEA. Figure 127 shows the panel displacement in impact direction of the test (a)) and of the FEA (b)) at a load of 30 kN. At this load level, the displacement of the test was slightly higher while the displacement of the FEA was slightly wider distributed.

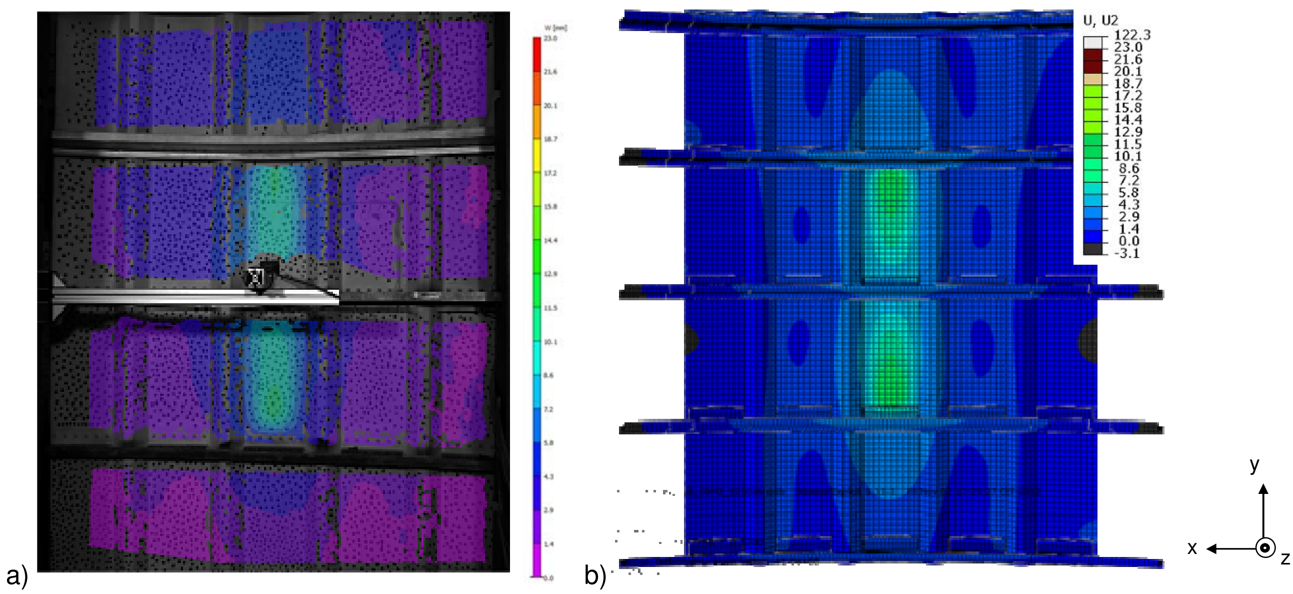

Figure 127 Displacement in impact direction: Test, 2nd load cycle, 30.0 kN, FEA: 30.4 kN

In Figure 128, the displacement in impact direction is displayed at the maximum load of the test (57.0 kN, a)) and after the load drop to 50.0 kN, b)). The indentation pattern got narrower at the load drop from maximum load while the load transfer through the centre shear tie was obviously changed when the damage in the centre shear tie grew

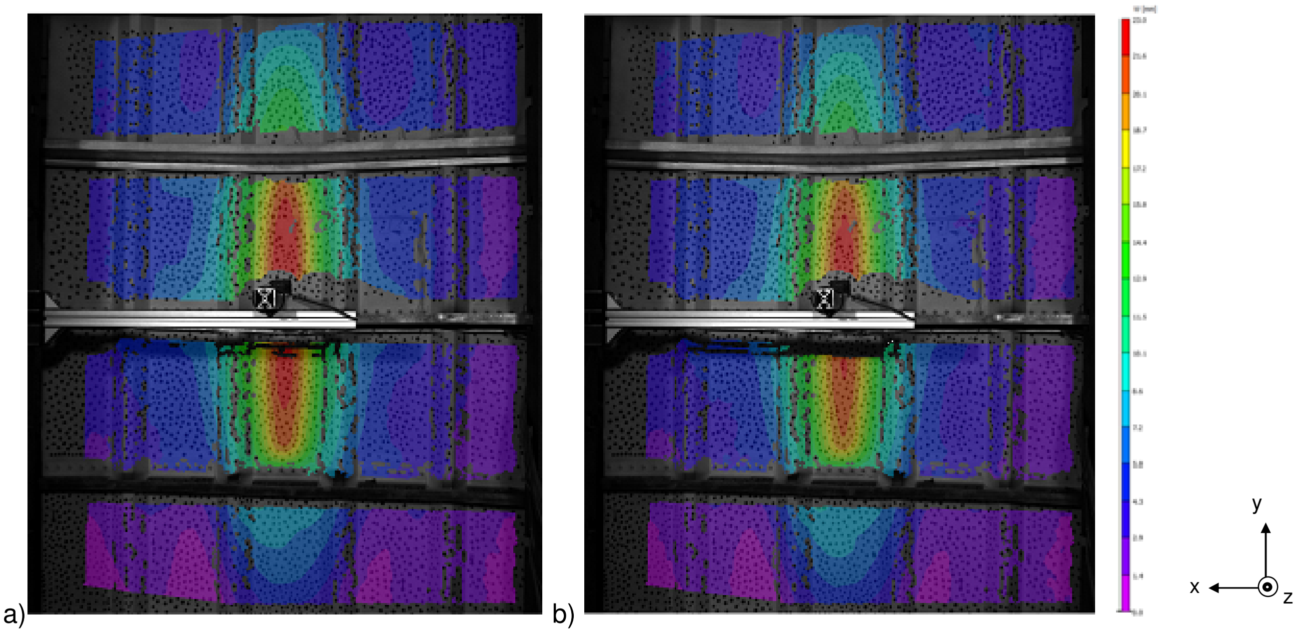

Figure 128 Displacement in impact direction: Test, 2nd load cycle: 57 kN, load drop to 50 kN

The FEA showed a generally lower displacement level than the test at the maximum load at the skin centre while the displacement of the actuator showed good agreement (see Figure 129).

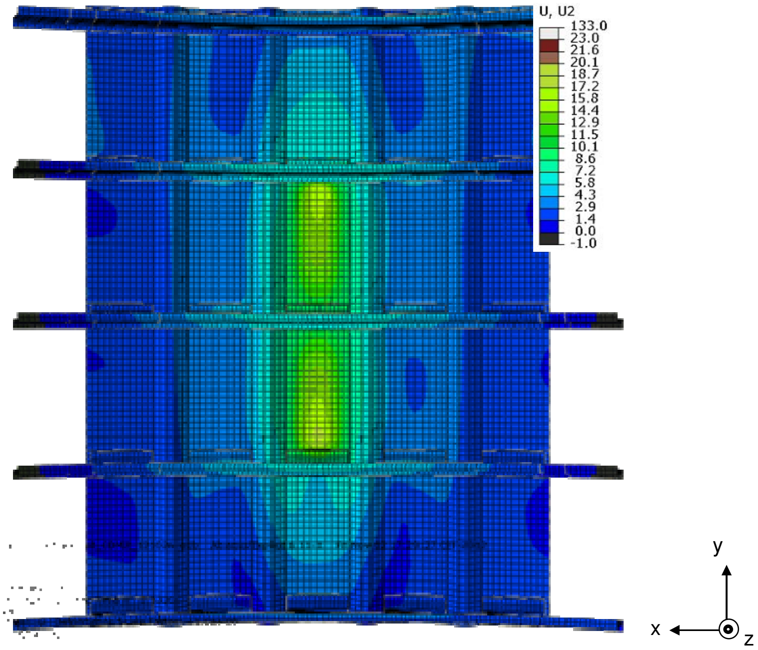

Figure 129 Displacement in impact direction: FEA: 57.4 kN

6.4.3 Strain comparison

The strain gauge positions and numbers can be found in Figure 130. In case of marked sets of two strain gauges at one defined position, the numbering follows the rules below.

- Skin: 1st SG circumferential, 2nd SG axial
- Frame: 1st SG on the inside (radially), 2nd SG on the outside (radially)
- Shear ties: 1st SG on the non-frame side, 2nd SG on the frame-side

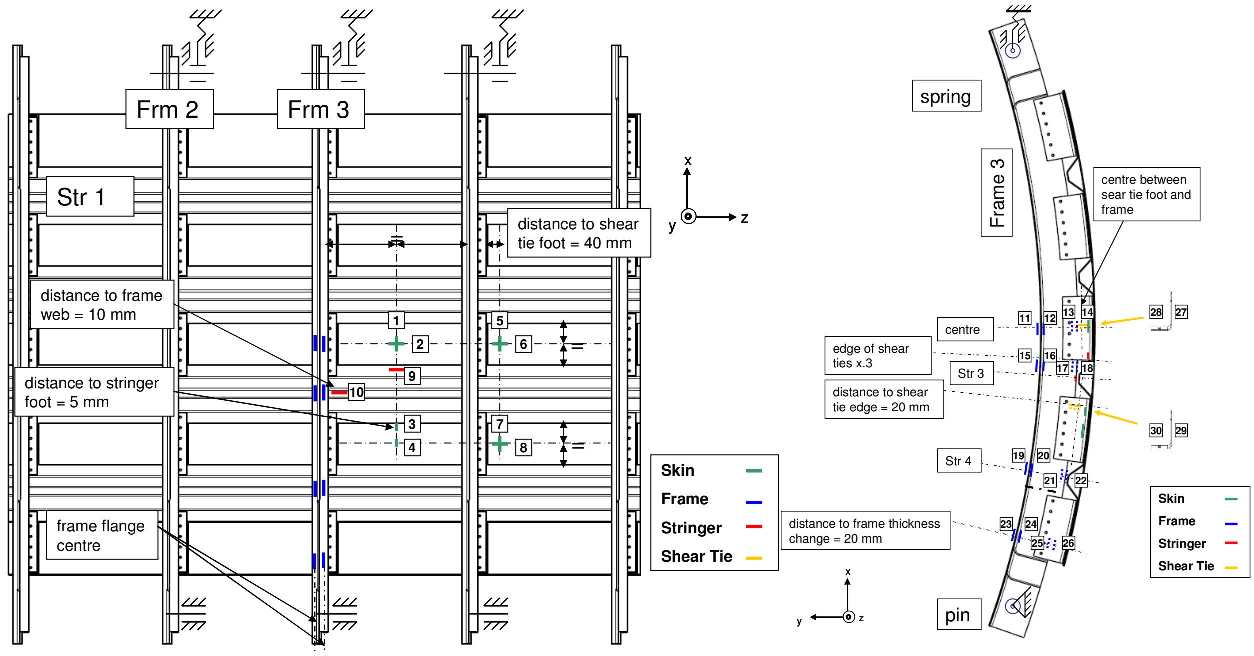

Figure 130 Strain gauge positions and numbering (see 5.7)

The skin strains in circumferential direction and in axial direction, in the loaded skin bay (frame 3-4, stringer 2-3, see Figure 131) shows good agreement. Only at high load the circumferential strain gets underestimated by the FEA.

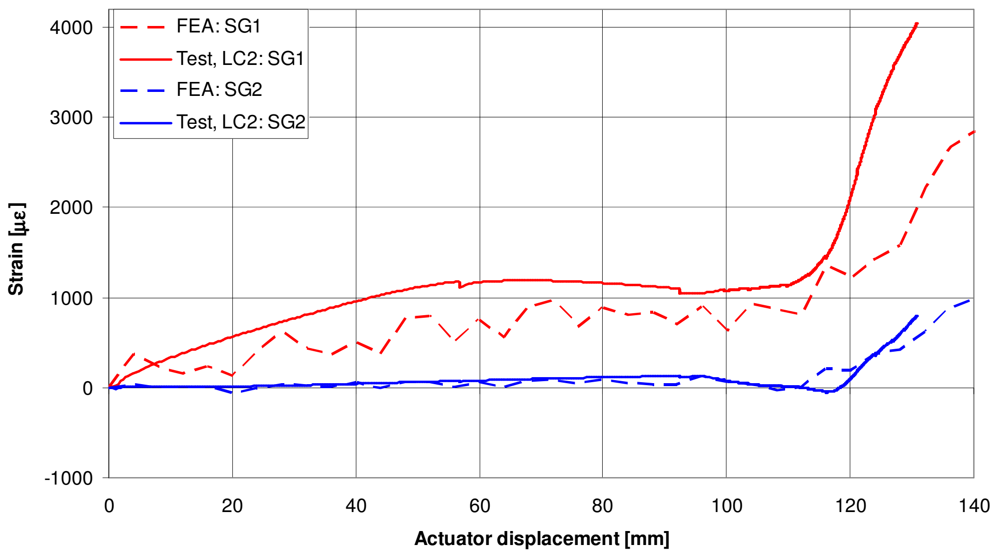

Figure 131 Test and FEA: Strains of strain gauges 1,2

The strains of the skin strain gauges 3, 4 and 5 show a good agreement of the test and the FEA (see Figure 132) while the FEA outputs clearly show dynamic effects due to the high loading rate of the simulations. However these dynamic effects are limited and are obvious only at low measured strains.

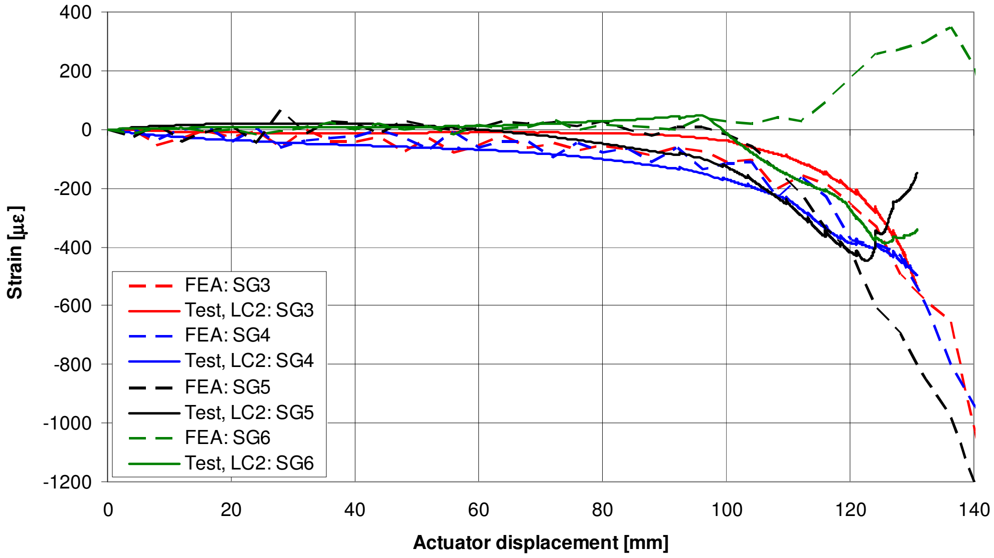

Figure 132 Test and FEA: Strains of strain gauges 3,4,5

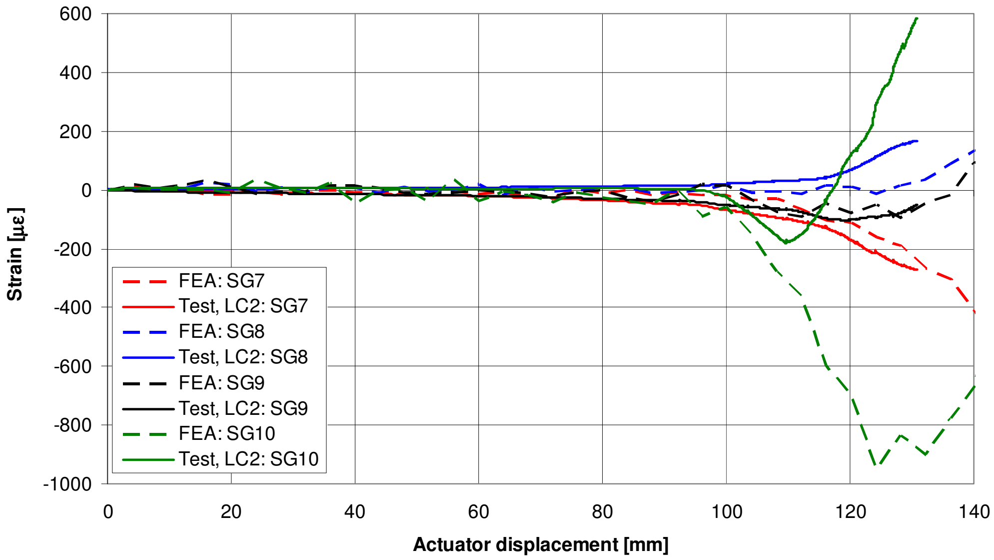

Figure 133 Test and FEA: Strains of strain gauges 7 to 10

The strain gauges on the flanges, in the centre region of frame 3, which are all aligned in circumferential direction, show general good accordance between the test and the FEA in Figure 134. Solely the strain of the outer flange in the centre position (SG13, 14) is significantly underestimated by the FEA.

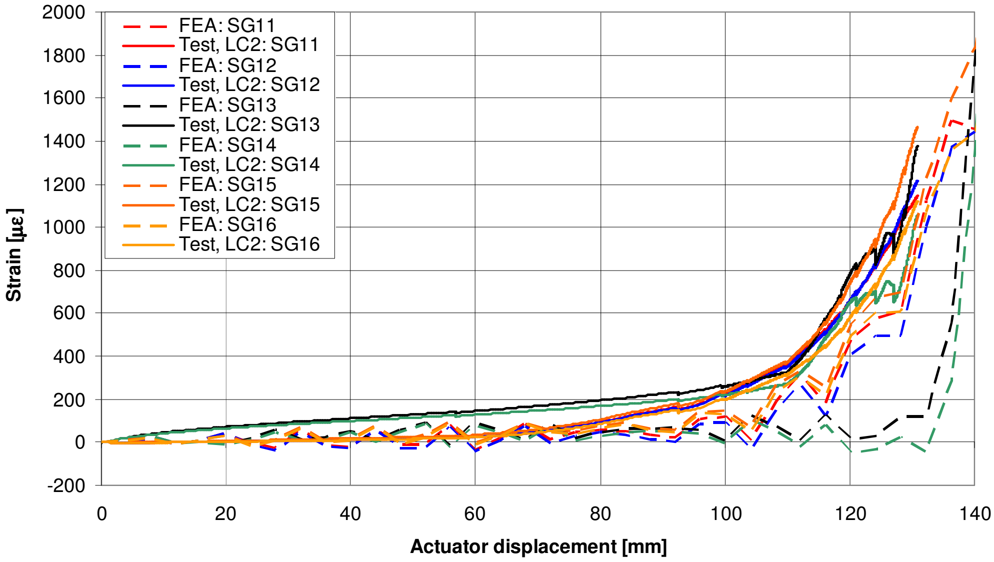

Figure 134 Test and FEA: Strains of strain gauges 11 to 15

At the frame position above stringer 4, the strain of the outer flange was underestimated by the FEA at high deformation level (see Figure 135) while the remaining strains are represented well.

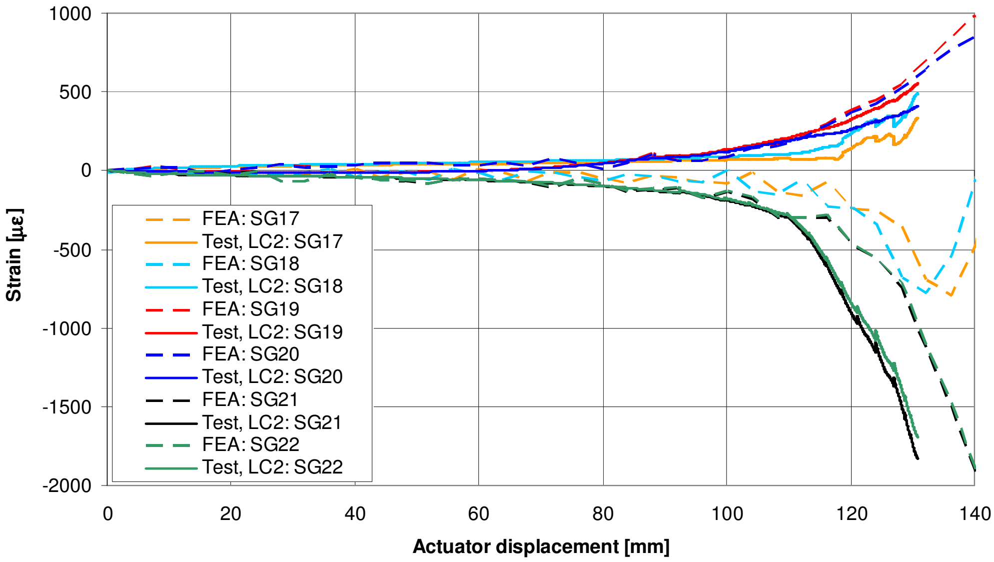

Figure 135 Test and FEA: Strains of strain gauges 19 to 22

The strains in the boundary region of frame 3 are well represented by the FEA (Figure 136) and proven to be sufficiently low in comparison to the test field in the centre of the panel. The test shows an effect of changing the bending direction after a low first level of bending to a higher level in the opposite direction.

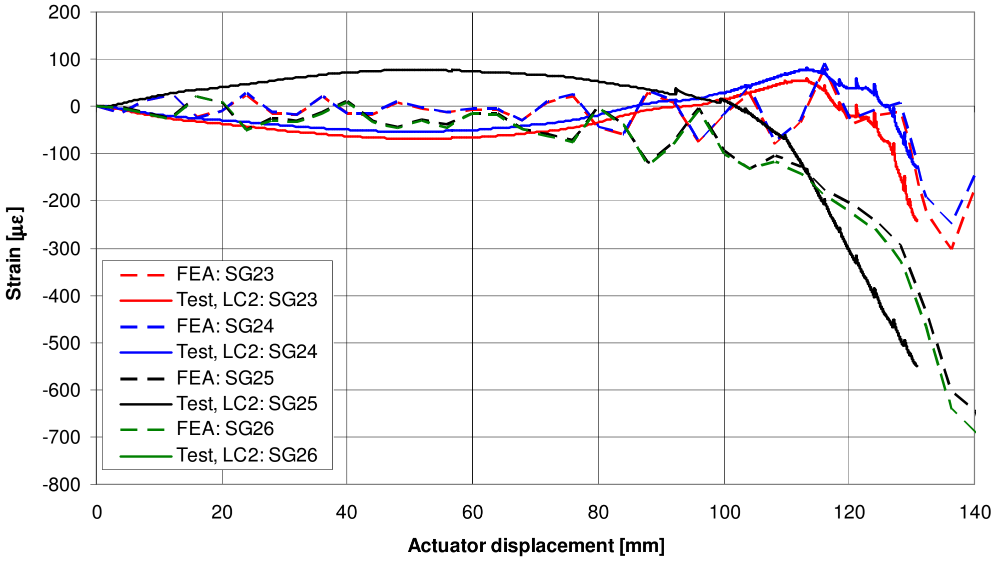

Figure 136 Test and FEA: Strains of strain gauges 23 to 26

The strain gauges that were applied in radial direction on the flanges of the two shear ties ST3_3 and ST3_4, reflect the observed bending in both the test and the FEA readings (see Figure 137). The strain level is clearly underestimated by the FEA at these positions. This might be related to the high deformation level in combination with damage sequencees in these regions and the limitation of the single element outputs that were read out of the FEA.

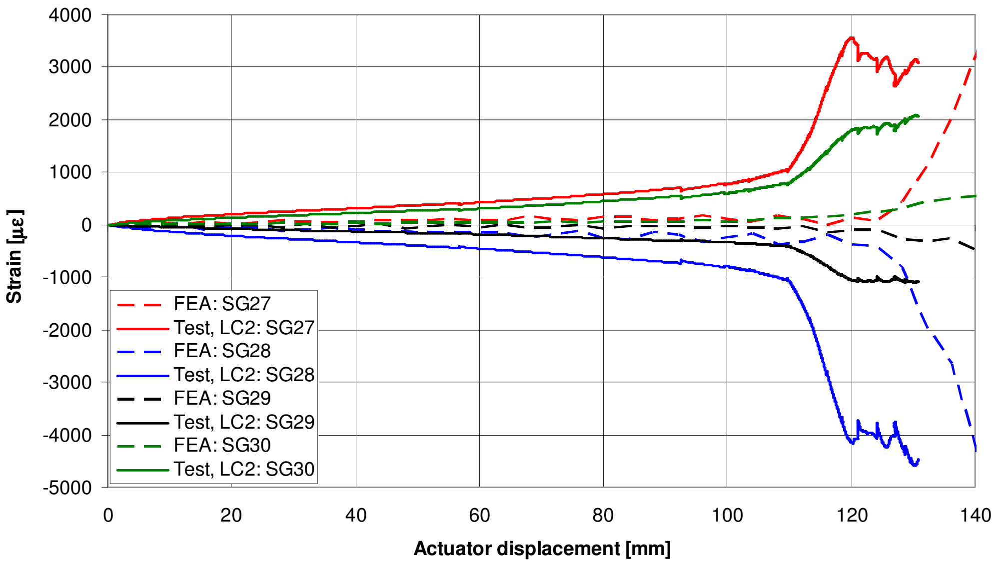

Figure 137 Test and FEA: Strains of strain gauges 27 to 30

For a direct comparison of the strains that were measured in the test and in the FEA, the strains at the maximum load that was reached in the test are plotted at their respective position on the panel. The values are represented by the surface of the plotted circles. The strains that were measured on the skin inside and on stringer 3, give a differentiated picture. Since the mesh of the FE model was not adjusted to provide nodes at the exact positions of the strain measurement, the accuracy of the strains that were extracted from elements or as interpolated output from nodes, was limited. The highest strain in the skin was measured in the impacted skin bay between the frames 3 and 4 and between the stringers 2 and 3. This circumferential strain was underestimated by the FEA while the axial strain was well represented. The strains in the skin bay between the frames 4 and 5 and between the stringers 2 and 3 indicate a slightly different shape of the zones of bi-axial skin bending outside the impact region, between the test and the FEA. While the axial component in the test shows compression that indicates a higher level of bending, the whole skin bay is under tension in the FEA and therefore undergoes less bending. The strain gauges between the stringers 3 and 4 show a similar behaviour in circumferential direction. The axial strain in the bay between the frames 3 and 4 and between the stringers 3 and 4 was found to be different, according to the described adjacent skin bay. The axial strain on the top of stringer 3, under frame 3 shows only a short phase of compression in the test, before it undergoes more significant tension. This position stays under compression in the FEA. The strain measurements from the test are shown in Figure 138, the strains from the FEA can be found in Figure 139.

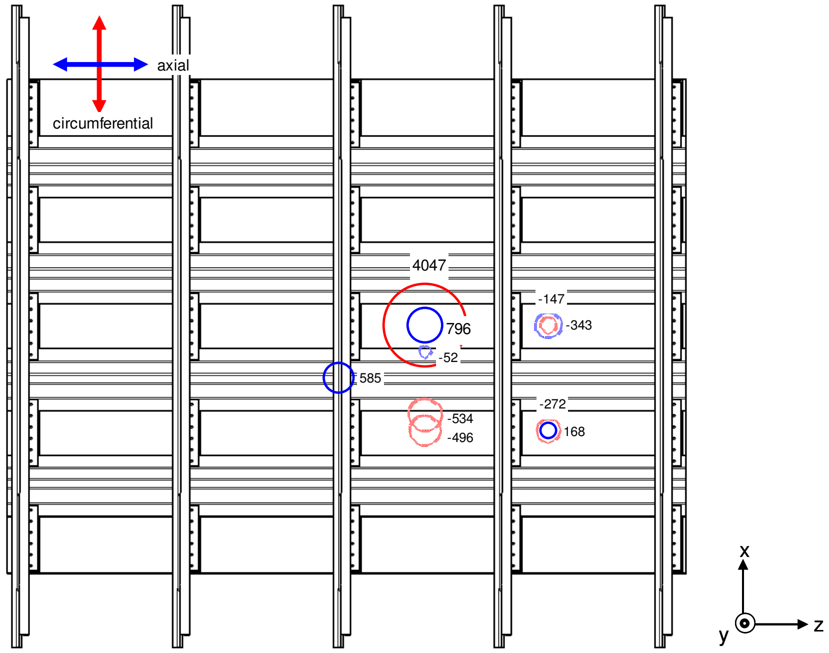

Figure 138 Strains at strain gauge positions, inside view: Test, 2nd load cycle, max. load

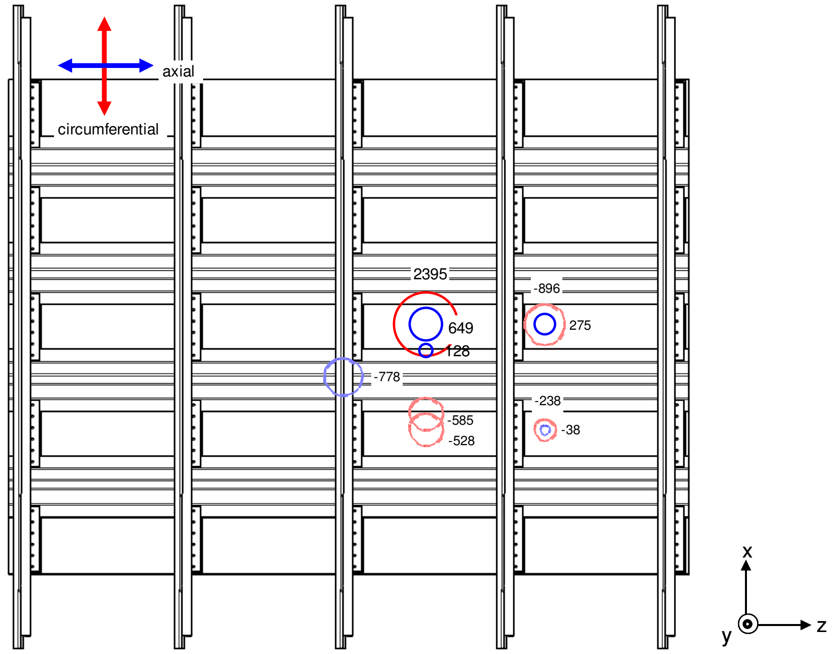

Figure 139 Strains at strain gauge positions, inside view: FEA, max. load of test

The strain measurements at the flanges of frame 3 and at two shear ties attached to frame 3 show a good agreement between the test and the FEA. The main deviation for this group of strain gauges is the different bending behaviour of the two shear ties. The bending tendency is the same. Yet the strain levels are increasing at a lower load level in the test. As the damage onset and the first major load drop due to damage (which was not reached in the CODAMEIN II test) were found to be well represented by the FEA, the damage behaviour of the centre shear ties and the related rotation of frame 3 were found to be not identical. The strain gauge outputs of the test are displayed in Figure 140, those of the FEA in Figure 141.

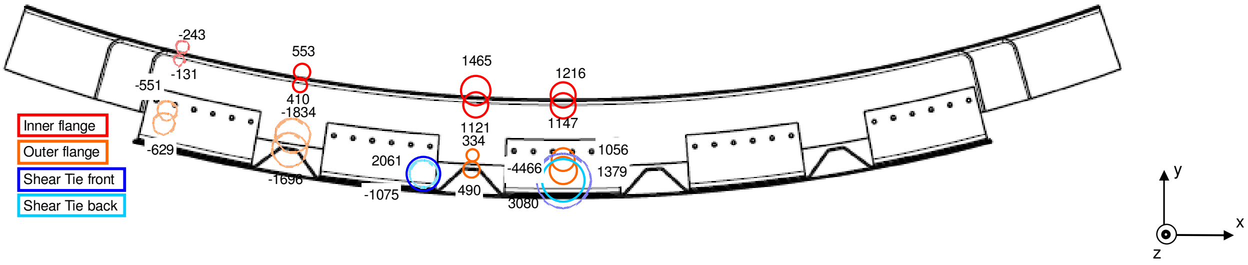

Figure 140 Strains at strain gauge positions, frame 3 top view, Test, 2nd load cycle, max. load

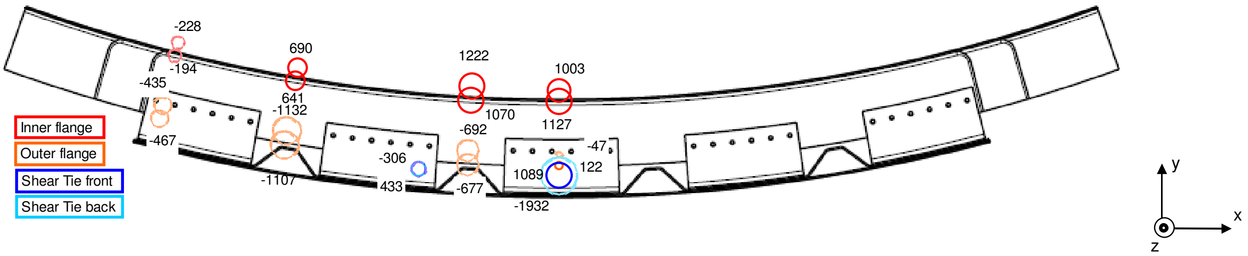

Figure 141 Strains at strain gauge positions, frame 3 top view, FEA, max load of test

6.4.4 Comparison with CODAMEIN panel

To maintain comparability of the performed FEA within CODAMEIN II, the sensitivity study as well as most of the panel analyses were performed under the boundary stiffness conditions of CODAMEIN (spring stiffness of 8500 N/mm per frame). The test results of CODAMEIN were used to assess the accuracy of the FE analyses. In the last step, the most mature state of the panel model was simulated with the changed boundary stiffness of CODAMEIN II which was 9500 N/mm per frame. Figure 142 indicates that the changed boundary stiffness had almost no influence on the global deformation of the panel. Small deviations were only visible in the past-damage phase. The very low influence of the boundary stiffness increased by 12% is expected to be due to the type of used boundary conditions which did not restrict axial rotation of the frame ends at their attachments.

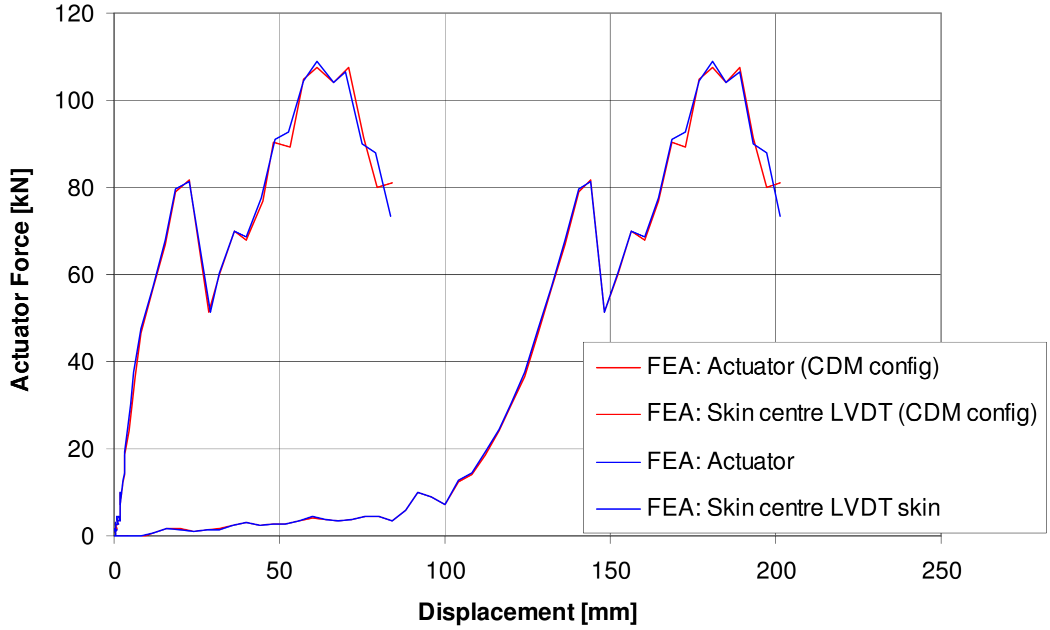

Figure 142 Load-displacement: FEA of CODAMEIN II and CODAMEIN

A comparison of the CODAMEIN II and CODAMEIN test in their 1st load cycle (LC1) and second load cycle (LC2) is displayed in Figure 143 and Figure 144. These charts show a similar response of the two test panels up to a load of approx. 25 kN which is below the first damages which were indicated audibly at 30 kN to 35 kN. The displacement measurement at the skin centre in CODAMEIN was stopped at maximum load when the used LVDT lost contact to the panel. The maximum load of the 1st load cycle was 45 kN in the CODAMEIN test and 39.5 kN in the CODAMEIN II test. Both load cycles were stopped upon a crack event.

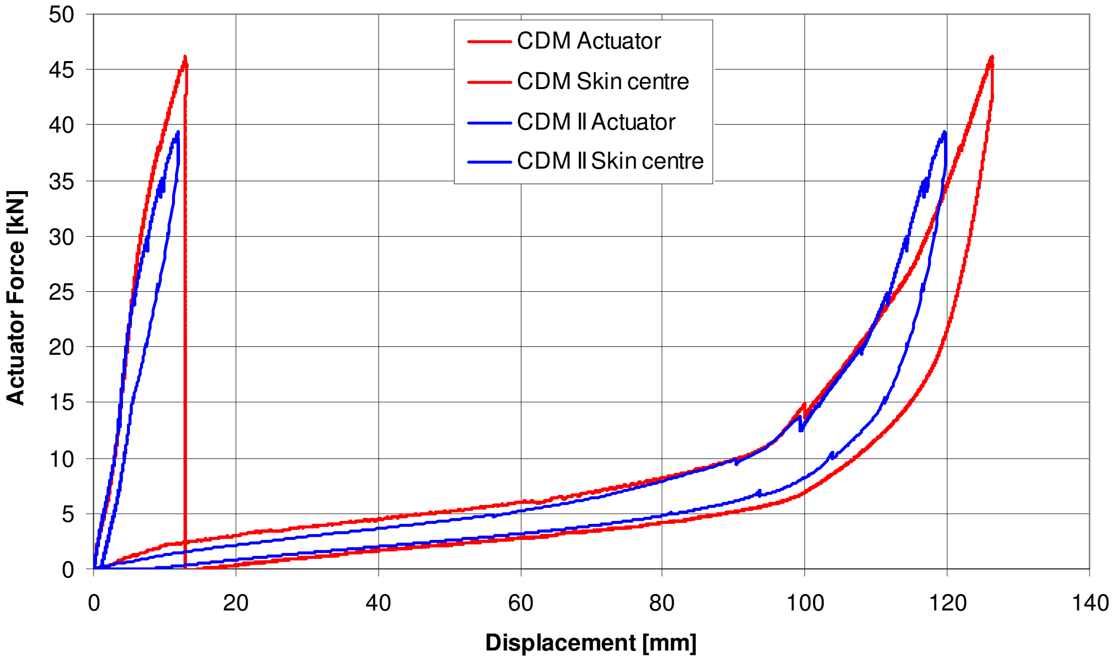

Figure 143 Load-displacement: Test of CODAMEIN II and CODAMEIN, LC 1

The second load cycles (LC2) of CODAMEIN and CODAMEIN II show different kinds of stiffness reduction as consequence of the damage in the panel which was found to be damage only in the radii of the centre shear ties.

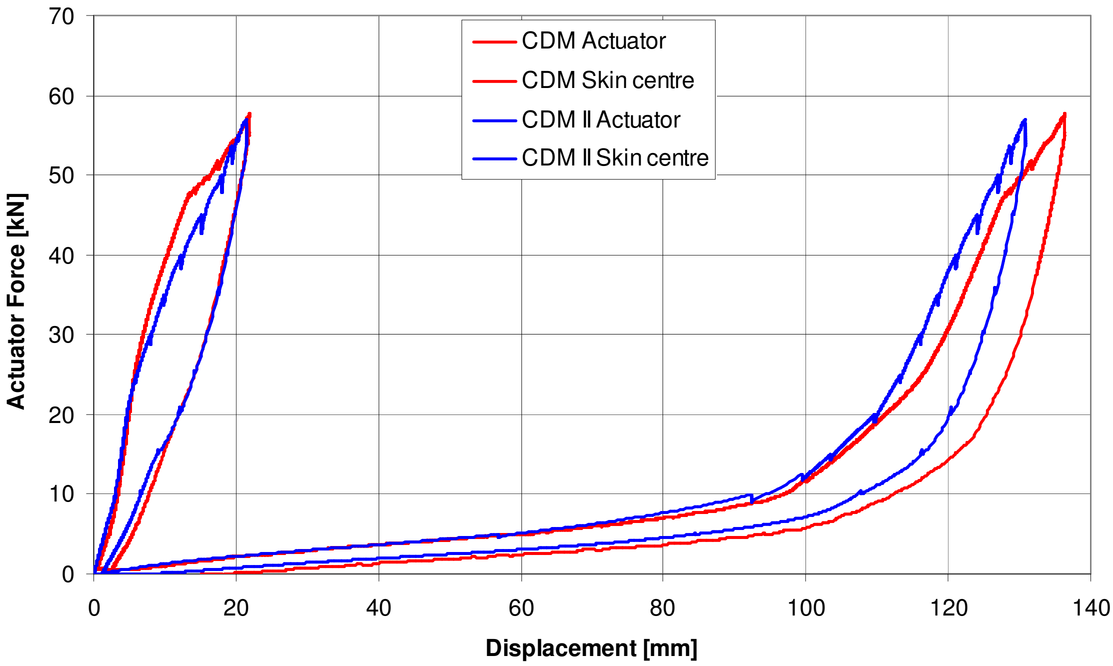

Figure 144 Load-displacement: Test of CODAMEIN II and CODAMEIN, LC 2

Figure 145 gives a comparison between the current FE panel analysis and the CODAMEIN panel analysis. The CODAMEIN panel model which did not include the rubber bumper compression phase and which was not able to reproduce the damage behaviour of the panel, shows a similar stiffness in the pre-damage phase.

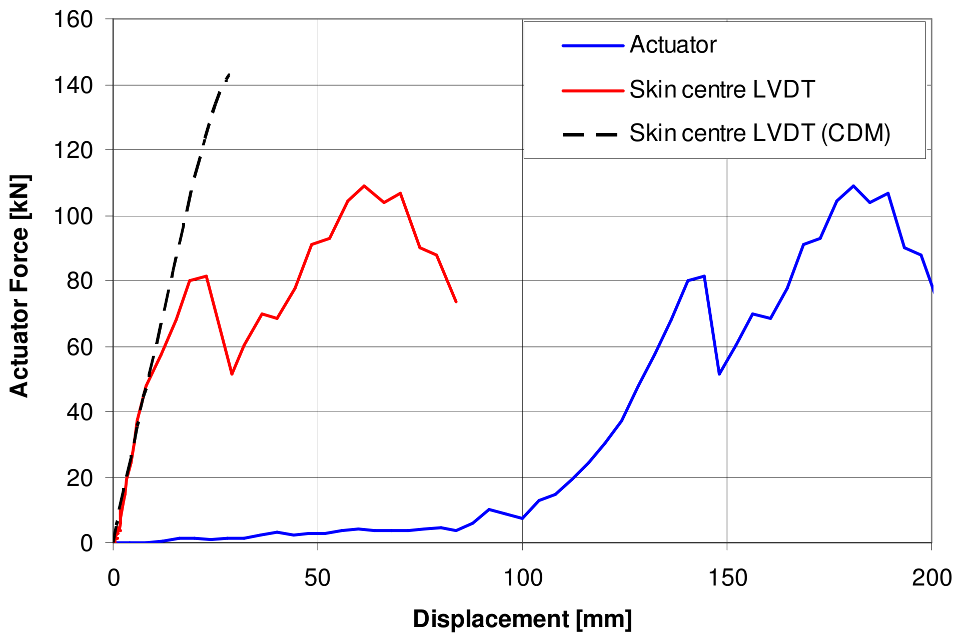

Figure 145 Load-displacement: CODAMEIN II and CODAMEIN

6.4.5 Energy trends

The impact energy that was imparted to the structure has been assessed using the impact force and the measured displacement in impact direction. Using the displacement of the actuator and of the skin centre, the energy fractions that compressed the rubber bumper and that deformed the panel were distinguished. The energy slopes highlight that the first phase of the actuator displacement only compresses the rubber bumper. At an impactor displacement of approx. 110 mm in the test, the rubber bumper was fully compressed and the panel started to deform. The point of full compression of the rubber bumper was indicated by the FEA at higher actuator displacement of approx. 128 mm. This matches the offset that was found in the load-displacement charts of the actuator and skin measurements of the test and the FEA. The rubber bumper thus did not exhibit an equally high stiffness in the FEA as in the test. This might be related to the simplified linear isotropic representation of the rubber material in the FEA, due to the absence of appropriate material parameters for the rubber material. The FEA deformed the bumper more to induce the same energy than the test. The maximum energy taken by the bumper was found to be larger in the FEA instead. It reached approx 900 J (affected by dynamic effects due to the high impact velocity) while a maximum of 700 J was found in the test. The simplified rubber material representation in the FEA may be the reason for the later increase of energies in the FEA compared to the test, which approach the tendency again at higher load levels, at the load where the CODAMEIN II test was stopped and beyond.

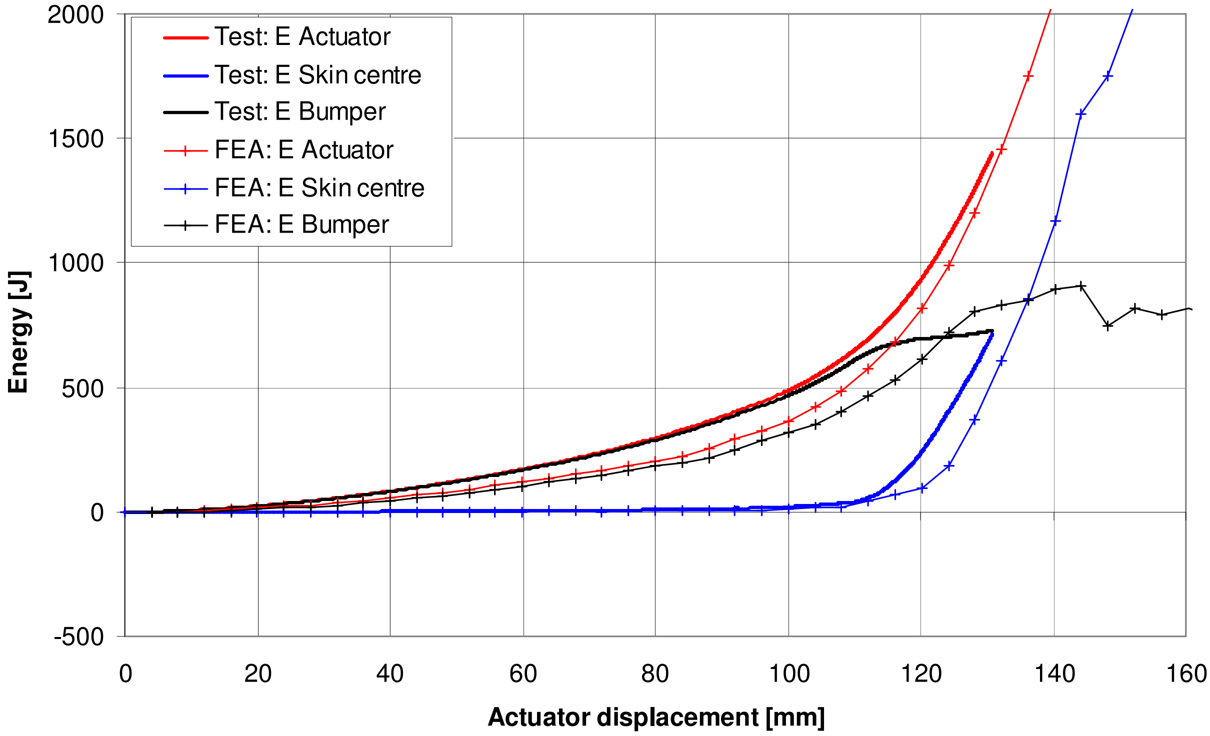

Figure 146 Deformation energy for panel and bumper: Test, FEA

The overall model energy outputs of the CODAMEIN II panel FEA are displayed in Figure 147. The curves of the single energy components comply with the expectations. No undesired peaks are found. The total strain energy ALLIE (ALLIE=ALLSE + ALLPD + ALLCD + ALLAE + ALLDMD+ ALLDC+ ALLFC) corresponds with the total external work ALLWK. The elastic strain energy ALLSE shows two plateaus indicating phases in which the bending of the frames and shear ties changes into another mode while major damage sequencees are found. The energy dissipated by damage ALLDMD highlights these phases, the damage onset and the second main phase of damage.

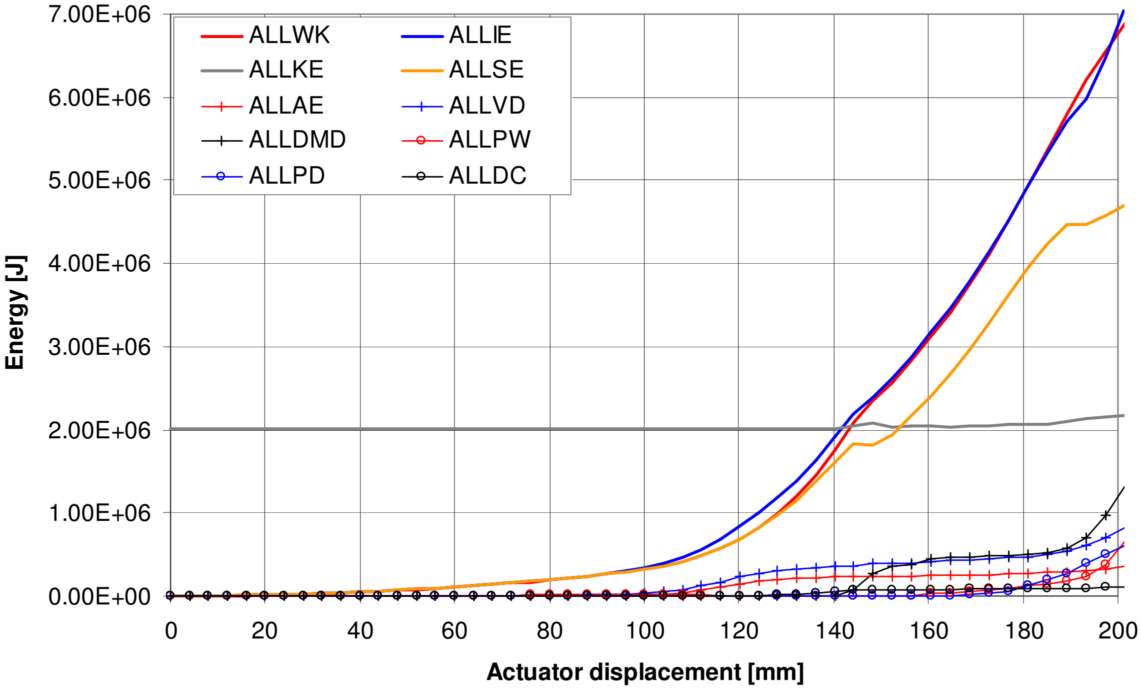

Figure 147 Panel model total energies

The energy dissipated for distortion control ALLDC is significant only at the rubber bumper which shows local significant element distortion at the locations of maximum compression by the bumper attachment bolts. The artificial strain energy ALLAE which is used to remove singular modes like hourglassings indicates that elements undergo stress-free modes like hourglassing, though these modes do not get obvious. The viscous dissipation or damping energy ALLVD is present in the phase of maximum bumper compression and increases less in the phase of damage. ALLVD which can be related to fastener failure or fracture mechanics, has to be considered since its level is not negligible in relation to the overall elastic energy. The plastic deformation of the frames is found to start in an early stage, but significantly increases only at an actuator displacement above 160 mm. In this late phase, the plastic frame deformation gets obvious by the output variable ALLPD. The contact penalty work ALLPW is negligible up to an actuator displacement of approx. 155 mm and increases significantly thereafter. This indicates the contact between the three inner frames and the two inner stringers which develops high contact pressures at very small contact surfaces. Figure 148 shows a detail view of the total energy components which are at a low level compared to the high level components like the total strain energy, the external work or the kinetic energy.

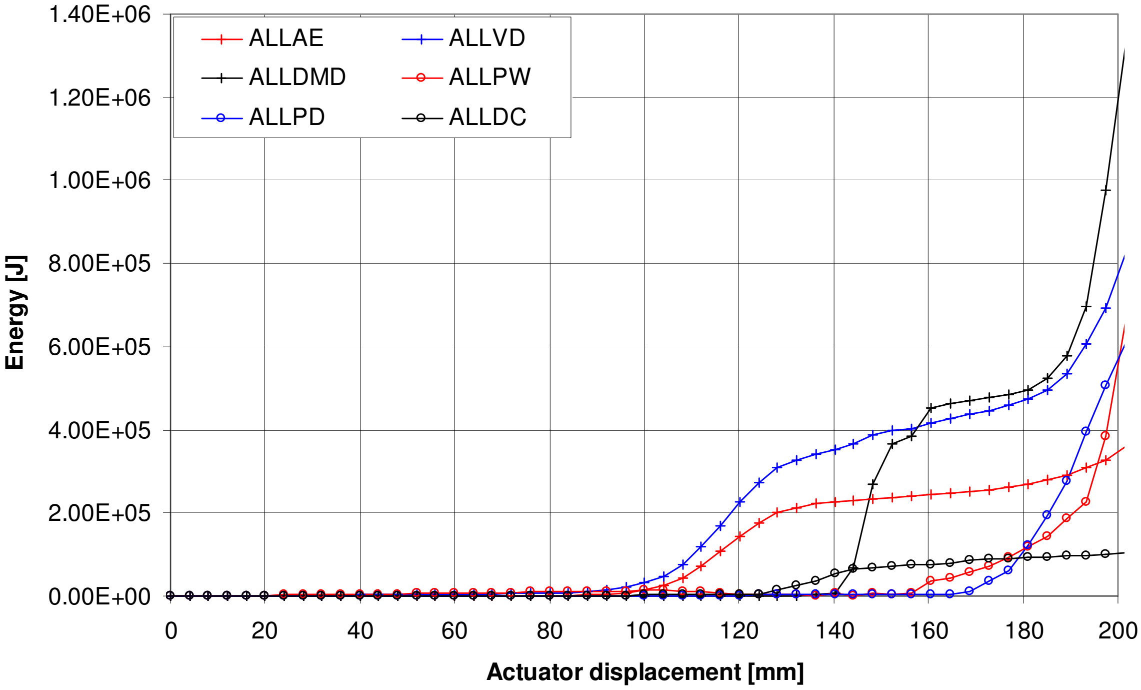

Figure 148 Panel model total energies, detail

The energy components of the panel model analysis were also extracted for a region around the centre shear tie ST3_3 (see Figure 149) which is most affected by the early damage phase.

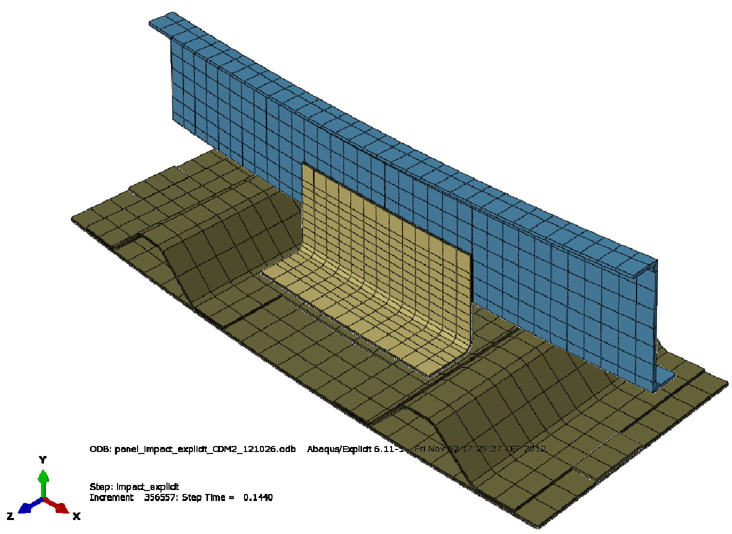

Figure 149 Panel model centre region for local energy output

The energy components of the panel centre region are displayed in Figure 150. The strain energy ELSE and the damage dissipation energy ELDMD are the dominating components. Damage in the composite material is indicated to start at an actuator displacement of 140 mm. Plasticity energy gets dissipated at low level from an actuator displacement of 160 mm and increases significantly at an actuator displacement of 180 mm. The viscous dissipation energy ELVD and the artificial strain energy ELASE which induces hourglassing and drilling stiffness are low but present. Hourglassing has been spotted within the model development process, in the phase of delamination and in-plane damage especially of the shear ties, combined with the out-of plane load by the rubber bumper. Though, this effect was not obvious in the present analysis. The ratio of ELVD and ELASE to the elastic strain energy ELSE is smaller than for the full panel model. Since the rubber bumper is not included in the cut-out, this indicates that a major part of the critical energy components are dissipated within the bumper and thus do not disturb the deformation and damage sequences in the panel.

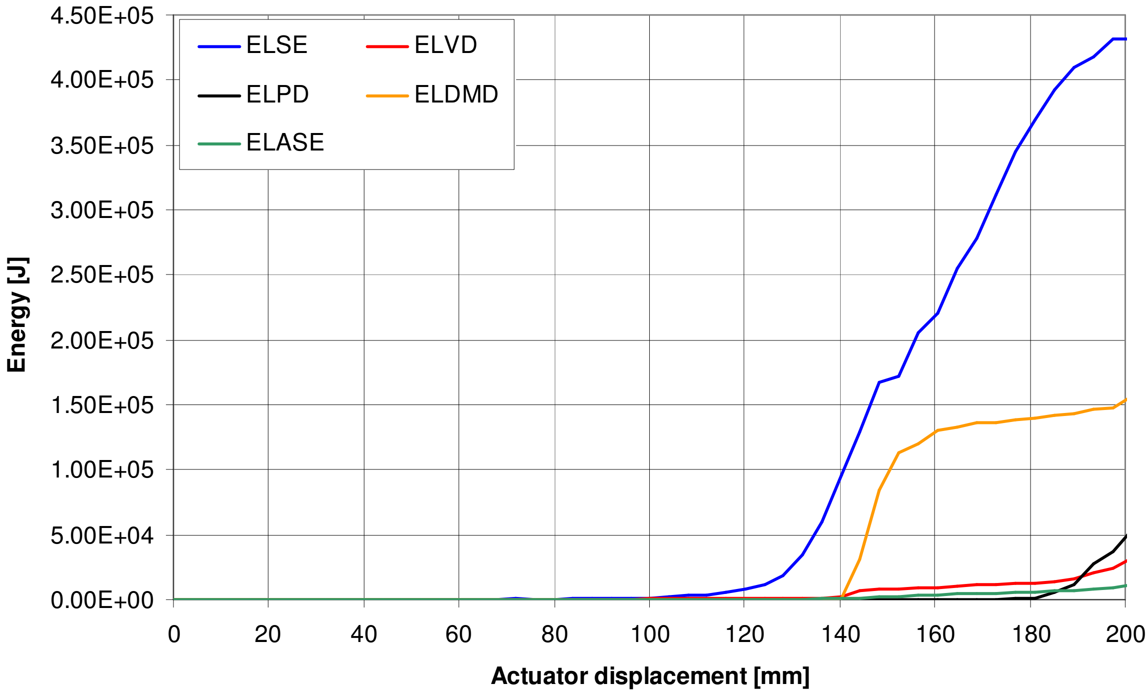

Figure 150 Energy components of the panel model centre region

6.4.6 Damage characteristics

The following damage sequence was found in the panel FE analysis.

Table 6 Order of damage events in the FEA

Damage stage	Type of damage	
1	Delamination and breakage of shear ties	Frame rotation
2	Frame-stringer contact	
3	Stringer severing, delamination	
4	Massive frame or stringer damage due to frame-stringer contact	

In the 1st load cycle of the test, the centre shear tie ST3_3 developed a crack in the radius starting expectedly at a load of approx. 30 kN and likely leading to a load drop at 39.5 kN at which the first load cycle was stopped. The crack in the shear tie ST3_3, marked after the 1st load cycle, is depicted in Figure 151.

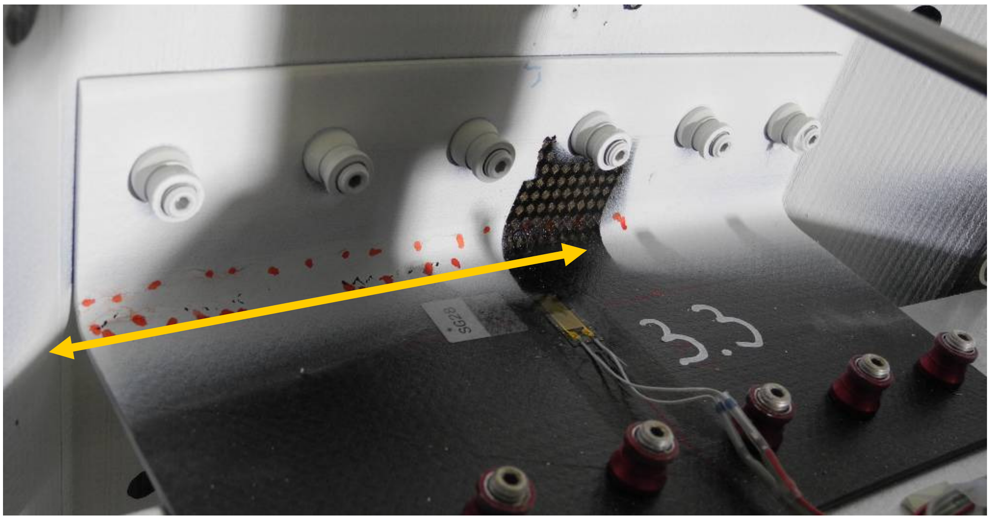

Figure 151 Crack in shear tie ST3_3 after the 1st load cycle

The load-displacement chart of the test's 1st load cycle, with the marked phase between the first indication of damage and the load drop which triggered the stop of the 1st load cycle, is shown in Figure 152.

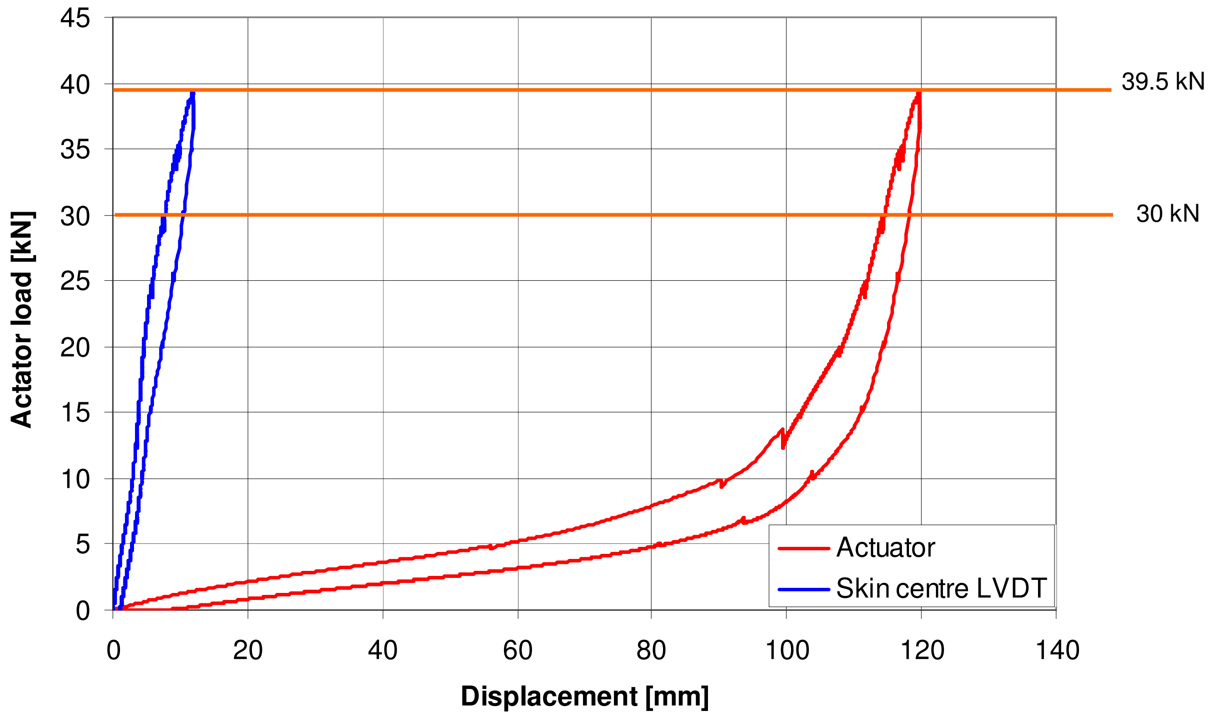

Figure 152 Load-displacement of the test's 1st load cycle

The FEA revealed damage onset in the form of delamination of the radius of the centre shear tie ST3_3, staring at both outer edges. The delamination onset which was found at an actuator load of 30 kN, is displayed in Figure 153.

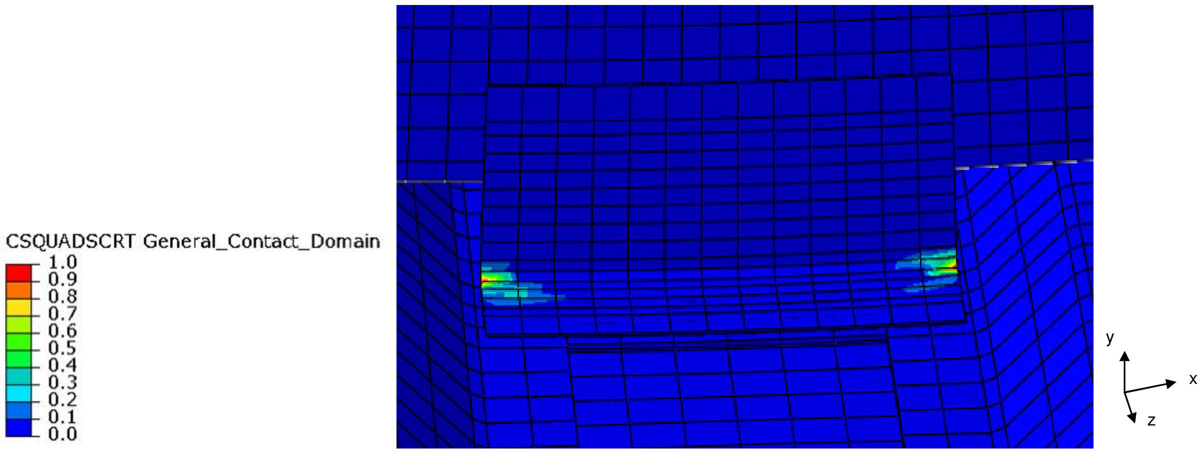

Figure 153 ST3_3 delamination onset at 30 kN (inc 30)

A progress of the delamination damage towards the centre of the shear tie started at a load of approx. 57 kN (see Figure 154). At this load, the onset of in-plane composite damage was found.

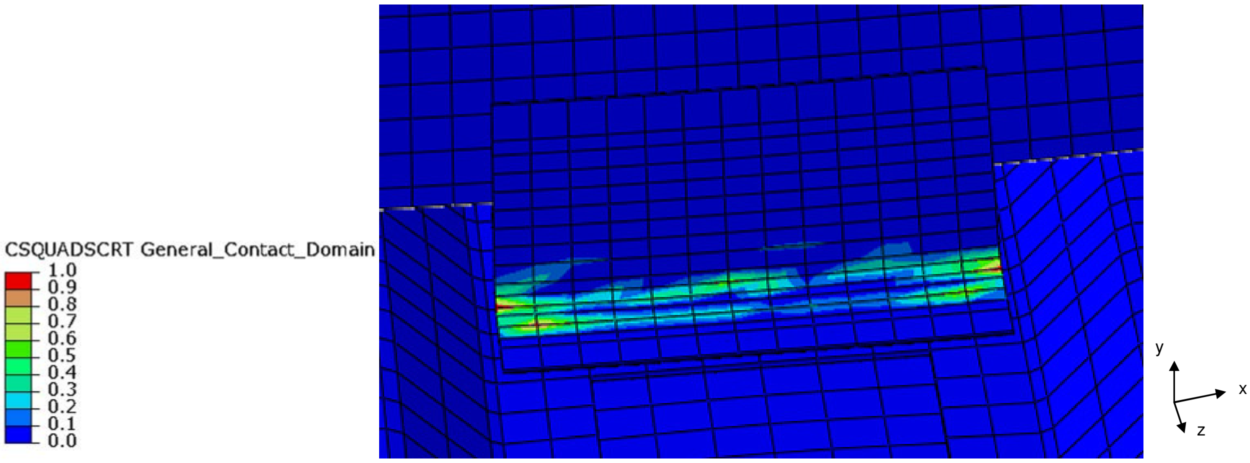

Figure 154 ST3_3 delamination at 57 kN (inc 33)

At a load of 82 kN, a sudden significant increase of the delaminated radii of the three centre shear ties (ST2_3, ST3_3, ST4_3) occurred, which delaminated almost the entire area between the rivet lines that attach them to the skin and the frames (see Figure 155).

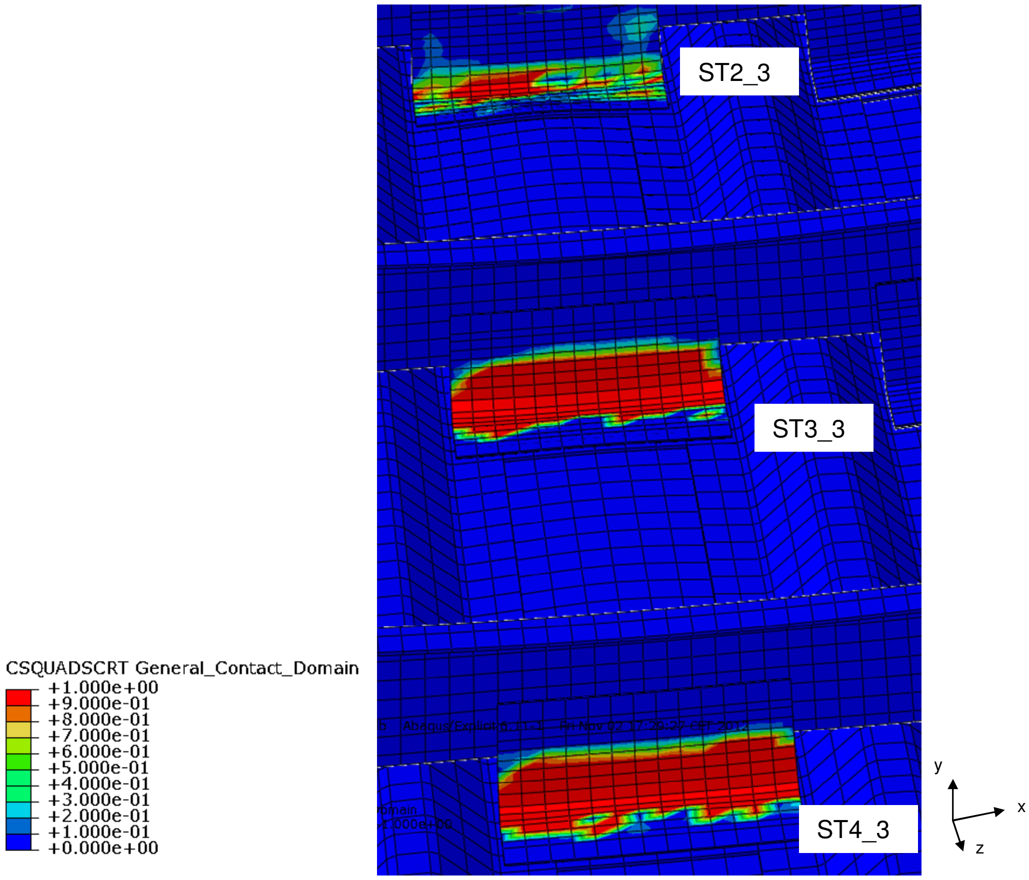

Figure 155 ST3_3 delamination at 82 kN (inc 36)

The point of onset of in-plane composite damage is displayed in Figure 156 and Figure 157. These picture show that the Hashin composite damage modes fibre compression as well as matrix compression and matrix tension initiate at the shear tie ST4_3. The pressure by the rubber bumper is not uniformly distributed since the attachment bolts inside the circular bumper are positioned in the regions of the two shear ties ST2_3 and ST4_3. Since the L-shaped shear ties are orientated in the same direction, this non-uniform loading by the rubber bumper is not induced symmetrically in the regions of these two shear ties.

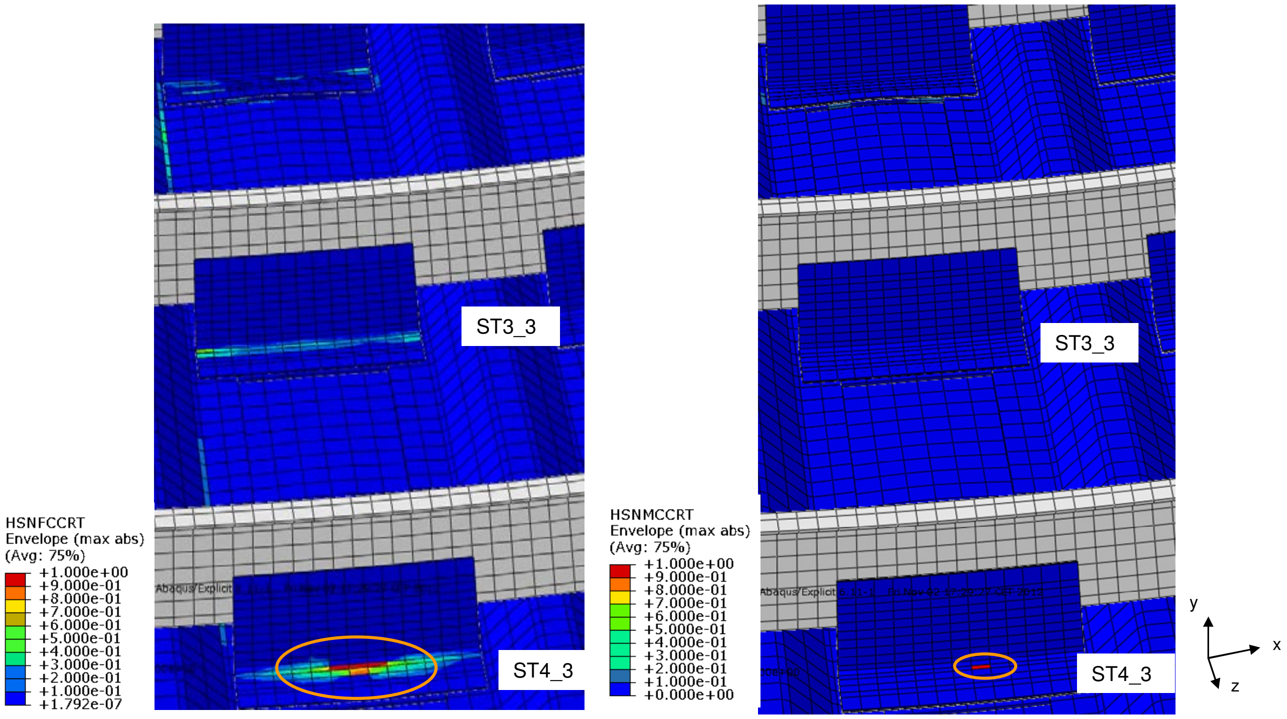

Figure 156 Fiber compression and matrix compression damage onset at 57 kN

Figure 157 also shows damage onset by matrix tension in the skin within the skin bay Frm 2-3, Str 2-3. This local damage onset in the skin, which was not found in any related test indicates a remaining imprecision here. The relatively coarse mesh at the transition from the reinforced skin with the attached shear tie to the basic skin as well as the modeling of the rubber bumper and the attachment bolts are expected to having influenced the development of the local skin damage in the FEA.

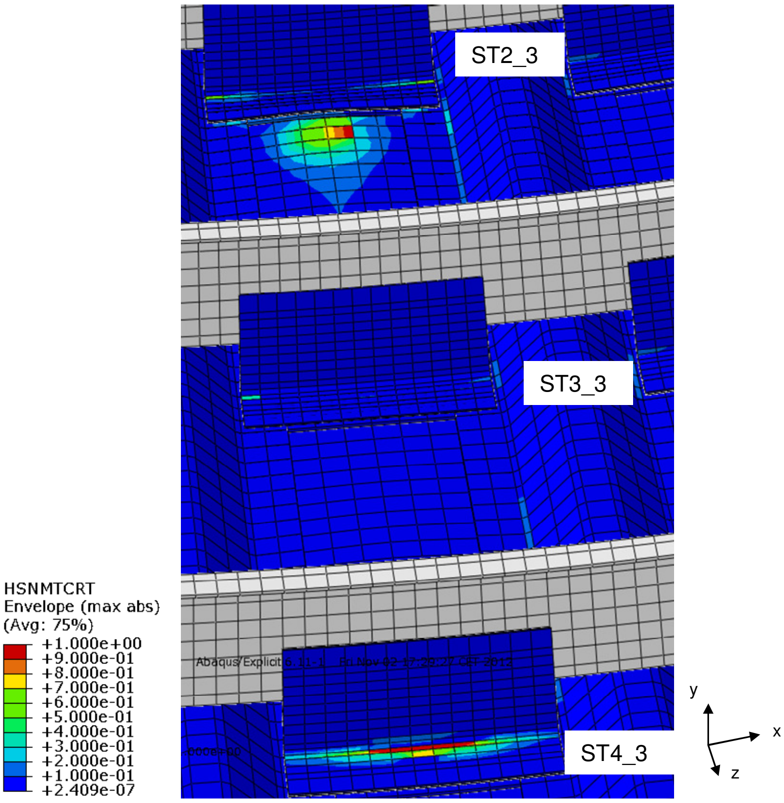

Figure 157 Matrix tension damage onset at 57 kN

Figure 158 shows the load-displacement chart of the panel FEA marking the load of delamination onset and of in-plane composite damage onset. The delamination onset load of approx. 30 kN corresponds with the load level at which first indications of damage were noticed in the test. The load of in-plane damage onset at 57 kN was not reached in the test.

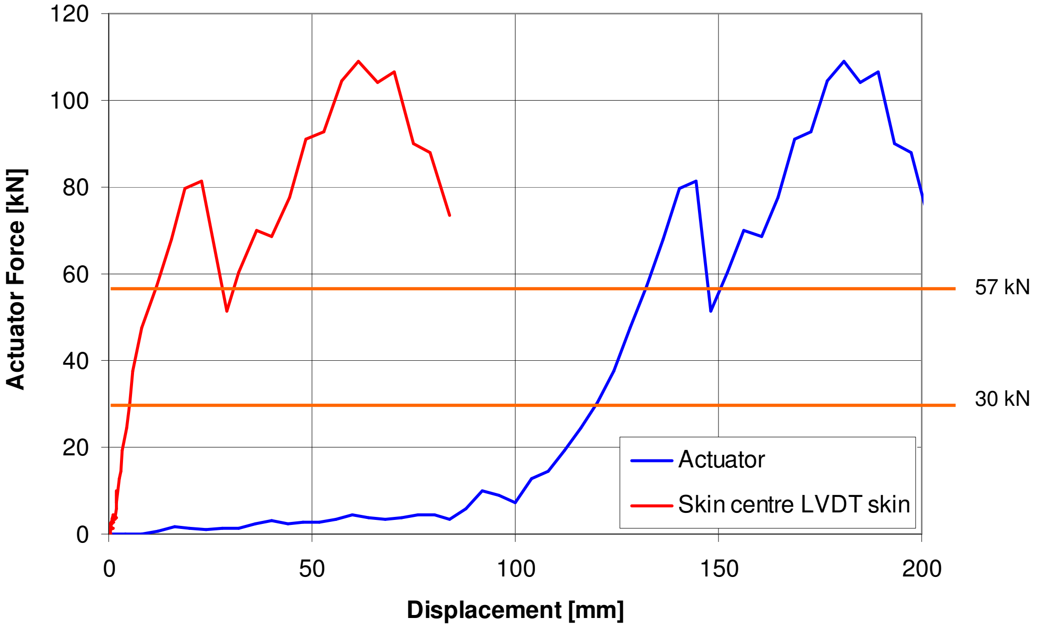

Figure 158 Load-displacement of the FEA

Figure 158 gives a summary of the FE analysis and the two load cycles performed within the CODAMEIN II test.

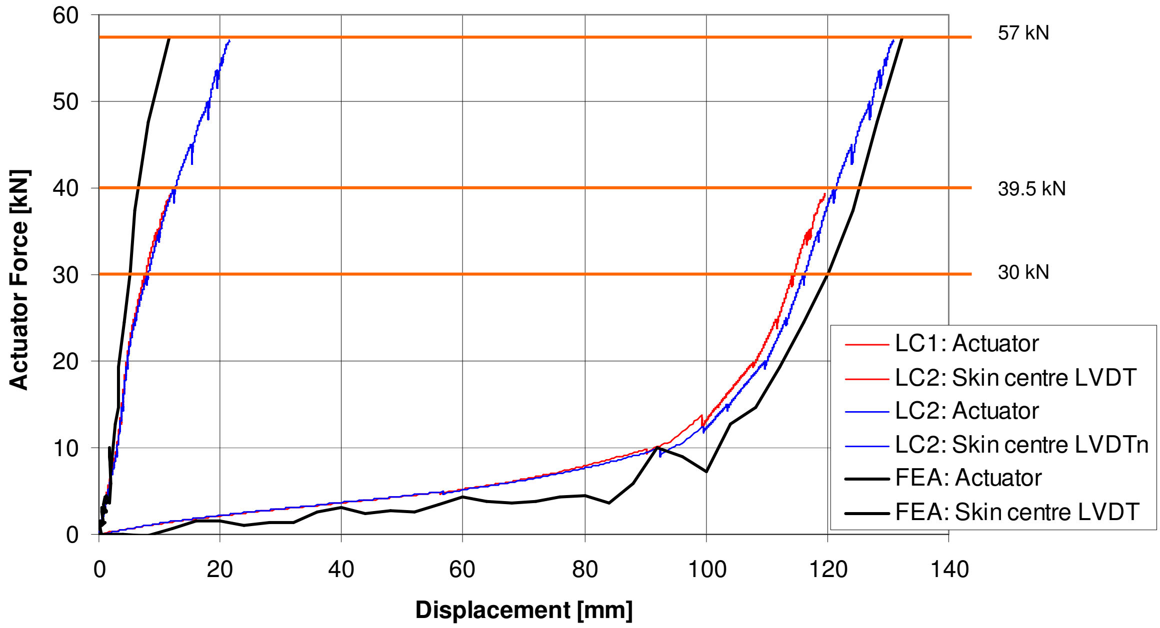

Figure 159 Load-displacement of both test load cycles and the FEA

6.4.7 Influence of frame attachment

The influence of the panel attachment using the three inner frames or using all five frames was assessed by FEA. While the CODAMEIN II test and all associated FE analyses were performed using a three-frame attachment, an additional simulation with an identical FE-model and a five-frame attachment was done. This analysis indicated no significant deviation of the global load-displacement due to the different number of frames attached, as displayed in the load-displacement chart in Figure 160. The deviation of the displacement at the first load drop is most likely overestimated since the FEA used a low output frequency and the two peak points lay on adjacent output points while the real peak points have less offset.

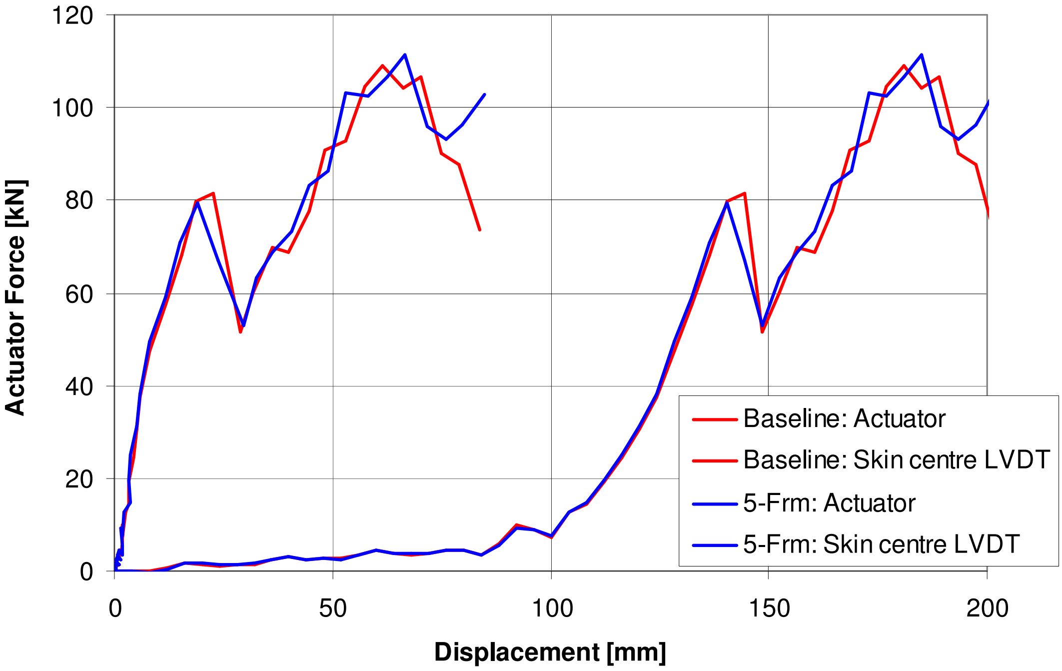

Figure 160 Load-displacement: 3-Frm. And 5-Frm. attachment

The CODAMEIN II test showed a very small influence of the boundary stiffness on the panel response. The compression of the test fixtures was found to be very low at the different spring stiffnesses while the boundary longitudinal rotation which was not restrained in the CODAMEIN / CODAMEIN II set-up, was more significant. It was proposed to use different test fixtures in future tests that provide longitudinal rotational stiffness. After numerical analyses with attachment of all five instead of the inner three frames were performed and the global response was compared to the baseline configuration, another set-up with five attached frames, the basic translational stiffness at one end of the frames as well as added rotational stiffness on both ends of all five frames was simulated. This corresponds to the test set-up that was used by Prof. Hyonny Kim's group at the UCSD to perform impact tests with all-composite panels of the size and configuration of the CODAMEIN and CODAMEIN II panels. The added rotational stiffness increased the global stiffness of the panel noticeably. As the rotation of the frame ends becomes more significant at a higher panel deformation, after the translational stiffness is dominating at low panel deformations, the global stiffness increases against the base configuration at higher loads as displayed in Figure 161.

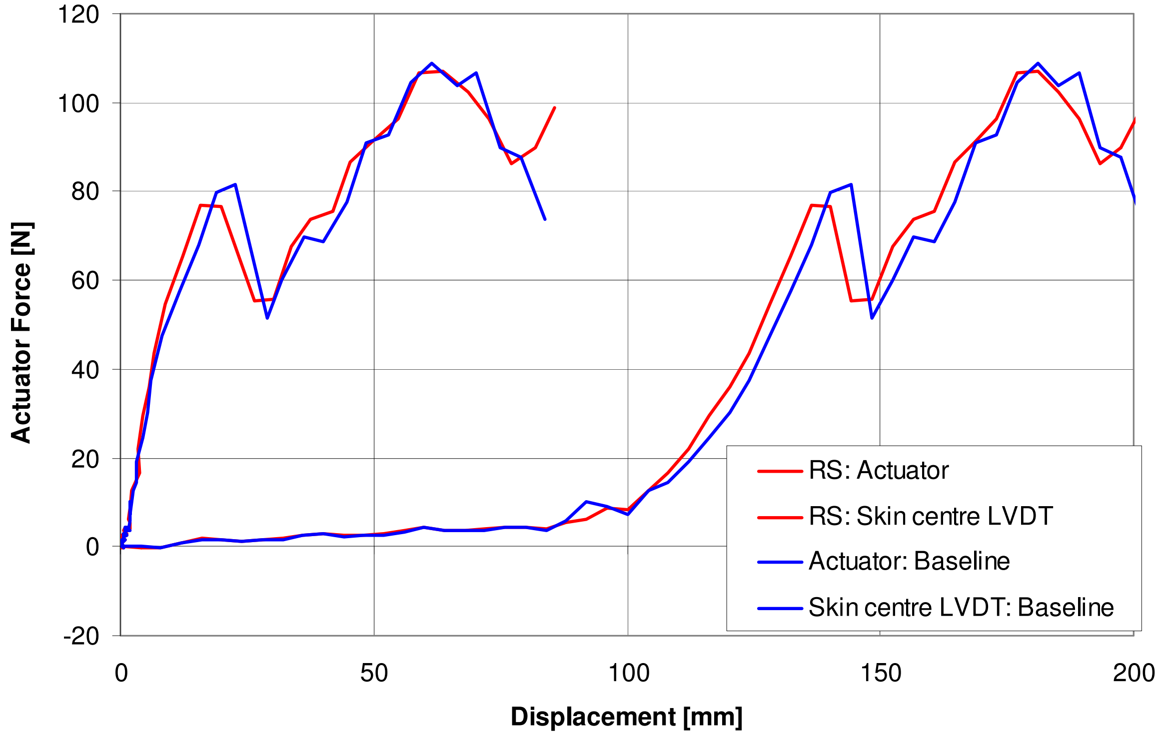

Figure 161 Load-displacement: Basic Set-up and 5-Frm attachm.+rotational stiffn.

7 Discussion of the results

The performed test delivered a broad platform of information which enabled a better understanding of the behaviour of the panel in the impact test. The general behaviour showed a high similarity to that recorded in the CODAMEIN test. The first damage events were noticed at slightly lower loads than in the CODAMEIN test. This might be caused by the increased boundary stiffness or by small deviations between the two mainly identical test panel as the parts of the panel were manufactured in a manual process and assembled using Hi-Lok fasteners. The quality control revealed an improved precision of the CODAMEIN II panel, likely due to reported improvements in the manufacturing process as result of the experience from the previous manufacturing process.

The comparison between the test measurements and the FEA results of CODAMEIN II showed different tendencies. Mainly the imperfections of the test panel and set-up and the limitations in their simulation caused the deviations documented by the displacement and strain measurements. The test fixture compression that was found to be much lower than predicted by the FEA, was described to be most likely caused by the imprecision of the test fixtures, and the contribution of their high mass. This obviously resulted in friction that's magnitude is unknown and that was not taken into account by the FEA. Also, the linear sliding ability of the test fixtures was assumed frictionless in the FEA. The test results however indicated that nameable friction appeared within the test fixtures. To adjust the FEA taking the friction into account, compression tests would have to be conducted with the test fixtures. An assessment of detrimental effects on the test fixtures and boundary conditions would have to be performed previously in order to judge the appropriate kind of fixture test and its reach to cover all influencing effects. Likely as a consequence of lower spring compression, the rotation of the pin joints was higher than expected. At a low load level, the strains in the panel centre were well predicted by the FEA as the influence of the boundary conditions was not significant yet. The mesh of the FE model however limited the accuracy in regions with high strain gradients. This obviously contributed to the better strain agreement in the skin bays and the worse agreement e.g. of the longitudinal strain of a stringer foot. The high number of strain gauges placed on the frame 3 revealed a complex strain distribution within the frame circumference. It proved that the boundary region did not undergo the highest strains, and the buckling tendency was maximal in the test field away from the boundary as desired. While the FEA predicted the frame flange strains well in most measurement positions, it revealed a significant deviation for the outer flange in the centre region. While in the test, the outer flange got compressed near the boundary but switched to significant tension towards the centre, it only reduced to approx. zero in the FEA. The reason for this could not be assigned to one specific factor. The deviation obviously arose in the simulation of the load transfer from the compressed bumper, through the skin and the centre shear tie (ST 3-3), into the centre frame (frame 3). The mass scaling that was used in the FEA to reduce the analysis time, was judged to have sufficiently low influence on the model response. The video correlation recordings showed a slight vertical non-symmetry of the skin indentation by the bumper. Since the possibilities to align the rubber bumper are limited, this cannot be compared to the CODAMEIN test in which no video correlation system was used.

The modification of the boundary stiffness of the test set-up was done based on the results of simulations of an improved fuselage barrel model. The used barrel model represents an advancement of the existing model of CODAMEIN including a representative inner structure which was added without increasing the general detail level of the model. The added inner fuselage structure slightly increased the stiffness of the barrel model under impact loading. The results of a numerical assessment of further boundary stiffnesses of the panel model however indicated that the single available component of boundary stiffness does not generate significant changes in the panel response. Hence, no change in the damage mode and sequence could be induced by a change of the boundary stiffness. The typical damage sequence which was documented by Prof. Hyonny Kim of UCSD and which was confirmed by both the CODAMEIN and CODAMEIN II tests proved to be robust against parameter variations.

Based on the results of the CODAMEIN test and the investigations of UCSD which all indicated that the shear ties are the first parts to fail within the test panel, a design change was considered to enable a different damage sequence. In line with a UCSD study, the replacement of the shear ties with stronger parts was considered. Thus, the target of the CODAMEIN II test was modified with the aim to retain the test panel in a condition that allows for a repair by replacing the shear ties and to avoid any further damage to the panel. After performing two load cycles in the test, the desired condition of the panel was maintained.

The FE model of the test panel was able to simulate the global response of the test panel and the damage modes that were found in the tests of CODAMEIN, CODAMEIN II and the UCSD tests. The model limitations that were found within CODAMEIN II are summarized below.

The used composite damage capability was a combination of the Hashin plane stress damage model and a single delamination line within the composite parts that used a cohesive surface definition. The size of the panel model did not allow to model the composite lay-ups in a detail level which would imply every ply as a separate layer of elements. Since this detail modelling would only be possible for extremely small sized models, maximum up to coupon size, simplifications were used. The Hashin damage model is able to capture the in-plane damage modes of fiber tension or compression and matrix tension or compression. Also the stiffness reduction capability of Hashin was used to simulate the damage progression. Since the detail level in terms of element size had to be limited, element side lengths of 4 mm at the most refined shear tie radii and 20 mm for the skin were used which limited the precision of capturing stress peaks, damage onset points and strains at strain gauge positions. The accuracy of the damage simulation was limited by the availability of material properties of the used materials that are necessary for the applied intralaminar and interlaminar damage models.

The cohesive surface definition that was used to enable delamination damage of the composite parts as well as debonding of co-cured parts, is influenced by the same limitation as the plane stress damage calculation. The definition of a single delamination plane in every composite part limits this damage criteria to the stresses in the centre of a part's thickness which might not be the position of maximum interlaminar peel or shear stresses in a specific case. Yet the centre position represents the most obvious approximation and permits the best mesh quality.

The test fixtures were integrated in the FE model as a perfect representation. The test however indicated that the mass of the test fixtures as well as panel manufacturing and test rig imprecision obviously generated significant friction and thus had nameable influence on the panel boundary response. These effects would have to be taken into account for further numerical analyses (see 10). The deviation between the displacements measured at the actuator and the panel centre in the test and the FEA also indicated a contribution of the rubber bumper implementation in the FEA which is expected to be mainly related to the representation of the rubber material. An improved material model would be needed to improve the representation of the rubber material.

The rubber bumper was integrated in the panel FE model in its undeformed shape and the compression was involved in the impact analysis. As no specific material data was available for the rubber bumper, linear elasticity was assumed with a stiffness that represented the behaviour of the test well. Since also the attachment bolts inside the rubber bumper were included in the FE model which enabled a more precise representation of the load distribution within the bumper, element distortion problems penalized the simulations. Thus, the rubber stiffness had to be locally increased to avoid detrimental element deformation in the regions of the bumper attachment bolts which stopped the FE calculations. The availability of more appropriate material data would permit a more stable behaviour of the rubber material (see 10).

The FE analyses of the panel model were very time consuming. This limitation required a high impact velocity. Using a velocity of 1 m/s, the numerical analyses could be performed in approx. three days each. The test was done statically for better control and a higher amount of gained measurement data. This led to deviations between the test and the FEA mainly in terms of dynamic effects such as vibration and inertia effects.

The FE analyses have been performed using the Abaqus explicit solver which avoided stability problems and other convergence issues that emerge for models of this size and complexity in implicit analyses. The usage of contact definitions, the different damage models and the high element deformation within the rubber bumper indicated that static FE analyses (Abaqus standard solver) would not be applicable.

8 Outreach

The conducted activities delivered a FE representation of the defined fuselage panel that is able to simulate the tested loading situation with acceptable precision. The FE model that was developed in CODAMEIN II showed good representation of the panel behaviour in the performed test. It proposes further usage of the model for simulations of different load cases, different positions and loading angles, further materials and panel designs. The gained test data and the FEA provided a significant amount of information that helps to understand the way damage forms in the investigated case of high energy low velocity blunt impact on composite or hybrid fuselage structure. This might be beneficial for aircraft design and certification as well as for ground handling and maintenance. Impact damage due to ground service collision can be avoided more effectively and the reporting of collisions may be adapted for the new fuselage materials. Using the results of this investigation, the specific traces of damage on the inside of the structure can be found in a targeted way.

9 Conclusions

Experimental tests were performed in which, based on the outcomes of the CODAMEIN project, a hybrid design fuselage panel was tested statically. The test panel was loaded by an impact load applied by a rubber bumper as typically used for ground service equipment. Damage with no external visibility was generated in the test panel. The testing concept as well as the test panel design of CODAMEIN was adopted. The test panel was rigged using pin joints at both ends of the three inner frames, giving longitudinal rotation DOF to both frame ends and translational spring stiffness normal to the impact direction to one end of the inner frames. For further development of the understanding on damage initiation and damage progression key phenomena, more measurement instrumentation was defined for the test. The numerical analyses were extended to include a higher detail level and deliver simulation results of the damage initiation and the damage progression.

The CODAMEIN II testing was in conjunction with the research activities of the UCSD' s research group in terms of the harmonized test panel design (the UCSD used all composite test panels while CODAMEIN uses a hybrid design with high similarity) and the same used rubber bumper being impacted at the same position of the panel. The test fixtures that were different to those of the UCSD, were adopted from the CODAMEIN test. The characteristic damage sequence of the CODAMEIN test and the UCSD tests was confirmed by the CODAMEIN II test and the associated numerical analyses. In this characteristic sequence, the loaded three centre shear ties (ST 2-3, 3-3, 4-3) started to bend first. While the L-shape of these shear ties opened and initiated damage in the radii, the centre regions of the three inner frames rotated. In the CODAMEIN test (not in the CODAMEIN II test) and the UCSD tests that were run up to panel failure, the centre shear tie failed first. Due to load redistribution, the centre shear ties of the adjacent frames failed at the same impactor displacement which made the centre frames contact the two centre stringers. The next step of damage that was only reached in tests of the UCSD, was either breaking of frames or perforation of stringers. At this damage level, the UCSD also found local debonding of the stringers. Stringer disbond was found neither in the CODAMEIN test nor in the CODAMEIN II test.

The test panel design and the test fixtures were reviewed at the beginning of CODAMEIN II. It was decided to use the same test fixtures as for the CODAMEIN test for comparability. The test panel design was slightly adapted by a frame reinforcement near the boundary that had no influence on the global panel behaviour while it reduced the risk of frame boundary failure at high test loads. The test fixtures which were used similarly in the CODAMEIN test and the CODAMEIN II test, where modified by increasing the translational spring stiffness based on numerical analysis results delivered by an advanced full barrel model implying stiffening inner structure.

The panel was tested in two load cycles. The expected general response of the panel and the similarity to the CODAMEIN test were confirmed. The energy levels 974 J and 1443 J were reached. In accordance with the UCSD research, the shear ties were found to be the parts to get damaged and to fail first while the inner frames rotated without reaching plasticity. To enable a replacement of shear ties for further testing in the future, as it has been done by the UCSD, the test was limited to an extent which only damages the shear ties and leaves the remaining panel undamaged for a shear tie replacement in a future test. Based on this decision, two load cycles were tested. Apart from damage to the shear ties, the test panel has not been further damaged. The characteristic damage sequence proposes that the usage of stronger shear ties is necessary to change that damage sequence, which would possibly lower the limits of external damage visibility. The increased boundary stiffness of the test fixtures was found to have no significant influence on the panel response. At high loads, the simulated rotational stiffness at the panel test fixtures, which was not implemented in the used test fixtures, indicated to be the more significant boundary stiffness, especially at higher panel deformations than have been reached in the test. Thus the used boundary conditions are expected to be insufficient against boundary conditions including rotational stiffness for high panel deformations.

Numerical analyses were performed, which implied a higher detail model than in the CODAMEIN numerical analyses. The overall panel response as well as damage onset and damage progression were represented by the analyses. Due to the high impact velocity, the panel model response showed significant dynamic effects. The damage sequence that was found in the testing campaigns of CODAMEIN / CODAMEIN and the UCSD research was represented by the analyses. The stiffness of the panel as well as the significant damage events (the damage sequence) including the specific damage types and the softening of the structure were represented by the numerical analyses.

The ability of the panel FE model to represent the test panel well proposes extended usage of this modelling approach for simulation of various impact scenarios. Within the investigated general panel design, different configurations may be analysed. Different boundary conditions, different impact situations regarding impactor type and size, impact position as well as direction and velocity would be applicable. A high quantity of information can thus be gained with a minimum of necessary tests.

The local damage and failure behaviour could not be fully represented by the analysis due to the necessary model simplifications. Thus, local frame plasticity was found in the analyses, clearly prior to the expected yield in the test. The analyses also showed local composite damage in the reinforced skin regions under the shear ties, which was not found in the test. A main reason for these observations was expected to be the model element size which was limited to minimum sizes between 10 mm and 20 mm in these regions. The response of the panel's fixtures could not be simulated well by the analysis since significant mass and friction effects in the test fixtures were concluded from the test results which were available after the completion of the numerical analyses. The test and the numerical analyses also showed a low influence especially of the boundary stiffness on the panel response. The rubber bumper was integrated in the numerical model with a high detail level that implied the attachment structure and the simulation of the bumper compression process. As no bumper material tests could be performed within this project, its material was simulated in a simplified way, using a stiffness that enabled compression behaviour similar to the test observations. Main parameters that govern the formation of impact damage were assessed in a sensitivity study.

The results of the sensitivity studies were used for the further improvement of the test panel numerical model. The possibilities of modifications to the design of components of the panel or to the used materials that would force a change of the characteristic damage sequence were assessed. As a result, basic modifications such as different boundary conditions or the exchange of parts of the panel with parts of different stiffness and strength are expected to be required to generate a change in the basic damage sequence.

The significance of damage with no or low visibility which was one of the basic subjects of CODAMEIN II as a threat to aircraft that consist of a high ratio of CFRP material, was confirmed. The test and the FEA proved that in the investigated case of high energy blunt impact, potential significant structural damage on the structure's inside may be generated while the outer skin returned to its original shape and remained visually undamaged. Even the threshold of invisible e.g. delamination damage to the skin is significantly higher than that of serious damage up to multiple failure of inner structure components.

10 Recommendations

Further testing based on the current project has been envisaged during the project. The possibility to gain information from a test which includes a different damage sequence was judged very important. It is recommended to perform further tests using the existing test panel with a new set of shear ties. Those should be designed within the aspects of which maximum stiffness and strength of shear ties is feasible for the present representative fuselage design and if a consequent change of the damage sequence can be expected.

Tests on coupon, element and component level are recommended to increase confidence in the developed and used modelling methods, to clarify questions that emerged during the performed investigation and to improve the accuracy of material parameters. Several material parameters such as the stiffness of the rubber bumper material shall be assessed via specific material tests.

The usage of different test fixtures is expected to enable an improvement of the structure representation and consequently of the value of information gained from a test. The test and the FEA in CODAMEIN II showed the limitations of the current boundary conditions. Especially the single boundary stiffness in translation in combination with free longitudinal rotation indicated disadvantages compared to the combined boundary stiffness incorporating rotational stiffness, already at low load. As the influence of the rotational boundary stiffness is expected to become more significant at higher loads, the incorporation of rotational stiffness, according to the test set-up used by the UCSD is judged necessary for future tests. The extension of the test fixture to all five frames instead of the three centre frames is recommended to improve the representation of the entire fuselage structure by providing an improved transition to the unaffected structure. The deviation between the currently used 3-frame attachment and the 5-frame attachment that was assessed using FE analyses, was found to be low at low impact loads and is expected to have significant influence at higher loads at the state of significant damage. The performed investigations have focused on a 5-frame 4-stringer fuselage cut-out with single curvature and with a boundary condition concept that incorporates only the frame ends. An extension of the boundary conditions to the skin and the stringers might provide an improved representation of the aircraft structure. The friction within the test fixtures indicated to have high influence on the panel behaviour. Thus, the test fixtures used for future tests shall be tested for friction, mass influence or damping, to integrate this behaviour in the FE analyses.

Based on the knowledge about the response of the tested structure gained in the CODAMEIN and CODAMEIN II tests and analyses, additional dynamic tests would be beneficial to assess the influence of the velocity of the impact process. Due to the limitations in the doability of FE simulations, a direct comparison between a static test and a dynamic test appears to be complicated. The computation time had important influence on the performed FE analyses and required a high impact velocity which deviated from the static test. The reduction of the computation time along with a reduction of the impact velocity is an important goal for a future FE investigation.

Material tests should be performed on the rubber bumper material. To integrate realistic rubber-elastic behaviour in the FE model, the necessary parameters would have to be assessed in a material test.

As the FE panel model developed within CODAMEIN II was able to simulate the test case of CODAMEIN II well, extensive usage of this modelling approach for the simulation of different load cases, different materials and impacted structures, including different skin curvature, possible double curvature and different boundary conditions is proposed. Comprehensive information on impacts can thus be gained prior to any experimental testing. To validate further configurations of FE models, the extension of the impact investigations to larger structures, up to a fuselage barrel is however recommended. The aft fuselage of aircraft which is highly prone for the investigated kind of ground impacts encloses double-curved structure, changing inner structure and changing skin thicknesses. The integration of more of these items might reveal new damage scenarios as well as new information about the criticality and detectability of damage.

Furthermore, specific recommendations relating to Airworthiness Certification, Continued Airworthiness and Maintenance as well as operational recommendations are made.

Airworthiness Certification

The design space around the assessed structure should be investigated to gain a better understanding regarding detrimental effects of design changes that e.g. lead to more critical damage situations or promote faster developing failure.

Continued Airworthiness and Maintenance

The impact of the damage without external visibility that was generated in the CODAMEIN and CODAMEIN II test on the residual strength of the structure could not be assessed within this investigation. Thus, the residual strength of structure implying damage like the generated type should be assessed in a future project. The level of damage to the inner structure which was generated in the CODAMEIN / CODAMEIN II tests and in the tests performed by the UCSD, indicates a reduction of the residual strength of the structure. As the developed FE model proved to be able to simulate the damage sequence that was found in the test, a strength and residual strength investigation using FEA is expected appropriate. The development of a set-up and loading approach for the strength and residual strength analysis is therefore recommended. As none of the impacts that were performed with a soft rubber bumper left external visible traces, it is important to either record the damage event or to use inspection techniques in the regular inspections that may detect damage to the frames, stringers and shear ties. Structural Health Monitoring (SHM) is one possible approach to detect impact damage using technology built-into the aircraft structure. SHM systems are subject to research, yet have not reached the maturity for application in CS-25 aircraft yet.

Should the investigated blunt impact prove to be able to reduce the residual strength to LL or below, the recording of the impact event would be mandatory to permit assessment of the damage. Since the investigated case of high energy blunt impact that showed the described threat potential is limited to ground service vehicle collision, damage recording would be ensured by the introduction of appropriate sensor technology in the ground service vehicles and of appropriate operation procedures.

Operational

While the visibility of impact damages at the aircraft can be low and therefore detection might be complicated, an improvement of the recording of impact events is an obvious approach. Both the equipment of ground service vehicles with collision and overload detection systems and the reporting procedures leave space for improvement. The standardisation of safety systems for ground service vehicles will reduce the threat of collisions. Also the reporting processes and the training of staff should be adapted to the requirements and the damage visibility characteristics at composite aircraft. Reporting principles covering every inadmissible contact must be followed to assess the specific risks of every event that potentially leads to impact damage. The rate of reported vehicle aircraft contacts of 50% [Kaiser, 2011] might otherwise further reduce due to the lack of visibility for composite hulls. Ground service vehicles which repeatedly make contact with the fuselage, such as mobile stairs and cargo loaders might be fitted with monitoring and assistance systems that would provide better visibility and assessment of the vehicle’s movement within a specified distance from the fuselage. Recording of sensor and camera data might support the complete reporting of incidents and their investigation.

Appendix A Hardware, Software

- Abaqus 6.11 CAE, Abaqus 6.11 Explicit solver
- Analyses on HP xw9400 Linux workstations using 4 AMD Opteron CPUs, 8, 16 or 32 GB RAM
- Analysis time of the panel model: minimum 40 h

Appendix B Drawings

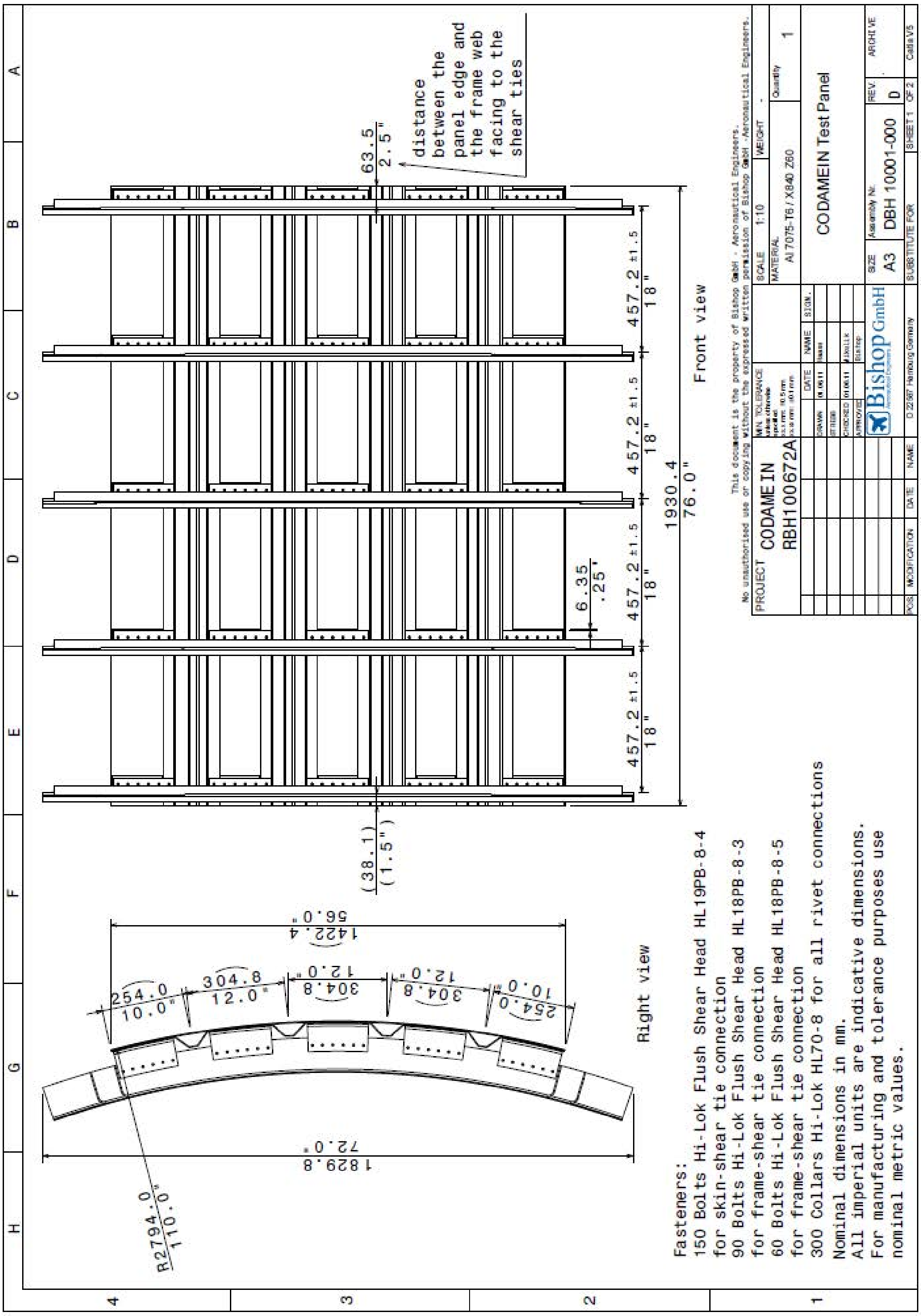

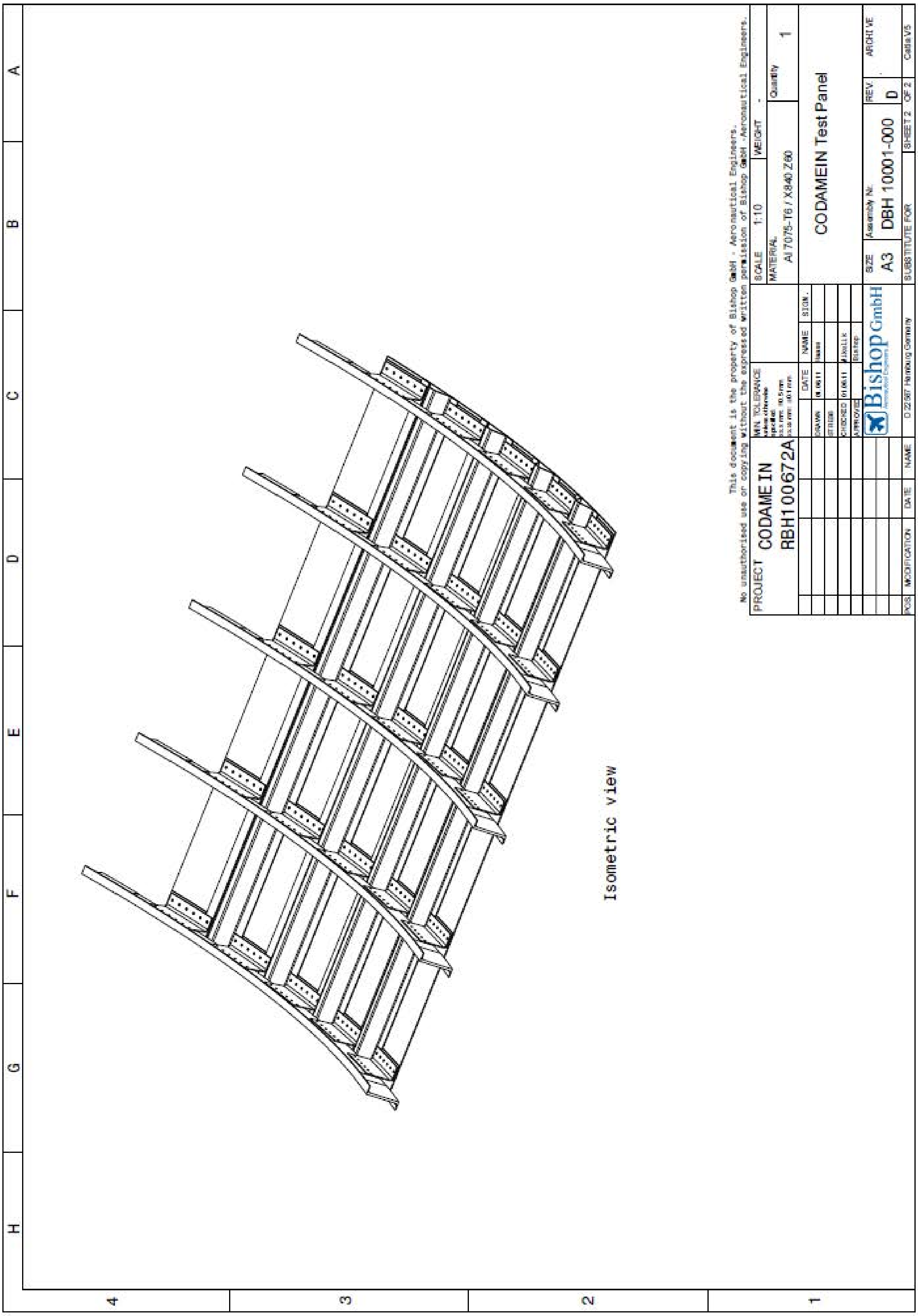

Isometric view
PROJECT CODAMEIN RBH100672A
SCALE 1:10
MATERIAL Al 7075-T6 / X840 Z60
CODAMEIN Test Panel
SIZE A3
Assembly Nr. DBH 10001-000
REV. D

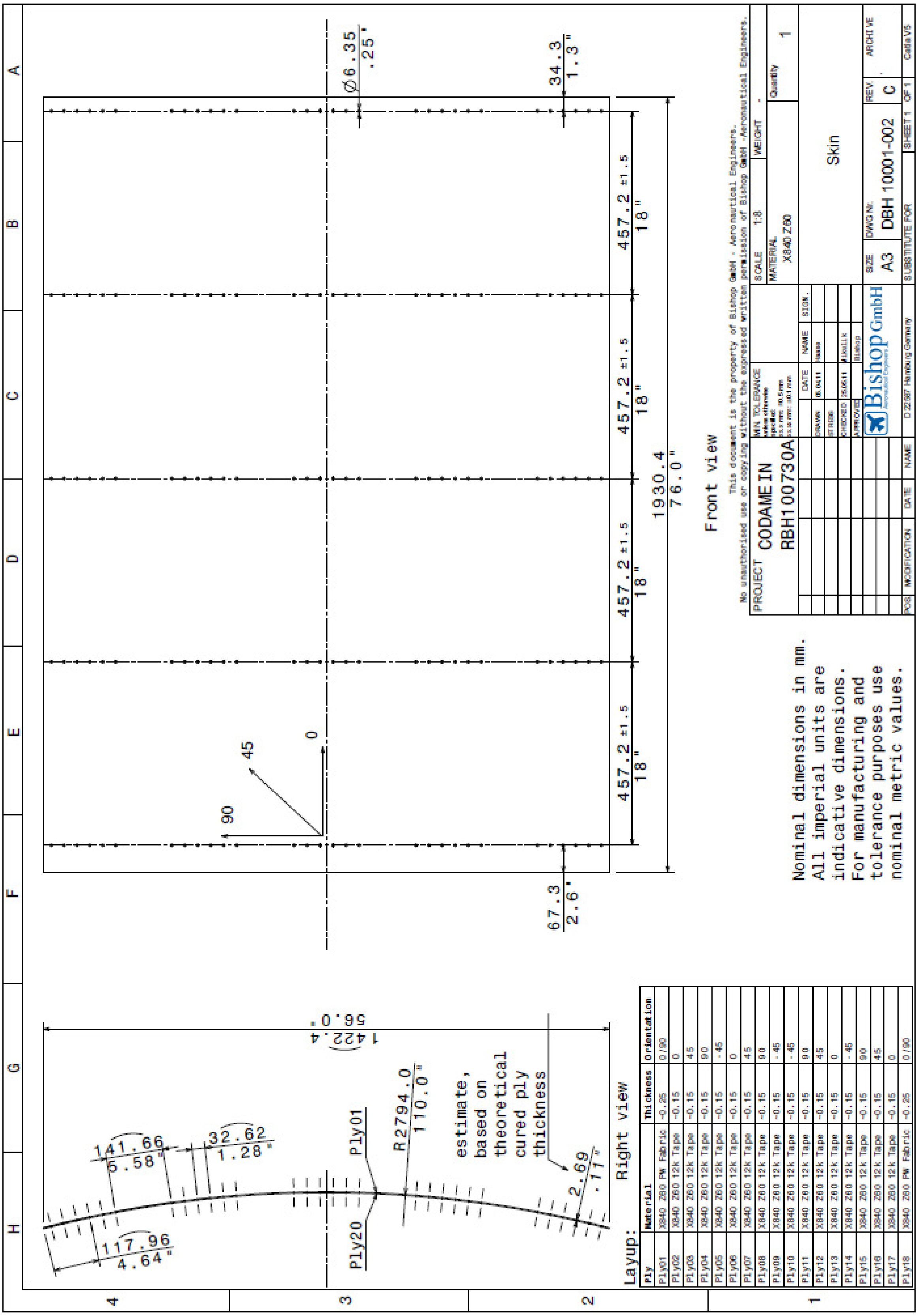

Layup:

Ply	Material	Thickness	Orientation
Ply01	X840 Z60 PW Fabric	~0.25	0/90
Ply02	X840 Z60 12k Tape	~0.15	0
Ply03	X840 Z60 12k Tape	~0.15	45
Ply04	X840 Z60 12k Tape	~0.15	90
Ply05	X840 Z60 12k Tape	~0.15	-45
Ply06	X840 Z60 12k Tape	~0.15	0
Ply07	X840 Z60 12k Tape	~0.15	45
Ply08	X840 Z60 12k Tape	~0.15	90
Ply09	X840 Z60 12k Tape	~0.15	-45
Ply10	X840 Z60 12k Tape	~0.15	-45
Ply11	X840 Z60 12k Tape	~0.15	90
Ply12	X840 Z60 12k Tape	~0.15	45
Ply13	X840 Z60 12k Tape	~0.15	0
Ply14	X840 Z60 12k Tape	~0.15	-45
Ply15	X840 Z60 12k Tape	~0.15	90
Ply16	X840 Z60 12k Tape	~0.15	45
Ply17	X840 Z60 12k Tape	~0.15	0
Ply18	X840 Z60 PW Fabric	~0.25	0/90

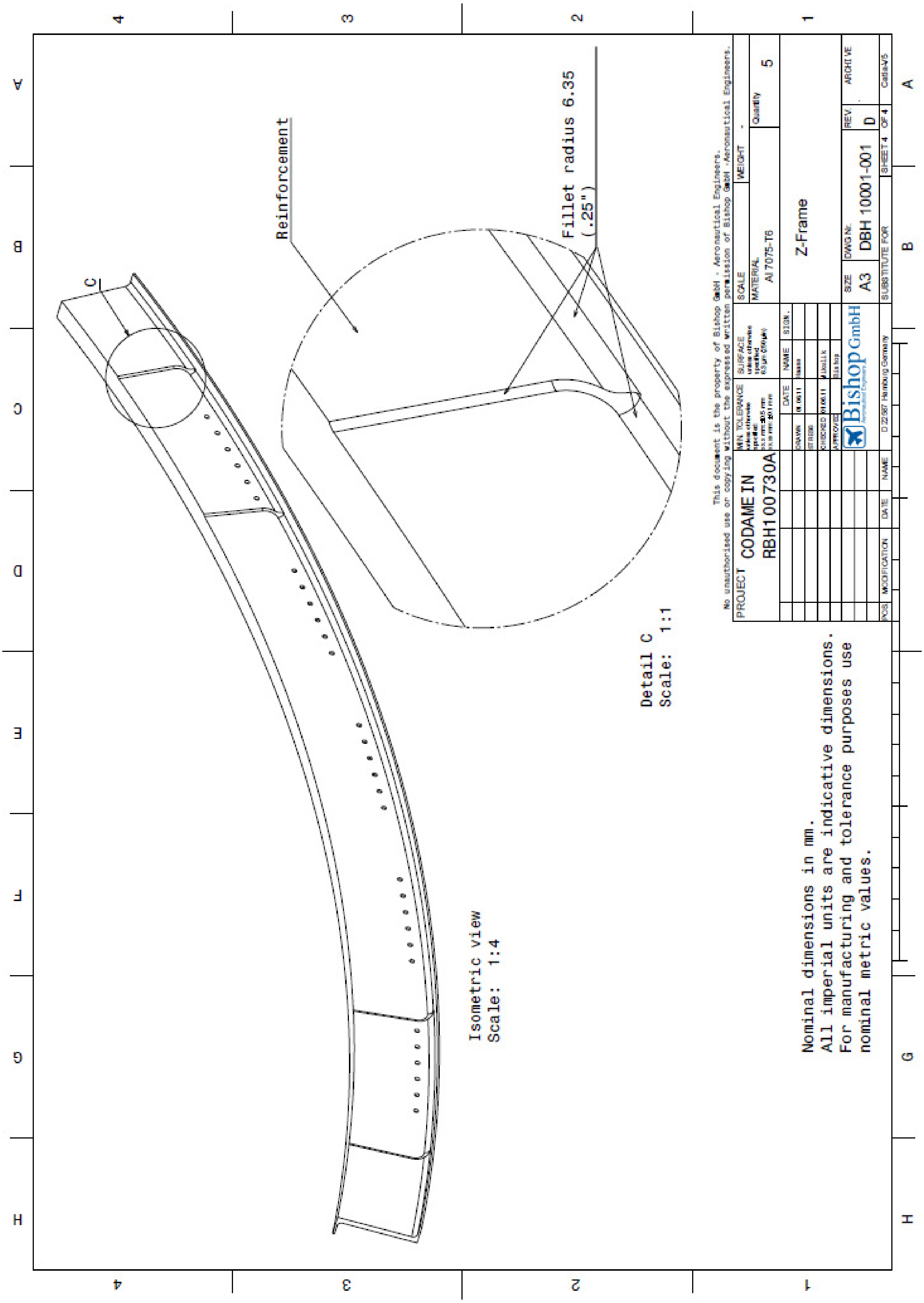

Reinforcement
Fillet radius 6.35 (.25")
C
Detail C
Scale: 1:1
Isometric view
Scale: 1:4
Nominal dimensions in mm.
All imperial units are indicative dimensions.
For manufacturing and tolerance purposes use nominal metric values.
PROJECT CODAMEIN RBH100730A
MATERIAL Al 7075-T6
Quantity 5
Z-Frame
SIZE A3
DWG Nr. DBH 10001-001
REV. D
SHEET 4 OF 4

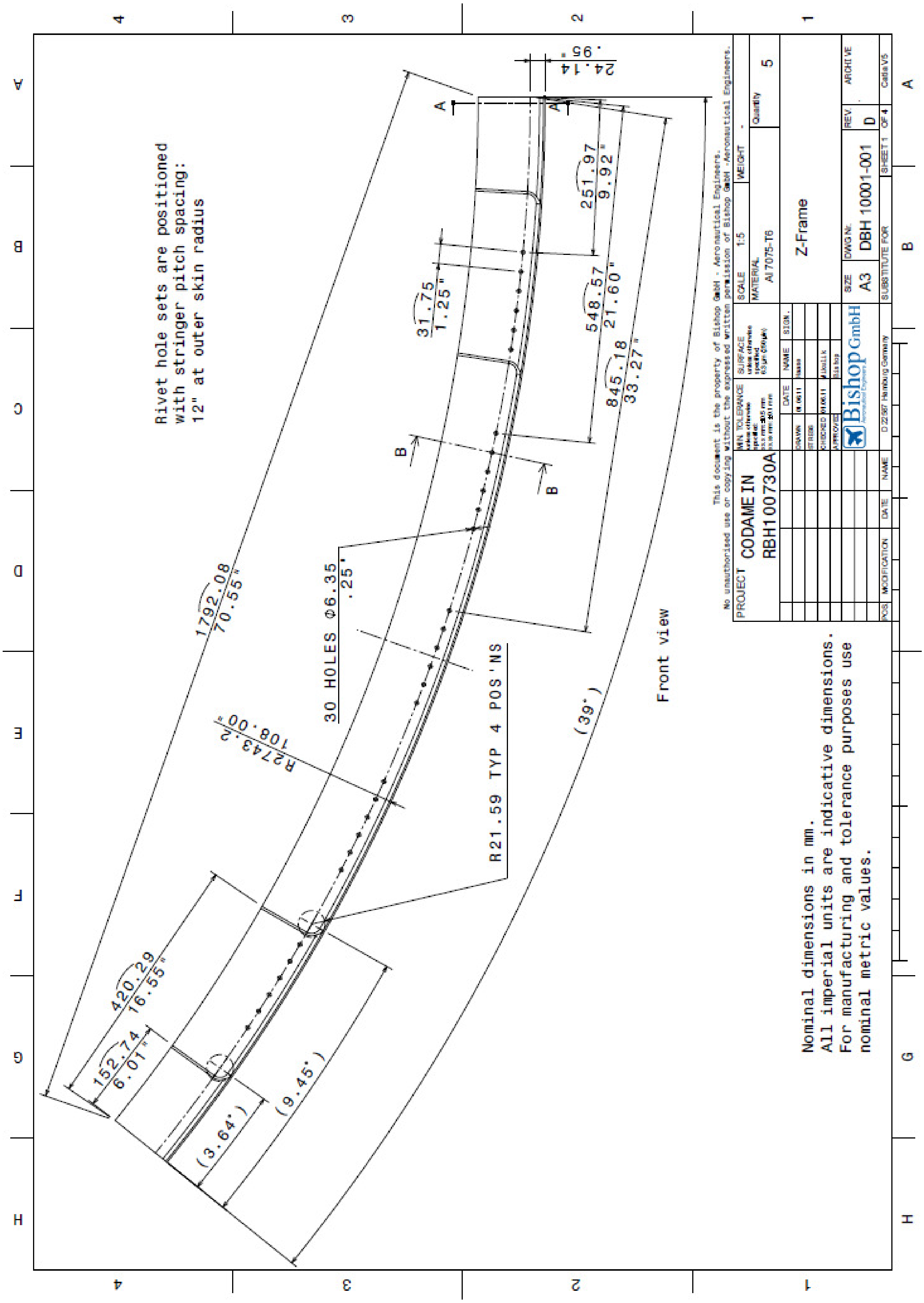

Rivet hole sets are positioned with stringer pitch spacing: 12" at outer skin radius
1792.08 70.55"
30 HOLES Φ6.35 .25"
R2743.2 108.00"
R21.59 TYP 4 POS'NS
31.75 1.25"
251.97 9.92"
548.57 21.60"
845.18 33.27"
24.14 .95"
420.29 16.55"
152.74 6.01"
(3.64')
(9.45')
(39')
Front view
Nominal dimensions in mm.
All imperial units are indicative dimensions.
For manufacturing and tolerance purposes use nominal metric values.
PROJECT CODAMEIN RBH100730A
MATERIAL Al 7075-T6
SCALE 1:5
Quantity 5
Z-Frame
SIZE A3
DWG No. DBH 10001-001
REV. D

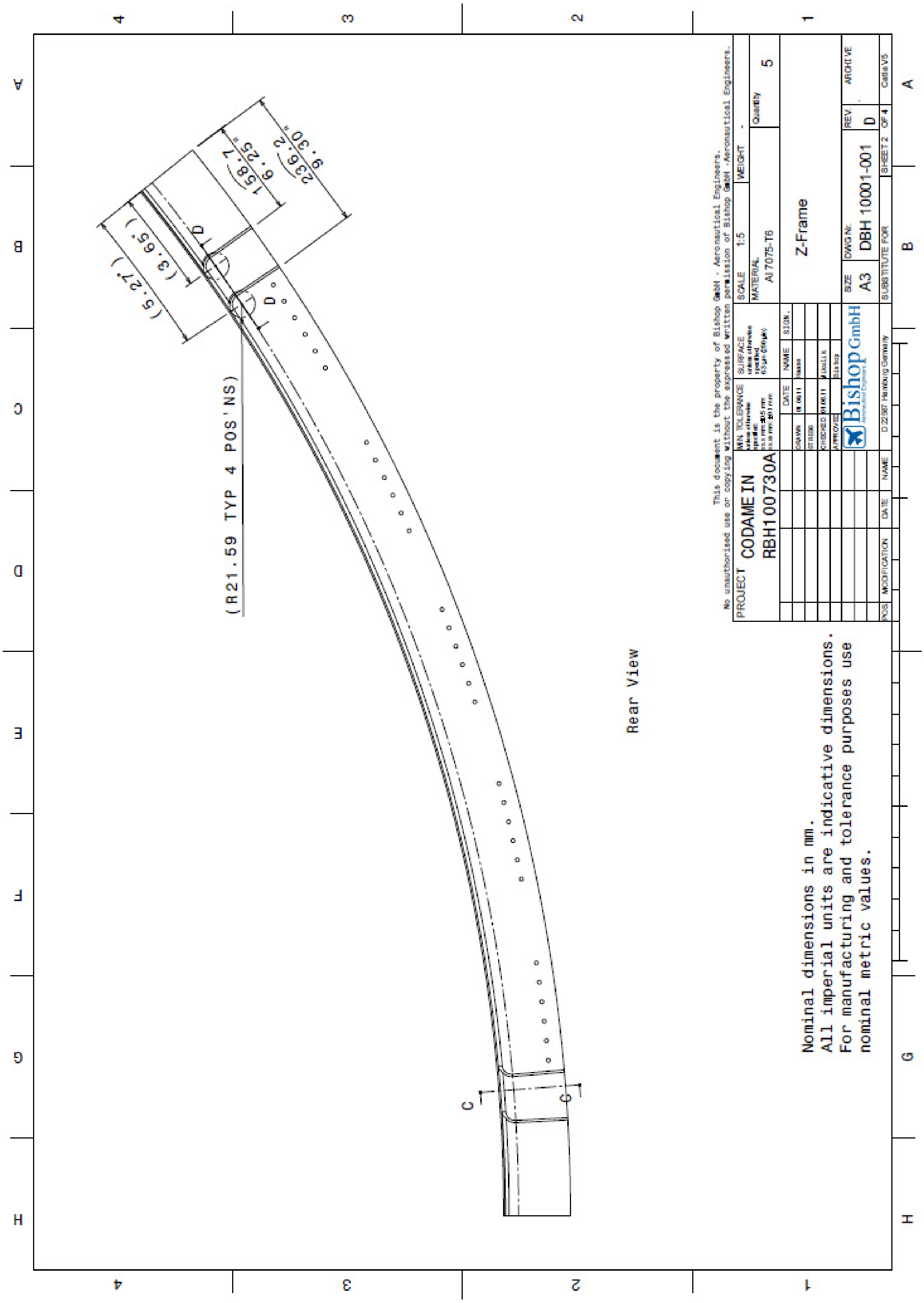
(R21.59 TYP 4 POS'NS)
Rear View
Z-Frame
CODAMEIN RBH100730A
Al 7075-T6
DBH 10001-001
A3
Nominal dimensions in mm.
All imperial units are indicative dimensions.
For manufacturing and tolerance purposes use
nominal metric values.

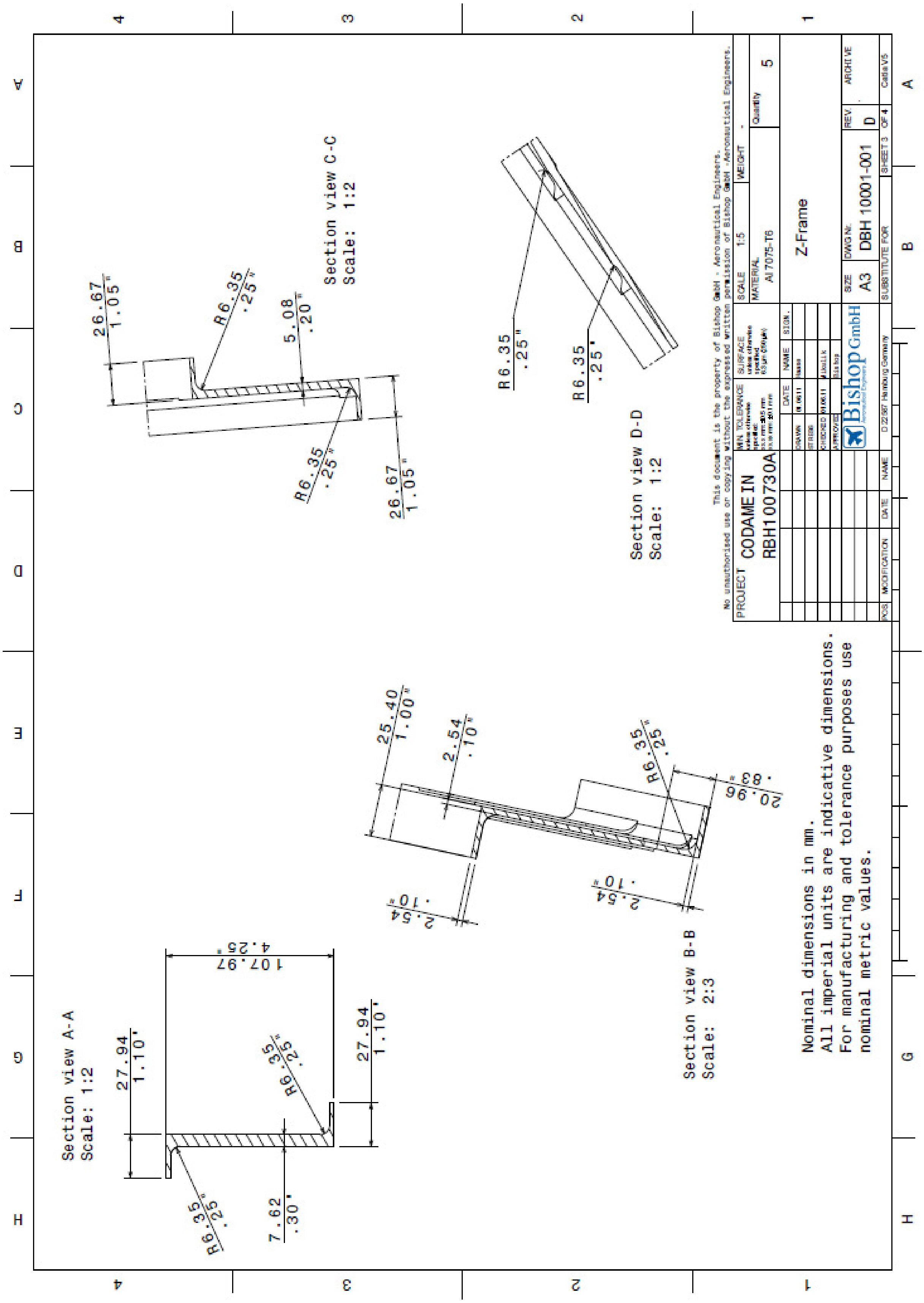
Section view C-C
Scale: 1:2
26.67
1.05"
R6.35
.25"
5.08
.20"
Section view D-D
Scale: 1:2
Section view B-B
Scale: 2:3
25.40
1.00"
2.54
.10"
20.96
.83"
Section view A-A
Scale: 1:2
107.97
4.25"
27.94
1.10"
7.62
.30"
Nominal dimensions in mm.
All imperial units are indicative dimensions.
For manufacturing and tolerance purposes use nominal metric values.
This document is the property of Bishop GmbH - Aeronautical Engineers.
No unauthorised use or copying without the expressed written permission of Bishop GmbH - Aeronautical Engineers.
PROJECT CODAMEIN RBH100730A
MATERIAL Al 7075-T6
SCALE 1:5
Quantity 5
Z-Frame
SIZE A3
DWG Nr. DBH 10001-001
REV. D
SHEET 3 OF 4
Catia V5
Bishop GmbH

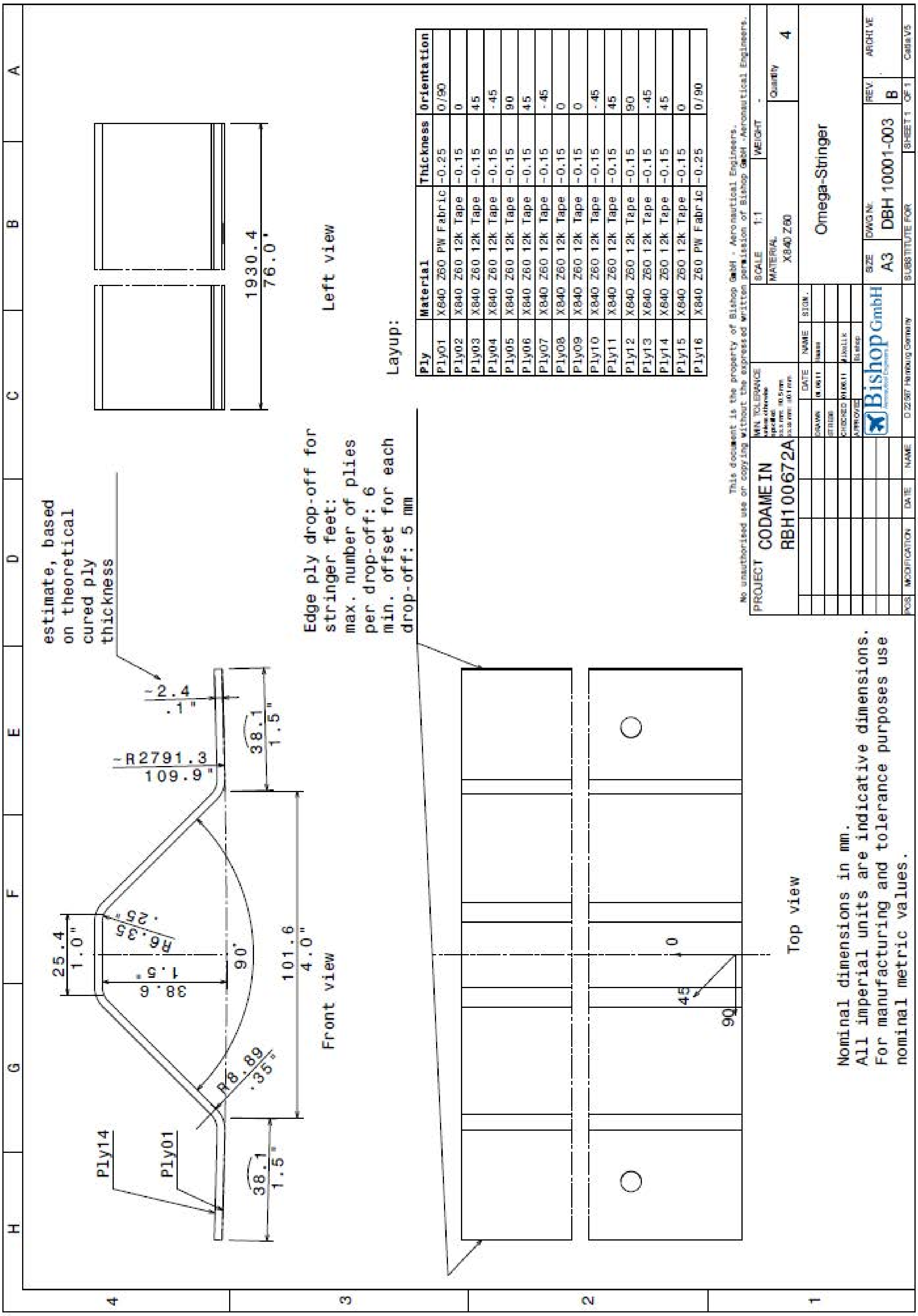

Ply	Material	Thickness	Orientation
Ply01	X840 Z60 PW Fabric	-0.25	0/90
Ply02	X840 Z60 12k Tape	-0.15	0
Ply03	X840 Z60 12k Tape	-0.15	45
Ply04	X840 Z60 12k Tape	-0.15	-45
Ply05	X840 Z60 12k Tape	-0.15	90
Ply06	X840 Z60 12k Tape	-0.15	45
Ply07	X840 Z60 12k Tape	-0.15	-45
Ply08	X840 Z60 12k Tape	-0.15	0
Ply09	X840 Z60 12k Tape	-0.15	0
Ply10	X840 Z60 12k Tape	-0.15	-45
Ply11	X840 Z60 12k Tape	-0.15	45
Ply12	X840 Z60 12k Tape	-0.15	90
Ply13	X840 Z60 12k Tape	-0.15	-45
Ply14	X840 Z60 12k Tape	-0.15	45
Ply15	X840 Z60 12k Tape	-0.15	0
Ply16	X840 Z60 PW Fabric	-0.25	0/90

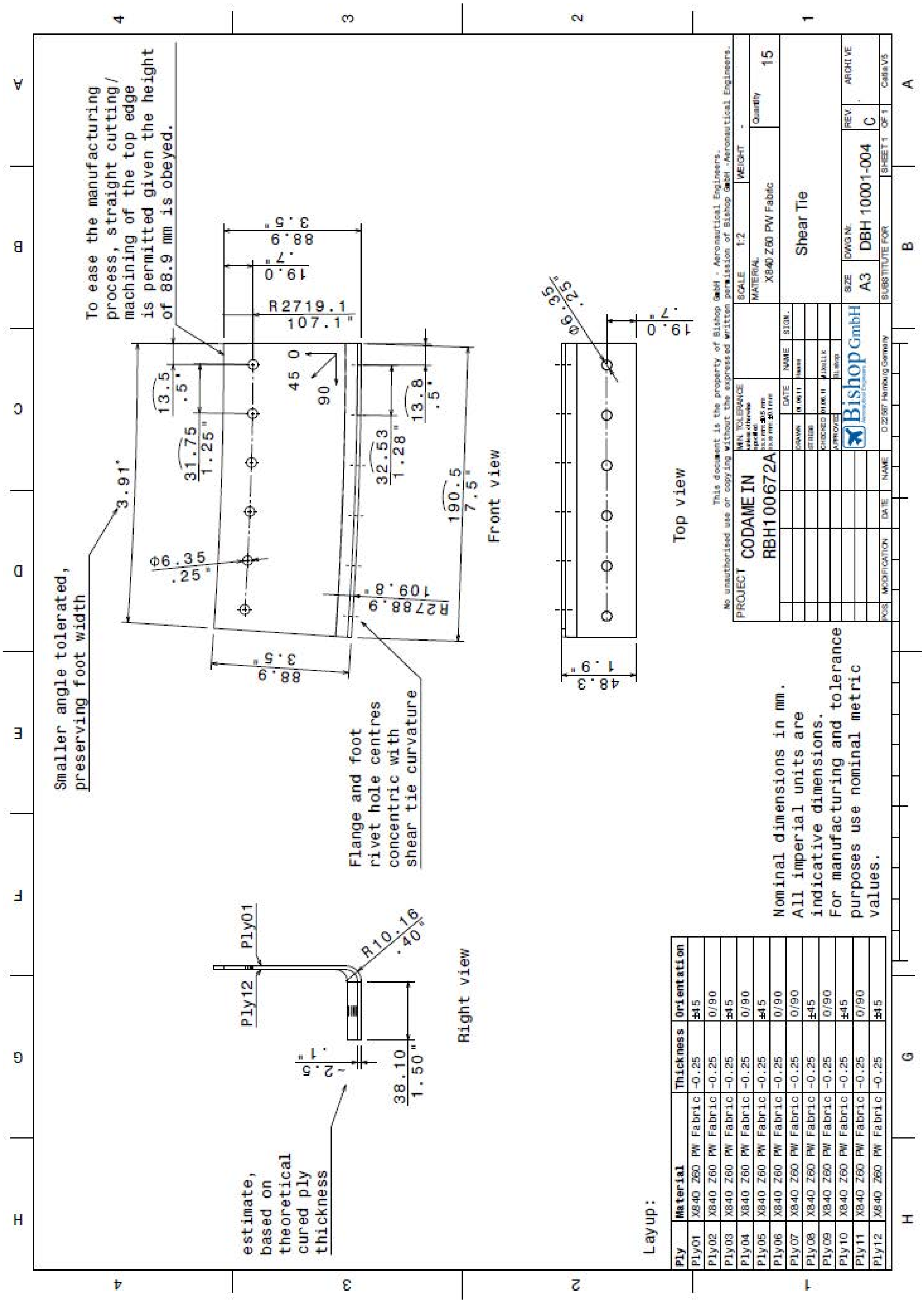

Ply	Material	Thickness	Orientation
Ply01	X840 Z60 PW Fabric	~0.25	±45
Ply02	X840 Z60 PW Fabric	~0.25	0/90
Ply03	X840 Z60 PW Fabric	~0.25	±45
Ply04	X840 Z60 PW Fabric	~0.25	0/90
Ply05	X840 Z60 PW Fabric	~0.25	±45
Ply06	X840 Z60 PW Fabric	~0.25	0/90
Ply07	X840 Z60 PW Fabric	~0.25	0/90
Ply08	X840 Z60 PW Fabric	~0.25	±45
Ply09	X840 Z60 PW Fabric	~0.25	0/90
Ply10	X840 Z60 PW Fabric	~0.25	±45
Ply11	X840 Z60 PW Fabric	~0.25	0/90
Ply12	X840 Z60 PW Fabric	~0.25	±45

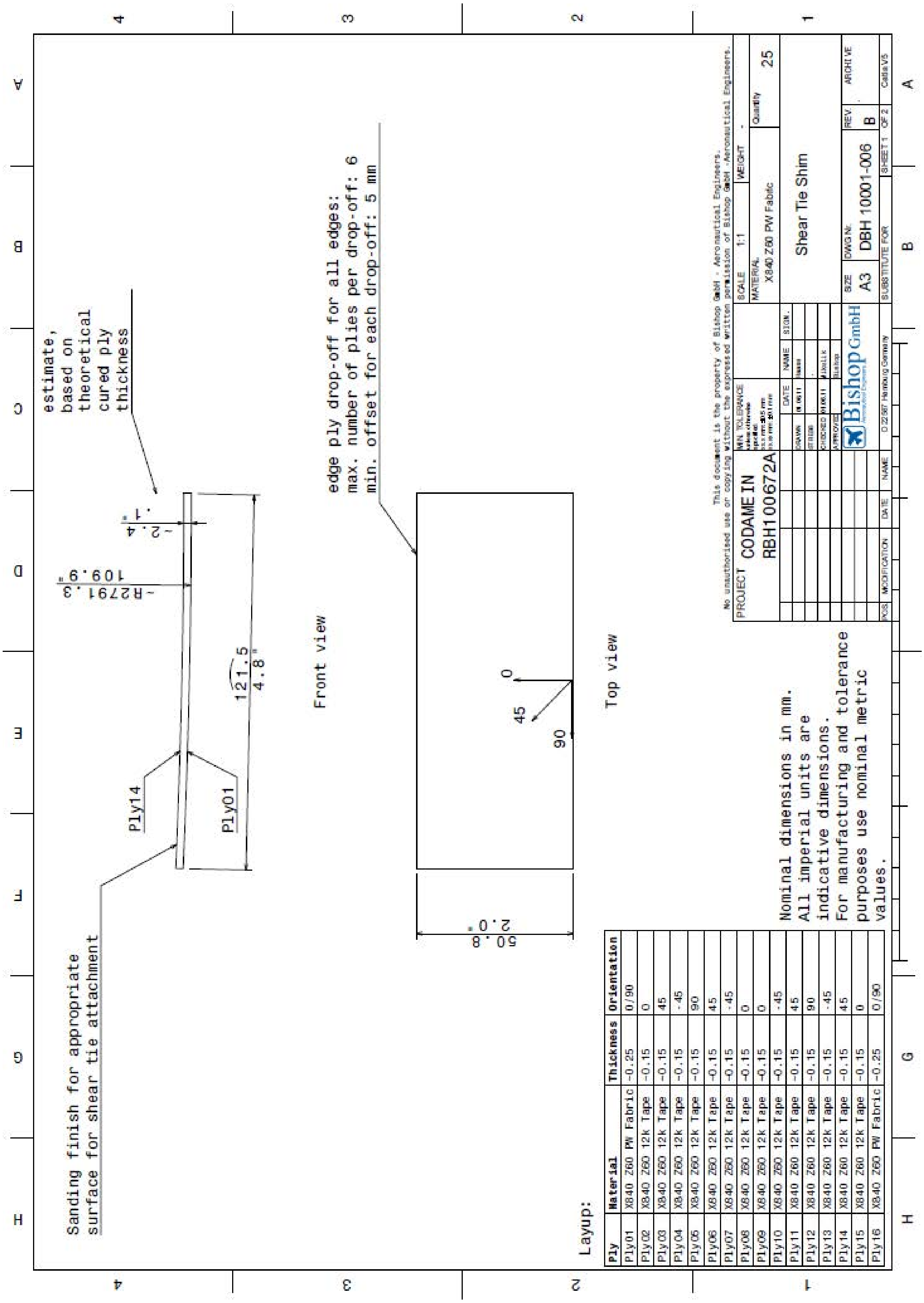

Ply	Material	Thickness	Orientation
Ply01	X840 Z60 PW Fabric	~0.25	0/90
Ply02	X840 Z60 12k Tape	~0.15	0
Ply03	X840 Z60 12k Tape	~0.15	45
Ply04	X840 Z60 12k Tape	~0.15	-45
Ply05	X840 Z60 12k Tape	~0.15	90
Ply06	X840 Z60 12k Tape	~0.15	45
Ply07	X840 Z60 12k Tape	~0.15	-45
Ply08	X840 Z60 12k Tape	~0.15	0
Ply09	X840 Z60 12k Tape	~0.15	0
Ply10	X840 Z60 12k Tape	~0.15	-45
Ply11	X840 Z60 12k Tape	~0.15	45
Ply12	X840 Z60 12k Tape	~0.15	90
Ply13	X840 Z60 12k Tape	~0.15	-45
Ply14	X840 Z60 12k Tape	~0.15	45
Ply15	X840 Z60 12k Tape	~0.15	0
Ply16	X840 Z60 PW Fabric	~0.25	0/90

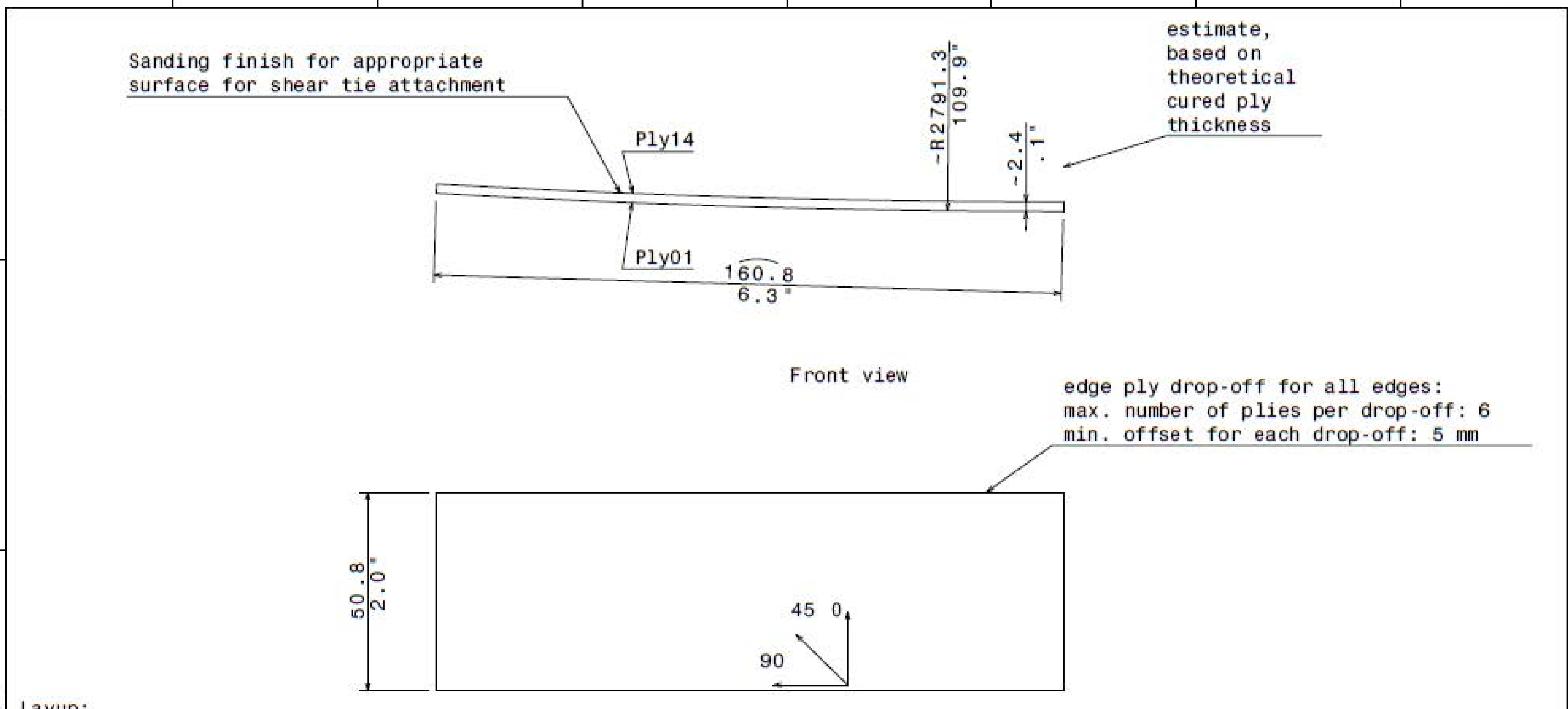

Top view

Layup:

Ply	Material	Thickness	Orientation
Ply01	X840 Z60 PW Fabric	-0.25	0/90
Ply02	X840 Z60 12k Tape	-0.15	0
Ply03	X840 Z60 12k Tape	-0.15	45
Ply04	X840 Z60 12k Tape	-0.15	-45
Ply05	X840 Z60 12k Tape	-0.15	90
Ply06	X840 Z60 12k Tape	-0.15	45
Ply07	X840 Z60 12k Tape	-0.15	-45
Ply08	X840 Z60 12k Tape	-0.15	0
Ply09	X840 Z60 12k Tape	-0.15	0
Ply10	X840 Z60 12k Tape	-0.15	-45
Ply11	X840 Z60 12k Tape	-0.15	45
Ply12	X840 Z60 12k Tape	-0.15	90
Ply13	X840 Z60 12k Tape	-0.15	-45
Ply14	X840 Z60 12k Tape	-0.15	45
Ply15	X840 Z60 12k Tape	-0.15	0
Ply16	X840 Z60 PW Fabric	-0.25	0/90

Nominal dimensions in mm.
All imperial units are indicative dimensions.
For manufacturing and tolerance purposes use nominal metric values.

PROJECT CODAMEIN RBH100730A
SCALE 1:1 | WEIGHT -
MATERIAL X840 Z60 PW Fabric | Quantity 10
DRAWN 27.03.12 Laeder
CHECKED 27.03.12 Haase
APPROVED Bishop
Shear Tie Shim Long
SIZE A3 | DWG Nr. DBH 10001-007 | REV. A | ARCHIVE
SUBSTITUTE FOR | SHEET 1 OF 1 | Catia V5
D 22587 Hamburg Germany

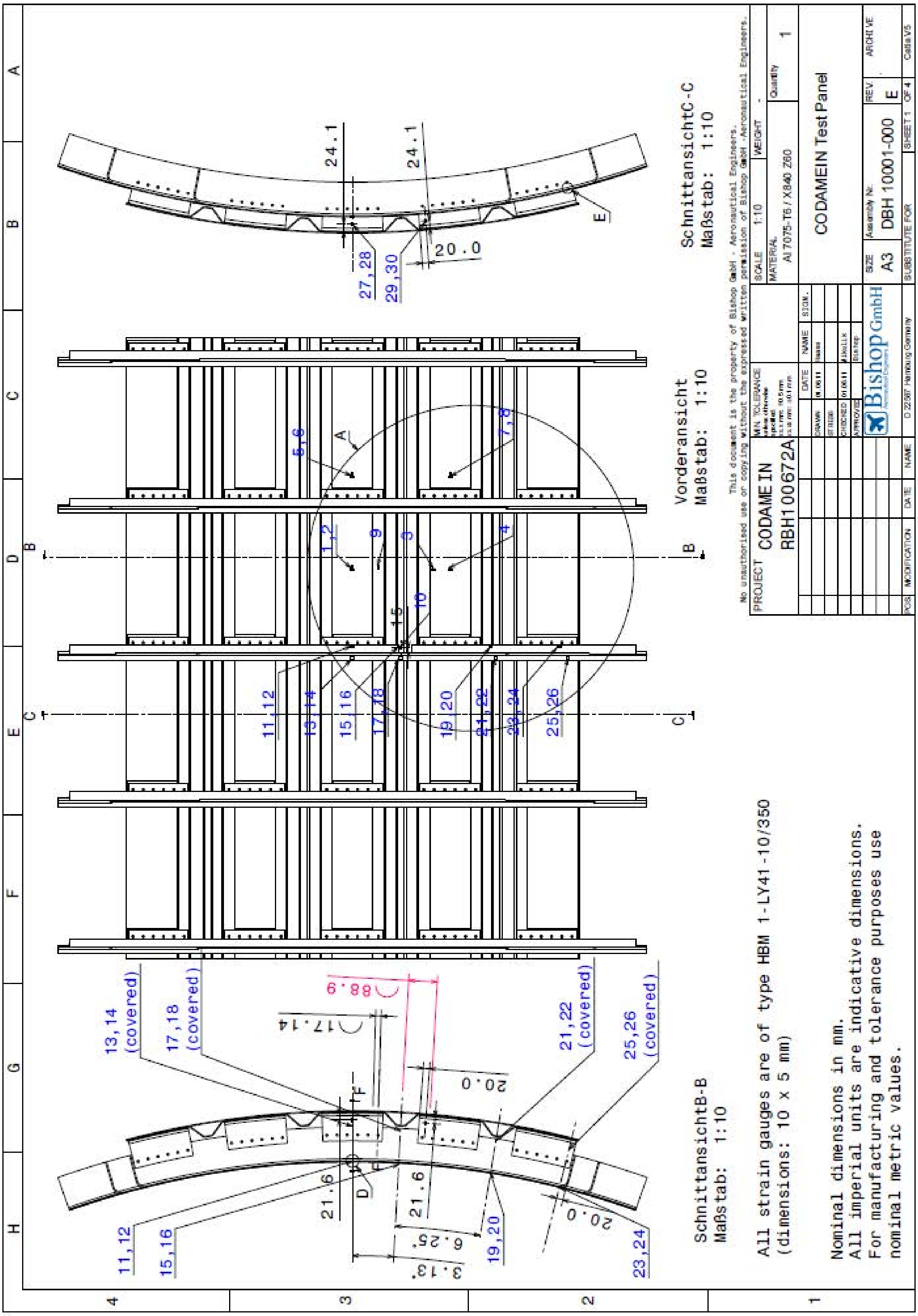
SchnittansichtC-C
Maßstab: 1:10
Vorderansicht
Maßstab: 1:10
SchnittansichtB-B
Maßstab: 1:10
All strain gauges are of type HBM 1-LY41-10/350
(dimensions: 10 x 5 mm)
Nominal dimensions in mm.
All imperial units are indicative dimensions.
For manufacturing and tolerance purposes use
nominal metric values.
13,14 (covered)
17,18 (covered)
21,22 (covered)
25,26 (covered)
CODAMEIN Test Panel
DBH 10001-000
CODAMEIN
RBH100672A
Al 7075-T6 / X840 Z60

Appendix C Test results (Strains)

The strain vs. time charts of all strain gauges are listed below for the test load cycles 1 and 2. The membrane and bending components are displayed for all two-sided strain gauge pairs.

1st load cycle

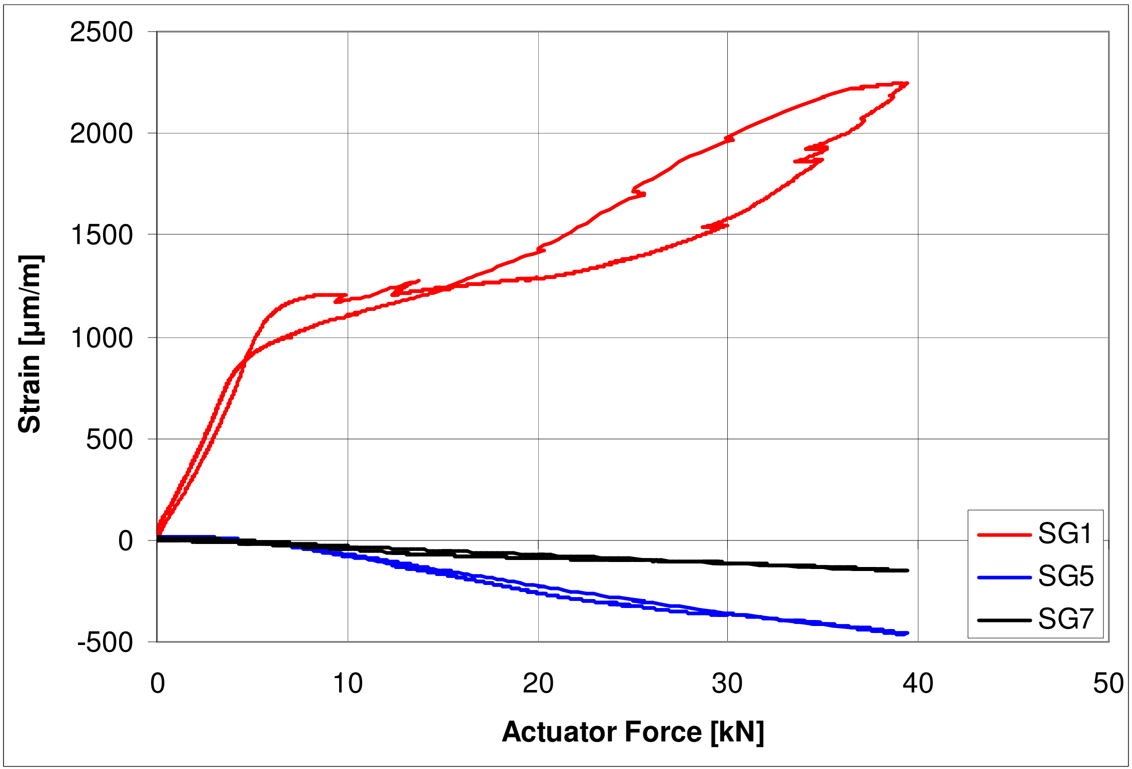

Figure 162 Skin circumferential Strain Gauges: Strain vs. Actuator Load

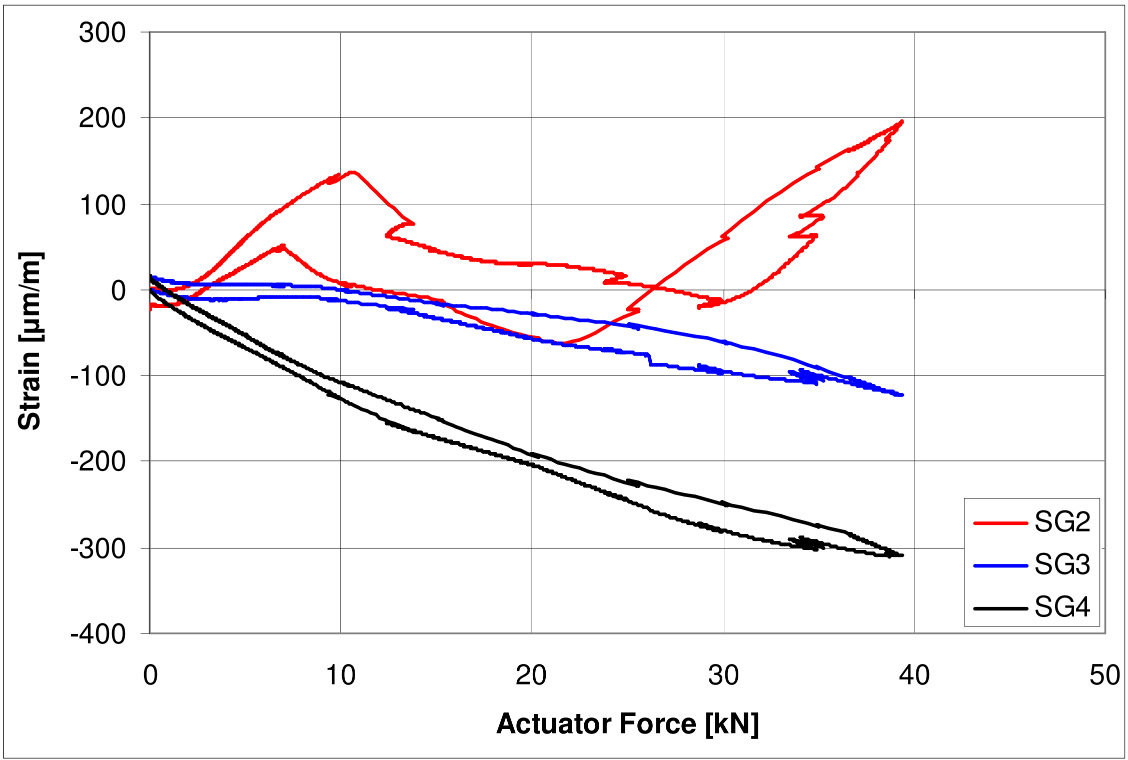

Figure 163 Skin axial Strain Gauges: Strain vs. Actuator Load

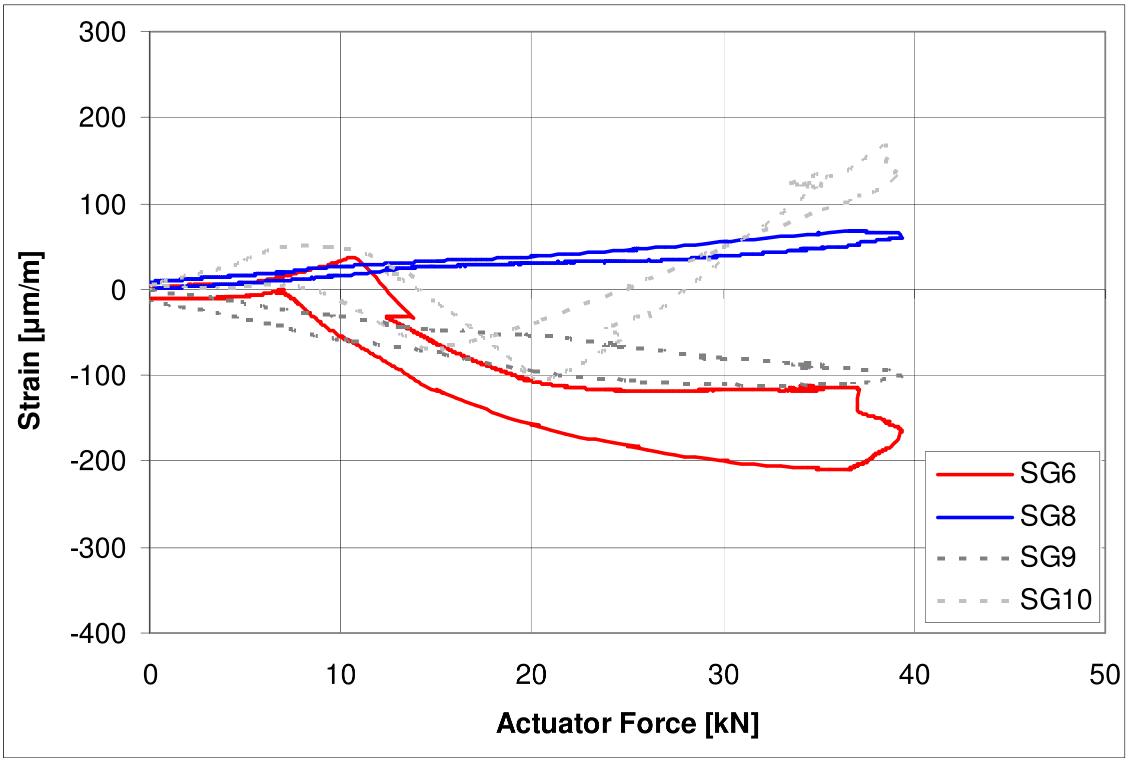

Figure 164 Skin & Stringer axial Strain Gauges: Strain vs. Actuator Load

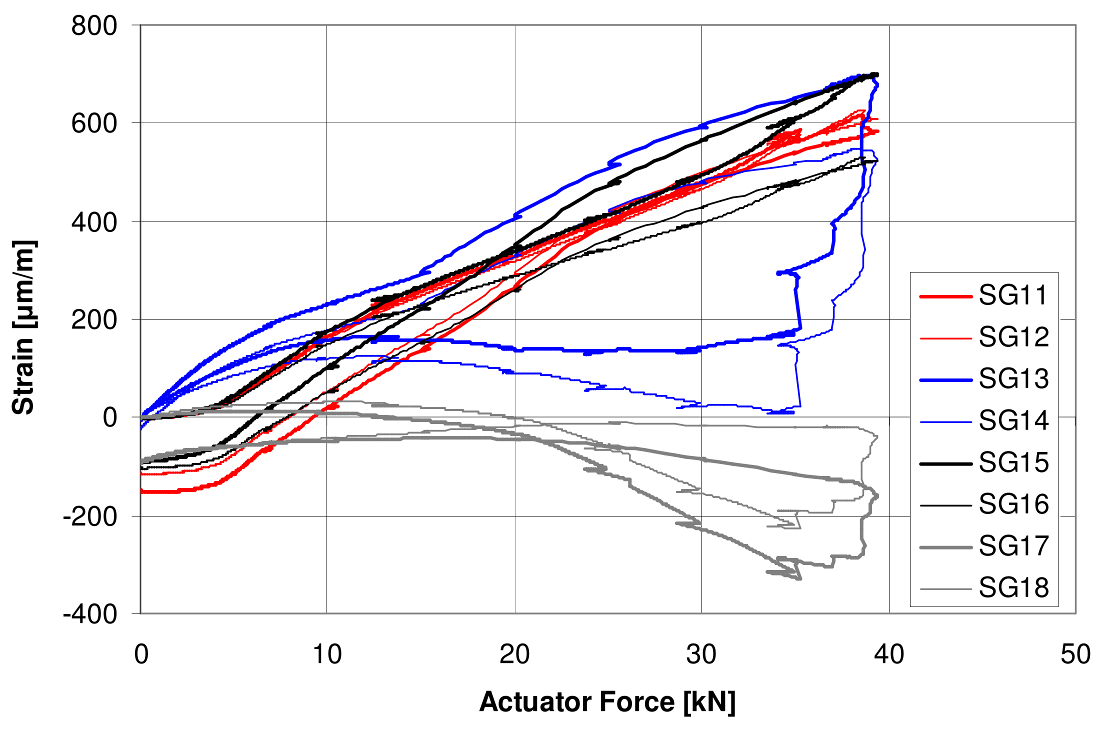

Figure 165 Frame Flange Strain Gauges 11 - 18: Strain vs. Actuator Load

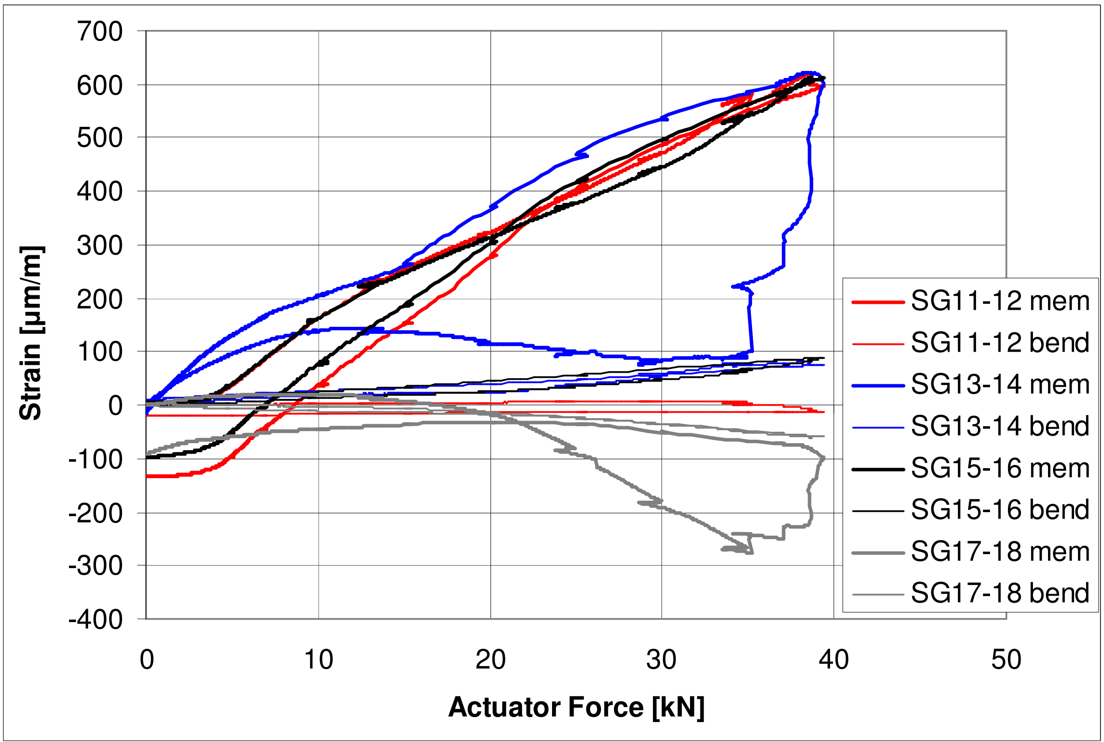

Figure 166 Frame Flange Strain Gauges 11 - 18: membrane, bending strains

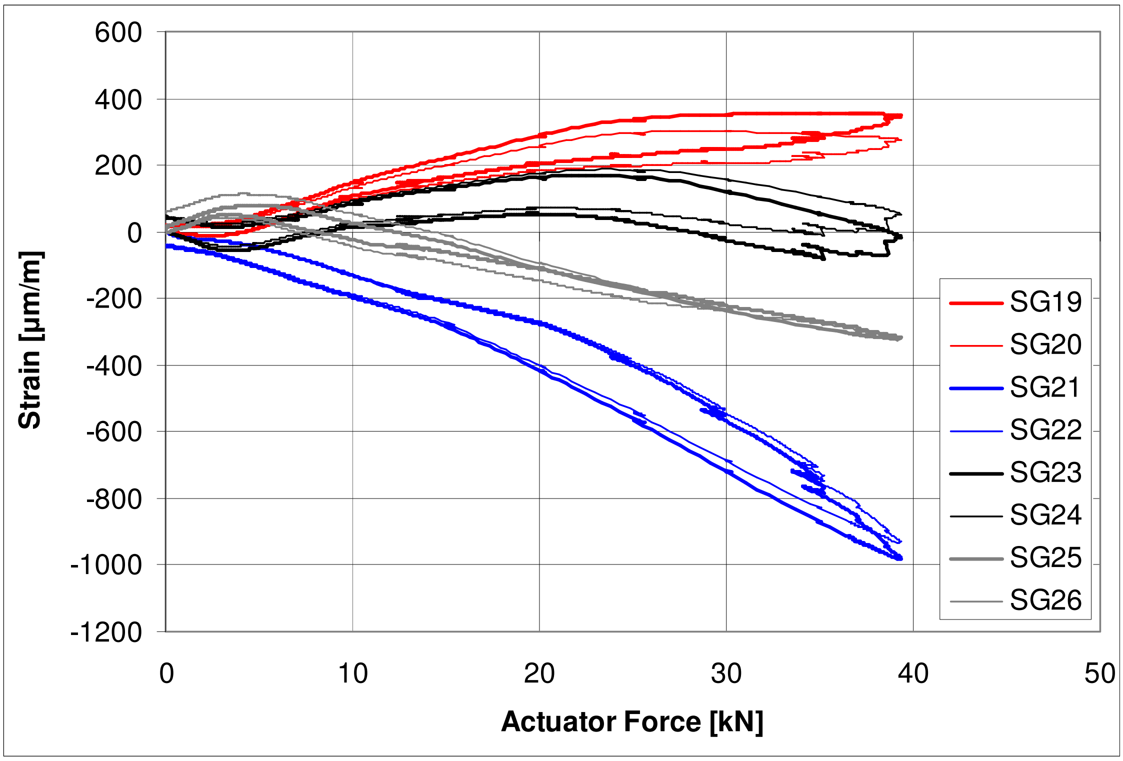

Figure 167 Frame Flange Strain Gauges 19 - 26: Strain vs. Actuator Load

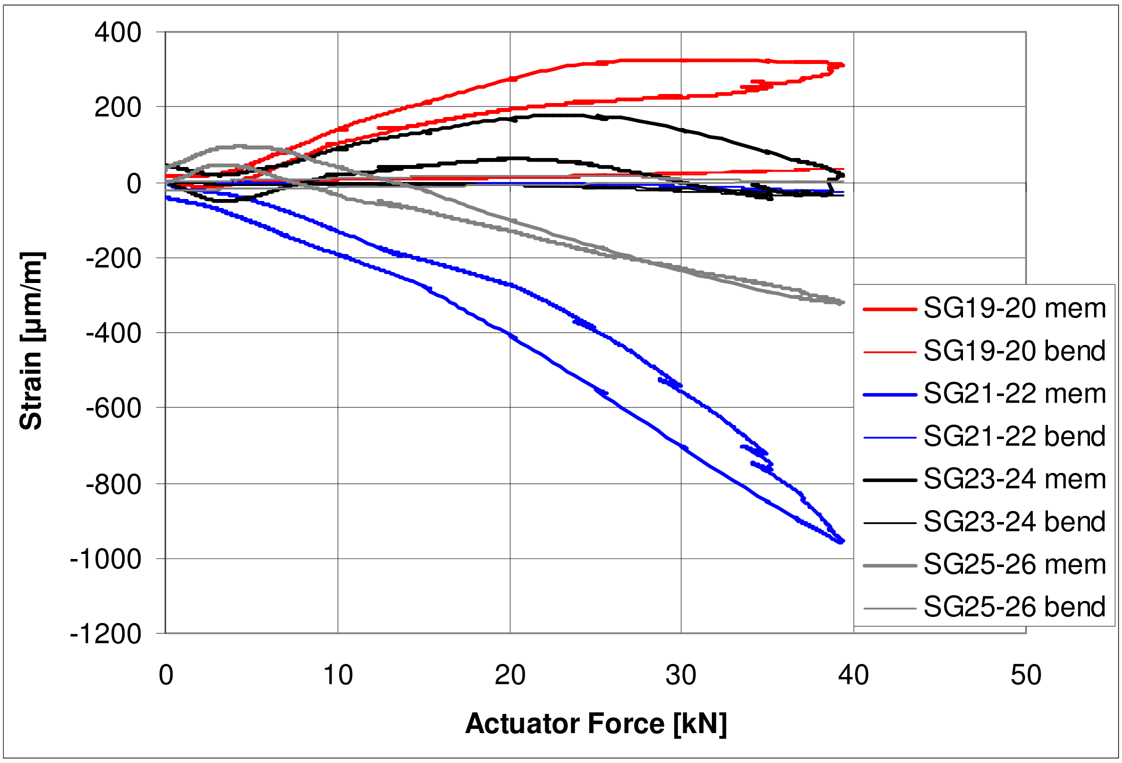

Figure 168 Frame Flange Strain Gauges 19 - 26: membrane and bending strains

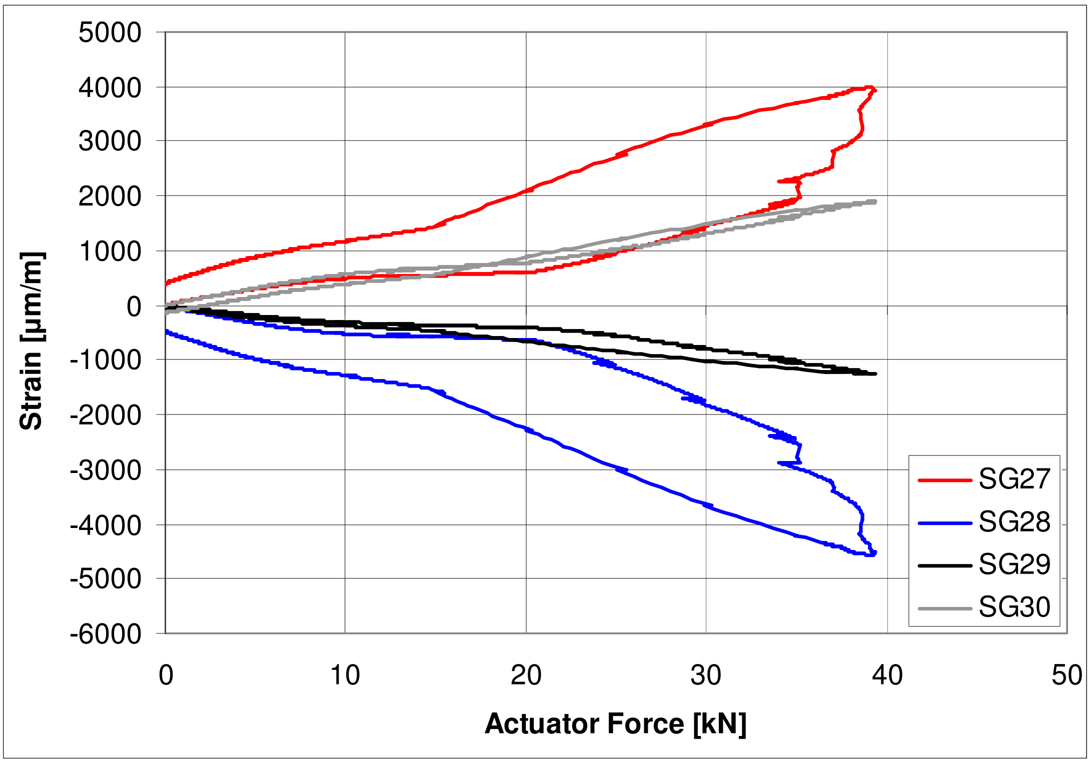

Figure 169 Shear Tie Strain Gauges: Strain vs. Actuator Load

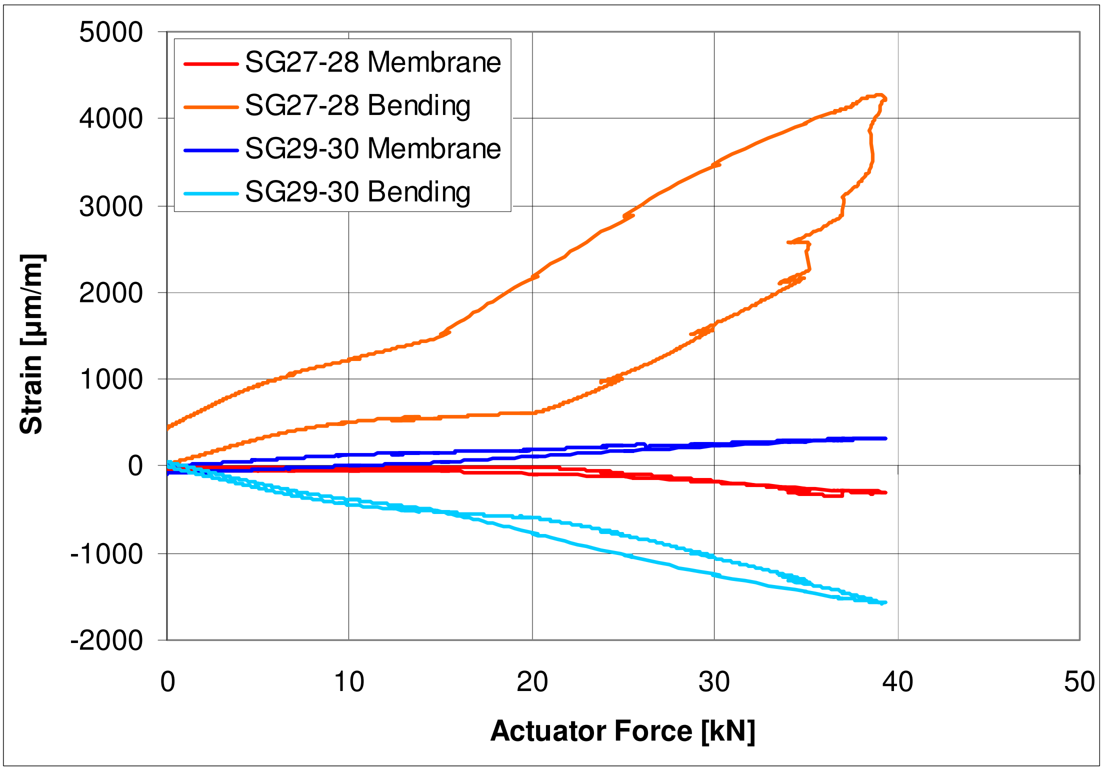

Figure 170 Shear Tie Strain Gauges, Membrane and Bending: Strain vs. Actuator Load

2nd load cycle

The displacement vs. load chart of the LVDTs 5,6,7 that were used to measure rotations, shows the measured displacements of these LVDTs (see Figure 171).

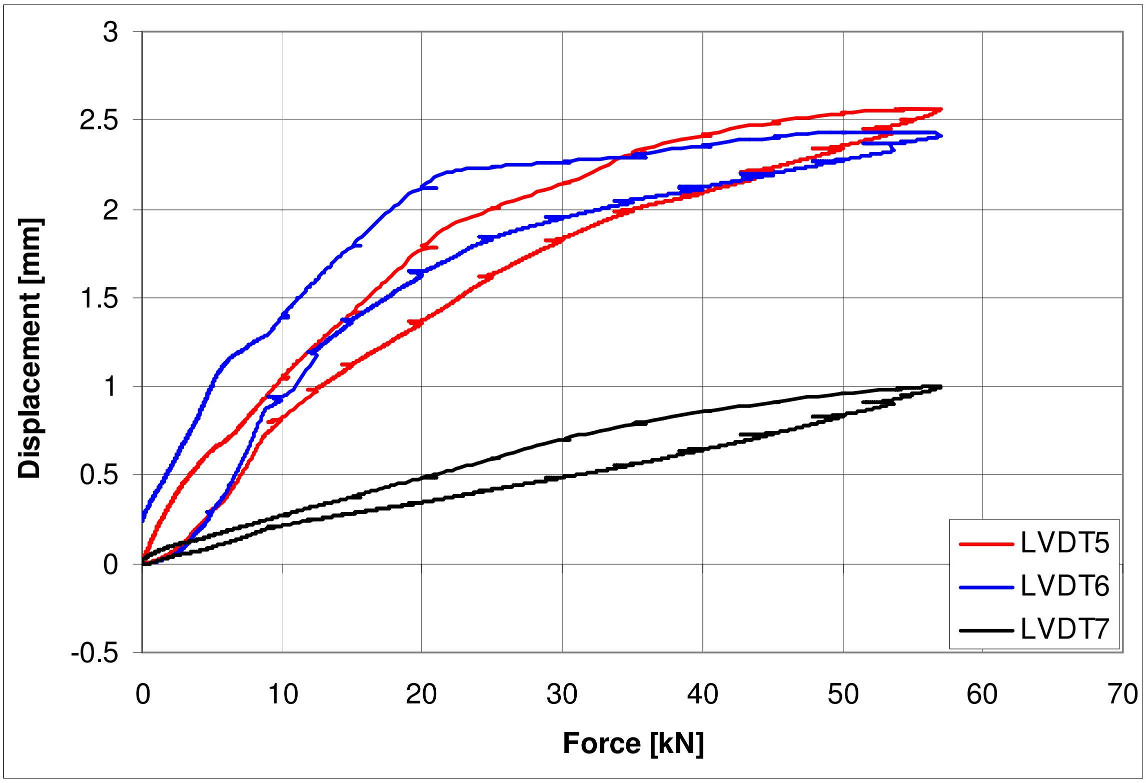

Figure 171 Displacement of LVDTs 5,6,7 vs. Actuator Load

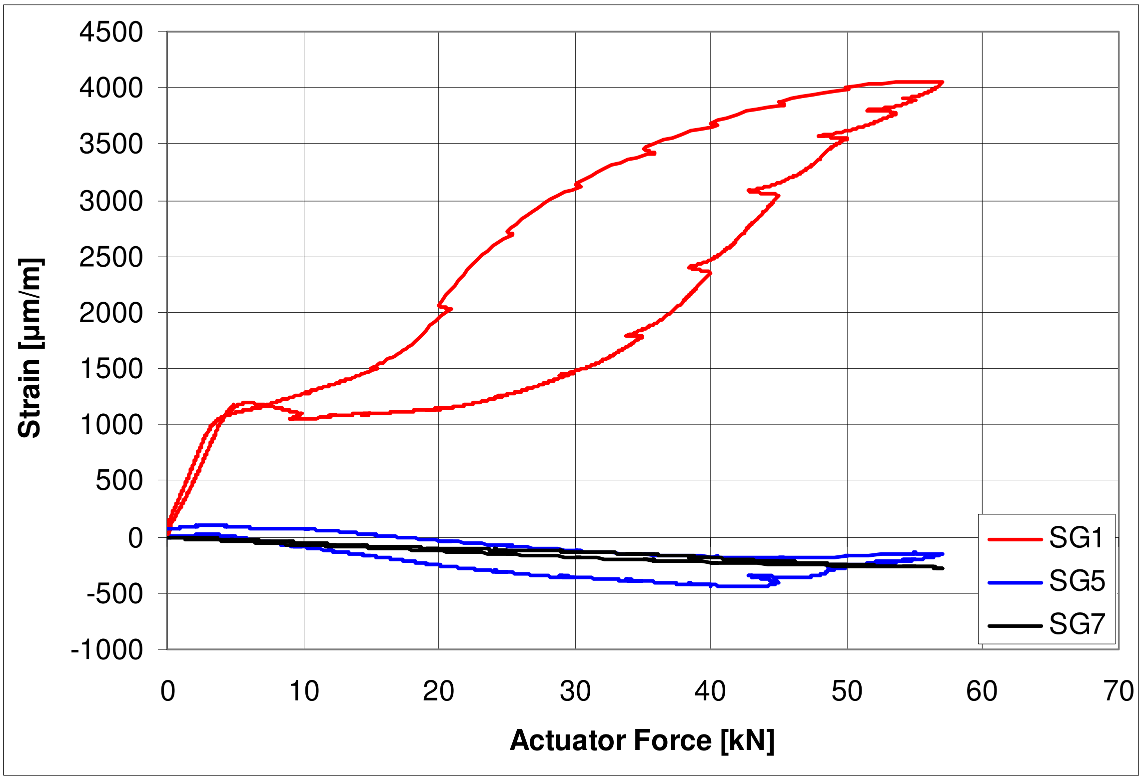

Figure 172 Skin circumferential Strain Gauges: Strain vs. Actuator Load

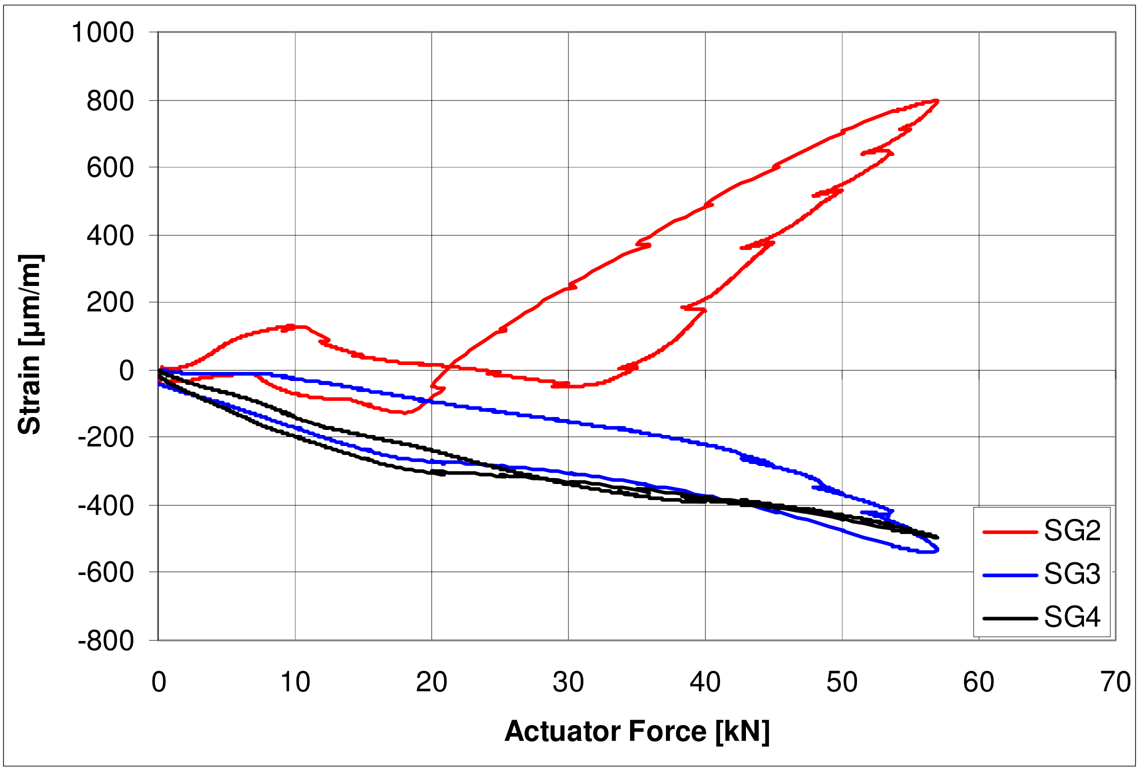

Figure 173 Skin axial Strain Gauges: Strain vs. Actuator Load

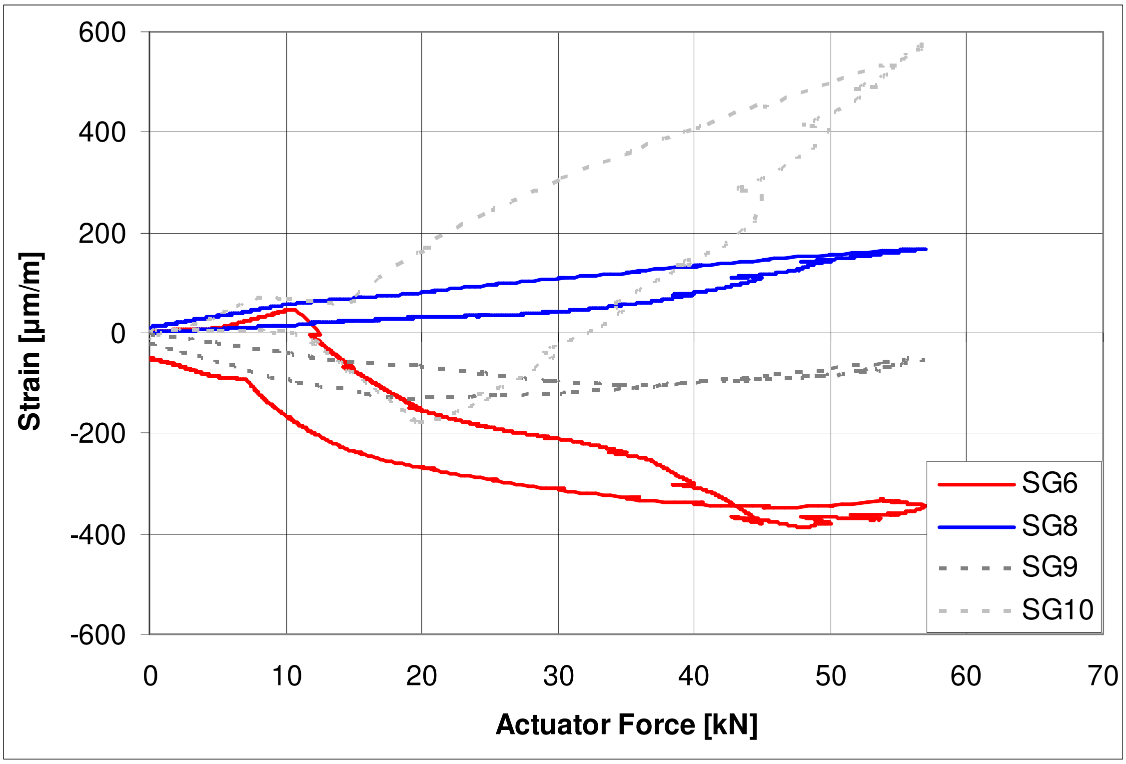

Figure 174 Skin & Stringer axial Strain Gauges: Strain vs. Actuator Load

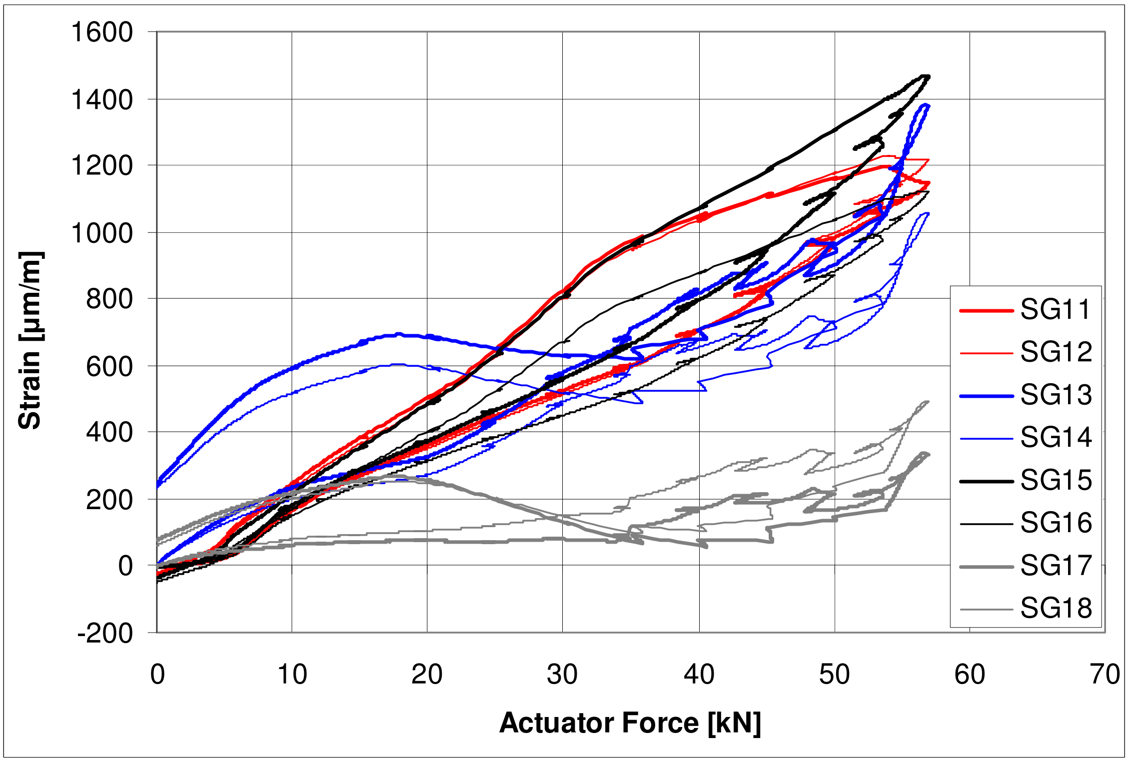

Figure 175 Frame Flange Strain Gauges 11 - 18: Strain vs. Actuator Load

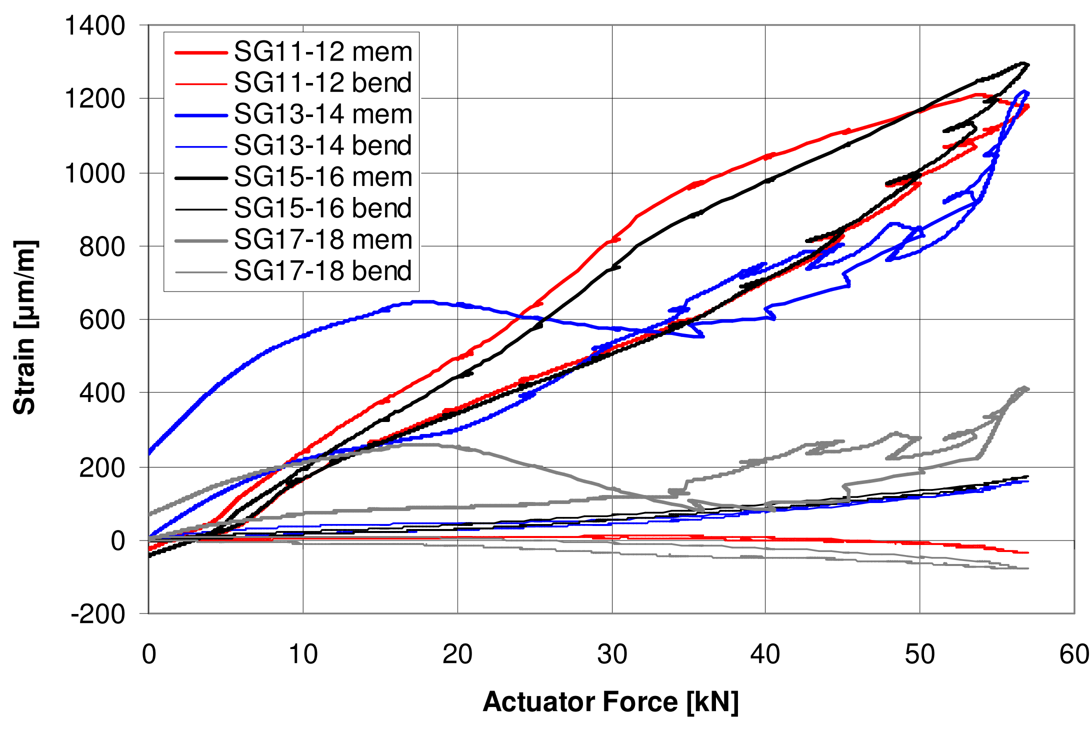

Figure 176 Frame Flange Strain Gauges 11 - 18: membrane and bending strains

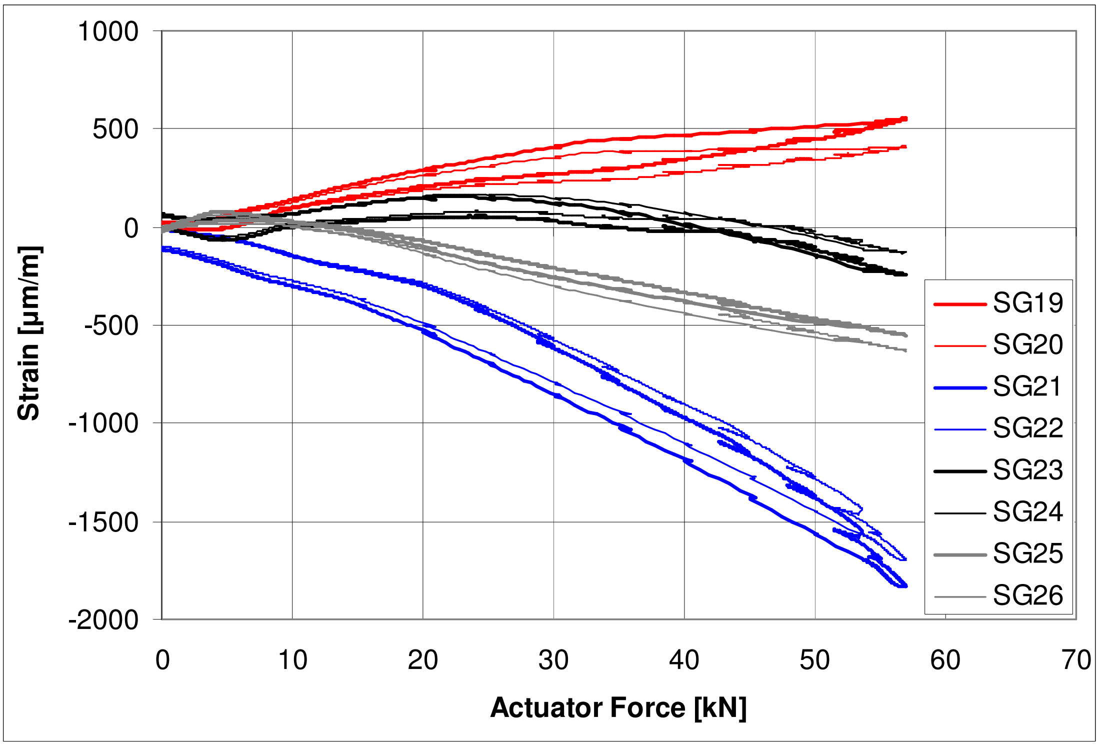

Figure 177 Frame Flange Strain Gauges 19 - 26: Strain vs. Actuator Load

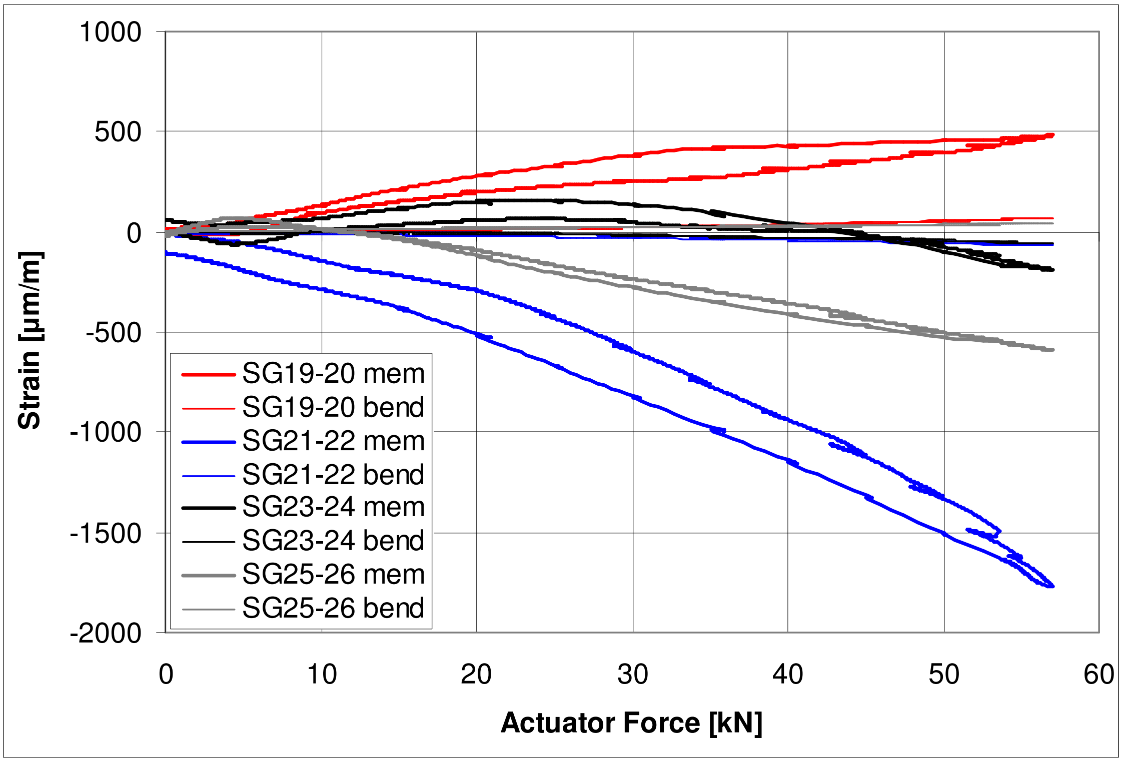

Figure 178 Frame Flange Strain Gauges 19 - 26: membrane and bending strains

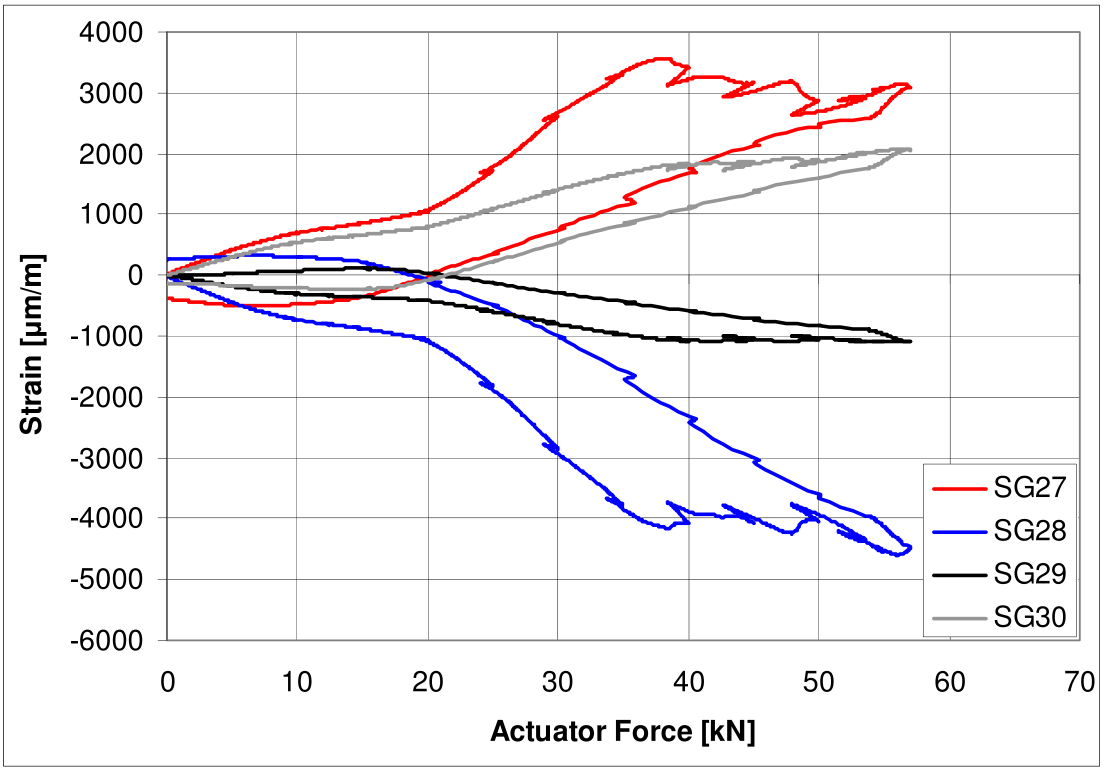

Figure 179 Shear Tie Strain Gauges: Strain vs. Actuator Load

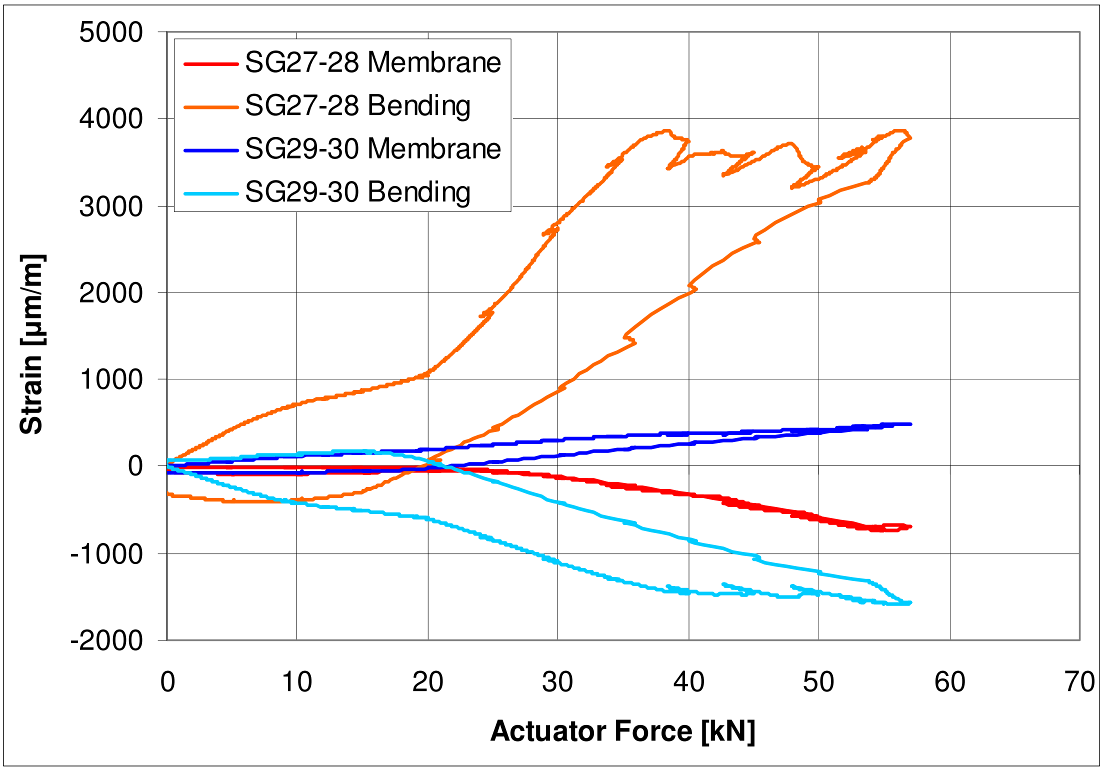

Figure 180 Shear Tie Strain Gauges, Membrane and Bending: Strain vs. Actuator Load

EUROPEAN AVIATION SAFETY AGENCY
AGENCE EUROPÉENNE DE LA SÉCURITÉ AÉRIENNE
EUROPÄISCHE AGENTUR FÜR FLUGSICHERHEIT

Postal address
Postfach 101253
50452 Cologne
Germany

Visiting address
Ottoplatz 1
50679 Cologne
Germany

Tel +49_221_89990-000
Fax +49_221_89990-999
Mail info@easa.europa.eu
Web easa.europa.eu